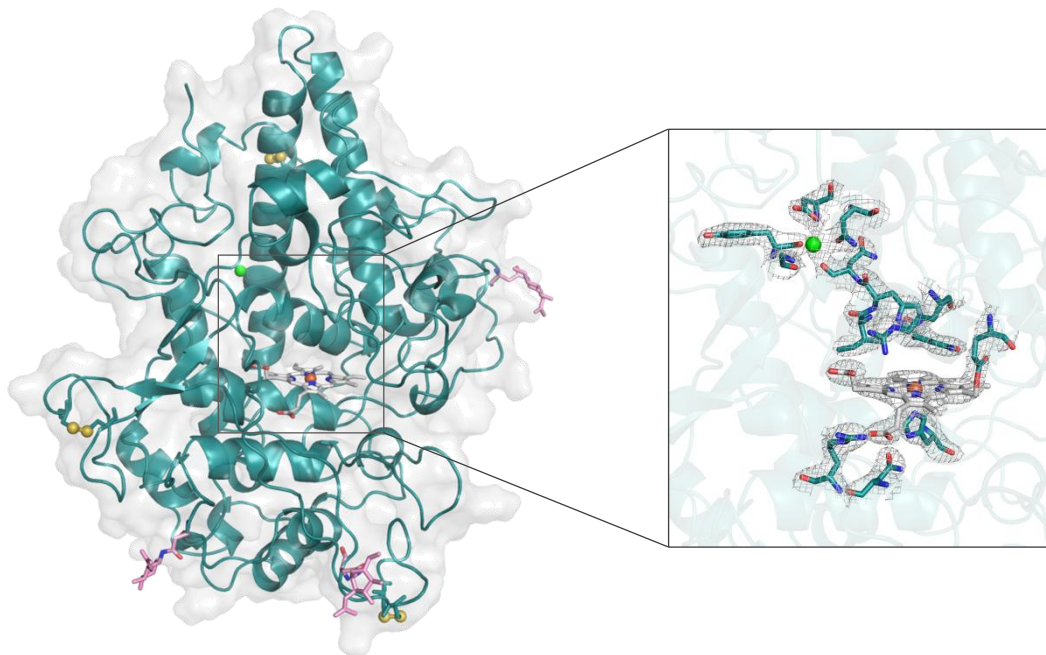


Enlightening the impact of covalent heme to protein bonds in ancestral peroxidases



PhD thesis

Andrea Nicolussi

Supervisor: Prof. Christian Obinger
December 2017

Protein Biochemistry Group, Department of Chemistry
BOKU - University of Natural Resources and Life Sciences
Muthgasse 18, 1190 Vienna, Austria

FWF



BiOP
Biomolecular
Technology of Proteins

Table of Contents

Acknowledgements	I
Declaration	II
Abstract	III
Zusammenfassung	IV
Introduction	1
Aims of the thesis	17
Publications	
How Covalent Heme to Protein Bonds Influence the Formation and Reactivity of Redox Intermediates of a Bacterial Peroxidase	20
Posttranslational Modification of Heme b in a Bacterial Peroxidase: The Role of Heme to Protein Ester Bonds in Ligand binding and Catalysis	33
Keeping it clean: Antibacterial Activity of a Secreted Peroxidase with One Covalent Heme to Protein Bond in the Social Amoeba <i>Dictyostelium discoideum</i>	51
Conclusion	87
Appendices	
Independent Evolution of Four Heme Peroxidase Superfamilies	95
Curriculum vitae	108

Acknowledgements

First and foremost, I would like to thank Christian Obinger for the opportunity to do my PhD thesis in the Protein Biochemistry group and for his supervision, motivation and constant support. Many thanks go also to Paul Furtmüller for his scientific guidance and advice during the last four years.

I also want to express my gratitude to Gianantonio Battistuzzi and Thierry Soldati for the chance to do my research stays in their labs in Modena and Geneva. Very special thanks go to Louise, Joe Dan, Ana, Cristina, Lyudmil, Elena, Caro and Nabil for their welcoming hospitality and all the fun during my time in Geneva.

Moreover I want to thank every single member of the Protein Biochemistry group for providing a supportive and cheerful atmosphere every single day. I really enjoyed working in this environment. Very special thanks go to my master students Georg and Julia and to my bachelor student Sonja, to everybody involved in the BioToP PhD program and especially to Christa for her advice in scientific as well as non-scientific topics.

Finally, I am forever grateful to my parents Johann and Elisabeth, my aunt Helga and my sister Eva-Maria for their constant support throughout my life and their faith in me. Special thanks go also to all of my friends for being there whenever I needed them. And last but not least I want to thank Stephan for his love and understanding during the challenging and the joyful times.

Declaration

All the laboratory work was carried out by the author of this thesis in the laboratory of Prof. Christian Obinger (BOKU Vienna, Department of Chemistry, Division of Protein Biochemistry, Muthgasse 18, 1190 Vienna, Austria), in the laboratory of Prof. Thierry Soldati (University of Geneva, Sciences II, 30, quai Ernest-Ansermet, 1211 Geneva, Switzerland), in the laboratory of Prof. Gianantonio Battistuzzi (University of Modena and Reggio Emilia, Department of Chemistry and Geology, via Campi 103, 41125 Modena, Italy) and in the laboratory of Prof. Prof. Kristina Djinović-Carugo (Max F. Perutz Laboratories, University of Vienna, Department for Structural and Computational Biology, 1030 Vienna, Austria).

Spectroelectrochemical measurements were performed with the help of Dr. Marzia Bellei (University of Modena and Reggio Emilia, Department of Life Sciences, via Campi 103, 41125 Modena, Italy).

Mass spectrometry was performed by Daniel Maresch, BSc. (BOKU Vienna, Department of Chemistry, Division of Protein Biochemistry, Muthgasse 18, 1190 Vienna, Austria). The lab work was supported by the master students Georg Schütz and Julia Weissensteiner and by the bachelor student Sonja Katz. *In-vivo* experiments were supported by Joe Dan Dunn, PhD. (University of Geneva, Sciences II, 30, quai Ernest-Ansermet, 1211 Geneva, Switzerland).

X-ray crystallography preparations were performed with support of Georg Mlynek, PhD (Max F. Perutz Laboratories, University of Vienna, Department for Structural and Computational Biology, Dr.-Bohr-Gasse 9, 1030 Vienna, Austria). Diffraction studies were carried out at the European Synchrotron Radiation Facility (ESRF, 71 Avenue des Martyrs, 38000 Grenoble, France).

Abstract

Heme peroxidases are found in all domains of life and typically catalyze the one- and two-electron oxidation of various organic or inorganic substrates. Four heme peroxidase superfamilies arose independently in evolution, and are therefore highly diverse regarding their secondary structure, active site architecture as well as catalytic activities. The redox cofactor is either a heme *b* or a posttranslationally modified heme that is coordinated by either a histidine or cysteine residue. The peroxidase-cyclooxygenase superfamily, which is composed of seven families, is unique in possessing a posttranslationally modified heme group. The heme can be covalently bound to the protein *via* one or two ester linkages between the 1-methyl and 5-methyl substituents of the porphyrin ring and adjacent acidic residues (aspartate and/or glutamate). The best-studied representatives of this superfamily are the mammalian peroxidases (family 1, e.g. myeloperoxidase or lactoperoxidase). However, recent phylogenetic analyses revealed that also ancestral peroxidases from prokaryotes and early eukaryotes (i.e. from Family 6) could possibly contain these posttranslational modifications.

In this thesis, occurrence and biosynthesis of these heme modifications in ancestral peroxidases from Family 6 were investigated. Two model enzymes were selected, namely a heme peroxidase with two covalent ester bonds from the cyanobacterium *Lyngbya* sp. PCC 8106 (LspPOX) and a peroxidase from the social amoeba *Dictyostelium discoideum* (DdPoxA) with one covalent ester bond. Studies on LspPOX demonstrate that both ester linkages have a drastic impact on the biophysical and biochemical properties of this heme enzyme. Compared to heme *b* proteins, the UV-vis maxima of the Soret bands are red-shifted, the standard reduction potential of the Fe(III)/Fe(II) couple is more positive and the thermal stability is increased. While the oxidation of the ferric enzyme by hydrogen peroxide is not affected by this posttranslational modification, the halogenation reaction rates increase significantly upon formation of the ester linkages. By mutating the relevant acidic amino acids, we were able to investigate the impact of each single ester bond.

Studies on DdPoxA showed that one ester linkage is sufficient to maintain a high thermal stability, but the oxidation capacity of Compound I is drastically decreased. Contrary to LspPOX, DdPoxA can oxidize bromide only at a very low rate. This work also includes the first X-ray structure of a peroxidase from family 6 (DdPoxA) and we elucidate the antibacterial role of DdPoxA in the life cycle of the social amoeba *D. discoideum*.

Zusammenfassung

Häm-Peroxidasen sind in allen Domänen des Lebens vertreten und katalysieren die Ein- oder Zweielektronen-Oxidation verschiedener organischer oder inorganischer Substrate. Vier Superfamilien von Häm-Peroxidasen haben sich evolutionär unabhängig voneinander entwickelt. Diese unterscheiden sich in ihrer Sekundärstruktur, ihrem aktiven Zentrum und ihrer katalytischen Aktivität. Als Redox-Kofaktor fungiert entweder Häm *b* oder ein posttranslational modifiziertes Häm, das durch ein Histidin oder Cystein koordiniert wird. In der Peroxidase-Cyclooxygenase Superfamilie (bestehend aus sieben Familien) kann die Häm Gruppe durch eine posttranslationale Modifikation kovalent an das Protein gebunden werden. Dabei werden eine oder zwei Esterbindungen zwischen der 1-Methyl und der 5-Methyl-Seitenkette des Porphyrinrings und benachbarten Aminosäureresten (Aspartat und/oder Glutamat) ausgebildet. Die am besten untersuchten Vertreter der Peroxidase-Cyclooxygenase Superfamilie sind die Säugetierperoxidasen (Familie 1, z.B. Myelo-peroxidase oder Lactoperoxidase). Jedoch zeigen phylogenetische Analysen, dass auch in Vertretern aus Prokaryoten und frühen Eukaryoten aus Familie 6 diese posttranslationalen Modifikationen vorkommen könnten.

In dieser Arbeit werden die strukturelle und funktionale Rolle dieser Häm-Modifikationen in zwei Modell-Peroxidasen aus Familie 6 untersucht, nämlich die Peroxidase aus dem Cyanobakterium *Lyngbya* sp. PCC 8106 mit zwei Häm-Protein Esterbindungen (LspPOX) und jene aus *Dictyostelium discoideum* mit einer kovalenten Bindung (DdPoxA). Untersuchungen an LspPOX zeigen, dass die beiden kovalenten Esterbindungen großen Einfluss auf die biophysikalischen und biochemischen Eigenschaften dieses Hämenzyms haben. Im Vergleich zu Häm *b* Proteinen sind die UV-vis Maxima bathochrom verschoben, das Reduktionspotential des Redoxpaares Fe(III)/Fe(II) ist positiver und die Thermostabilität erhöht. Während die Oxidation des Ferri-Enzyms durch H₂O₂ zu Compound I nicht durch diese posttranslationale Modifikation beeinflusst wird, sind die Halogenidoxidationsraten signifikant höher. Durch Mutationen an den relevanten Aminosäuren konnte der Einfluss der einzelnen Esterbindungen ermittelt werden.

Die Studien an DdPoxA zeigten, dass durch eine Esterbindung zwar noch eine hohe Thermostabilität gegeben ist, jedoch die Oxidationskapazität von Compound I drastisch vermindert ist. Im Gegensatz zu LspPOX kann DdPoxA Bromid nur mit sehr niedriger Rate oxidieren. Diese Arbeit inkludiert außerdem die erste Röntgenstruktur einer Peroxidase aus Familie 6 und die gibt Hinweise auf die antibakterielle Rolle von DdPoxA im Lebenszyklus der Amöbe *D. discoideum*.

Introduction

Heme peroxidases - an overview

Four heme peroxidase superfamilies evolved independently during evolution, differing in their overall fold, their active site architecture and in the catalyzed reactions. They are widely distributed among all kingdoms of life and catalyze the H₂O₂-mediated oxidation of various one- or two-electron donors. These donors can be aromatic (e.g. tyrosine, urate, coniferyl or sinapyl alcohol etc.) or aliphatic (e.g. ascorbic acid) molecules, cations (e.g. Mn²⁺), anions (e.g. halides or thiocyanate) or even other proteins (e.g. cytochrome *c*). In addition to these peroxidase activities, catalase, cyclooxygenase, chlorite dismutase and peroxygenase activities of heme peroxidases have been reported.^{1,2}

The cofactor in all these peroxidases is either heme *b* (Figure 1) or a modified heme. This iron-containing porphyrin macrocycle occurs in thousands of proteins and fulfills an enormous amount of different reactions. Prominent examples are electron transport (cytochromes), carriage or storage of dioxygen (hemoglobin or myoglobin), dismutation of hydrogen peroxide (catalases), detoxification reactions (cytochrome P450s), hormone biosynthesis (cytochrome P450s, thyroid peroxidase), cell wall biosynthesis (plant peroxidases) or innate immunity (myeloperoxidase or lactoperoxidase).^{2,3}

Phylogeny of the peroxidase-cyclooxygenase superfamily

The peroxidase-cyclooxygenase superfamily (Pfam accession number PF03098) is divided into seven families (Figure 2). Family 1 comprises the **vertebrate peroxidases** that have been under investigation for more than 40 years.⁴ In mammals, homodimeric myeloperoxidase (MPO) as well as monomeric lactoperoxidase (LPO) and eosinophil peroxidase (EPO) have been shown to be an essential part of host defense in the innate immunity of vertebrates.⁵ By releasing highly reactive and oxidizing reaction products like hypohalous acids, they comprise the front line defense against invading pathogens. Dimeric membrane-anchored thyroid peroxidase (TPO) catalyzes the synthesis of the thyroid hormones triiodothyronine (T₃) and thyroxine (T₄).⁶

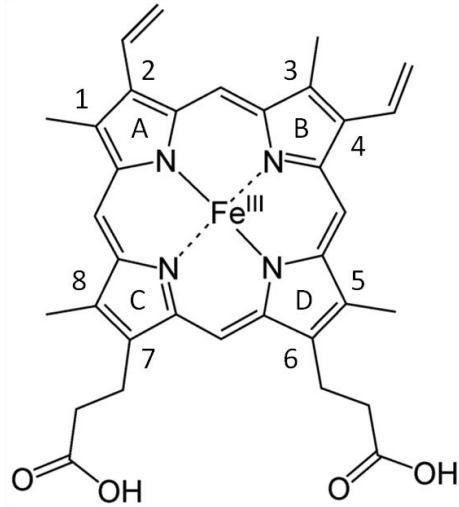


Figure 1: Structure of heme *b*. Porphyrin substituents 1, 3, 5, and 8: methyl groups; porphyrin substituents 2 and 4: vinyl groups, porphyrin substituents 6 and 7: propionate groups. A, B, C and D: four pyrrole rings linked by methine bridges. Figure was constructed with IsisDraw 2.3.

The first representative of Family 2 was detected in *Drosophila* in 1984.⁷ In this publication the name **peroxidasin** was first coined. Family 2 members are homotrimeric multidomain heme peroxidases found in invertebrates and vertebrates. Recently they have attracted attention due to their important role in extracellular matrix consolidation in mammals.⁸⁻¹¹ These multidomain peroxidases are secreted and comprised of leucine-rich domains, immunoglobulin domains and a C-terminal von Willebrand factor C domain in addition to the catalytic heme peroxidase domain. It has been proposed that their physiological role is providing hypobromous acid for the formation of specific collagen IV crosslinks in the extracellular matrix of mammals.^{9,12}

Family 3 contains heme peroxidases designated as **peroxinectins** with cell adhesion function(s) and putative function in innate immunity of invertebrates (Figure 2).¹³ Peroxinectins are fusion proteins of a heme peroxidase domain with an integrin-binding motif. No comprehensive biochemical and physiological studies on peroxinectins are available so far.

Family 4 of the peroxidase-cyclooxygenase superfamily is comprised of bacterial, fungal, plant and animal **cyclooxygenases** and especially the bacterial members are still at the level of putative protein sequences.² A few representatives from the animal phyla were cloned and analysed. In mammals, cyclooxygenases (COX-1 and COX-2), also known as prostaglandin-endoperoxide synthases (PTGS), are responsible for the formation of prostanoids, including thromboxanes and prostaglandins.

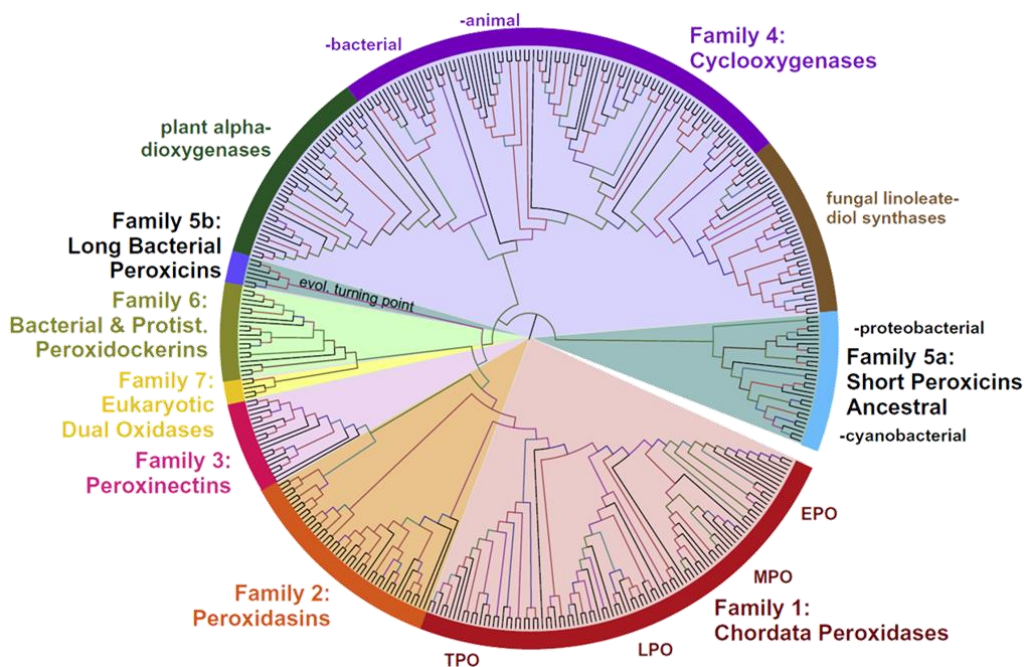


Figure 2: Reconstructed phylogenetic tree of the peroxidase-cyclooxygenase superfamily.² Family 1 comprises the mammalian peroxidases, while the two enzymes LspPOX (heme peroxidase from the cyanobacterium *Lyngbya* sp. PCC 8106) and DdPoxA (peroxidase A from *Dictyostelium discoideum*), which are investigated in this thesis, belong to Family 6 (peroxidockerins). EPO, eosinophil peroxidase; MPO, myeloperoxidase; LPO, lactoperoxidase, TPO, thyroid peroxidase.

The ancestral clade of short bacterial **peroxicins** of Family 5 is supposed to contain the oldest representatives of this superfamily.² From them, proteobacterial and actinobacterial peroxicins and, finally, long bacterial peroxicins evolved that in addition to the catalytic peroxidase contain additional domains like calcium-binding or hemolysin-type motifs. No biochemical and physiological data about Family 5 proteins are known.

Two enzymes from Family 6, the **peroxidockerins**, are investigated in this work (see below). Family 6 representatives are at the evolutionary basis of the peroxinectins, peroxidasins and chordata peroxidases like MPO or LPO. Descendants of variable length emerged in eubacteria as well as Amoebozoa, Heterolobosea and Chromalveolata.² This suggests that peroxidockerins were widely distributed among the early eukaryotic world.

Family 7 contains two-domain **dual oxidases** (DUOX), which were segregated from Family 6 at the level of primitive eukaryotes. The multidomain oxidases have retained an extracellular peroxidase domain of unknown function at the N-terminus followed by a transmembrane calcium-binding domain and a cytosolic flavodomain with homology to NADPH oxidase (NOX). In humans,

two members, hDUOX1 and hDUOX2 are found. The function of dual oxidases is superoxide and/or hydrogen peroxide generation, however the role and interaction of the two catalytic flavo- and heme-domain is still not clear.¹⁴

In five out of the seven families of the peroxidase-cyclooxygenase superfamily, representatives with a modified and covalently bound heme in their active site have been found, namely members of Family 1, 2, 3, 5 and 6.^{1,2} The most prominent examples containing these posttranslational modifications are the vertebrate peroxidases including MPO, LPO, TPO, EPO and peroxidasin 1.^{12,15,16} However, recent phylogenetic analyses revealed that the acidic amino acids that are responsible for covalent heme attachment can also be found in bacterial and early eukaryotic members of the peroxidase-cyclooxygenase superfamily.^{2,17,18}

Heme to protein ester bonds

Upon several described forms of covalent heme attachment³, this work focuses on ester bonds between conserved acidic amino acids, i.e. aspartate and glutamate, and the 1-methyl and 5-methyl groups of the heme porphyrin ring. This posttranslational modification is found exclusively in the peroxidase-cyclooxygenase superfamily and is the most striking structural feature of the mammalian peroxidases.¹ Prominent examples are the mammalian MPO, LPO, EPO and TPO, which have been studied with respect to their structure, function and their role in physiology. MPO, LPO and EPO have been shown to play important roles in innate immunity, while TPO contributes in hormone biosynthesis.^{6,19-21} The mammalian MPO is unique in having a third covalent link (a sulfonium ion bond) that is formed between a sulfur atom of a methionine and the C_β atom of the 2-vinyl group of the heme porphyrin ring.^{22,23}

The impact of these heme modifications has been postulated previously^{26,27}, but detailed investigations were diminished by the fact that these enzymes could not be produced recombinantly or purified from natural sources in satisfying amounts. Further, the production of mutants was hindered by the fact that these proteins could not be expressed in a simple bacterial expression host but in insect or mammalian cell culture.

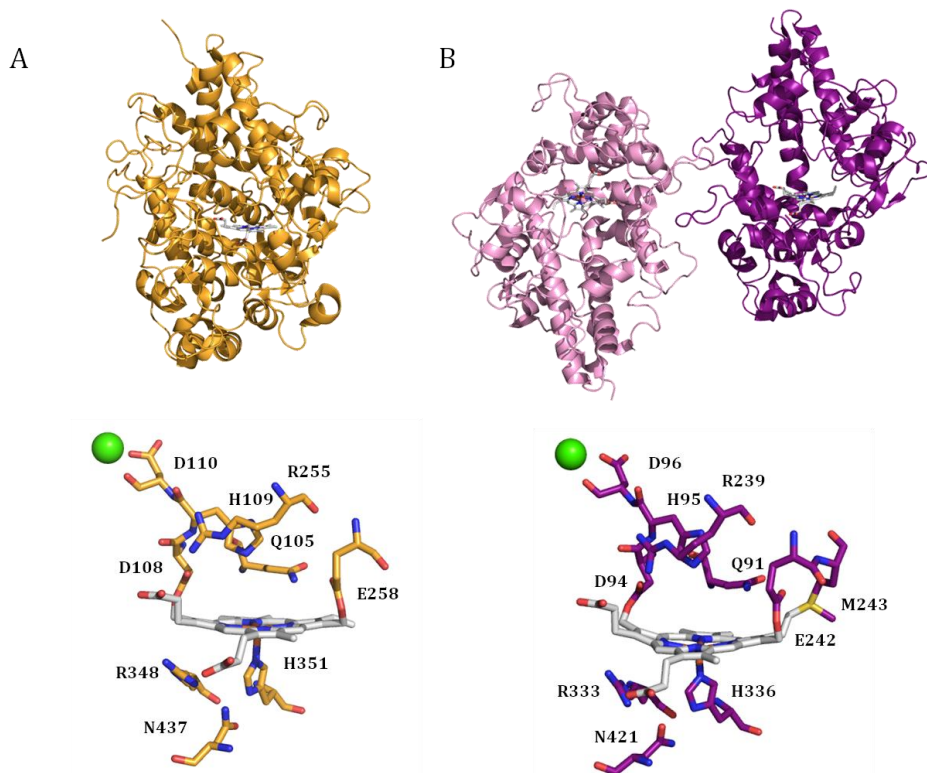


Figure 3: Overall and active site structures of monomeric caprine lactoperoxidase²⁴ (A) and dimeric human myeloperoxidase²⁵ (B) including the covalent heme to protein linkages (LPO: D109 and E258, MPO: D94, E242 and M243), distal residues and proximal histidine, asparagine and arginine.

Formation and consequences of heme to protein ester bonds

Formation of the covalent ester linkages has been shown to occur autocatalytically and posttranslationally, starting from hydrogen peroxide-mediated formation of Compound I.²⁸ Figure 4 shows a detailed reaction mechanism that was recently postulated by Ortiz de Montellano, including the following steps: formation of Compound I by the non-covalently linked holoprotein. Compound I oxidizes an adjacent carboxylic acid to the carboxylate radical, thereby reducing the heme to Compound II. The side chain radical performs hydrogen abstraction from the adjacent heme methyl group, yielding in a methylene radical and regeneration of the carboxylic acid anion. Subsequently, the unpaired electron is transferred from the methylene to the iron center, leading to a ferric heme and a methylene cation that traps the carboxylate anion, thereby forming the covalent ester linkage.²⁹

As a consequence of the ester bond formation, the porphyrin ring becomes distorted causing a bow-shaped out-of-plane structure, as has been shown by X-ray crystallography as well as by resonance Raman spectroscopy.^{25,30,31} This effect is much more pronounced in MPO due to the presence of the third (electron withdrawing) sulfonium ion linkage. As a consequence of distortion and electronic effects, the spectroscopic, redox and catalytic properties of vertebrate peroxidases (e.g. LPO and MPO) and heme *b* peroxidases (e.g. horseradish peroxidase) are significantly different.^{22,23} Closely related to those distinct biochemical and biophysical properties are the physiological roles of these oxido-reductases.^{22,26,32}

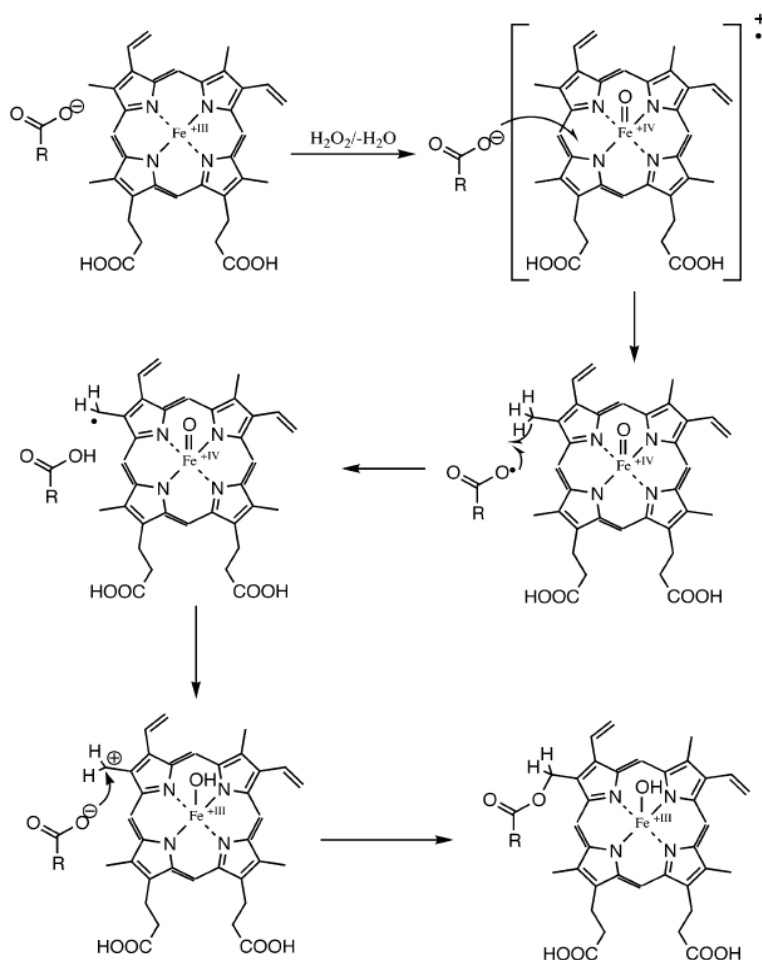


Figure 4: The postulated reaction mechanism for the formation of heme to protein ester bond follows a H₂O₂-mediated free radical mechanism starting with formation of Compound I.²⁹

Spectral features

The absorption spectrum of a heme protein is caused by electron transitions within the porphyrin as well as between the porphyrin, the iron and its ligands. Heme peroxidases containing unmodified heme *b*, such as HRP, typically exhibit Soret bands between 400 and 408 nm (Figure 5). Upon covalent attachment of the heme to the protein matrix, the spectral features change drastically. The formation of the two ester bonds causes a distortion of the heme and is sufficient to result in a significant red-shift of the Soret peak to 410 - 413 nm as was shown for LPO, EPO or a truncated peroxidasin 1 (HsPxd1 con4).^{11,12,22} Due to the additional MPO-typical sulfonium ion linkage the Soret peak is further red-shifted to 430 nm (Figure 5).³³ Mutants of MPO having Met243 is replaced by other amino acids (thus forming only two ester bonds) exhibit spectral properties similar to LPO or EPO.^{15,22,34} This clearly demonstrates that the additional covalent link in MPO is responsible for its unique spectral properties.

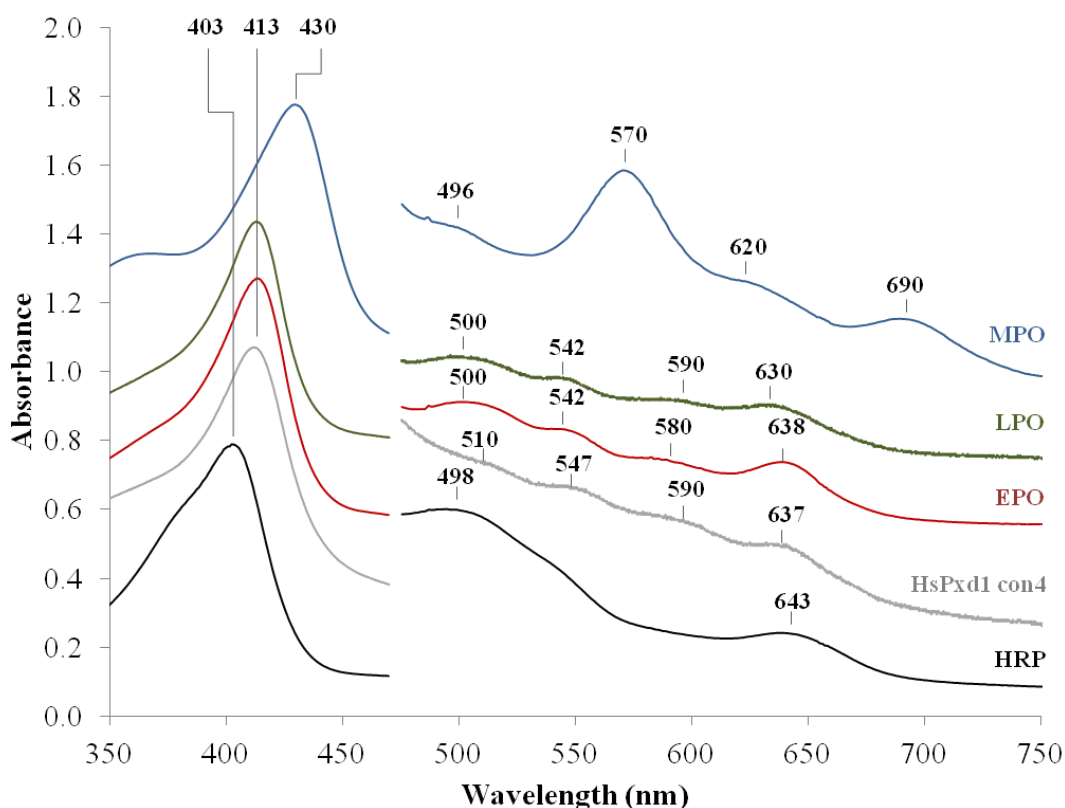


Figure 5: Spectral features of myeloperoxidase (MPO, blue), lactoperoxidase (LPO, green), eosinophil peroxidase (EPO, red), truncated human peroxidasin 1 (hsPxd01 con4, grey) and horseradish peroxidase (HRP, black). The wavelength region between 450 and 750 nm is multiplied by a factor of 5.

Standard reduction potential

Additionally, the covalent heme linkages greatly influence the redox properties of the mentioned heme peroxidases. Enzymes containing unmodified heme *b*, such as HRP, exhibit a standard reduction potential (E°) of the redox couple Fe(III)/Fe(II) around -300 mV (Table 1).³⁵ Lactoperoxidase, EPO and truncated human peroxidase 1 show slightly more positive standard reduction potentials (-176 mV, -126 mV and -128 mV, respectively) (Table 1).^{12,36} However, MPO is unique in having a positive Fe(III)/Fe(II) reduction potential of +5 mV similar to globins. This positive standard reduction potential of MPO is very likely due to the positive charge of the sulfur atom participating in the sulfonium ion linkage, which acts as an electron withdrawing group and decreases the electron density at the heme iron.³⁷

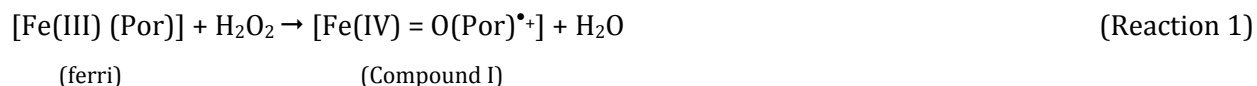
Only very little is known about the reduction potentials of the redox couples Compound I/Compound II and Compound II/Fe(III) (Table 1). There is only a small difference in the reduction potentials of Compound II/Fe(III) among the investigated peroxidases. But compared to heme *b* peroxidases such as HRP, the reduction potential of Compound I/Compound II is significantly higher in MPO and LPO (Table 1). Furthermore, this standard reduction potential is higher in MPO (1.35 V)³⁸ than in LPO (1.14 V).³⁹ This again underlines the role of the sulfonium ion linkage in further increasing the electron deficiency of the porphyrin π -cation radical of Compound I. Various substrates can act as one-electron donors for Compound I, but the reduction potential of the Compound II/Fe(III) couple is usually less positive. As a consequence, in most peroxidases reduction of Compound II to the ferric enzyme is the rate-limiting step.^{40,41}

Table 1: Standard reduction potentials of all relevant redox couples of myeloperoxidase (MPO), lactoperoxidase (LPO), eosinophil peroxidase (EPO), truncated human peroxidase 1 (HsPxd1 con4) and horseradish peroxidase (HRP). Cpd I, Compound I; Cpd II, Compound II, n.d. not determined.

E° (mV)	MPO	LPO	EPO	HsPxd1 con4	HRP
Fe(III)/Fe(II)	+5 (37)	-176 (36)	-126 (36)	-128 (12)	-306 (35)
Cpd I/Fe(III)	1160 (42)	1090 (43)	1100 (42)	n.d.	883 (44)
Cpd I/Cpd II	1350 (45)	1140 (43)	n.d.	n.d.	898 (44)
Cpd II/Fe(III)	970 (45)	1040 (43)	n.d.	n.d.	869 (44)

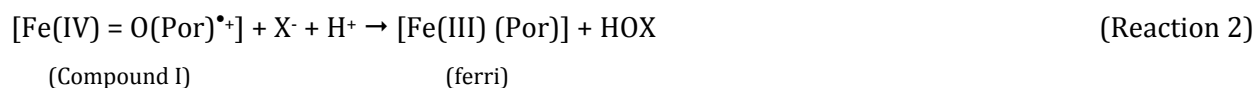
Catalysis

Peroxidases are able to catalyze halogenation as well as peroxidase reactions. Both reaction cycles start with the same initial redox reaction, namely the oxidation of the ferric resting state to the so-called Compound I mediated by hydrogen peroxide (Reaction 1).^{22,46}



Compound I is two oxidizing equivalents above the resting ferric state. In Family 1 peroxidases Compound I is an oxoiron(IV) species with a porphyrin π -cation radical.⁴⁶ The rate of Compound I formation is in the same order of magnitude for various investigated peroxidases from the four superfamilies ($1 - 5 \times 10^7 \text{ M}^{-1} \text{ s}^{-1}$)^{12,46-49}, regardless whether the heme is covalently attached to the protein or not (Table 2). Hence, posttranslational modification of the prosthetic heme group has no impact on Compound I formation.²²

By contrast, the presence of covalent heme to protein linkages has a strong impact on the oxidation capacity of Compound I. During the halogenation cycle of a peroxidase, Compound I is reduced directly to the ferric resting state by two-electron donors such as halides (iodide, bromide, chloride) or the (pseudo-)halide thiocyanate, thereby forming (pseudo-)hypohalous acids (Reaction 2).²²

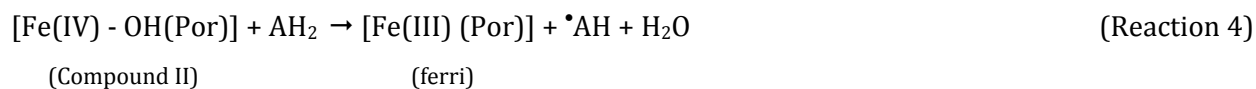
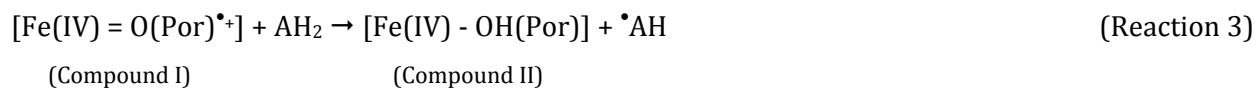


In general, the capability of peroxidases to oxidize (pseudo-)halides follows the hierarchy: $\text{SCN}^- > \text{I}^- > \text{Br}^- > \text{Cl}^-$. This order is based on the differences in the standard reduction potentials for the redox couples HXO/X^- , H_2O at pH 7.0: 1.27 V (Cl^-), 1.13 V (Br^-), 0.78 V (I^-) and 0.56 V (SCN^-).⁵⁰ Therefore, all peroxidases, regardless whether the heme group is covalently bound or not, can oxidize iodide and thiocyanate.⁴⁶ However, for the formation of HOBr or even HOCl, Compound I has to be a stronger oxidant. For LPO and EPO it was shown that the ester linkages increase the

standard reduction potential of the Compound I/Fe(III) couple in comparison to heme *b* peroxidases (Table 1).^{42,43} Only MPO is able to oxidize chloride at reasonable rates ($2.5 \times 10^4 \text{ M}^{-1} \text{ s}^{-1}$) due to the extraordinary high redox potential of the redox couple Compound I/Fe(III) of 1.16 V (Table 2).⁴⁸ The electron withdrawing effect of the vinyl-sulfonium ion linkage decreases the electron density at the heme group in Compound I, thereby enhancing the electron transfer from chloride to the electron deficient heme.⁴²

EPO is able to oxidize chloride to a very low extent ($3.1 \times 10^3 \text{ M}^{-1} \text{ s}^{-1}$), but bromide ($1.9 \times 10^7 \text{ M}^{-1} \text{ s}^{-1}$), iodide and thiocyanate ($\sim 10^8 \text{ M}^{-1} \text{ s}^{-1}$) at very high rates.⁵¹ LPO shows no reaction with chloride, but is able to oxidize bromide at reasonable rates ($4.1 \times 10^4 \text{ M}^{-1} \text{ s}^{-1}$), further it is an excellent oxidizer of iodide and thiocyanate ($> 10^8 \text{ M}^{-1} \text{ s}^{-1}$ for both reactions) (Table 2).⁴⁹ Compound I of a truncated version of human peroxidase 1 (HsPxd 1 con4) has recently been investigated intensively and shows a high reaction rate with bromide ($5.6 \times 10^6 \text{ M}^{-1} \text{ s}^{-1}$) as well as a reasonable rate with iodide and thiocyanate ($> 10^7 \text{ M}^{-1} \text{ s}^{-1}$ for both reactions).¹²

During the peroxidase cycle, Compound I is reduced back to the ferric resting state by a two step reaction *via* a oxoiron(IV) species called Compound II (Reactions 3 and 4). In these one-electron reactions, the peroxidase substrates (AH_2) are oxidized to their corresponding radicals ($\bullet\text{AH}$).^{22,26}



Various substrates can act as one-electron donors for the above described reactions, including physiological substrates such as tyrosine, ascorbate or serotonin. As mentioned before, the reduction of Compound II is the rate limiting step, since it shows a lower reaction rate than reduction of Compound I.⁵²⁻⁵⁵

Table 2: Apparent second-order rate constants for the reactions of myeloperoxidase (MPO), lactoperoxidase (LPO), eosinophil peroxidase (EPO), truncated peroxidasin 1 (HsPxd1 con4) and horseradish peroxidase (HRP) at pH 7.0 in their ferric, Compound I and Compound II state. Cpd I, Compound I; Cpd II, Compound II; ferri, ferric resting state; n.d., not determined.

Reaction/Substrate	MPO	LPO	EPO	HsPxd1 con4	HRP
	$\times 10^4 \text{ (M}^{-1} \text{s}^{-1}\text{)}$				
Ferri \rightarrow Cpd I H ₂ O ₂	(47) 1400	(49) 1100	(51) 4300	(12) 1800	(56) 1700
Cpd I \rightarrow ferri chloride bromide iodide thiocyanate	(48) 2.5 110 720 960	(49) - 4.1 12000 20000	(51) 0.31 1900 9300 10000	(12) - 560 1680 1830	(56) - - 130 -
Cpd I \rightarrow Cpd II tyrosine	(55) 77	(40) 11	(54) 35	n.d.	(53) 5
Cpd II \rightarrow ferri tyrosine	1.57	1	2.7	n.d.	0.1

Physiological relevance

It has been shown that (pseudo-) halides act as physiological substrates for various investigated vertebrate peroxidases. The resulting reaction products - (pseudo-) hypohalous acids - can act as strong oxidizers in innate host defense or have important roles in biosynthetic pathways.⁵

The vertebrate peroxidases MPO, LPO and EPO have crucial functions in the innate immune system. Myeloperoxidase is located in granules of neutrophils which are released upon phagocytosis of a pathogen. The hydrogen peroxide is derived from dismutated superoxide generated by NADPH oxidase. Subsequently, MPO oxidizes chloride into the anti-bacterial, highly reactive hypochlorous acid.⁵⁷ Lactoperoxidase is found in various human exocrine secretions such as tears, milk or saliva, where it contributes to the defense against invading microorganisms.⁵⁸ Eosinophil peroxidase is secreted by eosinophil cells and plays a role in defense against parasites.⁵⁹

In contrast, TPO is involved in hormone biosynthesis, where it catalyzes the iodination of tyrosine residues, resulting in the formation of the hormones triiodothyronine and thyroxine in the thyroid gland.⁶⁰ The recently discovered and investigated peroxidasin 1 contributes to the

formation of the extracellular matrix by formation of a sulfilimine link between the sulfur of a distinct methionine and the nitrogen of a hydroxylysine in collagen IV. This reaction is dependent on bromide, which is oxidized to hypobromous acid by peroxidase and subsequently mediates the formation of the sulfilimine bond.^{8,12}

Representatives of Family 6

In many cases, members of the peroxidase-cyclooxygenase superfamily are multidomain proteins with one heme binding domain with a mainly α -helical fold. Usually, Family 6 proteins are composed of a transmembrane domain, a sequence motif characteristic for planctomycete extracellular proteins, two dockerin type I repeats and a peroxidase domain. Most probably, the multidomain structure of these metalloenzymes has evolved from gene transfers between different species or endosymbiotic events.¹ In this work, two representatives of Family 6 are investigated, which are – in contrast to other enzymes of this Family – composed of only a peroxidase domain.

The first part of this work deals with the heme peroxidase LspPOX from the cyanobacterium *Lyngbya* sp. PCC 8106 (LspPOX). This oxidoreductase has been investigated previously, revealing that the active site is completely conserved compared to LPO, including the covalently bound, modified heme. This posttranslational modification leads to a substantial halogenation activity concerning the oxidation of bromide. Further it has been shown that the formation of the covalent linkages is an autocatalytic process that can be triggered by the incubation with hydrogen peroxide. The formation of the linkages drastically increases the halogenation activity as well as the stability of LspPOX.^{17,18}

In the second part of this thesis, the heme peroxidase from the social amoeba *Dictyostelium discoideum* (DdPoxA) is studied. This second representative of Family 6 family attracted our attention since *D. discoideum* is a professional phagocyte, showing striking parallels to MPO-secreting neutrophils in the mammalian immune defense. Further, sequence alignments revealed that DdPoxA shows high sequence similarity to the vertebrate heme peroxidases, but - in contrast to LspPOX and the Family 1 members - it shows only one acidic amino acid (Glu236) that could possibly form a covalent ester bond to the heme group.² The similarity on a cellular basis combined with the finding that both cell types express a closely related peroxidase makes DdPoxA an interesting research target for elucidating the cellular evolution of phagocytosis.

References

1. Zamocky, M., Jakopitsch, C., Furtmüller, P. G., Dunand, C., and Obinger, C. (2008) The peroxidase-cyclooxygenase superfamily. Reconstructed evolution of critical enzymes of the innate immune system. *Proteins* **71**, 589-605.
2. Zamocky, M., Hofbauer, S., Schaffner, I., Gasselhuber, B., Nicolussi, A., Soudi, M., Pirker, K.F., Furtmüller, P.G., and Obinger, C. (2015) Independent evolution of four heme peroxidase superfamilies. *Arch Biochem Biophys* **574**, 108-19.
3. Lin, Y. W. (2015) The broad diversity of heme-protein crosslinks: an overview. *Biochim Biophys Acta* **1854**, 844-59.
4. Klebanoff, S. J. (2005) Myeloperoxidase: friend and foe. *J Leuco Biol* **77**, 598-625.
5. Davies, M. J., Hawkins, C. L., Pattison, D. I., and Rees, M. D. (2008) Mammalian heme peroxidases: From molecular mechanisms to health implications. *Antioxid Redox Signal* **10**, 1199-1234.
6. Ruf, J., and Carayon, P. (2006) Structural and functional aspects of thyroid peroxidase. *Arch Biochem Biophys* **445**, 269-277.
7. Nelson, R. E., Fessler, L. I., Takagi, Y., Blumberg, B., Keene, D., R., Olson, P. F., Parker, C. G., and Fessler, J. H. (1994) Peroxidasin: a novel enzyme-matrix protein of *Drosophila* development. *EMBO J* **13**, 3438-3447.
8. Bhave, G., Cummings, C. F., Vanacore, R. M., Kumagai-Cresse, C., Ero-Tolliver, I. A., Rafi, M., Kang, J. S., Pedchenko, V., Fessler, L. I., Fessler, J. H., and Hudson, B. G. (2012) Peroxidasin forms sulfilimine chemical bonds using hypohalous acids in tissue genesis. *Nat Chem Biol* **8**, 784-790.
9. McCall, A. S., Cummings, C. F., Bhave, G., Vanacore, R., Page-McCaw, A., and Hudson, B. G. (2014) Bromine is an essential trace element for assembly of collagen IV scaffolds in tissue development and architecture. *Cell* **157**, 1380-1392.
10. Peterfi, Z., and Geiszt, M. (2014) Peroxidases: novel players in tissue genesis. *Trends Biochem Sci* **39**, 305-7.
11. Soudi, M., Paumann-Page, M., Delporte, C., Pirker, K.F., Bellei, M., Edenhofer, E., Stadlmayr, G., Battistuzzi, G., Boudjeltia, K.Z., Furtmüller, P.G., Van Antwerpen, P., and Obinger, C. (2015) Multidomain human peroxidasin 1 is a highly glycosylated and stable homotrimeric high spin ferric peroxidase. *J Biol Chem* **290**, 10876-90.
12. Paumann-Page, M., Katz, R.-S., Bellei, M., Schwartz, I., Edenhofer, E., Sevcnikar, B., Soudi, M., Hofbauer, S., Battistuzzi, G., Furtmüller, P.G., and Obinger, C. (2017) Pre-steady-state kinetics reveal the substrate specificity and mechanism of halide oxidation of truncated human peroxidase 1. *J Biol Chem* **292**, 4583-4592.
13. Vizzini, A., Parrinello, D., Sanfratello, M. A., Mangano, V., Parrinello, N., and Cammarata, M. (2013) Ciona intestinalis peroxinectin is a novel component of the peroxidase-cyclooxygenase gene superfamily upregulated by LPS. *Dev Comp Immunol* **41**, 59-67.
14. De Deken, X., Corvilain, B., Dumont, J. E., and Miot F. (2014) Roles of DUOX-mediated hydrogen peroxide in metabolism, host defense, and signalling. *Antioxid Redox Signal* **20**, 2776-2793.
15. Zederbauer, M., Furtmüller, P. G., Brogioni, S., Jakopitsch, C., Smulevich, G., and Obinger, C. (2007) Heme to protein linkages in mammalian peroxidases: impact on spectroscopic, redox and catalytic properties. *Nat Prod Rep* **24**, 571-584.
16. Fayadat, L., Niccoli-Sire, P., Lanet, J., and Franc, J.-L. (1999) Role of heme in intracellular trafficking of thyroperoxidase and involvement of H₂O₂ generated at the apical surface of thyroid cells in autocatalytic covalent heme binding. *J Biol Chem* **274**, 10533-10538.

17. Auer, M., Gruber, C., Bellei, M., Pirker, K. F., Zamocky, M., Kroiss, D., Teufer, A. S., Hofbauer, S., Soudi, M., Battistuzzi, G., Furtmüller, P. G., and Obinger, C. (2013) A stable bacterial peroxidase with novel halogenating activity and an autocatalytically linked heme prosthetic group. *J Biol Chem* **288**, 27181–27199.
18. Auer, M., Nicolussi, A., Schütz, G., Furtmüller, P. G., and Obinger, C. (2014) How covalent heme to protein bonds influence the formation and reactivity of redox intermediates of a bacterial peroxidase. *J Biol Chem* **289**, 31480–31491.
19. Nauseef, W. M. (2014) Myeloperoxidase in human neutrophil host defence. *Cell Microbiol* **16**, 1146-1155.
20. Ihalin, R., Loimaranta, V., and Tenovuo, J. (2006) Origin, structure and biological activities of peroxidases in human saliva. *Arch Biochem Biophys* **445**, 261-268.
21. Malik, A., and Batra, J.K. (2012) Antimicrobial activity of human eosinophil granule proteins: involvement in host defence against pathogens. *Crit Rev Microbiol* **38**, 168-181.
22. Zederbauer, M., Furtmüller, P. G., Ganster, B., Moguilevsky, N., and Obinger, C. (2007) The vinyl-sulfonium bond in human myeloperoxidase: Impact on compound I formation and reduction by halides and thiocyanate. *Biochem Biophys Res Commun* **356**, 450-456.
23. Battistuzzi, G., Stampfer, J., Bellei, M., Vlasits, J., Soudi, M., Furtmüller, P. G., and Obinger, C. (2011) Influence of the covalent heme-protein bonds on the redox thermodynamics of human myeloperoxidase. *Biochemistry* **50**, 7987-7994.
24. Singh, A. K., Singh, N., Sharma, S., Singh, S. B., Kaur, P., Bhushan, A., Srinivasan, A., and Singh, T. P. (2008) Crystal structure of lactoperoxidase at 2.4 Å resolution. *J Mol Biol*, **376**, 1060-1075.
25. Carpena, X., Vidossich, P., Schroettner, K., Calisto, B. M., Banerjee, S., Stampfer, J., Soudi, M., Furtmüller, P. G., Rovira, C., Fita, I., and Obinger, C. (2009) Essential role of proximal histidine-asparagine interaction in mammalian peroxidases, *J Biol Chem* **284**, 25929-37.
26. Furtmüller, P. G., Zederbauer, M., Jantschko, W., Helm, J., Bogner, M., Jakopitsch, C., and Obinger, C. (2006) Active site structure and catalytic mechanisms of human peroxidases, *Arch Biochem Biophys* **445**, 199-213.
27. Battistuzzi, G., Bellei, M., Bortolotti, C. A., and Sola, M. (2010) Redox properties of heme peroxidases. *Arch Biochem Biophys* **500**, 21-36.
28. Colas, C., and Ortiz de Montellano, P. R. (2003) Autocatalytic radical reactions in physiological prosthetic heme modification. *Chem Rev* **103**, 2305-2332.
29. Ortiz de Montellano, P. R. (2016) Heme peroxidases: selfprocessing of peroxidases (Raven, E. and Dunford, B., Eds) RSC Metallobiology Series No. 4, pp 3-30, The Royal Society of Chemistry, Cambridge, U.K.
30. Fiedler, T. J., Davey, C. A., and Fenna, R. E. (2000) X-ray crystal structure and characterization of halide-binding sites of human myeloperoxidase at 1.8 Å resolution. *J Biol Chem* **275**, 11964-11971.
31. Brogioni, S., Stampfer, J., Furtmüller, P. G., Feis, A., Obinger, C., and Smulevich, G. (2008) The role of the sulfonium linkage in the stabilization of the ferrous form of myeloperoxidase: A comparison with lactoperoxidase. *Biochim Biophys Acta* **1784**, 843-849.
32. DePillis, G., Ozaki, S., Kuo, J.M., Maltby, D.A., and Ortiz de Montellano, P.R. (1997) Autocatalytic processing of heme by lactoperoxidase produces the native protein-bound prosthetic group. *J Biol Chem* **272**, 8857-8860.
33. Kooter, I. M., Koehler, B. P., Moguilevsky, N., Bollen, A., Wever, R., and Johnson, M. K. (1999) The Met243 sulfonium ion linkage is responsible for the anomalous magnetic circular dichroism and optical spectral properties of myeloperoxidase. *J Biol Inorg Chem* **4**, 684-691.

34. Zederbauer, M., Jantschko, W., Neugschwandtner, K., Jakopitsch, C., Moquilevsky, N., Obinger, C., and Furtmüller, P. G. (2005) Role of the covalent glutamic acid 242-heme linkage in the formation and reactivity of redox intermediates of human myeloperoxidase. *Biochemistry* **44**, 6482-6491.
35. Battistuzzi, G., Borsari, M., Ranieri, A., and Sola, M. (2002) Redox thermodynamics of the Fe(3+)/Fe(2+) couple in horseradish peroxidase and its cyanide complex. *J Am Chem Soc* **124**, 26-27.
36. Battistuzzi, G., Bellei, M., Vlasits, J., Banerjee, S., Furtmüller, P. G., Sola, M., and Obinger, C. (2010) Redox thermodynamics of lactoperoxidase and eosinophil peroxidase. *Arch Biochem Biophys* **494**, 72-77.
37. Battistuzzi, G., Bellei, M., Zederbauer, M., Furtmüller, P. G., Sola, M., and Obinger, C. (2006) Redox thermodynamics of the Fe(III)/Fe(II) couple of human myeloperoxidase in its high-spin and low-spin forms. *Biochemistry* **45**, 12750-12755.
38. Furtmüller, P. G., Arnhold, J., Jantschko, W., Pichler, H., and Obinger, C. (2003) Redox properties of the couples compound I/compound II and compound II/native enzyme of human myeloperoxidase. *Biochem. Biophys Res Commun* **301**, 551-557.
39. Furtmüller, P. G., Arnhold, J., Jantschko, W., Zederbauer, M., Jakopitsch, C., and Obinger, C. (2005) Standard reduction potentials of all couples of the peroxidase cycle of lactoperoxidase. *J Inorg Biochem* **99**, 1220-1229.
40. Jantschko, W., Furtmüller, P. G., Allegra, M., Livrea, M. A., Jakopitsch, C., Regelsberger, G., and Obinger, C., (2002) Redox intermediates of plant and mammalian peroxidases: a comparative transient-kinetic study of their reactivity toward indole derivatives. *Arch Biochem Biophys* **398**, 12-22.
41. Jantschko, W., Furtmüller, P. G., Zederbauer, M., Neugschwandtner, K., Lehner, I., Jakopitsch, C., Arnhold, J., and Obinger, C. (2005) Exploitation of the unusual thermodynamic properties of human myeloperoxidase in inhibitor design. *Biochem Pharmacol* **69**, 1149-1157.
42. Arnhold, J., Furtmüller, P. G., Regelsberger, G., and Obinger, C. (2001) Redox properties of the couple compound I/native enzyme of myeloperoxidase and eosinophil peroxidase. *Eur J Biochem* **268**, 5142-5148.
43. Furtmüller, P. G., Arnhold, J., Jantschko, W., Zederbauer, M., Jakopitsch, C., and Obinger, C. (2005) Standard reduction potentials of all couples of the peroxidase cycle of lactoperoxidase. *J Inorg Biochem* **99**, 1220-1229.
44. Farhangrazi, Z. S., Fossett, M. E., Powers, L. S., Ellis, W. R. Jr. (1995) Variable-temperature spectroelectrochemical study of horseradish peroxidase. *Biochemistry* **34**, 2866-2871.
45. Furtmüller, P. G., Arnhold, J., Jantschko, W., Pichler, H., and Obinger, C. (2003) Redox properties of the couples compound I/compound II and compound II/native enzyme of human myeloperoxidase. *Biochem Biophys Res Commun* **301**, 551-557.
46. Dunford, H. B. (1999) Heme Peroxidases. WILEY-VCH, New York.
47. Marquez, L. A., Huang, J. T., and Dunford, H. B. (1994) Spectral and kinetic studies on the formation of myeloperoxidase compounds I and II: roles of hydrogen peroxide and superoxide. *Biochemistry* **33**, 1447-1454.
48. Furtmüller, P. G., Burner, U., and Obinger, C. (1998) Reaction of myeloperoxidase compound I with chloride, bromide, iodide, and thiocyanate. *Biochemistry* **37**, 17923-17930.
49. Furtmüller, P. G., Jantschko, W., Regelsberger, G., Jakopitsch, C., Arnhold, J., and Obinger, C. (2002) Reaction of lactoperoxidase compound I with halides and thiocyanate. *Biochemistry* **41**, 11895-11900.
50. Arnhold, J., Monzani, E., Furtmüller, P. G., Zederbauer, M., Casella, L., and Obinger, C. (2006) Kinetics and thermodynamics of halide and nitrite oxidation by mammalian heme peroxidases. *Eur J Inorg Chem* **19**, 3801-3811.

51. Furtmüller, P. G., Burner, U., Regelsberger, G., and Obinger, C. (2000) Spectral and kinetic studies on the formation of eosinophil peroxidase compound I and its reaction with halides and thiocyanate. *Biochemistry* **39**, 15578-15584.
52. Banerjee, S., Furtmüller, P. G., and Obinger, C. (2011) Bovine lactoperoxidase - a versatile one- and two-electron catalyst of high structural and thermal stability. *Biotechnol J* **6**, 231-243.
53. Ralston, I., Dunford, H. B. (1978) Horseradish peroxidase. XXXII. pH dependence of the oxidation of L-(-)-tyrosine by compound I. *Can J Biochem* **56**, 1115-1119.
54. Furtmüller, P. G., Jantschko, W., Regelsberger, G., and Obinger, C. (2001) Spectral and kinetic studies on eosinophil peroxidase compounds I and II and their reaction with ascorbate and tyrosine. *Biochim Biophys Acta* **1548**, 121-128.
55. Marquez, L. A., and Dunford, H. B. (1995) Kinetics of oxidation of tyrosine and dityrosine by myeloperoxidase compounds I and II. Implications for lipoprotein peroxidation studies. *J Biol Chem* **270**, 30434-30440.
56. Adak, S., Mazumdar, A., and Banerjee, R. K. (1996) Low catalytic turnover of horseradish peroxidase in thiocyanate oxidation. *J Biol Chem* **272**, 11049-11056.
57. Pattison, D. I., Davies, M. J., and Hawkins, C. L. (2012) Reactions and reactivity of myeloperoxidase-derived oxidants: differential biological effects of hypochlorous and hypothiocyanous acids. *Free Radic Res* **46**, 975-995.
58. Ihalin, R., Loimaranta, V., and Tenovuo, J. (2006) Origin, structure, and biological activities of peroxidases in human saliva. *Arch Biochem Biophys* **445**, 261-268.
59. Abu-Ghazaleh, R. I., Dunnette, S. L., Loegering, D. A., Checkel, J. L., Kita, H., Thomas, L. L., and Gleich, G. J. (1992) Eosinophil granule proteins in peripheral blood granulocytes. *J Leukoc Biol* **52**, 611-618.
60. Taurog, A. (1999) Molecular evolution of thyroid peroxidase. *Biochimie* **81**, 557-562.

Aims of the thesis

Recent phylogenetic analysis of the peroxidase-cyclooxygenase superfamily revealed the presence of prokaryotic and early eukaryotic heme peroxidases with homology to the mammalian counterparts. The aim of this thesis is to characterize a bacterial and a eukaryotic model heme peroxidase from Family 6 of the peroxidase-cyclooxygenase superfamily. Comprehensive biochemical and biophysical studies will provide the basis for (i) elucidation of structure-function relationships and (ii) comparison with the well investigated mammalian counterparts.

In detail this work focuses on heme peroxidases from the cyanobacterium *Lyngbya* sp. PCC 8106 (LspPOX) and from the social amoeba *Dictyostelium discoideum* (DdPoxA). In order to gain a better understanding of the underlying structure-function relationships of these two oxidoreductases, the project plan includes the following methods and experiments:

- ❖ Development of expression platforms and purification protocols for both peroxidases, yielding in sufficient amounts of functional recombinant proteins with high heme occupancy
- ❖ Design, expression and characterization of LspPOX mutants with disrupted ester bonds by exchanging of the respective aspartic and glutamic acids
- ❖ Investigation of the posttranslational heme to protein ester linkages of both enzymes including UV-vis, electronic circular dichroism and electron paramagnetic resonance spectroscopy, spectroelectrochemistry, mass spectrometry, differential scanning calorimetry and multi-angle light scattering
- ❖ Multimixing stopped-flow spectroscopy in order to investigate spectral properties and kinetics of interconversion of the redox intermediates ferric state, Compound I and Compound II as well as of low-spin complexes. Elucidation of apparent bimolecular rate constants of Compound I reduction by chloride, bromide, iodide and thiocyanate
- ❖ Comparison of biochemical and biophysical differences and similarities between LspPOX, DdPoxA and the mammalian counterparts myeloperoxidase (MPO), lactoperoxidase (LPO), eosinophil peroxidase (EPO) and peroxidasin 1 (HsPxd1)

- ❖ Solving the X-ray crystal structure of both LspPOX and DdPoxA in collaboration with the group of Prof. Djinovic-Carugo (MFPL, University of Vienna)
- ❖ Investigation of the *in vivo* role and putative substrates of DdPoxA by performing experiments in *D. discoideum* cell culture in collaboration with the group of Prof. Thierry Soldati (University of Geneva, Switzerland)

PUBLICATIONS

How Covalent Heme to Protein Bonds Influence the Formation and Reactivity of Redox Intermediates of a Bacterial Peroxidase

Auer, M., *Nicolussi, A.*, Schütz, G., Furtmüller, P. G., and Obinger, C.

Research article

Journal of Biological Chemistry (2014) **289**, 31480-31491.

doi: 10.1074/jbc.M114.595157

How Covalent Heme to Protein Bonds Influence the Formation and Reactivity of Redox Intermediates of a Bacterial Peroxidase*

Received for publication, July 13, 2014, and in revised form, September 22, 2014. Published, JBC Papers in Press, September 22, 2014, DOI 10.1074/jbc.M114.595157

Markus Auer, Andrea Nicolussi, Georg Schütz, Paul G. Furtmüller¹, and Christian Obinger²

From the Department of Chemistry, Division of Biochemistry, Vienna Institute of BioTechnology, University of Natural Resources and Life Sciences, Muthgasse 18, A-1190 Vienna, Austria

Background: The impact of autocatalytically formed covalent heme to protein bonds on formation and reactivity of redox intermediates of a peroxidase was analyzed.

Results: Posttranslational modification significantly changes the reactivity of the ferric protein and of compounds I and II.

Conclusion: Upon covalent attachment, the capacity of compound I to oxidize one- and two-electron donors is enhanced.

Significance: First direct evidence about the relation between H₂O₂-triggered covalent heme to protein bond formation and enzyme reactivity.

The most striking feature of mammalian peroxidases, including myeloperoxidase and lactoperoxidase (LPO) is the existence of covalent bonds between the prosthetic group and the protein, which has a strong impact on their (electronic) structure and biophysical and chemical properties. Recently, a novel bacterial heme peroxidase with high structural and functional similarities to LPO was described. Being released from *Escherichia coli*, it contains mainly heme *b*, which can be autocatalytically modified and covalently bound to the protein by incubation with hydrogen peroxide. In the present study, we investigated the reactivity of these two forms in their ferric, compound I and compound II state in a multi-mixing stopped-flow study. Upon heme modification, the reactions between the ferric proteins with cyanide or H₂O₂ were accelerated. Moreover, apparent bimolecular rate constants of the reaction of compound I with iodide, thiocyanate, bromide, and tyrosine increased significantly and became similar to LPO. Kinetic data are discussed and compared with known structure-function relationships of the mammalian peroxidases LPO and myeloperoxidase.

The most striking feature of the mammalian peroxidases myeloperoxidase (MPO),³ eosinophil peroxidase (EPO), lactoperoxidase (LPO), and thyroid peroxidase is the existence of two covalent ester bonds between the prosthetic group and the protein in the functional, mature enzyme (1). Myeloperoxidase is unique in having an additional vinyl-sulfonium bond (see Fig. 1) (1, 2). These posttranslational modifications (PTMs) cause a distortion of the porphyrin ring from planarity, which is more

pronounced in MPO (3–5) than in LPO (6). In MPO, the heme ring features a bow-shaped structure with less symmetry and a considerable out-of-plane location of the high-spin iron ion (3–5). Formation of these covalent heme to protein bonds has been proposed to occur autocatalytically (7–9) and has a deep impact on the biochemical and biophysical properties of these mammalian peroxidases (2, 10, 11). This includes significant modulation of the redox chemistry of these proteins, which provides the thermodynamic basis for the effective two-electron oxidation of halides, including bromide and chloride (11). The resulting reaction products, *i.e.* hypohalous acids, contribute to the antimicrobial role of MPO, EPO, and LPO in the innate immune system.

Analysis of the peroxidase-cyclooxygenase superfamily (12) suggested the occurrence of enzymatic domains with structural similarity to the vertebrate peroxidases (*i.e.* subfamily 1 including MPO, LPO, EPO, and thyroid peroxidase) in five of seven subfamilies. Interestingly, two new prokaryotic heme peroxidase subfamilies were found (12). Recently, the first bacterial representative of this subfamily was successfully produced in *E. coli* and biochemically characterized (13). The recombinant peroxidase from the cyanobacterium *Lyngbya* sp. PCC 8106 (LspPOX) was shown to have high similarities to mammalian LPO (see Fig. 1), including heme to protein linkages, redox and spectral properties as well as halogenation activity (13).

It was reported that the recombinant protein purified from *E. coli* was a mixture of two species with ~80% containing heme *b* (see Fig. 1B) and ~20% having the prosthetic group covalently bound to the protein via two ester linkages similar to LPO (Fig. 1D) (13). Most interestingly, this ratio shifted significantly when the recombinant protein was incubated with hydrogen peroxide. In this case, the majority (>70%) of the protein molecules showed covalently bound hemes. This strongly suggests autocatalytic formation of these covalent bonds triggered by hydrogen peroxide and resembles characteristics of mammalian peroxidases that also show intrinsic inhomogeneity regarding the heme to protein bonds. For example, the x-ray structure of human MPO purified from leukocytes clearly shows the side

* This work was supported by Austrian Science Fund Projects P20664 and P25270 and the Doctoral Program BioToP-Biomolecular Technology of Proteins (FWF W1224).

¹ To whom correspondence may be addressed: Tel.: 43-1-47654-6077; Fax: 43-1-47654-6059; E-mail: paul.furtmueller@boku.ac.at.

² To whom correspondence may be addressed: Tel.: 43-1-47654-6073; Fax: 43-1-47654-6059; E-mail: christian.obinger@boku.ac.at.

³ The abbreviations used are: MPO, myeloperoxidase; LspPOX, peroxidase from *Lyngbya* sp. PCC 8106; LspPOX (H₂O₂), peroxidase from *Lyngbya* sp. PCC 8106 incubated with hydrogen peroxide; LPO, lactoperoxidase; EPO, eosinophil peroxidase; X⁻, halide; PTM, posttranslational modification.

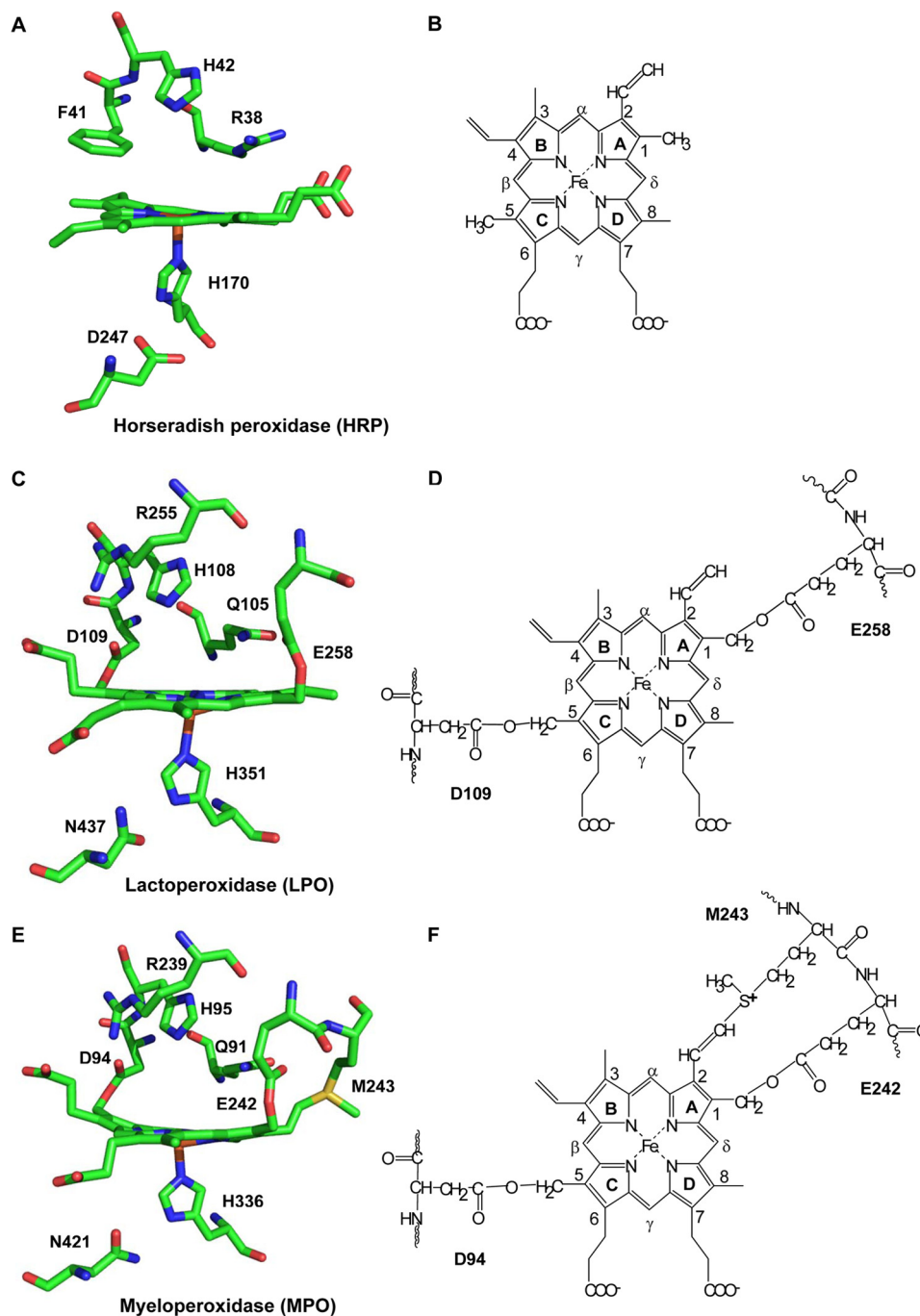


FIGURE 1. **Structures of active sites and prosthetic groups of HRP, LPO, and MPO.** The structure of active site of HRP (A) and (unmodified) heme *b* (B) is shown. The structure of the active site of bovine LPO (C) and its modified prosthetic group (ester linkages between Asp-109 and the carbon of the 5-methyl group of pyrrole ring C as well as between Glu-258 and the carbon of the methyl group of pyrrole ring A) (D) are shown. Shown are active site structure of human MPO (E) and its modified prosthetic group (two ester linkages similar to that in LPO and an additional sulfonium ion linkage between the sulfur atom of Met-243 and the β -carbon of the vinyl group of pyrrole ring A) (F). Figures were constructed using the coordinates deposited in the Protein Data Bank codes: 1ATJ (HRP), 2GJ1 (LPO), and 3F9P (MPO). Please note that covalent heme to protein bonds in LspPOX (H_2O_2) correspond to that in LPO (D).

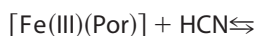
chain of Glu-242 (which is responsible for an ester bond linkage) in two distinct conformations (5). Moreover, both native and recombinantly produced LPO (7, 8) and EPO (9) contain heme *b*, which can be modified and covalently linked by external addition of 10–15 times molar excess of H_2O_2 .

A closer analysis of the effect of this posttranslational modification (PTM) in LPO, EPO, and MPO was so far hampered by the fact that the proteins could only be produced recombinantly in small amounts (or even failed in production) either in

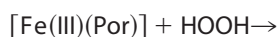
insect cell lines or animal cell factories. Moreover, the produced proteins often showed unsatisfactory heme occupancy. Now, for the first time, the cyanobacterial protein (LspPOX) with high similarity to LPO enables to directly monitor the impact of this PTM on the formation and reactivity of redox intermediates of a heme enzyme by a comprehensive multi-mixing stopped-flow study. LspPOX can easily and in relatively high amounts be produced in *E. coli* and has almost 100% heme occupancy (13). Moreover, upon incubation with hydrogen

Catalytic Role of the Heme to Protein Linkages

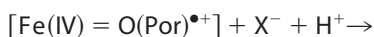
peroxide, it is posttranslationally modified (LspPOX (H₂O₂)) and forms heme to protein linkages to an extent that is similar to native mammalian peroxidases (13). This prompted us to investigate all relevant individual reaction steps of the halogenation and peroxidase cycle. For both ferric LspPOX and LspPOX (H₂O₂), we analyzed cyanide binding (Reaction 1) as well as the reaction with hydrogen peroxide forming compound I (*i.e.* oxoiron(IV) porphyrin π -cation radical) (Reaction 2). We investigated compound I reduction by the two-electron donors (X⁻) bromide, iodide, and thiocyanate to the corresponding (hypo)halous acids (Reaction 3) as well as all reactions involved in the peroxidase cycle, including compound I (Reaction 4) and compound II (*i.e.* oxoiron(IV)) reduction by one-electron donors (AH₂), thereby releasing radical species (\bullet AH) (Reaction 5). Furthermore, we monitored whether compound I reacts with H₂O₂ (Reaction 6), which is observed with MPO (14, 15). We report the kinetics of Reactions 1–6 of both LspPOX and LspPOX (H₂O₂) and demonstrate the significant impact of this PTM on the individual reaction steps. The reported apparent bimolecular rate constants are compared with those known from the mammalian counterparts and discussed with respect to the known structures of MPO (3–5) and LPO (6).



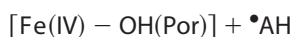
REACTION 1



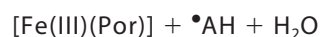
REACTION 2



REACTION 3



REACTION 4



REACTION 5



REACTION 6

EXPERIMENTAL PROCEDURES

Materials—Cloning, expression and purification of LspPOX were described in detail previously (13). LspPOX had a purity index (A_{412}/A_{280}) of ~ 0.7 . The ferric high-spin LspPOX and LspPOX pretreated with 15 times molar excess of hydrogen peroxide, *i.e.* LspPOX (H₂O₂), had a molar extinction coefficient at Soret maximum of $\epsilon_{412 \text{ nm}} = 94,670 \text{ M}^{-1} \text{ cm}^{-1}$ (13).

Hydrogen peroxide obtained as 30% solution was purchased from Sigma-Aldrich. Hydrogen peroxide was diluted with H₂O, and its concentration was determined at 240 nm using the extinction coefficient $39.4 \text{ M}^{-1} \text{ cm}^{-1}$ (16). H₂O₂ stock solutions were prepared freshly before the experiments. Cyanide, bromide, tyrosine, and all other chemicals were also purchased from Sigma-Aldrich at the highest grade available.

Stopped-flow Spectroscopy—Reactions of LspPOX or LspPOX (H₂O₂) with cyanide or H₂O₂ were measured in the conventional stopped-flow mode by following the decrease of absorbance at 412 nm (Soret maximum of ferric LspPOX) or 413 nm (Soret maximum of LspPOX (H₂O₂)) or at 431/432 nm (Soret bands of cyanide complex of LspPOX and LspPOX (H₂O₂)). In a typical experiment, one syringe contained 4 μM LspPOX or LspPOX (H₂O₂), and the second syringe contained at least 10 times molar excess of cyanide or hydrogen peroxide. All reactions were performed in 100 mM phosphate buffer, pH 7.0, at 25 °C. Three determinations were performed for each ligand or oxidant concentration. The mean of the pseudo-first-order rate constants, k_{obs} , was used in the calculation of the second-order rate constants obtained from the slope of a plot of k_{obs} versus ligand or oxidant concentration.

Because of the inherent instability of compound I of LspPOX and LspPOX (H₂O₂), the sequential stopped-flow (multi-mixing) technique was used for determination of rates of the reaction of compound I with one- and two-electron donors. Similar to bovine LPO, LspPOX (H₂O₂) compound I could be formed with equimolar concentrations of H₂O₂, whereas full compound I of LspPOX could only be generated with 6.7 times molar excess of H₂O₂. In a typical experiment, 4 μM of LspPOX (H₂O₂) or LspPOX were premixed with 4 μM or 26.8 μM H₂O₂ in the aging loop. After 100 ms, the formed compound I was mixed with increasing concentrations of various electron donors. Direct compound I reduction to the ferric state by halides was followed by monitoring of the absorbance change at 412 nm for LspPOX and at 413 nm for LspPOX (H₂O₂). Formation and reduction of compound II by tyrosine was investigated by following the biphasic reaction (at 432 nm) of compound I to compound II and further to the ferric state for both LspPOX and LspPOX (H₂O₂). All measurements were done in 100 mM phosphate buffer, pH 7.0, at 25 °C with a minimum of three repeats.

All spectral experiments were carried out with the stopped-flow apparatus SX.18MV and Pi-star-180 from Applied Photophysics in either conventional or sequential mode. The optical quartz cell with a path length of 10 mm had a volume of 20 μl . The fastest time for mixing two solutions and recording the first data point was 1 ms. All reactions were followed both at single wavelengths as well as by using a diode array detector. Polychromatic data were analyzed with Pro-Kineticist software from Applied Photophysics. The program simultaneously fits the kinetic traces at all wavelengths to the proposed reaction mechanism and simulates the spectra of all reactants, products, and intermediate species as well as their time-dependent distribution on the reaction coordinates. Monochromatic data were analyzed and fitted with Pro-Data Viewer software (Applied Photophysics) to calculate time-dependent rate constants.

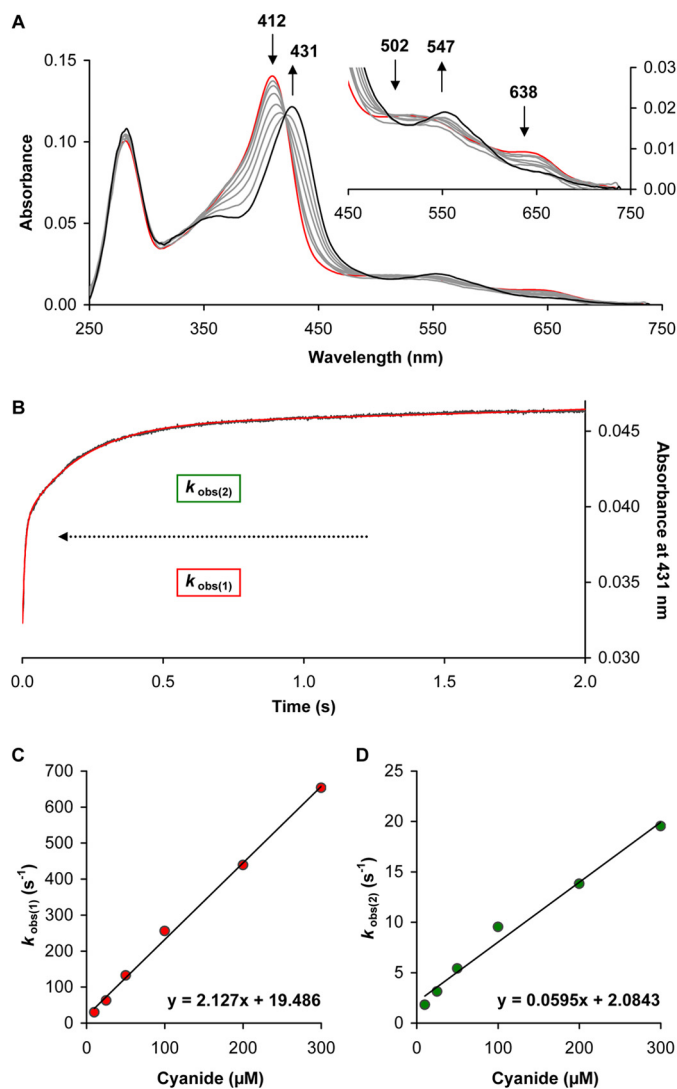


FIGURE 2. Reaction of ferric LspPOX with cyanide. *A*, spectral transition of the reaction of 2 μM LspPOX with 100 μM cyanide or 10 mM cyanide (final concentrations) measured in the conventional mixing stopped-flow mode. The first spectrum shows the ferric protein in its high-spin state (red). The second spectrum was recorded 1 ms after mixing with 100 μM cyanide, and subsequent spectra were measured at 3 ms, 6 ms, 80 ms, and 2 s. The last two spectra were recorded after mixing with 10 mM cyanide at 4 ms and 100 ms, showing the complete formation of the low-spin cyanide complex (black). Arrows indicate changes of absorbance with time. Final conditions were as follows: 100 mM phosphate buffer, pH 7, 25 °C. *B*, typical time trace at 431 nm and double-exponential fit (1 μM LspPOX and 50 μM cyanide). *C* and *D*, Dependence of $k_{obs(1)}$ (red) and $k_{obs(2)}$ values (green) from cyanide concentration. Final enzyme concentration was 1 μM LspPOX in 100 mM phosphate buffer, pH 7, 25 °C.

RESULTS

Cyanide Binding—Fig. 2*A* shows the spectral changes upon addition of 100 μM or 10 mM cyanide to 2 μM recombinant peroxidase from the cyanobacterium *Lyngbya* sp. PCC 8106 (LspPOX). Following Reaction 1, the ferric protein purified from *E. coli* was converted from the high-spin ($S = 5/2$) iron state to the low-spin ($S = 1/2$) state, thereby shifting the Soret peak from 412 nm to 431 nm with a clear isosbestic point at 421 nm. Concomitantly, in the visible range a new peak at 547 nm appeared. As depicted in Fig. 2*B*, the time traces were markedly biphasic with a rapid first phase and a dominating slower second phase. The corresponding pseudo-first-order rate con-

stants, $k_{obs(1)}$ and $k_{obs(2)}$, could be obtained from double-exponential fits. From the corresponding plots of k_{obs} versus cyanide concentration ($k_{obs} = k_{on} [CN^-] + k_{off}$) (Fig. 2, *C* and *D*), apparent second-order rate constants of $(2.13 \pm 0.06) \times 10^6 M^{-1} s^{-1}$ ($K_D = k_{off}/k_{on} = 9.2 \mu M$) and $(6.0 \pm 0.37) \times 10^4 M^{-1} s^{-1}$ ($K_D = 35 \mu M$) could be obtained (25 °C).

Interestingly, when LspPOX was incubated with 15 times stoichiometric excess of hydrogen peroxide for 1 h at room temperature (in the following designated as LspPOX (H_2O_2)), the kinetics of cyanide binding changed. Ferric LspPOX (H_2O_2) exhibits a Soret maximum at 413 nm and two additional peaks at 502 nm and 638 nm. Recently, spectral differences between LspPOX and LspPOX (H_2O_2) could be assigned by mass spectrometry to differences in the extent of heme to protein linkages, ranging from only 20% in the recombinant protein purified from *E. coli* to >70% in LspPOX (H_2O_2). Cyanide binding in the latter (low-spin complex with maxima at 432 nm and 547 nm and an isosbestic point at 423 nm) was also biphasic but now with a dominating fast phase (being responsible for ~85% of the absorbance change at 432 nm) followed by a second slower phase. The corresponding pseudo-first-order rate constants, $k_{obs(1)}$ and $k_{obs(2)}$, could be obtained from double-exponential fits and allowed the calculation of the apparent second-order rate constants to be $(2.06 \pm 0.02) \times 10^6 M^{-1} s^{-1}$ ($K_D = 7.9 \mu M$) (Fig. 3*C*) and $(4.6 \pm 0.26) \times 10^4 M^{-1} s^{-1}$ ($K_D = 22.1 \mu M$) (Fig. 3*D*), respectively, at pH 7.0 and 25 °C (Table 1).

In both, LspPOX and LspPOX (H_2O_2), cyanide binding was biphasic with a fast reaction followed a slower one. Both proteins exhibited almost identical rate constants for these two phases, suggesting that the slow reaction reflects cyanide binding to the heme *b* protein, whereas the fast reaction reflects cyanide binding to the protein modified by PTM. This is underlined by the fact that in LspPOX, the slower binding phase dominated, whereas in LspPOX (H_2O_2), the fast reaction was responsible for the large part of absorbance change. Moreover, the apparent bimolecular rate constant as well as the dissociation constant of the fast cyanide binding phase in the bacterial peroxidase are comparable with those of MPO ($1.3 \times 10^6 M^{-1} s^{-1}$, $K_D = 4.3 \mu M$) (17) and LPO ($1.3 \times 10^6 M^{-1} s^{-1}$, $K_D = 23.8 \mu M$) (18) at pH 7.0 and 25 °C.

Compound I Formation—Based on these significant differences in cyanide binding between LspPOX and LspPOX (H_2O_2), we further investigated the redox reactions between the respective high-spin ferric proteins and hydrogen peroxide (Reaction 2). With LspPOX, 6.7 times molar excess of H_2O_2 was necessary to obtain maximum hypochromicity at the Soret maximum (412 nm). An additional prominent peak of LspPOX compound I was observed at 663 nm (*black spectrum* in *bold-face* in Fig. 4*A*). Similar to cyanide binding, the kinetics of compound I formation showed a pronounced biphasicity with a rapid single exponential phase ($k_{obs(1)}$) responsible for ~15% absorbance change at 412 nm followed by a slower single exponential phase ($k_{obs(2)}$) responsible for ~85% absorbance change at the Soret maximum.

Compound I of LspPOX (H_2O_2) was characterized by a 45% decrease of absorbance at the Soret band (Fig. 5*A*). Already equimolar H_2O_2 was sufficient to reach the full hypochromicity at the Soret maximum (413 nm), very similar to EPO (20) and

Catalytic Role of the Heme to Protein Linkages

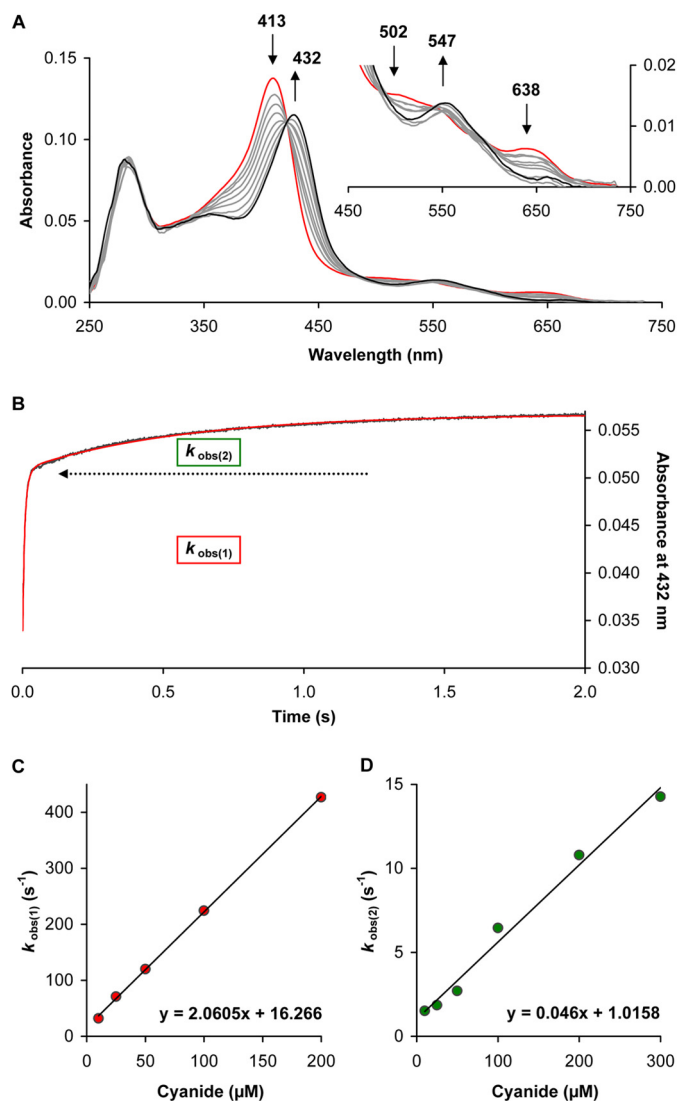


FIGURE 3. Reaction of ferric LspPOX (H₂O₂) with cyanide. *A*, spectral transition of the reaction of 2 μM LspPOX (H₂O₂) with 100 μM cyanide or 10 mM cyanide (final concentrations) measured in the conventional mixing stopped-flow mode. The first spectrum shows the ferric protein in its high-spin state (red). The second spectrum was recorded 1 ms after mixing with 100 μM cyanide, and subsequent spectra were measured at 3 ms, 6 ms, 80 ms, and 2 s. The last three spectra were recorded after mixing with 10 mM cyanide at 4 ms, 15 ms, and 100 ms showing the complete formation of the low-spin cyanide complex (black). Arrows indicate changes of absorbance with time. Final conditions were as follows: 100 mM phosphate buffer, pH 7, 25 °C. *B*, typical time trace at 432 nm and double-exponential fit (1 μM LspPOX (H₂O₂) and 50 μM cyanide). *C* and *D*, dependence of $k_{\text{obs}(1)}$ (red) and $k_{\text{obs}(2)}$ values (green) from cyanide concentration. The association rate constant was calculated from the slope, the dissociation rate constant from the intercept. Final enzyme concentration was 1 μM LspPOX (H₂O₂) in 100 mM phosphate buffer, pH 7, 25 °C.

LPO (21). Upon compound I formation, absorbance at 502 and 638 nm was lost, and a new peak at 663 nm appeared (black spectrum in Fig. 5A). Compound I formation of LspPOX (H₂O₂) was still biphasic but now showed a dominating rapid exponential decrease at 413 nm ($k_{\text{obs}(1)}$, responsible for $\sim 85\%$ absorbance change), followed by a slower decrease ($k_{\text{obs}(2)}$) at the Soret maximum (Fig. 5B).

Upon calculation of the apparent bimolecular rate constant of the initial rapid phase (*i.e.* $k_{\text{obs}(1)}$ values) of compound I formation (Figs. 4E and 5E), similar apparent bimolecular rate constants could be obtained for both metalloproteins, namely

TABLE 1

Apparent second-order rate constants for the reactions of LspPOX and LspPOX (H₂O₂) in their ferric, compound I and compound II state

In biphasic reactions, the amplitude of each phase is given in parentheses. Data are presented in comparison with MPO and LPO. For details, see "Experimental Procedures." C-I, compound I; C-II, compound II; nat. enzyme, ferric resting state.

$E^{\circ'}$ Fe(II)/Fe(III) (mV)	LspPOX	LspPOX (H ₂ O ₂)	MPO	LPO
	-184 (13)	-145 (13)	+5 (11)	-176 (25)
Reaction/Substrate	$\times 10^4$ (M ⁻¹ s ⁻¹)			
nat. enzyme \leftrightarrow complex			(17)	(18)
cyanide				
$k_{\text{obs}(1)}$	213 (15%)	206 (85%)	130	130
$k_{\text{obs}(2)}$	6.0 (85%)	4.6 (15%)		
nat. enzyme \rightarrow C-I			(14, 15)	(21, 24)
H ₂ O ₂				
$k_{\text{obs}(1)}$	5200 (15%)	4400 (85%)	1400	1100
$k_{\text{obs}(2)}$	168 (85%)	157 (15%)		
C-I \rightarrow nat. enzyme			(22)	(21)
chloride				
	no reaction	no reaction	2.5	no reaction
bromide				
	4.1	18	110	4.1
iodide				
	53	4200	720	12000
thiocyanate				
	5.3	2000	960	20000
C-I \rightarrow C-II				
H ₂ O ₂				
	no reaction	no reaction	4.4 (14, 15)	no reaction
tyrosine				
	32	62	77 (23)	11 (24)
C-II \rightarrow nat. enzyme				
tyrosine				
	5.5	11	1.57 (23)	1 (24)

(5.2 ± 0.24) $\times 10^7$ M⁻¹ s⁻¹ for LspPOX and (4.4 ± 0.15) $\times 10^7$ M⁻¹ s⁻¹ for LspPOX (H₂O₂). Moreover, the apparent second-order rate constants calculated from the $k_{\text{obs}(2)}$ values (Figs. 4F and 5F) were almost identical, *i.e.* (1.7 ± 0.07) $\times 10^6$ M⁻¹ s⁻¹ and (1.6 ± 0.17) $\times 10^6$ M⁻¹ s⁻¹, respectively. Together with the correlation between absorbance changes and k_{obs} values of the fast and slower phase in the respective proteins (see above), these data nicely reflect that (i) in LspPOX (H₂O₂) compound I formation is ~ 30 times faster compared with LspPOX and that (ii) $\sim 85\%$ of LspPOX (H₂O₂) contains covalently bound heme, which reflects the mass spectrometric findings reported recently (13). The bimolecular rate constant of LspPOX (H₂O₂) is faster compared with MPO (14, 15) and LPO (21) (Table 1).

Besides the discrepancy in the apparent bimolecular rate constants between the heme *b* protein and the posttranslationally modified peroxidase, the corresponding plots also showed differences in *y* axis intercepts (compare Figs. 4E and 5E with Figs. 4F and 5F), which might reflect differences in (i) H₂O₂ binding (*e.g.* faster dissociation from the initial complex between the protein and the peroxide in the modified peroxidase) and/or in (ii) reactivity and stability of the resulting compound I. As will be shown below, compound I of LspPOX(H₂O₂) is a stronger oxidant of bromide compared with that of LspPOX. The increased reactivity is also reflected by a more positive reduction potential of the Fe(III)/Fe(II) couple of LspPOX (H₂O₂) (13).

With both proteins, compound I was not stable. In case of LspPOX (H₂O₂), compound I decayed (Fig. 5C) directly to an intermediate with spectral features very similar to those of an

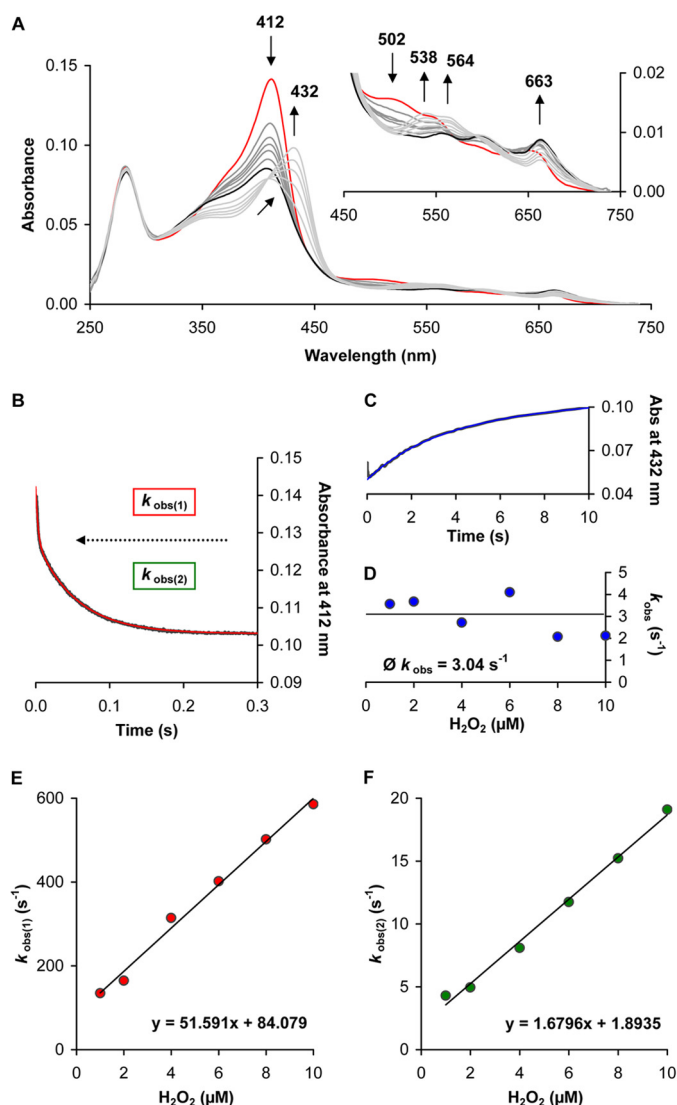


FIGURE 4. Reaction of ferric LspPOX with hydrogen peroxide. *A*, spectral transition upon mixing of 2 μM ferric LspPOX with 13.4 μM hydrogen peroxide (6.7 times excess of H_2O_2). The *red spectrum* indicates the ferric enzyme at the beginning of the reaction. The first spectrum was measured 5 ms after mixing, and subsequent spectra were measured at 15 ms, 26 ms, 38 ms, 58 ms, 100 ms (*i.e.* compound I formation, *black spectra*) and 1.1 s, 2.5 s, 4.3 s, 6.2 s, and 10 s (decay of compound I, *gray spectra*). *Arrows* show the direction of absorbance changes with time. Final conditions were as follows: 100 mM phosphate buffer, pH 7, 25 °C. The *inset* to *A* depicts the spectral transition in the visible range. The spectrum of compound I is highlighted in *black* (100 ms after mixing). *Arrows* indicate absorbance changes with time. Shown is a typical time trace with double-exponential fit (*red*) of the reaction of ferric LspPOX with 6.7 times excess of H_2O_2 followed at 412 nm for the first 300 ms (*B*) and typical time trace with single-exponential fit (*blue*) of the decay of compound I followed at 432 nm for 10 s (*C*). Conditions were as described in *A*. *D*, pseudo-first-order rate constants k_{obs} (*blue*) of the decay of compound I plotted against hydrogen peroxide concentration. *E* and *F*, pseudo-first-order rate constants $k_{\text{obs}(1)}$ (*red*) and $k_{\text{obs}(2)}$ (*green*) of the biphasic compound I formation (monitored at 412 nm) plotted against hydrogen peroxide concentration. Final enzyme concentration was 2 μM in 100 mM phosphate buffer, pH 7, 25 °C.

oxoiron(IV) species (Fig. 5*A*, *light gray spectra*) with maxima at 432, 538, and 564 nm (rate of decay of $\sim 3 \text{ s}^{-1}$). After adding a 6.7 times molar excess of H_2O_2 to LspPOX, it took at least 100 ms to reach full hypochromicity at the Soret absorbance, but the resulting compound I also decayed (Fig. 4*C*) to an intermediate with spectral features identical to those of LspPOX

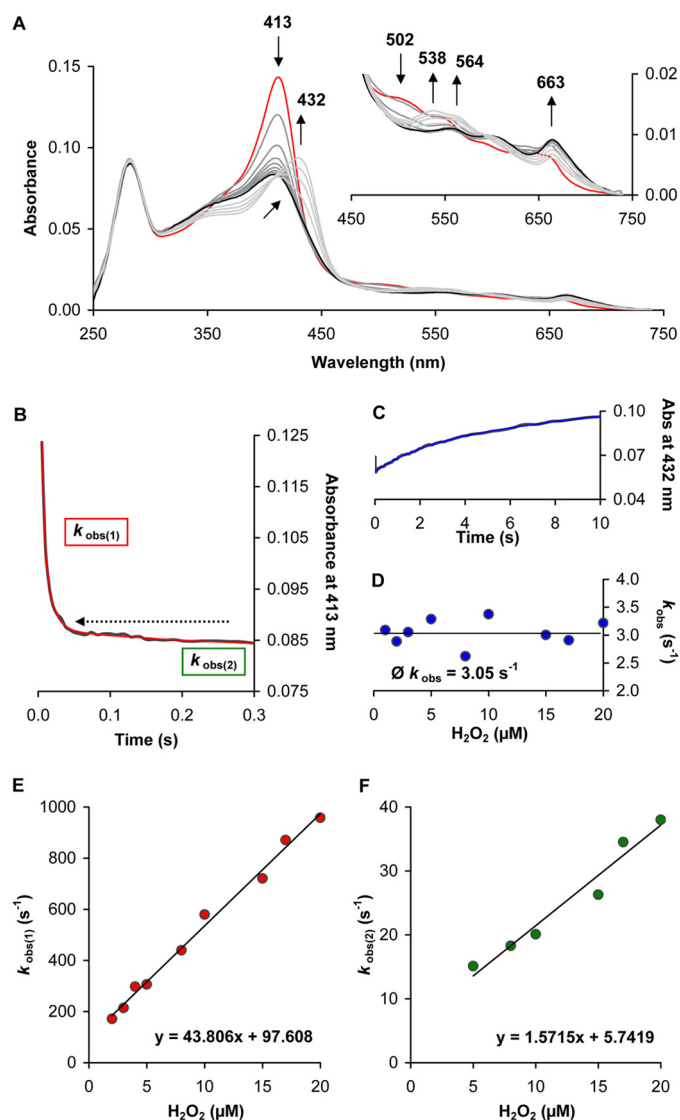


FIGURE 5. Reaction of ferric LspPOX (H_2O_2) with hydrogen peroxide. *A*, spectral transition upon mixing of 2 μM ferric LspPOX (H_2O_2) with 2 μM hydrogen peroxide. The *red spectrum* indicates the ferric enzyme. The first spectrum was measured 5 ms after mixing, and subsequent spectra were measured at 10 ms, 15 ms, 20 ms, 26 ms, 38 ms, 58 ms, 140 ms (*i.e.* compound I formation, *black spectra*) and 1.72 s, 3.9 s, 6.5 s, and 10 s (*i.e.* compound I decay, *gray spectra*). *Arrows* show the direction of absorbance changes with time. Final conditions were 100 mM phosphate buffer, pH 7, 25 °C. The *inset* to *A* shows the spectral transition in the visible range. The spectrum of compound I is highlighted in *black* (140 ms after mixing). *Arrows* indicate absorbance changes with time. Shown is a typical time trace with double-exponential fit (*red*) of the reaction of ferric LspPOX (H_2O_2) with equimolar H_2O_2 followed at 413 nm for the first 300 ms (*B*) and typical time trace with single-exponential fit (*blue*) of the decay of compound I followed at 432 nm for 10 s (*C*). Conditions were as described in *A*. *D*, pseudo-first-order rate constants k_{obs} (*blue*) of the decay of compound I plotted against hydrogen peroxide concentration. *E* and *F*, pseudo-first-order rate constants $k_{\text{obs}(1)}$ (*red*) and $k_{\text{obs}(2)}$ (*green*) of the biphasic compound I formation (monitored at 413 nm) plotted against hydrogen peroxide concentration. Final enzyme concentration was 2 μM in 100 mM phosphate buffer, pH 7, 25 °C.

(H_2O_2) (Fig. 4*A*, *gray spectra*). In both cases, formation of this species with compound II-like spectral properties did not depend on the concentration of hydrogen peroxide (Figs. 4*D* and 5*D*). Formation of an oxoiron(IV) protein radical species in the absence of exogenous electron donors has also been demonstrated with LPO and EPO (19). Only in MPO, compound I can be reduced with hydrogen peroxide to compound II with a

Catalytic Role of the Heme to Protein Linkages

bimolecular rate-constant of $4.4 \times 10^4 \text{ M}^{-1} \text{ s}^{-1}$ according to Reaction 6 (Table 1) (14, 15). Oxidation of H_2O_2 to superoxide by compound I is typical for myeloperoxidase (14, 15), but neither LspPOX (H_2O_2) nor EPO (20) or LPO (21) can catalyze this reaction.

Reaction of Compound I with Two-electron Donors—Next, we studied the effect of the posttranslational modification on the reactivity of compound I with halides and thiocyanate according to Reaction 3. In detail, we premixed LspPOX with 6.7 times excess H_2O_2 and LspPOX (H_2O_2) with equimolar H_2O_2 in the aging loop for 100 ms to get a maximum of compound I. For both species, this guaranteed a minimum decay of compound I. With chloride (up to 100 mM) as electron donor, no reaction occurred, and compound I of both proteins decayed to the oxoiron(IV) species described above.

Upon mixing compound I of LspPOX with bromide, formation of this compound II-like species was suppressed to some extent and the absorbance at the Soret maximum (412 nm) increased, indicating the occurrence of a direct transition of compound I back to ferric LspPOX (Fig. 6A). The higher the bromide concentration, the more negligible was the decay of compound I to the oxoiron(IV) species (shoulder at 432 nm). Fig. 6B depicts typical time traces at 412 and 432 nm for the reaction with $50 \mu\text{M}$ bromide. The observed initial steady-state phase is consistent with the presence of excess of hydrogen peroxide that had to be used for compound I formation of LspPOX. Ferric enzyme produced by reaction of compound I with bromide was immediately reoxidized by excess of H_2O_2 to compound I, which could react again with bromide or decay to the oxoiron(IV) species. The higher the bromide concentration, the faster H_2O_2 was consumed and the shorter was this initial steady-state phase. The increase of absorbance at 412 nm (after this initial phase) could be fitted with a double-exponential function (Fig. 6B). The slope of the plot of pseudo-first-order rate constant, $k_{\text{obs}(1)}$, against bromide concentration gave an apparent bimolecular rate constant of $(4.1 \pm 0.3) \times 10^4 \text{ M}^{-1} \text{ s}^{-1}$ at pH 7.0 and 25°C (Fig. 6C). With iodide and thiocyanate, similar time traces were observed, and apparent bimolecular rate constants could be calculated to be $(5.3 \pm 0.32) \times 10^5 \text{ M}^{-1} \text{ s}^{-1}$ (iodide) and $(5.3 \pm 0.57) \times 10^4 \text{ M}^{-1} \text{ s}^{-1}$ (thiocyanate), respectively (Fig. 6, D and E). The y intercepts of the plots ($2.0\text{--}4.4 \text{ s}^{-1}$) might reflect the instability and decay of compound I as described above.

By contrast, with LspPOX (H_2O_2) an almost direct transition of compound I (built with equimolar H_2O_2) to ferric LspPOX (H_2O_2) was observed (Fig. 7A). Typical time traces at 413 nm still showed a double-exponential character (Fig. 7B) with the first fast phase of the reaction being strongly dependent on the halide concentration (Fig. 7C), whereas the second slower part being independent of the halide concentration and reflecting the formation of the oxoiron(IV) species. In Fig. 7C, the apparent second-order rate constant was calculated from the slope of the linear plot of pseudo-first-order rate constant, $k_{\text{obs}(1)}$, against bromide concentration to be $(1.8 \pm 0.05) \times 10^5 \text{ M}^{-1} \text{ s}^{-1}$, which is about four times faster compared with LspPOX and LPO (21) but slower compared with MPO (22) (Table 1). With iodide and thiocyanate similar spectral transitions were obtained. The impact of the instability of compound I was significantly smaller due to the higher reactivity with both

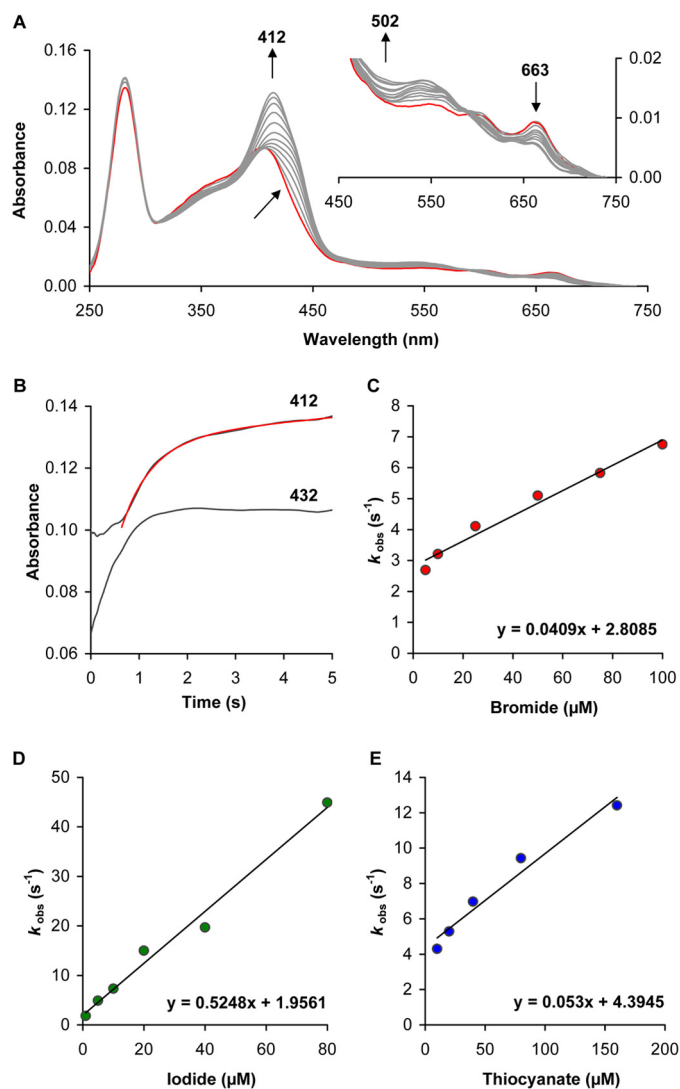


FIGURE 6. Reaction of LspPOX compound I with (pseudo-)halides. A, spectral transition after addition of $50 \mu\text{M}$ bromide to LspPOX compound I ($2 \mu\text{M}$) in the sequential mixing stopped-flow mode. Compound I was performed with 6.7 times excess of H_2O_2 (red) as described under "Experimental Procedures." After a 100-ms delay, the first spectrum was recorded at 2 ms, and subsequent spectra were recorded at 101 ms, 251 ms, 406 ms, 551 ms, 707 ms, 860 ms, 1.04 s, 1.4 s, 2.03 s, 3.1 s, and 5 s. The reaction was carried out in 100 mM phosphate buffer, pH 7.0, 25°C , with a 100-ms delay time. B, typical time traces at 412 nm and 432 nm as well as a double-exponential fit (red) of the reaction of LspPOX compound I with $50 \mu\text{M}$ bromide followed at 412 nm. Conditions were as described in A. C, pseudo-first-order rate constants k_{obs} (red) plotted against bromide concentration. Final conditions were 100 mM phosphate buffer, pH 7.0, 25°C , $1 \mu\text{M}$ LspPOX and $6.7 \mu\text{M}$ H_2O_2 , with a 100-ms delay time. D, pseudo-first-order rate constants k_{obs} (green) plotted against iodide concentration. Final conditions were 100 mM phosphate buffer, pH 7.0, 25°C , $1 \mu\text{M}$ LspPOX, and $6.7 \mu\text{M}$ H_2O_2 , with a 100-ms delay time. E, pseudo-first-order rate constants k_{obs} (blue) plotted against thiocyanate concentration. Final conditions were 100 mM phosphate buffer, pH 7.0, 25°C , $1 \mu\text{M}$ LspPOX and $6.7 \mu\text{M}$ H_2O_2 , with a 100-ms delay time.

iodide and thiocyanate (Fig. 7, D and E). Inspection of the corresponding plots reveals a higher intercept compared with those for LspPOX, which could reflect differences in iodide or thiocyanate binding to compound I in these two species. In any case, the reactions between iodide or thiocyanate and compound I of LspPOX (H_2O_2) were extremely fast, *i.e.* $(4.2 \pm 0.27) \times 10^7 \text{ M}^{-1} \text{ s}^{-1}$ (iodide) and $(2.0 \pm 0.07) \times 10^7 \text{ M}^{-1} \text{ s}^{-1}$ (thiocyanate). The big differences in reaction rates between

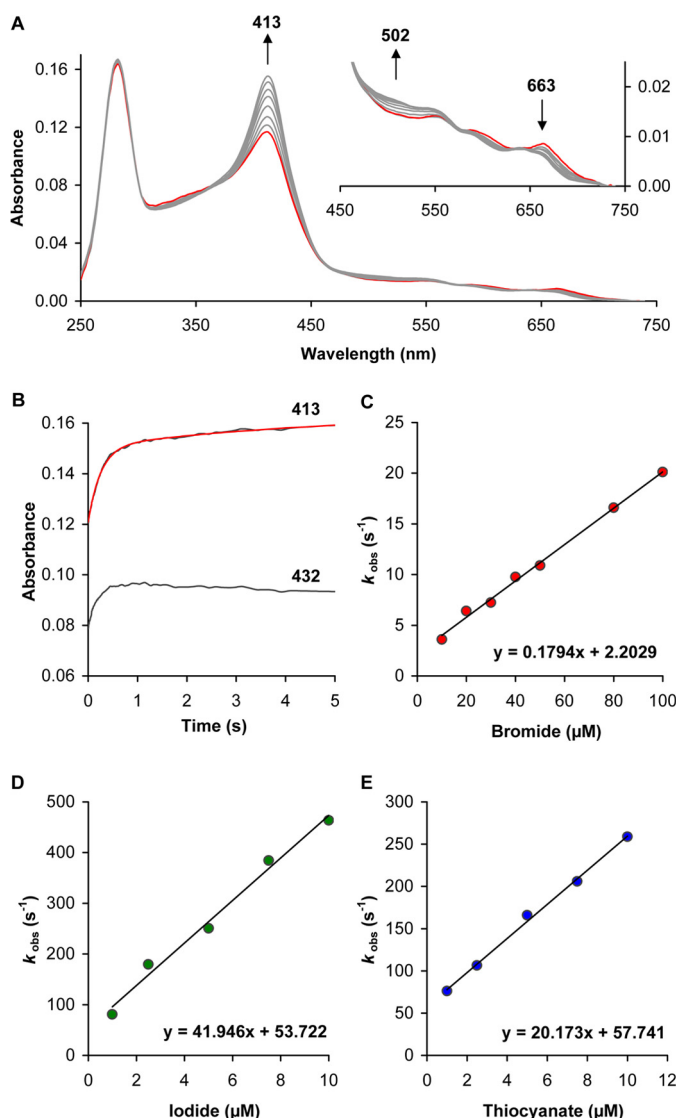


FIGURE 7. Reaction of LspPOX (H_2O_2) compound I with (pseudo-)halides. A, spectral transition after addition of $10 \mu\text{M}$ bromide to LspPOX (H_2O_2) compound I ($2 \mu\text{M}$) in the sequential mixing stopped-flow mode. Compound I was preformed with equimolar H_2O_2 as described under "Experimental Procedures." After a 100-ms delay, the first spectrum was recorded at 2 ms, and subsequent spectra were recorded at 37 ms, 123 ms, 212 ms, 347 ms, 609 ms, 1.77 s, and 5 s. The reaction was carried out in 100 mM phosphate buffer, pH 7.0, 25 °C, with a 100-ms delay time. B, typical biphasic time trace and double-exponential fit (red) of the reaction of LspPOX (H_2O_2) compound I with $10 \mu\text{M}$ bromide followed at 413 nm. Conditions were as described in A. C, pseudo-first-order rate constants k_{obs} (red) plotted against bromide concentration. Final conditions were 100 mM phosphate buffer, pH 7.0, 25 °C, $1 \mu\text{M}$ LspPOX (H_2O_2), $1 \mu\text{M}$ H_2O_2 , with a 100-ms delay time. D, pseudo-first-order rate constants k_{obs} (green) plotted against iodide concentration. Final conditions were 100 mM phosphate buffer, pH 7.0, 25 °C, $0.6 \mu\text{M}$ LspPOX (H_2O_2), $1 \mu\text{M}$ H_2O_2 , with a 100-ms delay time. E, pseudo-first-order rate constants k_{obs} (blue) plotted against thiocyanate concentration. Final conditions were 100 mM phosphate buffer, pH 7.0, 25 °C, $0.6 \mu\text{M}$ LspPOX (H_2O_2), $1 \mu\text{M}$ H_2O_2 , with a 100-ms delay time.

LspPOX and LspPOX (H_2O_2) are obvious, *i.e.* 80 times (iodide) or 345 times (thiocyanate) higher rates in LspPOX (H_2O_2) (Table 1). Iodide and thiocyanate oxidation by LspPOX (H_2O_2) is faster than with MPO compound I (22) but slower compared with the LPO intermediate (21).

Reactions between Compound I and Compound II and Tyrosine—Finally, we analyzed compound I (Reaction 4) and compound II reduction (Reaction 5) of both proteins by tyro-

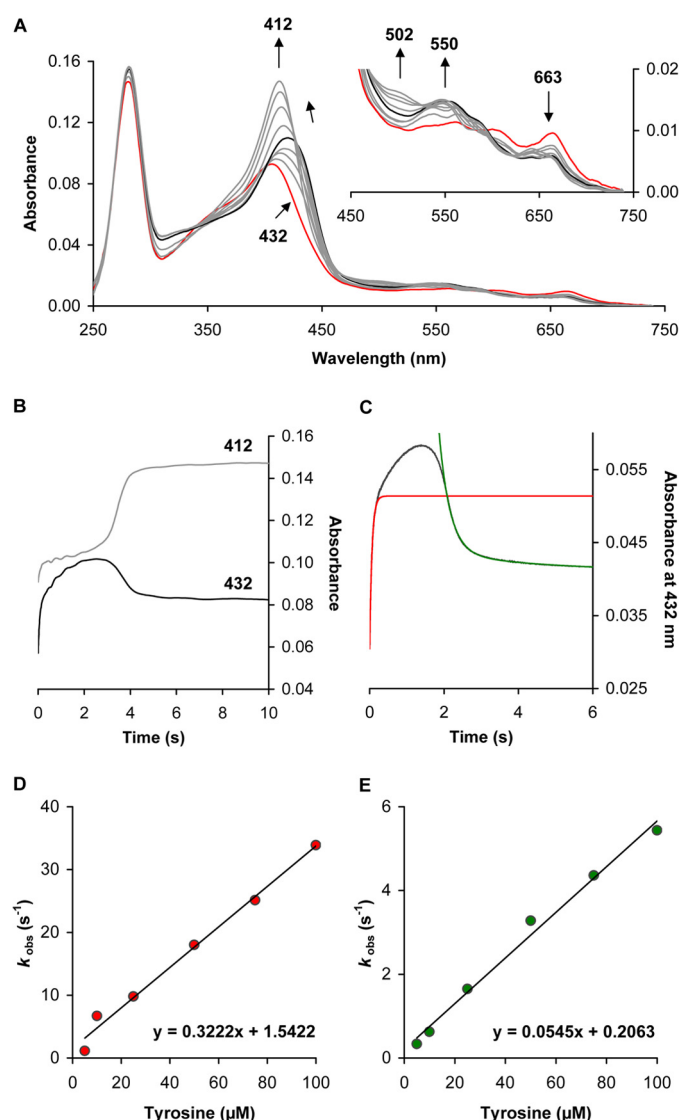


FIGURE 8. Reduction of LspPOX compound I and compound II by tyrosine. A, spectral changes upon addition of $50 \mu\text{M}$ tyrosine to $2 \mu\text{M}$ compound I in the sequential mixing stopped-flow mode. Compound I was formed with ferric LspPOX and 6.7 times excess of H_2O_2 (red). After a 100-ms delay, the first spectrum was recorded at 5 ms, and subsequent spectra were recorded at 100 ms, 298 ms, 900 ms, 2.4 s (compound II-like, black labeled) and 3.2 s, 3.5 s, 3.9 s, and 10 s. The inset to Fig. 8A shows the spectral transition in the visible range. Final reaction conditions were 100 mM phosphate buffer, pH 7.0, 25 °C, with a delay time of 100 ms. B, typical time traces at 432 nm, the maximum absorbance of compound II and 412 nm, the maximum absorbance of ferric LspPOX. Conditions were as described in A. C, multiphasic time trace at 432 nm with both single-exponential fits, (i) the initial phase of compound II formation (red) and (ii) the last phase of compound II reduction (green). Final conditions were 100 mM phosphate buffer, pH 7.0, 25 °C, $1 \mu\text{M}$ LspPOX and $6.7 \mu\text{M}$ H_2O_2 , 100-ms delay time, $50 \mu\text{M}$ tyrosine. D and E, pseudo-first-order rate constants for LspPOX compound I reduction (red) at 432 nm (D) and (in green) at 432 nm) compound II reduction (E) both plotted against tyrosine concentrations. Conditions were as described in C.

sine. Upon addition of tyrosine to LspPOX compound I (Fig. 8A, red line), compound II (black line) was formed, and after a distinct steady-state phase (caused by excess of hydrogen peroxide in the system), compound II was converted to the ferric protein. The length of this steady-state phase depended on the tyrosine concentration. The corresponding time traces at 412 and 432 nm (*i.e.* Soret maximum of compound II) are shown in Fig. 8B. From the time traces at 432 nm, pseudo-first-order rate

Catalytic Role of the Heme to Protein Linkages

constants of compound II formation and reduction were obtained by fitting the respected phases by single-exponential equations (Fig. 8C). Apparent second-order rate constants were calculated from the corresponding linear plots (Fig. 8, D and E) to be $(3.2 \pm 0.17) \times 10^5 \text{ M}^{-1} \text{ s}^{-1}$ (compound I reduction) and $(5.5 \pm 0.27) \times 10^4 \text{ M}^{-1} \text{ s}^{-1}$ (compound II reduction) (Table 1).

Upon addition of tyrosine to LspPOX (H_2O_2) compound I (red line), sequential formation of compound II (black line) and its reduction was observed (Fig. 9A). Transition of compound I to compound II showed a defined isosbestic point at 413 nm, whereas the transition of compound II to ferric LspPOX (H_2O_2) exhibited an isosbestic point at 425 nm. Fig. 9B shows a typical biphasic time trace observed at 432 nm, which was obtained when LspPOX (H_2O_2) compound I was mixed with the one-electron donor tyrosine. After initial formation of compound II (Soret maximum at 432 nm), the reaction continues and ferric LspPOX (H_2O_2) was formed (decrease at 432 nm and increase at 413 nm). Both parts of the time trace could be fitted with a single-exponential function (Fig. 9C), and the apparent second-order rate constants were determined to be $(6.2 \pm 0.15) \times 10^5 \text{ M}^{-1} \text{ s}^{-1}$ for compound I reduction and $(1.1 \pm 0.07) \times 10^5 \text{ M}^{-1} \text{ s}^{-1}$ for compound II reduction (Fig. 9, D and E). Both rate constants are similar or even higher than those reported for MPO (23) or LPO (Table 1) (24).

DISCUSSION

Heme proteins conduct a myriad of different biological functions, including oxygen transport, storage and reduction, electron transfer, and redox catalysis. Thus, it is challenging to investigate and understand the role of (posttranslational) modifications of the prosthetic group and/or of its protein environment in fine-tuning of biophysical and biochemical features of these oxidoreductases. In the majority of heme peroxidase families unmodified heme *b* (e.g. in horseradish peroxidase (HRP) (Fig. 1A)) is found at the active site (Fig. 1B). So far, prominent exceptions included vertebrate (including human) peroxidases that constitute the cornerstone of the innate immune system. These halogenating enzymes (e.g. LPO, EPO, and MPO) have modified 1- and 5-methyl groups on pyrrole rings A and C of the heme group, allowing formation of ester linkages with the carboxyl groups of conserved glutamate and aspartate residues (1, 2, 6). Myeloperoxidase is unique in having a third covalent bond, which connects the β -carbon of the vinyl group on pyrrole ring A with the sulfur atom of methionine 243, giving rise to a sulfonium ion linkage (Fig. 1, E and F) (3–5).

Recently, we demonstrated for the first time the occurrence of bacterial peroxidases that are highly homologous to LPO in many respects (13). The prosthetic group of the protein from *Lyngbya* sp. is covalently bound via ester bonds between a conserved aspartate (Asp-100) and/or a glutamate residue (Glu-229) similar to LPO (Fig. 1, C and D) (13). It was interesting to see that the recombinant protein produced by *E. coli* contained mainly unmodified heme *b*. An external addition of 15 times molar excess of H_2O_2 to the recombinant peroxidase was sufficient to promote the posttranslational modification. It is reasonable to assume that the native protein synthesized by *Lyngbya* sp. PCC 8106 corresponds to LspPOX (H_2O_2). The cyanobacterium *Lyngbya* sp. accommodates an oxygenic

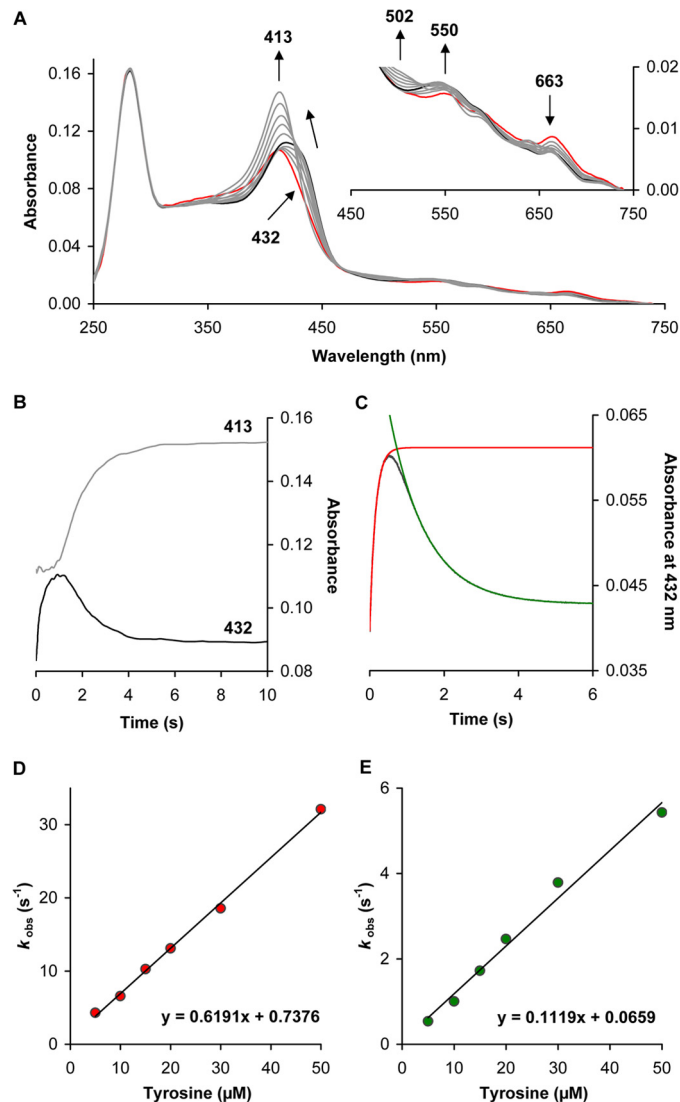


FIGURE 9. Reduction of LspPOX (H_2O_2) compound I and compound II by tyrosine. A, spectral changes upon addition of $10 \mu\text{M}$ tyrosine to $2 \mu\text{M}$ compound I in the sequential mixing stopped-flow mode. Compound I was formed with ferric LspPOX (H_2O_2) and equimolar H_2O_2 (red). With a delay time of 100 ms, the first spectrum was recorded at 5 ms, and subsequent spectra were recorded at 100 ms, 216 ms, 450 ms, 900 ms (compound II-like, black labeled) and 1.3 s, 1.6 s, 1.9 s, 2.7 s, and 10 s. The inset to Fig. 9A shows the spectral transition in the visible range. Final reaction conditions were 100 mM phosphate buffer, pH 7.0, 25 °C, with a delay time of 100 ms. B, typical time traces at 432 nm, the maximum absorbance of compound II and 413 nm, the maximum absorbance of ferric LspPOX (H_2O_2). Conditions were as described in A. C, biphasic time trace at 432 nm with both single-exponential fits, (i) for the initial phase of compound II formation (red) and (ii) the second phase of compound II reduction (green). Final conditions were 100 mM phosphate buffer, pH 7.0, 25 °C, $1 \mu\text{M}$ LspPOX (H_2O_2), and equimolar H_2O_2 , 100-ms delay time, $10 \mu\text{M}$ tyrosine. D and E, pseudo-first-order rate constants for LspPOX (H_2O_2) compound I reduction (red) at 432 nm (D) and (in green at 432 nm) compound II reduction (E) both plotted against tyrosine concentrations. Conditions were as described in C.

photosynthetic together with a respiratory electron transport chain within a single prokaryotic (non-compartmentalized) cell, thereby performing oxygen activation and generation of hydrogen peroxide at high rates.

Most likely via H_2O_2 -mediated oxidation and compound I formation, the nearby located carboxyl side chains of Asp-100 and Glu-229 were oxidatively attacked, finally leading to ester bond formation as described for its mammalian counterparts

(7–9). Thereby, most likely the symmetry of the heme group as well as its planarity were lowered as was evident by distinct changes of the UV-visible electronic absorption, circular dichroism, and electronic paramagnetic resonance spectra as described recently (13). It was interesting to see that during this autocatalytic process the spectral properties of the ferric and ferrous forms of the bacterial peroxidase became very similar to LPO. Moreover, the standard reduction potential (E°) of the Fe(III)/Fe(II) couple (-145 mV) became similar to that of LPO (-176 mV) (25) and EPO (-126 mV) (25). This result compares with reported E° values of -190 mV and -306 mV for the heme *b* proteins cytochrome *c* peroxidase and horseradish peroxidase (26). It reflects the impact of heme to protein ester bonds on heme distortion by promoting the out of plane displacement of the heme iron in mammalian peroxidases (6, 25, 26) and most probably also in ferric LspPOX (H_2O_2).

The possibility to monitor the peroxide driven transition from a predominantly heme *b* in LspPOX to mainly modified and covalently linked heme in LspPOX (H_2O_2) motivated us to study the impact of this PTM on the kinetics of the formation and reaction of all relevant redox intermediates of the halogenation and peroxidase cycles. For the mammalian counterparts (e.g. MPO or LPO), this could not be followed so far (despite the presence of comparable inhomogeneities regarding the covalent heme to protein bonds both in MPO or LPO).

Upon incubation of recombinant ferric LspPOX with hydrogen peroxide both cyanide binding and H_2O_2 -mediated oxidation to compound I was accelerated, and the K_D value for cyanide was decreased. It has to be mentioned that in regard to the rate of compound I formation, there are no obvious differences between peroxidases with and without covalently linked heme. The k_{app} values of this bimolecular reaction in mammalian peroxidases as well as plant-type peroxidases (such as horseradish peroxidase) are within $(1.1 - 5.6) \times 10^7 \text{ M}^{-1} \text{ s}^{-1}$ at pH 7.0 (1, 2). This result clearly suggests that upon transition from LspPOX to LspPOX (H_2O_2), changes of both (i) the structure of the distal heme cavity as well as of (ii) the access channel to the active site occurred. Both cyanide and hydrogen peroxide binding to the ferric state need the distal (catalytic) histidine to act as proton acceptor before the resulting anions bind to the ferric heme. Additionally, in heme peroxidases the distal histidine is involved in hydrogen bonding of the resulting cyanide complexes as well as of higher oxidation states such as compound II (1, 4). Modification of the prosthetic group and formation of covalent bonds with the protein will have an impact on these interactions. Moreover, because the substrate channel opens into the heme cavity close to the δ -meso bridge between pyrrole rings A and D (Fig. 1), these PTMs will also affect the accessibility of ligands and substrates. This result has been demonstrated for MPO variants, where the exchange of this glutamate residue (i.e. Glu-242) significantly reduced the rate of cyanide binding and compound I formation, most likely because the flexible side chain blocked the entrance to the heme cavity (27, 28). A similar scenario supposedly accounts for the lower reactivity in LspPOX with mainly unmodified glutamate.

Compound I of LspPOX (H_2O_2) could be formed with equimolar concentration of hydrogen peroxide. This fact as well as the spectral features of the resulting intermediate are

very similar to LPO compound I (1, 24). In the absence of exogenous electron donors, the protein moiety of the bacterial protein is oxidized resulting in an oxoiron(IV) intermediate with a compound II-like spectrum. This effect is also observed with LPO and reflects the similar redox properties of the two enzymes (13, 19, 25).

The oxidation capacity of compound I of LspPOX was significantly increased upon PTM. Similar to LPO, chloride could not act as electron donor in LspPOX (H_2O_2). Chloride oxidation is known from MPO and closely related to the existence of its electron-withdrawing sulfonium ion linkage and its strongly distorted and asymmetric heme group (3–5, 29), which results in the extraordinary positive reduction potential of its Fe(III)/Fe(II) couple (Table 1) (11, 27). By contrast, bromide acts as two-electron donor of compound I of LspPOX (H_2O_2) and the calculated apparent bimolecular rate constant was even higher compared with LPO compound I, which nicely reflects the recently published steady-state bromination data (13) but also the slightly more positive reduction potential of the Fe(III)/Fe(II) couple of LspPOX (H_2O_2). Although not directly involved in the catalytic cycle, the hierarchy of reduction potentials of the Fe(III)/Fe(II) couple often reflects the hierarchy of the reduction potential (E°) of the compound I/Fe(III) couple. Based on this, the hierarchy of E° (compound I/Fe(III)) is suggested to be MPO > EPO > LspPOX (H_2O_2) > LPO (11, 13).

An interesting observation was also the drastic increase of apparent bimolecular rate constants of the reactions of compound I with iodide and thiocyanate after PTM. This cannot be related with the increase of the oxidation capacity of the bacterial peroxidase as oxidation of these two-electron donors is not challenging thermodynamically (30). As already discussed above, probably in LspPOX, the negatively charged and flexible glutamate impedes the accessibility of these (bigger) anionic electron donors. Upon PTM and covalent bond formation, the negative charge disappears and additionally (most likely) the accessibility to the active site is increased (27–29).

Finally, we could demonstrate that the PTM also modulated the peroxidase cycle of this novel bacterial peroxidase (Reactions 2, 4, and 5). Both relevant redox intermediates, namely compound I and compound II, exhibited increased oxidation rates of tyrosine after the autocatalytic transformation (Table 1). Importantly, the observed UV-visible spectral features of compound II are also similar to LPO and significantly different to heme *b* peroxidases. With tyrosine ($E^\circ = 0.93$ V (31)) as model substrate, it was demonstrated that the apparent bimolecular rate constants of both compound I reduction (Reaction 4) and compound II reduction (Reaction 5) of LspPOX (H_2O_2) were about two times higher compared with LspPOX (Table 1). Both compound I and compound II of LspPOX (H_2O_2) are stronger oxidants compared with the corresponding redox intermediates of lactoperoxidase (Table 1) and horseradish peroxidase (32). In both horseradish peroxidase and mammalian peroxidases, the oxidation of aromatic electron donors has been proposed to take place in the vicinity of the δ -mesocarbon and pyrrole ring D (compare Fig. 1, B, D, and F) (1, 32). Based on the sequence homology of the bacterial protein with LPO (13), it is reasonable to assume that the oxidation site of tyrosine in LspPOX (H_2O_2) is very similar. This, together with the hierar-

Catalytic Role of the Heme to Protein Linkages

chy of the reduction potential of the Fe(III)/Fe(II) couples of these peroxidases (11, 13, 25, 32), suggests that the E° values of the couples compound I/compound II as well as compound II/Fe(III) follow the hierarchy LspPOX (H_2O_2) > LPO > HRP. It demonstrates that the bacterial peroxidase is an efficient catalyst of both two- and one-electron oxidation reactions. These properties together with its high conformational and thermal stability (13) render this novel class of heme proteins very interesting for application as catalyst in biotechnology.

Summing up, for the first time a recombinant heme peroxidase allowed monitoring of the effect of hydrogen peroxide-driven formation of covalent heme to protein bonds on its biochemical and biophysical properties. Distinct changes in spectral and redox properties during this structural transition were observed (13). This posttranslational modification alters the architecture of the heme cavity thereby improving the binding of cyanide and H_2O_2 . Upon covalent bond formation, the reduction potentials of the relevant redox intermediates and their reactivity toward one- and two-electron donors are increased. Additionally, the accessibility to the (pseudo-)halide binding and oxidation site seems to be increased.

It has to be mentioned that the physiological role of these bacterial heme peroxidases is completely unknown so far. LspPOX is the first studied representative of a novel peroxidase family, which can be regarded as phylogenetic origin in the evolution of the vertebrate peroxidases, including LPO and MPO (13). By sharing structural, biophysical and catalytic properties, one might speculate whether these bacterial proteins also share similar biological roles, *i.e.* unspecific defense reactions by production of halogenating and antimicrobial products such as hypohalous acids.

REFERENCES

1. Furtmüller, P. G., Zederbauer, M., Jantschko, W., Helm, J., Bogner, M., Jakopitsch, C., and Obinger, C. (2006) Active site structure and catalytic mechanisms of human peroxidases. *Arch. Biochem. Biophys.* **445**, 199–213
2. Zederbauer, M., Furtmüller, P. G., Brogioni, S., Jakopitsch, C., Smulevich, G., and Obinger, C. (2007) Heme to protein linkages in mammalian peroxidases: impact on spectroscopic, redox and catalytic properties. *Nat. Prod. Rep.* **24**, 571–584
3. Fiedler, T. J., Davey, C. A., and Fenna, R. E. (2000) X-ray crystal structure and characterization of halide-binding sites of human myeloperoxidase at 1.8 Å resolution. *J. Biol. Chem.* **275**, 11964–11971
4. Blair-Johnson, M., Fiedler, T., and Fenna, R. (2001) Human myeloperoxidase: structure of a cyanide complex and its interaction with bromide and thiocyanate substrates at 1.9 Å resolution. *Biochemistry* **40**, 13990–13997
5. Carpena, X., Vidossich, P., Schroettner, K., Calisto, B. M., Banerjee, S., Stampler, J., Soudi, M., Furtmüller, P. G., Rovira, C., Fita, I., and Obinger, C. (2009) Essential role of proximal histidine-asparagine interaction in mammalian peroxidases. *J. Biol. Chem.* **284**, 25929–25937
6. Singh, A. K., Singh, N., Sharma, S., Singh, S. B., Kaur, P., Bhushan, A., Srinivasan, A., and Singh, T. P. (2008) Crystal structure of lactoperoxidase at 2.4 Å resolution. *J. Mol. Biol.* **376**, 1060–1075
7. DePillis, G. D., Ozaki, S. i., Kuo, J. M., Maltby, D. A., and Ortiz de Montellano, P. R. (1997) Autocatalytic processing of heme by lactoperoxidase produces the native protein-bound prosthetic group. *J. Biol. Chem.* **272**, 8857–8860
8. Colas, C., Kuo, J. M., and Ortiz de Montellano, P. R., (2002) Asp-225 and Glu-375 in autocatalytic attachment of the prosthetic heme group of lactoperoxidase. *J. Biol. Chem.* **277**, 7191–7200
9. Oxvig, C., Thomsen, A. R., Overgaard, M. T., Sorensen, E. S., Højrup, P., Bjerrum, M. J., Gleich, G. J., and Sottrup-Jensen, L. (1999) Biochemical evidence for heme linkage through esters with Asp-93 and Glu-241 in human eosinophil peroxidase. The ester with Asp-93 is only partially formed *in vivo*. *J. Biol. Chem.* **274**, 16953–16958
10. Brogioni, S., Stampler, J., Furtmüller, P. G., Feis, A., Obinger, C., and Smulevich, G. (2008) The role of the sulfonium linkage in the stabilization of the ferrous form of myeloperoxidase: a comparison with lactoperoxidase. *Biochim. Biophys. Acta* **1784**, 843–849
11. Battistuzzi, G., Stampler, J., Bellei, J., Vlasits, J., Soudi, M., Furtmüller, P. G., and Obinger, C. (2011) Influence of the covalent heme-protein bonds on the redox thermodynamics of human myeloperoxidase. *Biochemistry* **50**, 7887–7994
12. Zamocky, M., Jakopitsch, C., Furtmüller, P. G., Dunand, C., and Obinger, C. (2008) The peroxidase-cyclooxygenase superfamily: reconstructed evolution of critical enzymes of the innate immune system. *Proteins* **72**, 589–605
13. Auer, M., Gruber, C., Bellei, M., Pirker, K. F., Zamocky, M., Kroiss, D., Teufer, S. A., Hofbauer, S., Soudi, M., Battistuzzi, G., Furtmüller, P. G., and Obinger, C. (2013) A stable bacterial peroxidase with novel halogenating activity and an autocatalytically linked heme prosthetic group. *J. Biol. Chem.* **288**, 27181–27199
14. Marquez, L. A., Huang, J. T., and Dunford, H. B. (1994) Spectral and kinetic studies on the formation of myeloperoxidase compounds I and II: roles of hydrogen peroxide and superoxide. *Biochemistry* **33**, 1447–1454
15. Furtmüller, P. G., Burner, U., Jantschko, W., Regelsberger, G., and Obinger, C. (2000) Two-electron reduction and one-electron oxidation of organic hydroperoxides by human myeloperoxidase. *FEBS Lett.* **484**, 139–143
16. Nelson, D. P., and Kiesow, L. A. (1972) Enthalpy of decomposition of hydrogen peroxide by catalase at 25 degrees C (with molar extinction coefficients of H_2O_2 solutions in the UV). *Anal. Biochem.* **49**, 474–478
17. Bolscher, B. G., and Wever, R. (1984) A kinetic study of the reaction between human myeloperoxidase, hydroperoxides and cyanide. Inhibition by chloride and thiocyanate. *Biochim. Biophys. Acta* **788**, 1–10
18. Dolman, D., Dunford, H. B., Chowdhury, D. M., and Morrison, M. (1968) The kinetics of cyanide binding by lactoperoxidase. *Biochemistry* **7**, 3991–3996
19. Lardinois, O. M., Medzihradsky, K. F., and Ortiz de Montellano, P. R. (1999) Spin trapping and protein cross-linking of the lactoperoxidase protein radical. *J. Biol. Chem.* **274**, 35441–35448
20. Furtmüller, P. G., Burner, U., Regelsberger, G., and Obinger, C. (2000) Spectral and kinetic studies on the formation of eosinophil peroxidase compound I and its reaction with halides and thiocyanate. *Biochemistry* **39**, 15578–15584
21. Furtmüller, P. G., Jantschko, W., Regelsberger, G., Jakopitsch, C., Arnhold, J., and Obinger, C. (2002) Reaction of lactoperoxidase compound I with halides and thiocyanate. *Biochemistry* **41**, 11895–11900
22. Furtmüller, P. G., Burner, U., and Obinger, C. (1998) Reaction of myeloperoxidase compound I with chloride, bromide, iodide, and thiocyanate. *Biochemistry* **37**, 17923–17930
23. Marquez, L. A., and Dunford, H. B. (1995) Kinetics of oxidation of tyrosine and dityrosine by myeloperoxidase compounds I and II. Implications for lipoprotein peroxidation studies. *J. Biol. Chem.* **270**, 30434–30440
24. Banerjee, S., Furtmüller, P. G., and Obinger, C. (2011) Bovine lactoperoxidase - a versatile one- and two-electron catalyst of high structural and thermal stability. *Biotechnol. J.* **6**, 231–243
25. Battistuzzi, G., Bellei, M., Vlasits, J., Banerjee, S., Furtmüller, P. G., Sola, M., and Obinger, C. (2010) Redox thermodynamics of lactoperoxidase and eosinophil peroxidase. *Arch. Biochem. Biophys.* **494**, 72–77
26. Battistuzzi, G., Bellei, M., Bortolotti, C. A., and Sola, M. (2010) Redox properties of heme peroxidases. *Arch. Biochem. Biophys.* **500**, 21–36
27. Zederbauer, M., Jantschko, W., Neugschwandtner, K., Jakopitsch, C., Moguevsky, N., Obinger, C., and Furtmüller, P. G. (2005) Role of the covalent glutamic acid 242-heme linkage in the formation and reactivity of redox intermediates of human myeloperoxidase. *Biochemistry* **44**, 6482–6491
28. Zederbauer, M., Furtmüller, P. G., Bellei, M., Stampler, J., Jakopitsch, C., Battistuzzi, G., Moguevsky, N., and Obinger, C. (2007) Disruption of the

- aspartate to heme ester linkage in human myeloperoxidase: impact on ligand binding, redox chemistry, and interconversion of redox intermediates. *J. Biol. Chem.* **282**, 17041–17052
29. Zederbauer, M., Furtmüller, P. G., Ganster, B., Moguilevsky, N., and Obinger, C. (2007) The vinyl-sulfonium bond in human myeloperoxidase: impact on compound I formation and reduction by halides and thiocyanate. *Biochem. Biophys. Res. Commun.* **356**, 450–456
30. Arnhold, J., Monzani, E., Furtmüller, P. G., Zederbauer, M., Casella, L., and Obinger, C. (2006) Kinetics and thermodynamics of halide and nitrite oxidation by mammalian heme peroxidases. *Eur. J. Inorg. Chem.* **19**, 3801–3811
31. Harriman, A. (1987) Further comments on the redox potentials of tryptophan and tyrosine. *J. Phys. Chem.* **91**, 6102–6104
32. Jantschko, W., Furtmüller, P. G., Allegra, M., Livrea, M. A., Jakopitsch, C., Regelsberger, G., and Obinger, C. (2002) Redox intermediates of plant and mammalian peroxidases: a comparative transient-kinetic study of their reactivity toward indole derivatives. *Arch. Biochem. Biophys.* **398**, 12–22

Posttranslational Modification of Heme *b* in a Bacterial Peroxidase: The Role of Heme to Protein Ester Bonds in Ligand Binding and Catalysis

Nicolussi, A., Auer, M., Weissensteiner, J., Schütz, G., Katz, S., Maresch, D., Hofbauer, S., Bellei, M., Battistuzzi, G., Furtmüller, P. G., and Obinger, C.

Research article

Biochemistry (2017) **56**, 4525-4538

doi: 10.1021/acs.biochem.7b00632

Posttranslational Modification of Heme *b* in a Bacterial Peroxidase: The Role of Heme to Protein Ester Bonds in Ligand Binding and Catalysis

Andrea Nicolussi,[†] Markus Auer,[†] Julia Weissensteiner,[†] Georg Schütz,[†] Sonja Katz,[†] Daniel Maresch,[†] Stefan Hofbauer,[†] Marzia Bellei,[‡] Gianantonio Battistuzzi,[§] Paul G. Furtmüller,[†] and Christian Obinger^{*,†}

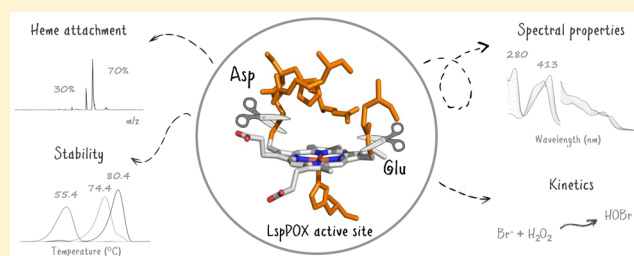
[†]Department of Chemistry, Division of Biochemistry, Vienna Institute of BioTechnology, BOKU-University of Natural Resources and Life Sciences, Muthgasse 18, A-1190 Vienna, Austria

[‡]Department of Life Sciences, University of Modena and Reggio Emilia, via Campi 103, 41125 Modena, Italy

[§]Department of Chemistry and Geology, University of Modena and Reggio Emilia, via Campi 103, 41125 Modena, Italy

S Supporting Information

ABSTRACT: The existence of covalent heme to protein bonds is the most striking structural feature of mammalian peroxidases, including myeloperoxidase and lactoperoxidase (LPO). These autocatalytic posttranslational modifications (PTMs) were shown to strongly influence the biophysical and biochemical properties of these oxidoreductases. Recently, we reported the occurrence of stable LPO-like counterparts with two heme to protein ester linkages in bacteria. This study focuses on the model wild-type peroxidase from the cyanobacterium *Lyngbya* sp. PCC 8106 (LspPOX) and the mutants D109A, E238A, and D109A/E238A that could be recombinantly produced as apoproteins in *Escherichia coli*, fully reconstituted to the respective heme *b* proteins, and posttranslationally modified by hydrogen peroxide. This for the first time allows not only a direct comparison of the catalytic properties of the heme *b* and PTM forms but also a study of the impact of D109 and E238 on PTM and catalysis, including Compound I formation and the two-electron reduction of Compound I by bromide, iodide, and thiocyanate. It is demonstrated that both heme to protein ester bonds can form independently and that elimination of E238, in contrast to exchange of D109, does not cause significant structural rearrangements or changes in the catalytic properties neither in heme *b* nor in the PTM form. The obtained findings are discussed with respect to published structural and functional data of human peroxidases.



Four heme peroxidase superfamilies arose independently during evolution, which differ in overall fold, active site architecture, and enzymatic activity.¹ The redox cofactor is either heme *b* or modified heme that is coordinated by either cysteine or histidine. Posttranslational modification (PTM) of the heme cofactor leading to covalent heme to protein bonds is found exclusively in members of the peroxidase-cyclooxygenase superfamily (Pfam accession number PF03098).² Its members are widely distributed among all domains of life. In at least five of the seven main families, the heme is covalently linked via one or two ester linkages formed by conserved glutamate and aspartate residues and the heme 1- and 5-methyl substituents.³ Only in one representative [i.e., myeloperoxidase (MPO)] of family 1 is a third covalent bond formed between a Met and the 2-vinyl substituent of the heme.^{3,4} Generally, family 1 (i.e., chordata) peroxidases are the best studied representatives of this superfamily with respect to structural and functional characterization and their role in physiology. Besides MPO, eosinophil peroxidase (EPO), lactoperoxidase (LPO), and thyroid peroxidase (TPO) are well-known and were shown to

participate in innate immunity (MPO, EPO, and LPO) and thyroid hormone biosynthesis (TPO).^{5–8}

Importantly, formation of the heme to protein bonds in vertebrate peroxidases was shown to occur autocatalytically proceeding via a free radical mechanism that includes H₂O₂-mediated formation of Compound I as proposed by Ortiz de Montellano.⁹ Compound I formed by the noncovalently bound heme–protein complex oxidizes a nearby carboxylic acid to the carboxylate radical, concomitantly reducing the heme center to the Compound II state. Finally, the side-chain radical abstracts a hydrogen atom from the nearby heme methyl group, yielding a methylene radical and regenerating the carboxylic acid anion. Intramolecular transfer of the unpaired electron from the methylene to the iron leads to regeneration of the ferric state and a methylene cation that traps the carboxylate anion and

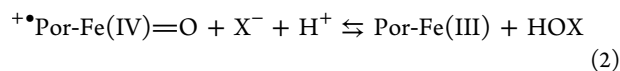
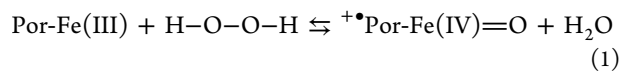
Received: July 5, 2017

Revised: July 31, 2017

Published: August 1, 2017

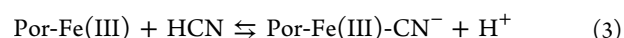
forms the ester bond.⁹ As a consequence of these PTMs, the heme is distorted causing a bowing of the structure as is demonstrated by X-ray crystallography and resonance Raman spectroscopy.^{3,4} The effect is much more pronounced in MPO than in LPO.^{3,4,10–12} As a result of this distortion and the MPO-specific electronic effects of the vinyl sulfonium linkage, the spectroscopic and redox properties of vertebrate peroxidases (e.g., LPO and MPO) and heme *b* peroxidases (e.g., horseradish peroxidase) differ substantially.^{3,13,14}

Vertebrate peroxidases, like heme peroxidases from all four superfamilies, catalyze the one-electron oxidation of diverse organic substrates.^{15–17} However, they have an additional and physiologically important function, namely the two-electron oxidation of halides and thiocyanate. Thereby, they follow the halogenation cycle that includes Compound I [i.e., oxoiron(IV) porphyrin radical, $^{+}\text{Por-Fe(IV)=O}$] formation (reaction 1) and the direct two-electron reduction of Compound I to the ferric state by halides or thiocyanate (reaction 2).^{3,18} The produced hypohalous acids (HOX) or hypothiocyanite are responsible for the antimicrobial role of MPO, EPO, and LPO in the mammalian innate immune system or thyroid hormone biosynthesis by TPO.^{5–8} Importantly, the PTMs were shown to significantly modulate the oxidation capacity of these peroxidases. For example, because of the vinyl–sulfonium bond, MPO is the only human enzyme that is able to oxidize chloride to hypochlorite at reasonable rates.^{3,5,14,19}



Phylogenetic analysis of the peroxidase-cyclooxygenase superfamily revealed that peroxidases homologous to mammalian counterparts are also found in bacteria and early eukaryotes,^{1,2} which poses a question about the origin of oxidant-based innate immunity. Recently, we have published biochemical studies of the first bacterial representative of the peroxidase-cyclooxygenase superfamily, namely a heme peroxidase from the cyanobacterium *Lyngbya* sp. PCC 8106 (LspPOX).^{20,21} Its sequence is highly homologous with that of LPO and the presence of all relevant heme cavity residues, including D109 and E238. The corresponding residues in LPO (but also EPO, TPO, and MPO) have been shown to be responsible for the two heme to protein ester bonds.¹² Furthermore, we could demonstrate that recombinant LspPOX isolated from *Escherichia coli* has a mixture of heme *b* and covalently bound heme and that addition of hydrogen peroxide increased the fraction of posttranslationally modified enzyme.^{20,21}

In this work, we aimed to study (i) the catalytic differences between heme *b* LspPOX and the posttranslationally modified (PTM) protein and (ii) the role of D109 and E238 in both the autocatalytic process and catalysis. Four proteins (wild-type, single mutants D109A and E238A, and double mutant D109A/E238A) were produced as apo forms, loaded with heme *b*, and, finally, incubated with a 15-fold molar excess of H_2O_2 for autocatalytic posttranslational modification. The corresponding heme *b* and PTM versions of those proteins were studied, and their spectral and redox properties, thermal stability, and ligand binding (reaction 3) and the two individual reaction steps of the halogenation cycle, i.e., Compound I formation and reduction (reactions 1 and 2), were compared.



MATERIALS AND METHODS

Materials. Chemicals and enzymes were purchased from the following sources. The pET-52b(+) vector was from Novagen, and the competent *E. coli* BL21 Star (DE3) cells were from Thermo Fisher Scientific. For site-directed mutagenesis, the QuikChange Lightning Site-directed Mutagenesis Kit (Agilent) was used. The chelating Sepharose Fast Flow column was from Amersham Biosciences, Centripreps-30 were from Amicon, whereas protease inhibitor tablets (SIGMAFAST Protease Inhibitor Cocktail Tablets EDTA-free), hydrogen peroxide (as a 30% solution), and PD-10 columns were purchased from Sigma-Aldrich. Membrane filters (hydrophilic 0.45 μm membrane filter) were from Merck Millipore. All other chemicals were purchased from Sigma-Aldrich at the highest available grade.

Cloning, Site-Directed Mutagenesis, and Expression. The preparation of the LspPOX gene from the *Lyngbya* sp. strain was described previously.^{20,21} A hexahistidine tag (His₆ tag) was fused at the N-terminus of the LspPOX gene and a Strep tag at the C-terminus. The pET-52b(+) plasmid containing the LspPOX gene was used for expression with the T7 expression system (Novagen). Mutants of LspPOX were produced using site-directed mutagenesis, and the designed primers (Table S1) were purchased from Sigma-Aldrich. For the introduction of point mutations, the polymerase chain reaction-based site-directed mutagenesis kit (Agilent Technologies) with two complementary primers with the specific mutation in the middle of their sequence was used. Chemically competent *E. coli* BL21 Star (DE3) cells were transformed with the mutated, purified plasmids by heat shock transformation for expression screening and final protein production.

Next, 12 mL of LB_{amp} medium [10 g/L peptone, 5 g/L yeast extract, and 5 g/L NaCl (pH 7.0), supplemented with 5 mg/L ampicillin] was inoculated with the transformed *E. coli* BL21 Star (DE3) cells, incubated overnight at 37 °C and 180 rpm, and used as the inoculum for 1 L of M9ZB_{amp} medium (20 g/L peptone, 10 g/L yeast extract, 5 g/L NaCl, and 1 g/L NH_4Cl , supplemented with 6 g/L $\text{Na}_2\text{HPO}_4 \cdot 7\text{H}_2\text{O}$, 3 g/L KH_2PO_4 , 1 g/L glucose, 25 mg/L $\text{MgSO}_4 \cdot 7\text{H}_2\text{O}$, and 5 mg/L ampicillin). The cultures were grown in two 2 L Erlenmeyer flasks at 37 °C and 180 rpm, until the optical density at 600 nm (A_{600}) reached a value of 0.6–0.8. Protein expression was induced using isopropyl β -D-1-thiogalactopyranoside (final concentration of 0.5 mM). The cells were grown for 4 h at 20 °C and 180 rpm. The cultures were harvested by centrifugation at 2700g and 4 °C for 15 min. The cell pellet was frozen at –80 °C.

Purification of Apoproteins and Reconstitution with Heme. Using the N-terminal His₆ tag, the protein was purified by metal chelate affinity chromatography. The cell pellet of 1 L of *E. coli* culture was thawed and resuspended in 20 mL of lysis buffer [50 mM Tris-HCl (pH 8.0) containing 2 mM Na_2EDTA , 0.1% Triton X-100, 1 mM phenylmethanesulfonyl fluoride, and a protease inhibitor cocktail tablet]. The cell suspension was cooled on ice during lysis by ultrasonication (50% pulse, three times for 40 s) and then centrifuged at 45000g and 4 °C for 25 min. The pellet was discarded, and the remaining supernatant containing apo-LspPOX was filtered through a hydrophilic 0.45 μm membrane filter (Merck Millipore) and used for metal chelate affinity chromatography. After the addition of 0.5 M

NaCl and 20 mM imidazole (final concentration), the solution was loaded on a chelating Sepharose gel column (1.6 cm × 12 cm) charged with Ni²⁺ (5 mg/mL) and equilibrated with 67 mM phosphate buffer (pH 7.2) containing 0.5 M NaCl and 20 mM imidazole. The column was washed with equilibration buffer, and bound proteins were eluted with 90 mL of a gradient of 20 to 250 mM imidazole in equilibration buffer. Fractions showing a pure band on sodium dodecyl sulfate–polyacrylamide gel electrophoresis (SDS–PAGE) were collected. The protein was concentrated by ultrafiltration (Amicon CentriPrep-30) with a weight cutoff of 30 kDa, desalted with PD-10 columns, and stored in 10 mM phosphate buffer (pH 7.0) at –80 °C.

The purified apoprotein was mixed with an equimolar amount of hemin chloride and incubated for approximately 10 min at room temperature in 50 mM phosphate buffer (pH 7.0). For the production of the respective PTM form with covalently linked heme, the protein solution was incubated with a 15-fold stoichiometric excess of hydrogen peroxide for 1 h at room temperature. The protein was desalted with PD-10 columns, concentrated by ultrafiltration (Amicon CentriPrep-30), and stored in 10 mM phosphate buffer (pH 7.0) at –80 °C.

Mass Spectrometry. To detect the fraction of protein containing covalently bound heme, intact protein mass spectrometry analyses were conducted. Therefore, 3 μg of wild-type LspPOX or mutants in 10 mM phosphate buffer (pH 7.0) was analyzed using a Dionex Ultimate 3000 system directly linked to a QTOF instrument (maXis 4G ETD, Bruker) equipped with the standard electrospray ionization (ESI) source in positive ion mode. Mass spectrometric scans were recorded in a range from *m/z* 400 to 3800. The instrument was calibrated using an ESI calibration mixture (Agilent). For separation of the proteins, a Thermo ProSwift RP-4H analytical separation column (250 mm × 0.200 mm) was used. A gradient from 80% solvent A and 20% solvent B [solvent A being 0.05% trifluoroacetic acid (TFA) and solvent B being 80.00% acetonitrile (ACN), 19.95% H₂O, and 0.05% TFA] to 65% B over 20 min was applied, followed by a 15 min gradient from 65 to 95% B, at a flow rate of 8 μL/min and 70 °C. The obtained data were processed using Data Analysis 4.0 (Bruker), and the spectrum was deconvoluted by MaxEnt (maximum entropy method, low mass of 40000, high mass of 200000, instrument resolving power of 10000).

Differential Scanning Calorimetry. Differential scanning calorimetry (DSC) measurements were taken on a VP-DSC microcalorimeter (MicroCal) controlled by the VP-viewer program and equipped with a 137 μL cell and an autosampler for 96-well plates. Studies were performed with 10 μM protein in 100 mM buffer (pH 7.0). Samples were analyzed using a programmed heating scan rate of 60 °C/h and a 4.1 bar cell pressure in a temperature range of 20–100 °C. Data analysis was performed with the MicroCal Origin 7 software. Raw DSC data were baseline-corrected with buffer and normalized for protein concentration. Individual endotherms were fitted by a non-two-state transition model.

Spectroelectrochemistry. Standard reduction potential *E*^{o'} of the Fe(III)/Fe(II) couple of the heme proteins was measured using a homemade OTTLE (optically transparent thin layer spectroelectrochemical) cell in a three-electrode configuration, consisting of a gold mini-grid working electrode (Buckbee-Mears), a homemade Ag/AgCl/KCl_{sat} microreference electrode, separated from the working solution by a Vycor set, and a platinum wire as counter electrode. The reference

electrode was calibrated against a saturated calomel electrode (AgCl) before each set of measurements. All potentials are referenced to the standard hydrogen electrode. Potentials were applied using an Amel model 2053 potentiostat/galvanostat. Ultraviolet–visible (UV–vis) spectra were recorded using a Varian Cary C50 spectrophotometer. Spectroelectrochemical titrations were performed using samples containing 10 μM wild-type LspPOX or mutants in 100 mM phosphate buffer and 100 mM NaCl at pH 7.0 and 25 °C. As redox mediators, 100 μM methyl viologen and 2 μM lumiflavin 3-acetate, methylene blue, phenazine methosulfate, and indigo disulfonate were used.

UV–Vis and ECD Spectroscopy. UV–vis spectra of wild-type and mutant LspPOX in both the heme *b* and PTM form were recorded using a Hitachi U-3900 spectrophotometer from 200 to 800 nm at 25 °C in 50 mM phosphate buffer (pH 7.0). The molar extinction coefficient of wild-type LspPOX has been determined previously by the method of Bradford and was 94670 M⁻¹ cm⁻¹.²⁰ It was used for all calculations of protein concentrations of LspPOX and its mutants.

Electronic circular dichroism (ECD) measurements were conducted using a Chirascan device (Applied Photophysics, Leatherhead, U.K.). UV–vis and ECD spectra were measured simultaneously. The machine was flushed with nitrogen at a flow rate of 5 L/min before and throughout the measurements. In the far-UV region (180–260 nm), the path length was 1 mm, using a bandwidth of 3 nm at a constant temperature of 25 °C, and the scan time was 10 s per point. The concentration of LspPOX and its mutants was 0.25 mg/mL in 10 mM phosphate buffer (pH 7.0). In the near-UV and visible region (250–470 nm), the instrument parameters were as follows: path length of 10 mm, spectral bandwidth of 1 nm, temperature of 25 °C, and scan time of 10 s per point. Concentrations for measurements in the near-UV and visible range were 5 mg/mL.

Temperature-dependent single-wavelength ECD measurements were conducted in a temperature range of 25–95 °C at a heating rate of 60 °C/h and a wavelength of 408 nm, revealing the unfolding of the heme cavity. The instrument setup was the same as that for near-UV and visible ECD measurements, and unfolding curves were fitted with a sigmoid regression curve to yield the midterm temperature (*T*_m) of unfolding of the heme cavity.

Stopped-Flow Spectroscopy. Pre-steady state kinetic measurements were performed to study the reaction intermediates of wild-type and mutant proteins in both the heme *b* and PTM forms. The experiments were performed with a stopped-flow apparatus (model SX-18MV and Pi-star-180, Applied Photophysics) equipped in the conventional mode or sequential mode. An optical quartz cell with a path length of 10 mm and a volume of 20 μL was used. The fastest time for mixing two solutions and recording the first data point was 1.0 ms. All measurements were performed at 25 °C. A minimum of three replicates was performed for each measurement. The spectra were followed with the diode array detector, and the single-wavelength time traces were obtained using a monochromator (both from Applied Photophysics). Cyanide binding and reaction with hydrogen peroxide were performed in the conventional stopped-flow mode by measuring the decrease in absorbance at 412 nm. One syringe contained a 4 μM protein solution in 50 mM phosphate buffer (pH 7.0), and the second syringe contained cyanide or hydrogen peroxide solutions at varying concentrations. The pseudo-first-order rate constants, *k*_{obs}, were used to calculate the second-order rate constants using the slope of the plotted *k*_{obs} values versus cyanide

concentration to calculate k_{on} , k_{off} , and K_D values. Apparent bimolecular rate constants of Compound I formation were calculated by plotting the obtained k_{obs} values against hydrogen peroxide concentration.

Sequential, multimixing stopped-flow spectroscopy was performed to monitor the reduction of Compound I using the (pseudo) halides Cl^- , Br^- , I^- , and SCN^- . Halide oxidation was followed by measuring the absorbance change at 412 nm. In detail, an 8 μM protein solution was premixed with varying hydrogen peroxide concentrations in the aging loop for varying time spans (see Table S2). Finally, Compound I was allowed to react with varying concentrations of electron donors. The measured time traces were fitted to obtain the corresponding pseudo-first-order rate constants, k_{obs} , which were further used to calculate the apparent bimolecular rate constants from the slope of the plot of k_{obs} versus (pseudo)halide concentration.

RESULTS

Production of Apoproteins, Heme *b* Proteins, and PTMs of the Prosthetic Group.

Wild-type peroxidase from the cyanobacterium *Lyngbya* sp. PCC 8106 (LspPOX) and the three mutants were successfully produced with an N-terminal His₆ tag as apoproteins. The respective supernatants of the lysed *E. coli* cells were purified by affinity chromatography, and the purity of the four proteins was proven by SDS-PAGE and Western blotting, using an anti-His₆ tag antibody. After optimization of the expression conditions, a yield of ~10 mg/L of *E. coli* culture could be obtained for all four proteins. Spectral investigation demonstrated the complete absence of heme in these samples. Aliquots of these apoproteins were stored at -80°C in 10 mM phosphate buffer (pH 7.0) until they were used for further investigation. Next, the apoproteins were reconstituted by stepwise addition of protein to a heme chloride solution to yield a final 1:1 stoichiometry. Spectral monitoring of this reconstitution procedure clearly showed monophasic transitions with isosbestic points (Figure 1). The typical heme spectra [maxima at 385 nm (shoulder at 360 nm) and 611 nm (red spectrum in Figure 1)] were converted to heme *b* spectra with Soret maxima at 411 nm (wild-type LspPOX and variant E238A) or at 404 nm (variants D109A and D109A/E238A). The resulting purity numbers (RZ, A_{Soret}/A_{280}) of approximately 0.85–0.90 indicated 90–95% heme occupancy. Mass spectrometric analysis confirmed the purity and homogeneity of the proteins (Figure 2) with molar masses of 60662 Da (wild-type), 60616 Da (D109A), 60602 Da (E238A), and 60560 Da (D109A/E238A). Note that during sample preparation for MS analysis (noncovalently bound) heme *b* is lost (see Materials and Methods).

Importantly, upon incubation of the heme *b* proteins with H_2O_2 at a 15-fold stoichiometric excess, the prosthetic heme group (612 Da) was modified and covalently linked with the protein, i.e., generation of the PTM form. Figure 2 demonstrates that 66–70% of wild-type LspPOX and mutants D109A and E238A showed additional MS peaks at 61272 Da (wild-type), 61229 Da (D109A), and 61216 Da (E238A), reflecting the presence of covalently bound heme. These data clearly suggest that both aspartate 109 and glutamate 238 can participate in ester bond formation even in the absence of the second acidic amino acid (Figure 2A–C). In the double mutant, heme *b* cannot be posttranslationally modified (Figure 2D).

The effect of the PTMs on the overall secondary and tertiary structure of the wild-type and mutant proteins is negligible. The

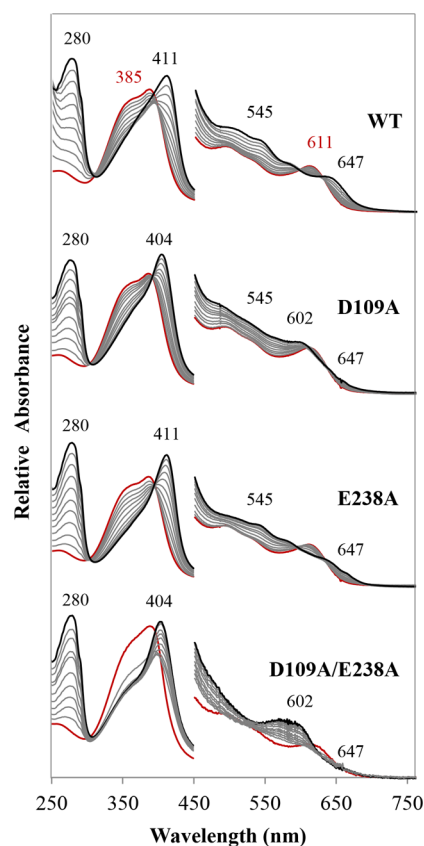


Figure 1. Conversion of apoproteins to the heme *b* forms followed by UV-vis spectroscopy. Purified apoproteins (wild-type, WT) and mutants D109A, E238A, and D109A/E238A were stepwise added to heme chloride (red spectrum) at room temperature in 50 mM phosphate buffer (pH 7.0). Spectra were recorded when no further spectral changes occurred (typically 5 min after each step). The final heme *b* spectra (90–95% heme occupancy) are shown in bold black.

heme *b* and posttranslationally modified versions of all four proteins exhibited almost identical CD spectra in the far-UV (185–250 nm) and near-UV (250–350 nm) regions (Figure 3A,B). Deconvolution of the spectra revealed the presence of approximately 30% α -helices, 25% β -sheets, 19% β -turns, and 26% random coil structure. However, in the visible region, both the wild-type protein and variant E238A showed significant differences between the heme *b* and PTM forms. Incubation with H_2O_2 increased the ellipticity of the respective minima. Additionally, the Soret minima slightly shifted to higher wavelengths (wild-type, from 409 to 411 nm; D109A, from 408 to 409 nm; E238A, from 410 to 412 nm). These findings clearly reflect rearrangements in the heme cavity caused by PTM. The ellipticity of the Soret region of double mutant D109A/E238A was small and did not change upon incubation of the protein with hydrogen peroxide.

Covalent bond formation was also reflected by changes in the UV-vis spectra. Upon incubation with H_2O_2 , the Soret bands of wild-type LspPOX and mutant E238A slightly narrowed and the maxima shifted from 411 to 412 nm. In addition, the Q-band at 545 nm and the CT1 band at 642 nm became more pronounced (Figure 4). It is important to note that the spectra of the heme *b* versions of D109A and D109A/E238A varied depending of the sample age and storage conditions. Freshly prepared heme *b* samples exhibited Soret maxima at 404 nm, whereas frozen and defrosted proteins showed maxima of ~410

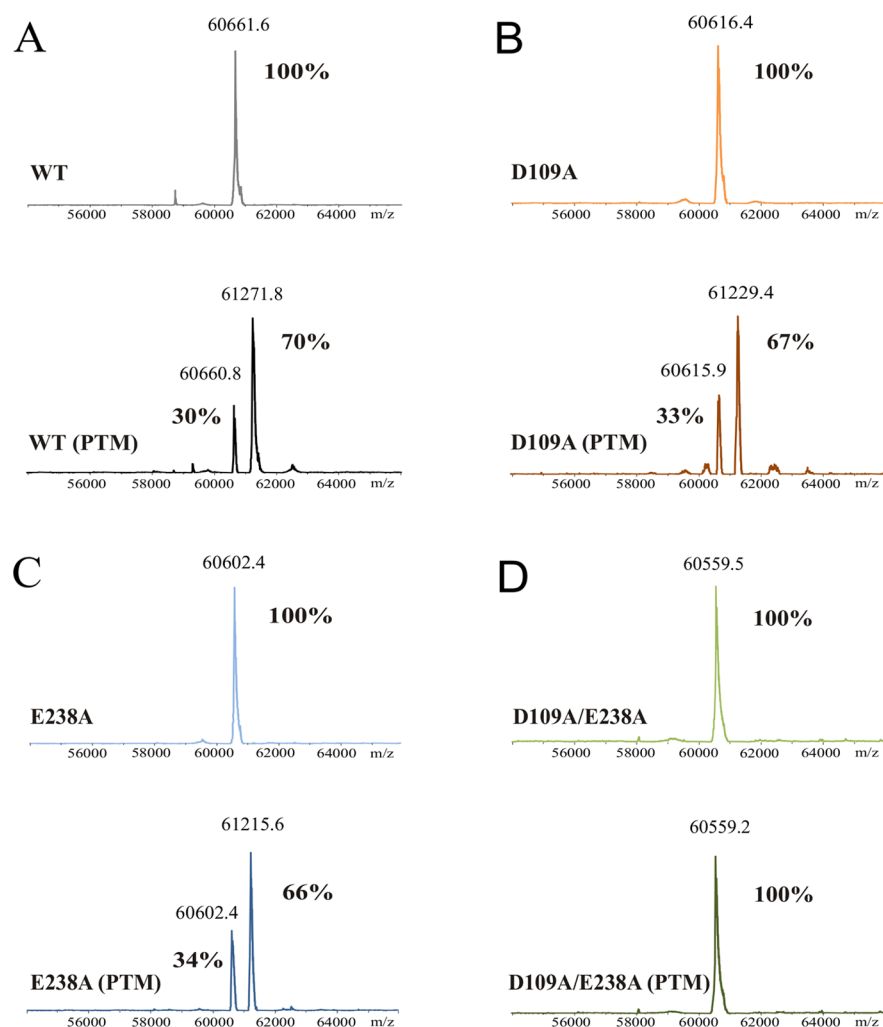


Figure 2. Mass spectrometry analysis of (A) wild-type LspPOX and mutants (B) D109A, (C) E238A, and (D) D109A/E238A in both the heme *b* and PTM forms. For intact protein analysis, 3 μg of the protein sample in 10 mM phosphate buffer (pH 7.0) was directly injected into the liquid chromatography–mass spectrometry system and analyzed by a QTOF instrument equipped with the standard ESI source in positive ion mode. The PTM versions were obtained by incubation of the heme *b* proteins with a 15-fold stoichiometric excess of H_2O_2 at room temperature for 1 h.

nm despite the fact that 100% heme *b* was still present in the active site.

Incubation with H_2O_2 significantly narrowed the Soret band of D109A and shifted the Soret maximum to 411 nm (67% covalently bound heme), whereas no spectral changes in the double mutant were evident (100% heme *b*) (Figure 4).

Impact of PTM on the Thermal Stability of Wild-Type and Mutant Proteins. Next, we analyzed the thermal stability of wild-type LspPOX and the three mutants in the heme *b* and PTM states by both differential scanning calorimetry (DSC) and ECD spectroscopy in the Soret region at 408 nm (Figure 5). DSC thermograms of the wild-type apoprotein showed an endotherm with a midterm transition at 55.4 $^{\circ}\text{C}$, whereas the presence of heme *b* significantly stabilized the overall fold ($T_m = 74.4$ $^{\circ}\text{C}$). Establishment of covalent ester bonds further stabilized the protein ($T_m = 80.4$ $^{\circ}\text{C}$). It was interesting to see that the thermal stabilities of the three variants in the heme *b* states were higher than those of the wild-type protein. The thermal stabilities of both D109A and the double mutant remained unchanged after incubation with H_2O_2 (T_m values of 79.7 and 77.4 $^{\circ}\text{C}$, respectively), whereas the T_m shifted from 75.2 to 78.6 $^{\circ}\text{C}$ in the case of E238A (Figure 5A). In the temperature-dependent CD studies, we focused on unfolding of

the heme cavity only and thus monitored the loss of heme Soret ellipticity at 408 nm (Figure 5B). The respective T_m values for the heme *b* and PTM states were determined to be 73.5 and 75.6 $^{\circ}\text{C}$ (wild-type LspPOX), 75.6 and 75.9 $^{\circ}\text{C}$ (D109A), and 72.2 and 75.0 $^{\circ}\text{C}$ (E238A), respectively. Double mutant D109A/E238A showed one distinct T_m value of 76.2 $^{\circ}\text{C}$ in the absence and presence of hydrogen peroxide.

Impact of PTMs on Cyanide Binding and Low-Spin Complex Formation. Furthermore, we were interested in the impact of the heme to protein bonds on the kinetics of cyanide binding and the stability of the resulting low-spin complex. Cyanide binding can easily be followed by UV–vis stopped-flow spectroscopy, because binding of the ligand converts the high-spin Fe(III) state ($S = 5/2$) into the low-spin Fe(III) state ($S = 1/2$) (reaction 3). When cyanide bound to wild-type heme *b* LspPOX, the Soret maximum was shifted from 411 to 429 nm in a monophasic reaction with a clear isosbestic point at 418 nm (Figure 6A). Concomitantly, in the visible region, the bands at 502 and 647 nm disappeared and the typical low-spin peak at 548 nm arose. The single exponentially fitted pseudo-first-order rate constant (k_{obs}) values were plotted against the cyanide concentration to yield apparent second-order rate constants (k_{on}) of $3.0 \times 10^4 \text{ M}^{-1} \text{ s}^{-1}$ (Table 1). The dissociation constant

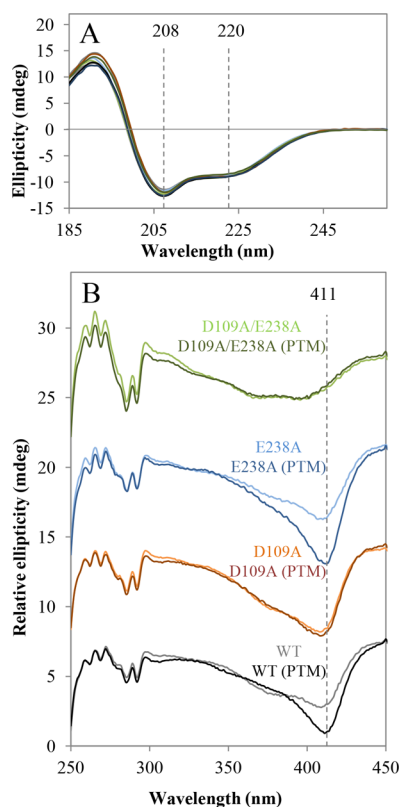


Figure 3. Electronic circular dichroism spectra of wild-type LspPOX and mutants D109A, E238A, and D109A/E238A in both the heme *b* and PTM forms. (A) Electronic circular dichroism (ECD) spectra of heme *b* and PTM forms of wild-type LspPOX and mutants in the far-UV region from 185 to 260 nm. The protein concentration was 0.25 mg/mL in 10 mM phosphate buffer (pH 7.0) at 25 °C (path length of 1 mm). (B) Electronic circular dichroism spectra of heme *b* and PTM forms of wild-type LspPOX and mutants in the near-UV and visible (250–450 nm) regions. The protein concentration was 0.5 mg/mL in 10 mM phosphate buffer (pH 7.0) at 25 °C (path length of 10 mm). The PTM versions were obtained by incubation of the heme *b* proteins with a 15-fold stoichiometric excess of H₂O₂ at room temperature for 1 h.

($K_D = k_{\text{off}}/k_{\text{on}}$) was calculated to be 96 μM , with k_{off} corresponding to the intercept (inset of Figure 6A). Upon autocatalytic PTM mediated by H₂O₂, the high-spin (413 nm) to low-spin (429 nm) conversion with added cyanide became faster and biphasic with two distinct values for the pseudo-first-order rate constants responsible for $\sim 70\%$ (k_{obs1}) and $\sim 30\%$ (k_{obs2}) of the absorbance decrease (Figure 6B). Plotted against the concentration of cyanide, k_{obs1} and k_{obs2} reveal two apparent second-order rate constants of $1.2 \times 10^6 \text{ M}^{-1} \text{ s}^{-1}$ (k_{on1}) and $2.7 \times 10^4 \text{ M}^{-1} \text{ s}^{-1}$ (k_{on2}), respectively. The corresponding dissociation constants (K_D) were found to be 25.7 μM (K_{D1}) and 112 μM (K_{D2}). The biphasic kinetics of cyanide binding reflects the heterogeneity of PTM as determined by mass spectrometry (see above). Hence, k_{on1} and K_{D1} are associated with the PTM form of the protein, whereas k_{on2} and K_{D2} are related to the heme *b* species. Formation of the heme to protein bonds significantly increased the binding rate of cyanide and stabilized the resulting complex. This is also supported by similar apparent k_{on} rates reported for lactoperoxidase and myeloperoxidase (i.e., $\sim 1.3 \times 10^6 \text{ M}^{-1} \text{ s}^{-1}$).^{18,22,23}

Exchange of aspartate 109 by alanine decelerates binding of cyanide to the heme *b* protein ($5.0 \times 10^3 \text{ M}^{-1} \text{ s}^{-1}$) and

destabilizes the resulting complex ($K_D = 780 \mu\text{M}$) (Figure 6C). As for the wild-type protein, incubation with H₂O₂ induced heterogeneity and biphasic cyanide binding (Figure 6D) with rates of $3.7 \times 10^5 \text{ M}^{-1} \text{ s}^{-1}$ (k_{on1}) and $6.6 \times 10^3 \text{ M}^{-1} \text{ s}^{-1}$ (k_{on2}) as well as 129 μM (K_{D1}) and 424 μM (K_{D2}). By contrast, incubation of the E238A mutant with hydrogen peroxide had no impact on the monophasic kinetics of cyanide binding or on the stability of the resulting complex (Figure 6E,F). Both the heme *b* protein and the PTM version showed a monophasic binding behavior with rates of $6.7 \times 10^5 \text{ M}^{-1} \text{ s}^{-1}$ ($K_D = 4.8 \mu\text{M}$) and $7.0 \times 10^5 \text{ M}^{-1} \text{ s}^{-1}$ ($K_D = 7.1 \mu\text{M}$), respectively (Table 1). Binding of cyanide to double mutant D109A/E238A revealed minor spectral changes that did not depend on cyanide concentration (Figure S1A), thus hindering the calculation of the apparent second-order rate constant (k_{on}) or the dissociation constant (K_D) for D109A/E238A.

Impact of PTM on Compound I Formation and

Reduction. Next, we studied the impact of the heme modifications on the formation of Compound I. The peroxidase cycle is induced by the two-electron oxidation of the ferric enzyme to the Compound I state mediated by hydrogen peroxide (reaction 1). In most heme peroxidases, including LspPOX, an oxoiron(IV) porphyrin π -cation radical that exhibits hypochromicity in the Soret band region is formed. Figure 7A shows the monophasic reaction of wild-type heme *b* LspPOX with hydrogen peroxide leading to $\sim 45\%$ hypochromicity and formation of peaks at 602 and 663 nm. A 2-fold stoichiometric excess of H₂O₂ was necessary to obtain full hypochromicity (Table S2). The apparent bimolecular rate constant, k_{app} , was calculated to be $2.6 \times 10^6 \text{ M}^{-1} \text{ s}^{-1}$ (Table 1). Induction of PTM by preincubation with H₂O₂ induced heterogeneity and rendered Compound I formation biphasic with k_{app1} ($\sim 70\%$ of the absorbance decrease) and k_{app2} ($\sim 30\%$ of the absorbance decrease) being 6.0×10^7 and $2.5 \times 10^6 \text{ M}^{-1} \text{ s}^{-1}$, respectively (Figure 7B).

Panels C and D of Figure 7 show the kinetics of Compound I formation of heme *b* D109A and the PTM version of this mutant. In the heme *b* protein, a 2-fold excess of H₂O₂ was necessary to achieve full hypochromicity ($k_{\text{app}} = 1.4 \times 10^6 \text{ M}^{-1} \text{ s}^{-1}$) in a monophasic reaction. In the PTM version of the mutant, equimolar addition of hydrogen peroxide already led to a full absorbance decrease at 411 nm in a biphasic transition with k_{app1} and k_{app2} being 3.2×10^7 and $1.4 \times 10^6 \text{ M}^{-1} \text{ s}^{-1}$, respectively. Similar to cyanide binding, preincubation of the E238A mutant with hydrogen peroxide had no impact on the oxidation of the respective ferric proteins by H₂O₂. For both the heme *b* and the PTM protein, Compound I formation was monophasic with very similar calculated apparent bimolecular rate constants of 2.0×10^7 and $2.5 \times 10^7 \text{ M}^{-1} \text{ s}^{-1}$, respectively (Table 1). Double mutant D109A/E238A showed only low hypochromicity (11%) upon Compound I formation; nevertheless, the spectral changes depended on hydrogen peroxide concentration (Figure S1B). An apparent rate constant of $9.3 \times 10^6 \text{ M}^{-1} \text{ s}^{-1}$ could be calculated. However, the kinetics did not change upon pretreatment with hydrogen peroxide ($k_{\text{app}} = 1.0 \times 10^7 \text{ M}^{-1} \text{ s}^{-1}$) (Table 1).

Finally, we investigated the reaction of Compound I with the two-electron donors (X^-) bromide, iodide, and the pseudohalide thiocyanate (reaction 2), because those represent the physiological substrates of the mammalian counterparts of LspPOX. When the halides (X^-) are mixed with preformed Compound I in the sequential-mixing stopped-flow mode, the

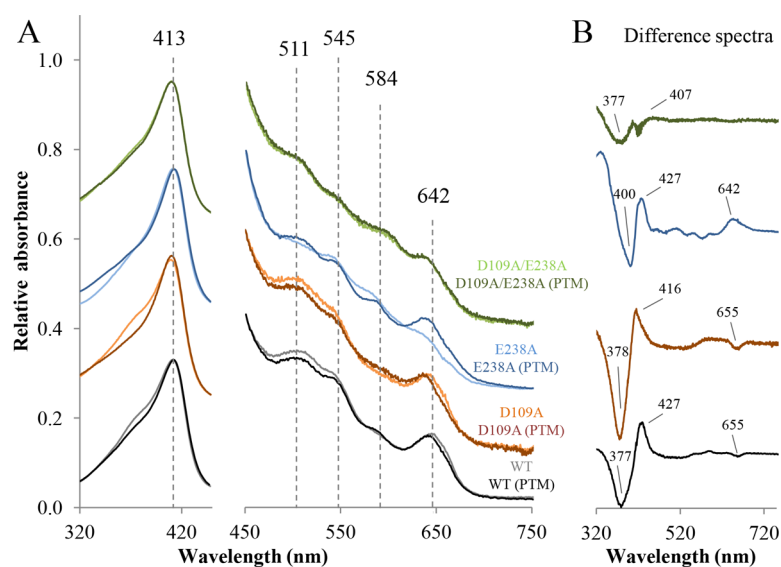


Figure 4. UV-vis spectra of wild-type LspPOX and mutants D109A, E238A, and D109A/E238A in both the heme *b* and PTM forms. (A) UV-vis spectra of heme *b* and PTM forms of wild-type LspPOX and its mutants. Conditions: 3 μM heme protein in 100 mM phosphate buffer (pH 7.0) at 25 $^{\circ}\text{C}$. The PTM versions were obtained by incubation of the heme *b* proteins with a 15-fold stoichiometric excess of H_2O_2 at room temperature for 1 h. The wavelength range between 450 and 750 nm is expanded by a factor of 15 for better visibility. Dashed lines represent the absorbance maxima of wild-type PTM LspPOX: 413, 511, 545, 584, and 642 nm. (B) Difference spectra (PTM form minus heme *b* form) of wild-type LspPOX and its mutants.

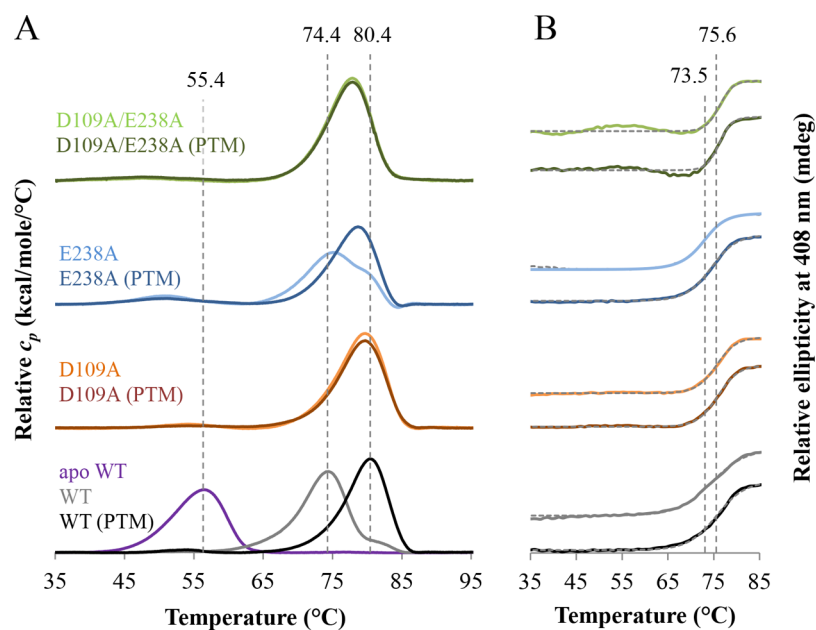


Figure 5. Thermal stability of wild-type LspPOX and mutants D109A, E238A, and D109A/E238A in both the heme *b* and PTM forms. (A) Normalized differential scanning calorimetric (DSC) thermograms of wild-type LspPOX and its mutants after baseline correction. Measurements were performed with 5 μM protein in 100 mM phosphate buffer (pH 7.0) in the range of 35–95 $^{\circ}\text{C}$ using a heating rate of 1 $^{\circ}\text{C}/\text{min}$. Vertical dashed lines have been inserted for presentation of respective melting temperatures of wild-type LspPOX in the apo form (55.4 $^{\circ}\text{C}$), heme *b* form (74.4 $^{\circ}\text{C}$), and PTM form (80.4 $^{\circ}\text{C}$). (B) Temperature-mediated unfolding of LspPOX and its mutants monitored by circular dichroism at a constant wavelength of 408 nm (Soret minimum) in a temperature range of 35–85 $^{\circ}\text{C}$. The protein concentration was 0.5 mg/mL, and measurements were taken with a heating rate of 1 $^{\circ}\text{C}/\text{min}$. Vertical dashed lines represent T_m values of wild-type heme *b* (73.5 $^{\circ}\text{C}$) and PTM LspPOX (75.6 $^{\circ}\text{C}$) reflecting unfolding of the heme cavity. The PTM versions were obtained by incubation of the heme *b* proteins with a 15-fold stoichiometric excess of H_2O_2 at room temperature for 1 h.

corresponding hypohalous acids (HOX and ^-OX) and the ferric protein are formed.

Chloride was unable to reduce Compound I of all four investigated proteins. Figure 8A shows the monophasic reaction between wild-type heme *b* LspPOX Compound I and bromide.

The reaction catalyzed by the heme *b* protein was relatively slow ($2.0 \times 10^2 \text{ M}^{-1} \text{ s}^{-1}$) but significantly accelerated upon induction of PTM, resulting in a biphasic Compound I reduction reaction with a $k_{\text{app}1}$ of $1.3 \times 10^6 \text{ M}^{-1} \text{ s}^{-1}$ and a $k_{\text{app}2}$ of $1.3 \times 10^2 \text{ M}^{-1} \text{ s}^{-1}$ (Figure 8B). Similarly, iodide and

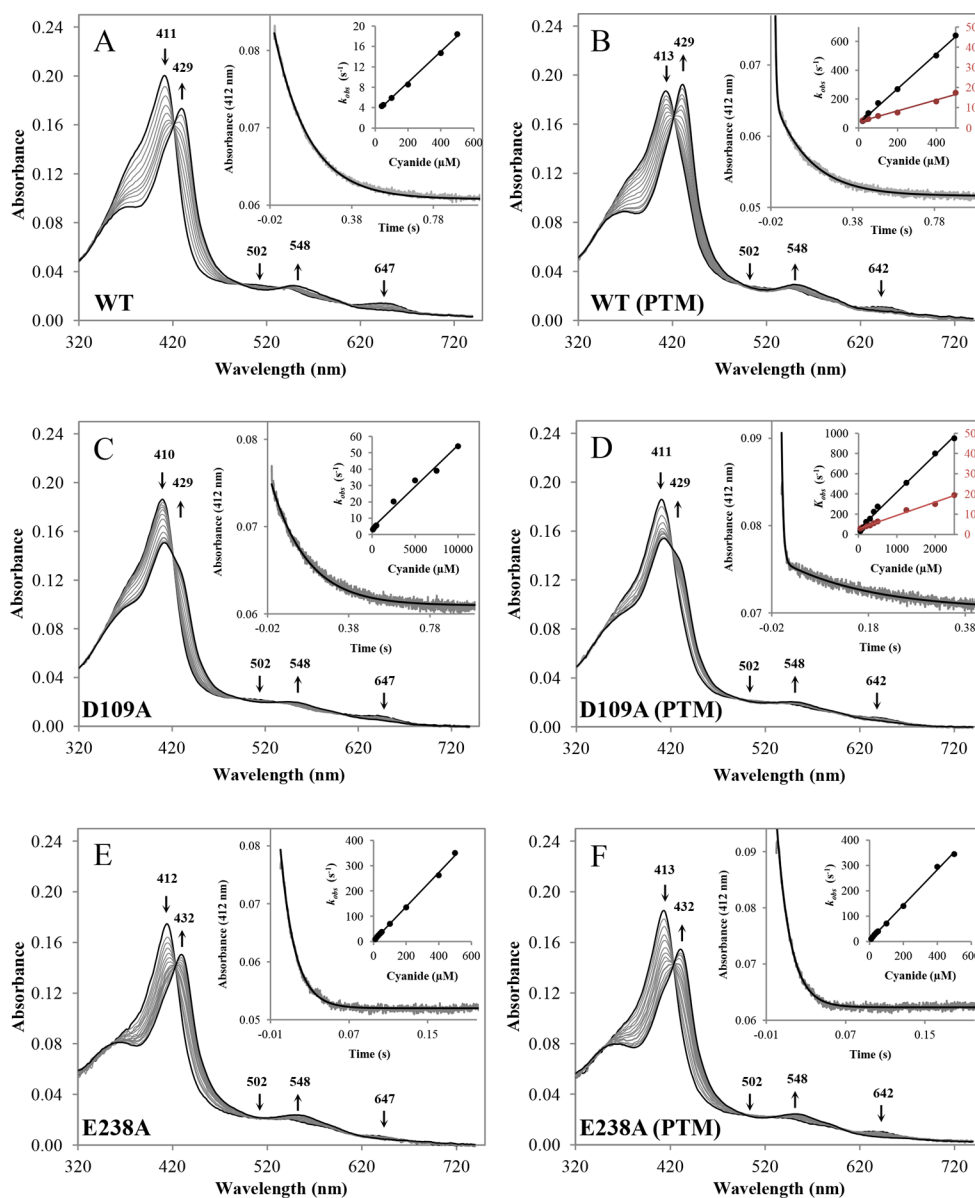


Figure 6. Reaction of ferric wild-type LspPOX and mutants D109A and E238A in both the heme *b* and PTM forms with cyanide. All stopped-flow measurements were performed in 50 mM phosphate buffer (pH 7.0) at 25 °C. (A and B) Spectral transition during reaction of 2 μM wild-type heme *b* and PTM LspPOX with 500 μM cyanide measured in conventional stopped-flow mode. The first bold black spectrum shows the ferric protein in its high-spin state with absorbance maxima at 412 nm (heme *b*) and 413 nm (PTM). The following spectra show the formation of the low-spin complex with an absorbance maximum at 429 nm. Arrows indicate directions of spectral transitions upon cyanide binding. Inset 1 shows a typical time trace at 412 nm upon reaction of 1 μM protein with 100 μM cyanide with a single-exponential fit for the heme *b* version and a double-exponential fit for the PTM form. Inset 2 shows the linear dependence of k_{obs} on cyanide concentration. The apparent association rate constants (k_{on}) were obtained from the slope, and the apparent dissociation rate constant (k_{off}) was calculated from the intercept. (C and D) Spectral transition during reaction of 2 μM heme *b* and PTM forms of D109A with 400 μM cyanide. Conditions and data presentation as in panels A and B. Inset 1 shows a typical time trace at 412 nm upon reaction of 1 μM protein with 400 μM cyanide (single-exponential fit for heme *b* D109A and double-exponential fit for PTM D109A). (E and F) Spectral changes upon reaction of 2 μM heme *b* and PTM E238A with 100 μM cyanide. Conditions and data presentation as in panels A and B. Inset 1 shows a typical time trace at 412 nm upon reaction of 1 μM protein with 100 μM cyanide (single-exponential fit for both forms). The PTM versions were obtained by incubation of the heme *b* proteins with a 15-fold stoichiometric excess of H₂O₂ at room temperature for 1 h.

thiocyanate oxidation by wild-type heme *b* LspPOX Compound I was monophasic (1.4×10^3 and 1.9×10^4 M⁻¹ s⁻¹, respectively) but became biphasic and dramatically faster upon formation of the heme to protein bonds (4.2×10^7 and 2.8×10^5 M⁻¹ s⁻¹, respectively, for iodide and 2.5×10^7 and 4.2×10^6 M⁻¹ s⁻¹, respectively, for thiocyanate) (not shown) (Table 1).

The heme *b* D109A mutant Compound I was a very poor oxidizer of bromide (40 M⁻¹ s⁻¹) (Figure 8C). However, establishment of the covalent ester bond of E238 with the heme increased the reduction rate of Compound I by a factor of 13500 (k_{app1} of 5.4×10^5 M⁻¹ s⁻¹ and k_{app2} of 1.1×10^3 M⁻¹ s⁻¹) (Figure 8D). Heme *b* D109A Compound I oxidized iodide and thiocyanate in monophasic reactions with apparent rate constants of 3.2×10^3 and 3.0×10^3 M⁻¹ s⁻¹, respectively,

Table 1. Apparent Second-Order Rate Constants ($\times 10^4 \text{ M}^{-1} \text{ s}^{-1}$) of Heme *b* and PTM Wild-Type LspPOX and Mutants D109A, E238A, and D109A/E238A for Cyanide Binding and Compound I (Cpd I) Formation and Reduction^a

$E^{\circ'}$ [Fe(III)/Fe(II)] (mV)	WT	WT (PTM)	D109A	D109A (PTM)	E238A	E238A (PTM)	D109A/E238A	D109A/E238A (PTM)
	-158 ± 10	nd ^b	-145 ± 10	nd ^b	-198 ± 10	-209 ± 10	-227 ± 10	-212 ± 10
Cyanide Binding								
k_{on1}	–	121	–	37	67	70	nd ^b	nd ^b
k_{off1} (s^{-1})	–	31.1	–	48	3.2	4.9	nd ^b	nd ^b
K_{D1} (μM)	–	25.7	–	129	4.8	7.1	nd ^b	nd ^b
k_{on2}	3	2.7	0.5	0.66	–	–	–	–
k_{off2} (s^{-1})	2.9	3	3.9	2.8	–	–	–	–
K_{D2} (μM)	96.3	111.9	780	424	–	–	–	–
Cpd I Formation								
k_{app1}	–	6000	–	3200	2000	2520	930	1020
k_{app2}	260	245	142	143	–	–	–	–
Cpd I Reduction								
chloride	–	–	–	–	–	–	–	–
bromide	–	–	–	–	–	–	–	–
k_{app1}	–	126	–	54	1.1	2.1	nd ^b	nd ^b
k_{app2}	0.02	1.16	0.04	0.11	–	–	nd ^b	nd ^b
iodide	–	–	–	–	–	–	–	–
k_{app1}	–	4190	–	1540	1110	2860	nd ^b	nd ^b
k_{app2}	0.14	28.5	0.32	3	–	53	nd ^b	nd ^b
thiocyanate	–	–	–	–	–	–	–	–
k_{app1}	–	2450	–	816	570	1185	nd ^b	nd ^b
k_{app2}	1.86	41.6	0.3	1.32	–	7.9	nd ^b	nd ^b

^aAdditionally, the standard reduction potential of the Fe(III)/Fe(II) couple is given. ^bNot determined.

whereas after PTM, the rates of both iodide and thiocyanate oxidation were significantly enhanced (1.5×10^7 and $3.0 \times 10^4 \text{ M}^{-1} \text{ s}^{-1}$, respectively, for iodide and 8.2×10^6 and $1.3 \times 10^4 \text{ M}^{-1} \text{ s}^{-1}$, respectively, for thiocyanate) (not shown).

As already seen in the studies of cyanide binding and Compound I formation, conversion of the heme *b* form of E238A to the PTM version had no impact on catalysis. In both cases, bromide oxidation was monophasic and occurred at similar rates (k_{app} values of 1.1×10^4 and $2.1 \times 10^4 \text{ M}^{-1} \text{ s}^{-1}$, respectively) (Figure 8D,E). This applies also for iodide (1.1×10^7 and $2.9 \times 10^7 \text{ M}^{-1} \text{ s}^{-1}$, respectively) and thiocyanate oxidation (5.7×10^6 and $1.2 \times 10^7 \text{ M}^{-1} \text{ s}^{-1}$, respectively) (not shown).

Double mutant D109A/E238A shows no halogenation reactions at all. Preformed Compound I of D109A/E238A showed no spectral changes upon being mixed with halides (Figure S1C).

Impact of PTM on the Standard Reduction Potential of the Fe(III)/Fe(II) Couple. Finally, spectroelectrochemical studies of the heme *b* and PTM forms of wild-type LspPOX and the mutants were performed to elucidate the standard reduction potential ($E^{\circ'}$) of the Fe(III)/Fe(II) couple (Table 1). The $E^{\circ'}$ values of the heme *b* forms were calculated to be $-0.158 \pm 0.005 \text{ V}$ (wild-type), $-0.145 \pm 0.010 \text{ V}$ (D109A), and $-0.198 \pm 0.011 \text{ V}$ (E238A). Unfortunately, because of the presence of two protein species in solution [which reflects the heterogeneity induced by PTM (see above)], we were not able to calculate reliable $E^{\circ'}$ values for the PTM forms of both the wild-type protein and mutant D109A. In the case of mutant E238A, formation of the covalent bond between the modified heme and D109 had no impact on the standard reduction potential of the Fe(III)/Fe(II) couple (PTM form, $-0.209 \pm 0.010 \text{ V}$). Likewise, incubation with H_2O_2 did not significantly alter the $E^{\circ'}$ value of the double mutant (heme *b*, $-0.227 \pm 0.010 \text{ V}$; PTM form, $-0.212 \pm 0.010 \text{ V}$).

DISCUSSION

Reconstructing the phylogenetic relationships of the main evolutionary lines of the mammalian peroxidases lactoperoxidase and myeloperoxidase revealed the presence of novel bacterial families within the peroxidase-cyclooxygenase superfamily.² By studying the peroxidase from the cyanobacterium *Lyngbya* sp. PCC 8106, we could demonstrate that this enzyme exhibits a high thermal stability, shows LPO-like spectral features, and possesses a high bromination activity.²⁰ Most importantly, both sequence alignment and biochemical analysis suggested that the recombinant protein purified from *E. coli* exhibits two heme to protein ester linkages like all vertebrate peroxidases investigated so far.^{1,2} Detailed mass spectrometric analysis demonstrated that both D109 and E238 are involved in those ester bonds.^{1,2} Furthermore, it could be demonstrated that the recombinant peroxidase isolated from *E. coli* cell cultures is heterogeneous with respect to the establishment of covalent heme to protein bonds and that incubation with hydrogen peroxide could increase the fraction with fully established linkages.²¹ This supports the hypothesis that these posttranslational modifications occur autocatalytically and need H_2O_2 -mediated Compound I formation for induction of the subsequent free radical mechanisms⁹ as demonstrated for LPO,^{24,25} EPO,²⁶ human peroxidase 1,^{27,28} and engineered horseradish peroxidase.²⁹ Moreover, we could demonstrate that the posttranslationally modified peroxidase exhibited a bromide oxidation rate higher than that of the protein isolated from *E. coli* without subsequent incubation with H_2O_2 .²¹ These findings raised the question about the functional role of these heme modifications. From studies of mammalian enzymes, it was concluded that these linkages contribute to heme distortion,^{4,12} more positive reduction potentials of relevant redox intermediates,^{13,14,30–32} higher oxidation capacity,¹⁴ and/or protection of heme from produced hypohalous acid.^{33,34} Whereas the

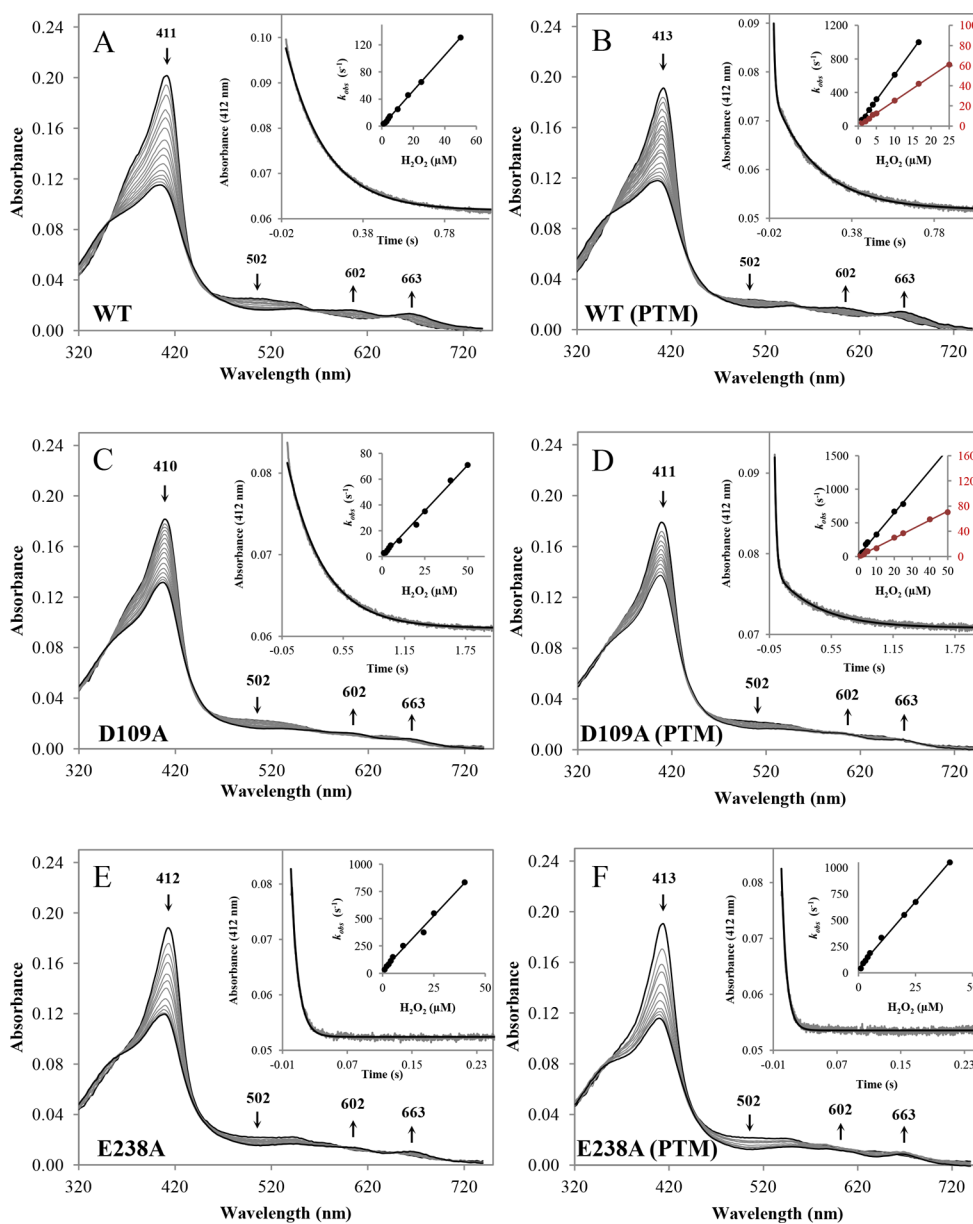


Figure 7. Reaction of ferric wild-type LspPOX and mutants D109A and E238A in both the heme *b* and PTM forms with hydrogen peroxide. All measurements were performed in 50 mM phosphate buffer (pH 7.0) at 25 °C. (A and B) Spectral changes upon reaction of 2 μM wild-type (WT) heme *b* and PTM LspPOX with 4 μM H_2O_2 measured in conventional stopped-flow mode. The first spectra (bold black) represent the ferric proteins in the resting state. The following spectra represent the formation of Compound I following a typical decrease in the absorbance in the Soret region. Inset 1 shows a typical time trace at 412 nm upon reaction of 1 μM enzyme with 2 μM H_2O_2 . Inset 2 shows the linear dependence of k_{obs} on H_2O_2 concentration. The apparent bimolecular rate constants (k_{app}) were obtained from the slope of the regression line. (C and D) Spectral changes upon reaction of 2 μM heme *b* and PTM forms of D109A with 4 μM H_2O_2 . Conditions and data presentation as in panels A and B. Inset 1 shows a typical time trace at 412 nm upon reaction of 1 μM mutant with 2 μM H_2O_2 . (E and F) Spectral changes upon reaction of 1 μM heme *b* and PTM forms of E238A with 2 μM H_2O_2 . Conditions and data presentation as in panels A and B. Inset 1 shows a typical time trace at 412 nm upon reaction of 1 μM mutant with 4 μM H_2O_2 .

unique role of the electron-withdrawing sulfonium ion link exclusively found in MPO (besides the two ester bonds) in catalysis has been demonstrated in numerous publications,^{2–5,9,11,14,17–19} the individual contribution of the ester bonds between conserved aspartate and glutamate residues on structure and catalysis remained mainly unclear.

In this work, LspPOX served as a model peroxidase that shows an ~30% overall amino acid identity and almost 100% identity regarding active site residues with LPO (Figure 9) and can easily be produced in *E. coli* and thus genetically engineered. For the first time, the pure heme *b* version and

the PTM version could be studied in a comparative way. As demonstrated by CD spectroscopy in the near- and far-UV regions, neither the PTM nor the exchange of D109 or E238 caused rearrangement of the secondary or tertiary structure, but both UV–vis and CD in the visible region clearly showed differences in the active site architecture of the studied variants that were reflected by differences in the catalytic properties.

The autocatalytic conversion of heme *b* to the modified heme and formation of the ester bonds are relatively slow and need a slight excess of hydrogen peroxide. However, a >20-fold stoichiometric excess of H_2O_2 led to bleaching of heme *b*

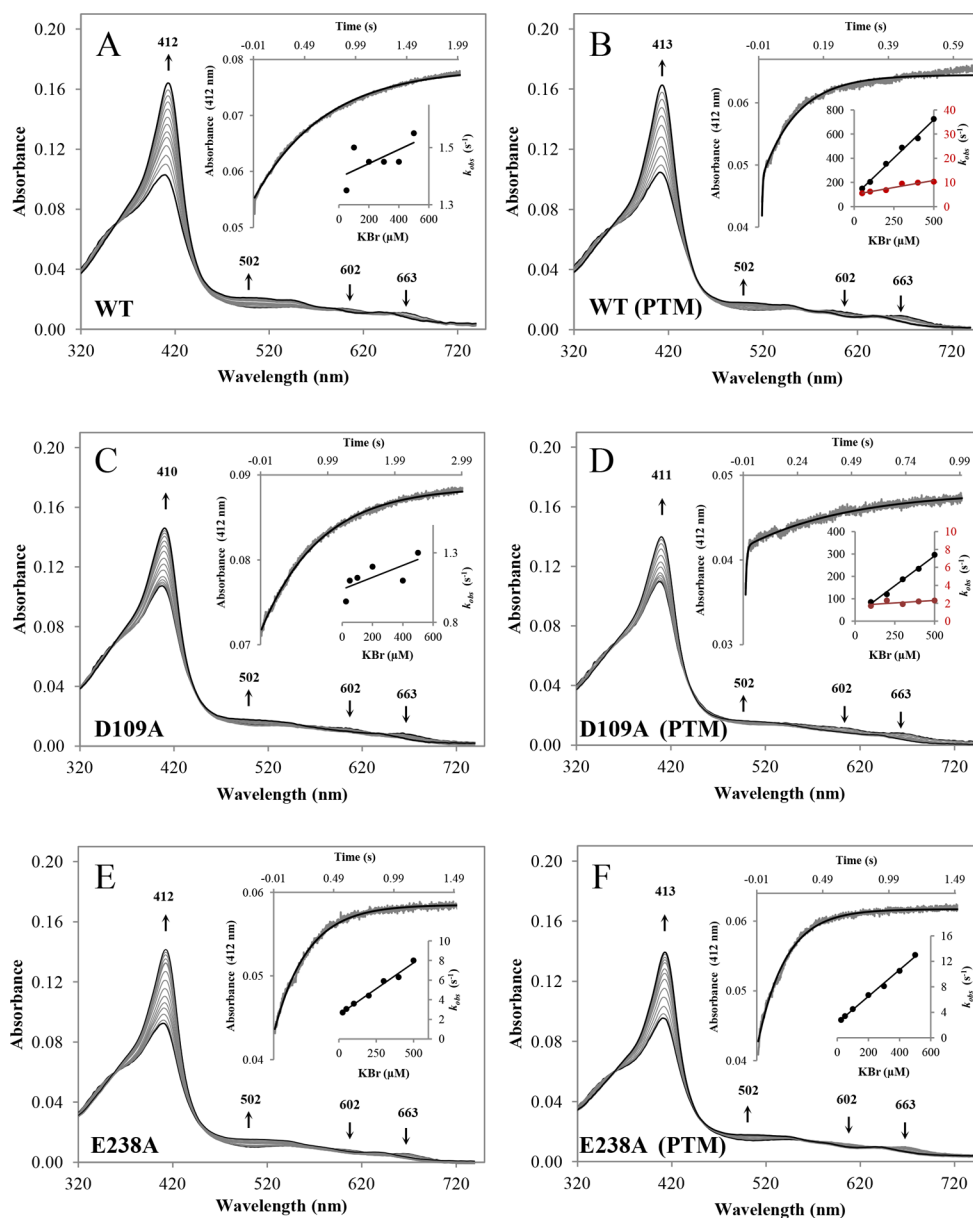


Figure 8. Reaction of Compound I of wild-type LspPOX and mutants D109A and E238A in both the heme *b* and PTM forms with bromide. (A and B) Spectral transition after adding 50 μM bromide to 2 μM wild-type heme *b* and PTM LspPOX in the sequential stopped-flow mode. All measurements were performed in 50 mM phosphate buffer (pH 7.0) at 25 °C. Compound I was performed using 4 μM hydrogen peroxide and a 400 ms delay time for heme *b* LspPOX and a 300 ms delay time for the PTM form. Inset 1 shows a typical time trace at 412 nm of 1 μM Compound I with 300 μM bromide. Inset 2 shows the linear dependence of the pseudo-first-order constant (k_{obs}) on bromide concentration. The corresponding k_{app} values were obtained from the slope of the linear regression. (C and D) Spectral transition after adding 50 μM bromide to 2 μM heme *b* and PTM forms of D109A. Compound I was performed using 4 μM hydrogen peroxide and a 500 ms delay time for heme *b* D109A and 2 μM H₂O₂ and a 300 ms delay time for the PTM form. Inset 1 shows a typical time trace at 412 nm of 1 μM Compound I with 400 μM bromide. (E and F) Spectral transition after adding 50 μM bromide to 2 μM heme *b* and PTM forms of E238A. Compound I was performed using 2 μM hydrogen peroxide and a 100 ms delay time for heme *b* and PTM E238A. Inset 1 shows a typical time trace at 412 nm of 1 μM Compound I with 100 μM bromide.

without the establishment of covalent bonds. Because the PTM involves Compound I formation, which is also very fast in wild-type heme *b* LspPOX (this work), it is reasonable to assume that the following radical process that involves oxidation of the carboxylic groups is the rate-limiting step. During our stopped-flow studies of the Compound I formation of the heme *b* proteins, we saw no indication of Compound II formation that should be an intermediate during the postulated autocatalytic radical process (see above).

In the wild-type protein, formation of the heme to protein bonds increased the rates for cyanide binding and Compound I

formation by factors of 40 and 23, respectively. For both reactions, the position of the distal histidine (H110) is crucial as it acts as a proton acceptor for both HCN and H₂O₂ and supports the heterolytic cleavage of hydrogen peroxide. Because it is the neighboring amino acid of D109, which is covalently bound to the heme after PTM, it is reasonable to assume that this structural rearrangement optimizes the position of H110 for catalysis (Figure 9). This is also reflected by the affinity of cyanide for the PTM protein that is significantly higher than that of the heme *b* version. The determined apparent rate constants for cyanide binding and Compound I formation of

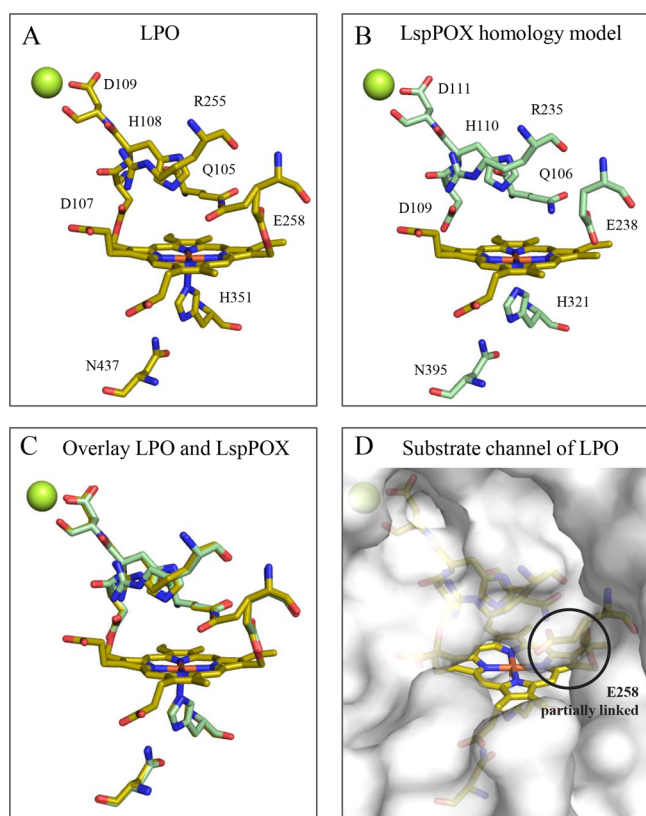


Figure 9. Active site structures of lactoperoxidase and LspPOX. Comparison of active site structures of lactoperoxidase (LPO, yellow) and a homology model of wild-type LspPOX (pale green). (A) Active site structure of bovine LPO (Protein Data Bank entry 5wv3) showing the split conformation of Glu258, partially linked to the heme group. The Ca^{2+} ion is colored green. (B) Homology model of LspPOX without covalent heme to protein bonds. This model was built with the online module Protein Model Portal (PMP) provided on the expasy homepage (<http://www.expasy.org/>). (C) Overlay of the bovine LPO and LspPOX homology model, revealing the conservation of the entire active site. (D) View into the substrate channel of bovine LPO, showing how the partially unbound Glu258 sticks out into the substrate access channel.

the mature bacterial peroxidase are very similar to the rates reported for MPO,³⁵ LPO,³⁶ and EPO,³⁷ suggesting similar active site architectures and modifications induced by PTM. Moreover, the structural rearrangement by bond formation between D109 and the prosthetic group should also impact the nearby Ca^{2+} -binding site because the ligand D111 is part of the most characteristic amino acid motif of this superfamily, namely -X104-G105-Q106-X107-X108-D109-H110-D111-X112-, with Q106 being also fully conserved and involved in halide binding (Figure 9A–C).^{18,38} As a consequence of PTM, the T_m values of the wild-type protein and the E238A variant are increased by 6 and 3.4 °C, respectively.

Besides the increase in the rates of formation of the cyanide complex and of Compound I formation, oxidation of halides and thiocyanate was significantly enhanced when the wild-type heme *b* protein was posttranslationally modified. In contrast to chloride, bromide can react with Compound I by donating two electrons, thereby forming the ferric enzyme and releasing hypobromous acid. The reaction is slow with the heme *b* protein but enhanced by a factor of 6300 due to PTM. Additionally, iodide and thiocyanate oxidation became

significantly faster by 3–4 orders of magnitude after incubation of the bacterial enzyme with H_2O_2 .

Halide and thiocyanate binding occurs at the distal heme site and involves a pronounced hydrogen bonding network that includes Q106, H110, and R235. The latter is part of the second conserved distal site motif that also includes E238 involved in ester bond formation (-X234-R235-X236-X237-E238-X239) (Figure 9). These findings clearly demonstrate that formation of the heme to protein ester bonds optimizes binding and oxidation of Br^- , I^- , and SCN^- at the distal heme cavity.

Furthermore, our data clearly demonstrate that elimination of E238 has almost no impact on the structural rearrangement that occurs during PTM. Comparison of the heme *b* and PTM forms of mutant E238A showed very similar E^o values of the Fe(III)/Fe(II) couple as well as similar kinetics of interconversion of redox intermediates, including cyanide binding, Compound I formation, and Compound I reduction. Moreover, the absolute values of the obtained apparent rate constants were very similar to those for the mature (PTM) wild-type protein. This was also reflected by almost identical spectral features of the wild-type protein and mutant E238A. Elimination of glutamate 238 still allowed formation of the ester linkage between D109 and the modified heme as determined by mass spectrometry. However, formation of this bond apparently did not change the structure of the heme or the distal protein environment of E238A, clearly suggesting that the carboxylate group of D109 is already placed in the vicinity of the 5-methyl substituent in heme *b* E238A. The autocatalytic free radical PTM mechanism includes formation of a carboxylate radical by Compound I followed by the transfer of hydrogen from the methyl substituent to the carboxylate radical, which needs the proximity of the involved reaction partners. As already outlined above, in contrast to E238A, the wild-type protein experienced a pronounced structural rearrangement during PTM most probably because of the subsequent formation of two ester bonds between D109 and E238 with the 5- and 1-methyl substituents of the prosthetic group. In the E238A mutant, the degree of conformational freedom at position 238 is increased, which apparently already allows the occupancy of the identical conformation of D109 in the heme *b* and PTM form, whereas this is not possible in the wild-type protein.

Interestingly, the X-ray structures of both native mature leukocyte MPO⁴ or recombinant proMPO³⁹ and bovine LPO⁴⁰ show always 100% ester bond formation involving the respective conserved aspartic acid, whereas the electron density of the glutamate residue is always split (Figure 9A,D). This heterogeneity of native mammalian peroxidases purified from natural sources (neutrophils or milk) is not reflected by spectral properties or (biphasic) kinetics,^{35,36} suggesting that (i) there is no difference in the overall heme cavity architecture between the protein fractions with unmodified glutamate or glutamate involved in the second ester bond formation and (ii) the heterogeneity seen in the PTM version of wild-type LspPOX most probably derives from conformational changes around aspartate 109.

In contrast to E238A, mutant D109A showed significant structural differences in the heme cavity between the heme *b* form and the PTM version. Mass spectrometry demonstrated that ~67% of the E238 residues became involved in ester bond formation during posttranslational modification of this mutant. Incubation of heme *b* D109A with hydrogen peroxide

significantly improved and accelerated cyanide binding as well as Compound I formation and reduction, reaching wild-type-like apparent rate constants. Because of the absence of D109 and the increased flexibility around position 109, the prosthetic group seems to be incorporated incorrectly immediately after reconstitution of the apoprotein with heme, which was also reflected by a Soret maximum at 404 nm in the beginning that slowly changed to 411 nm with increasing sample age, thus underlining the massive structural rearrangement. As determined by mass spectrometry, the 404 and 411 nm species still contained 100% heme *b* that could be converted to the PTM version by H₂O₂. In this process, the E238 to heme bond was formed that, finally, seemed to rearrange the prosthetic group into a wild-type-like conformation. Because E238 is located close to the substrate entrance channel (Figure 9D), it seems to impede to some extent the access of ligands and substrate to the active site. Upon PTM, the conformational flexibility is lost, which is also reflected by significantly increased rates of ligand binding as well as iodide and thiocyanate oxidation rates. Similar conclusions were also drawn for the respective myeloperoxidase mutants.^{41,42}

In summary, the LPO-like bacterial peroxidase from *Lyngbya* sp. PCC 8106 was shown to be a perfect model peroxidase for studying the consequences of PTMs that are typical for the whole peroxidase-cyclooxygenase superfamily. The bacterial protein is unglycosylated and can easily be produced in *E. coli* as the apoprotein, 100% reconstituted to the heme *b* form, and autocatalytically and posttranslationally modified to the mature enzyme by a slow process that needs the addition of hydrogen peroxide. As a consequence, two heme to protein ester bonds between conserved aspartate and glutamate residues and the modified prosthetic group are established. We could demonstrate that during this PTM significant structural rearrangements at the distal heme cavity occurred that increased the rate of formation and the stability of the cyanide complex as well as significantly increased the rates for Compound I formation and reduction by two-electron donors like bromide, iodide, and thiocyanate. Mutational analysis showed that ester bond formation at each site occurs independently and elimination of E238 resulted in enzymatic features very similar to those of mature (PTM) wild-type peroxidase. By contrast, mutation at D109 significantly altered the heme *b* protein structure and negatively affected the catalytic properties. However, upon induction of PTM by H₂O₂, the respective D109A mutant could be rescued and also exhibited wild-type-like catalytic properties. Formation of those ester bonds significantly improved bromide oxidation but did not allow the production of hypochlorous acid. The latter reaction is catalyzed by only myeloperoxidase (member of family 1 of the peroxidase-cyclooxygenase superfamily) that forms a unique electron-withdrawing sulfonium ion bond between a conserved methionine and the 2-vinyl substituent of heme in addition to the two heme to protein ester bonds.

■ ASSOCIATED CONTENT

📄 Supporting Information

The Supporting Information is available free of charge on the ACS Publications website at DOI: 10.1021/acs.biochem.7b00632.

List of primers used for construction of mutants D109A, E238A, and D109A/E238A by site-directed mutagenesis (Table S1), conditions and delay times for pre-steady

state kinetics followed by stopped-flow spectroscopy in sequential mixing mode (Table S2), and reaction of ferric D109A/E238A with cyanide and hydrogen peroxide and reduction of D109A/E238A Compound I with bromide followed by stopped-flow spectroscopy in sequential mixing mode (Figure S1) (PDF)

■ AUTHOR INFORMATION

Corresponding Author

*Phone: +43-1-47654-77273. Fax: +43-1-47654-77259. E-mail: christian.obinger@boku.ac.at.

ORCID

Christian Obinger: 0000-0002-7133-3430

Funding

This project was supported by the Austrian Science Fund, FWF [Doctoral program BioToP-Biomolecular Technology of Proteins (W1224) and Project P25538].

Notes

The authors declare no competing financial interest.

■ ABBREVIATIONS

heme *b* LspPOX, recombinant peroxidase from *Lyngbya* sp. PCC 8106 carrying unmodified heme *b* in the active site; PTM, posttranslational modification; PTM LspPOX, recombinant peroxidase from *Lyngbya* sp. PCC 8106 posttranslationally modified by incubation with a 15-fold stoichiometric excess of hydrogen peroxide; MPO, myeloperoxidase; LPO, lactoperoxidase; EPO, eosinophil peroxidase; TPO, thyroid peroxidase; X⁻, halide; HOX, hypohalous acid; E^{o'}, standard reduction potential; ECD, electronic circular dichroism; DSC, differential scanning calorimetry.

■ REFERENCES

- (1) Zamocky, M., Hofbauer, S., Schaffner, I., Gasselhuber, B., Nicolussi, A., Soudi, M., Pirker, K. F., Furtmüller, P. G., and Obinger, C. (2015) Independent evolution of four heme peroxidase superfamilies. *Arch. Biochem. Biophys.* 574, 108–119.
- (2) Zamocky, M., Jakopitsch, C., Furtmüller, P. G., Dunand, C., and Obinger, C. (2008) The peroxidase-cyclooxygenase superfamily. Reconstructed evolution of critical enzymes of the innate immune system. *Proteins: Struct., Funct., Genet.* 72, 589–605.
- (3) Zederbauer, M., Furtmüller, P. G., Brogioni, S., Jakopitsch, C., Smulevich, G., and Obinger, C. (2007) Heme to protein linkages in mammalian peroxidases: impact on spectroscopic, redox and catalytic properties. *Nat. Prod. Rep.* 24, 571–584.
- (4) Carpena, X., Vidossich, P., Schroettner, K., Calisto, B. M., Banerjee, S., Stampfer, J., Soudi, M., Furtmüller, P. G., Rovira, C., Fita, I., and Obinger, C. (2009) Essential role of proximal histidine-asparagine interaction in mammalian peroxidases. *J. Biol. Chem.* 284, 25929–25937.
- (5) Nauseef, W. M. (2014) Myeloperoxidase in human neutrophil host defence. *Cell. Microbiol.* 16, 1146–1155.
- (6) Ihalin, R., Loimaranta, V., and Tenovou, J. (2006) Origin, structure, and biological activities of peroxidases in human saliva. *Arch. Biochem. Biophys.* 445, 261–268.
- (7) Malik, A., and Batra, J. K. (2012) Antimicrobial activity of human eosinophil granule proteins: involvement in host defence against pathogens. *Crit. Rev. Microbiol.* 38, 168–181.
- (8) Ruf, J., and Carayon, P. (2006) Structural and functional aspects of thyroid peroxidase. *Arch. Biochem. Biophys.* 445, 269–277.
- (9) Ortiz de Montellano, P. R. (2016) *Heme peroxidases: self-processing of peroxidases* (Raven, E., and Dunford, B., Eds) RSC Metallobiology Series No. 4, pp 3–30, The Royal Society of Chemistry, Cambridge, U.K.

- (10) Zbylut, S. D., and Kincaid, J. R. (2002) Resonance Raman evidence for protein-induced out-of-plane distortion of the heme prosthetic group of mammalian lactoperoxidase. *J. Am. Chem. Soc.* 124, 6751–6758.
- (11) Brogioni, S., Feis, A., Marzocchi, M. P., Zederbauer, M., Furtmüller, P. G., Obinger, C., and Smulevich, G. (2006) Resonance assignment of myeloperoxidase and the selected mutants Asp94Val, and Met242Thr. Effect of heme distortion. *J. Raman Spectrosc.* 37, 263–276.
- (12) Singh, A. K., Singh, N., Sharma, S., Singh, S. B., Kaur, P., Bhushan, A., Srinivasan, A., and Singh, T. P. (2008) Crystal structure of lactoperoxidase at 2.4 Å resolution. *J. Mol. Biol.* 376, 1060–1075.
- (13) Battistuzzi, G., Bellei, M., Bortolotti, C. A., and Sola, M. (2010) Redox properties of heme peroxidases. *Arch. Biochem. Biophys.* 500, 21–36.
- (14) Battistuzzi, G., Stampfer, J., Bellei, M., Vlasits, J., Soudi, M., Furtmüller, P. G., and Obinger, C. (2011) Influence of the covalent heme–protein bonds on the redox thermodynamics of human myeloperoxidase. *Biochemistry* 50, 7987–7994.
- (15) Burner, U., Jantschko, W., and Obinger, C. (1999) Kinetics of oxidation of aliphatic and aromatic thiols by myeloperoxidase compounds I and II. *FEBS Lett.* 443, 290–296.
- (16) Burner, U., Furtmüller, P. G., Kettle, A. J., Koppenol, W., and Obinger, C. (2000) Mechanism of reaction of myeloperoxidase with nitrite. *J. Biol. Chem.* 275, 20597–20601.
- (17) Jantschko, W., Furtmüller, W., Allegra, M., Livrea, M. A., Jakopitsch, C., Regelsberger, G., and Obinger, C. (2002) Redox intermediates of plant and mammalian peroxidases: a comparative transient-kinetic study of their reactivity toward indole derivatives. *Arch. Biochem. Biophys.* 398, 12–22.
- (18) Furtmüller, P. G., Zederbauer, M., Jantschko, W., Helm, J., Bogner, M., Jakopitsch, C., and Obinger, C. (2006) Active site structure and catalytic mechanisms of human peroxidases. *Arch. Biochem. Biophys.* 445, 199–213.
- (19) Arnhold, J., Monzani, E., Furtmüller, P. G., Zederbauer, M., Casella, L., and Obinger, C. (2006) Kinetics and thermodynamics of halide and nitrite oxidation by heme peroxidases. *Eur. J. Inorg. Chem.* 2006, 3801–3811.
- (20) Auer, M., Gruber, C., Bellei, M., Pirker, K., Zamocky, M., Kroiß, D., Teufer, A. S., Hofbauer, S., Soudi, M., Battistuzzi, G., Furtmüller, P. G., and Obinger, C. (2013) A stable bacterial peroxidase with novel halogenating activity and an autocatalytically linked heme prosthetic group. *J. Biol. Chem.* 288, 27181–27199.
- (21) Auer, M., Nicolussi, A., Schütz, G., Furtmüller, P. G., and Obinger, C. (2014) How covalent heme to protein bonds influence the formation and reactivity of redox intermediates of a bacterial peroxidase. *J. Biol. Chem.* 289, 31480–31491.
- (22) Banerjee, S., Furtmüller, P. G., and Obinger, C. (2011) Bovine lactoperoxidase – a versatile one- and two-electron catalyst of high structural and thermal stability. *Biotechnol. J.* 6, 231–243.
- (23) Sharma, S., Singh, A. K., Kaushik, S., Sinah, M., Singh, R. P., Sharma, P., Sirohi, H., Kaur, P., and Singh, T. P. (2013) Lactoperoxidase: structural insights into the function, ligand binding and inhibition. *Int. J. Biochem. Mol. Biol.* 4, 108–128.
- (24) DePillis, G. D., Ozaki, S., Kuo, J. M., Maltby, D. A., and Ortiz de Montellano, P. R. (1997) Autocatalytic processing of heme by lactoperoxidase produces the native protein-bound prosthetic group. *J. Biol. Chem.* 272, 8857–8860.
- (25) Colas, C., Kuo, J. M., and Ortiz de Montellano, P. R. (2002) Asp 225 and Glu 375 in autocatalytic attachment of the prosthetic heme group of lactoperoxidase. *J. Biol. Chem.* 277, 7191–7200.
- (26) Oxvig, C., Thomsen, A. R., Overgaard, M. T., Sorensen, E. S., Højrup, P., Bjerrum, M. J., Gleich, G. J., and Sottrup-Jensen, L. (1999) Biochemical evidence for heme linkage through esters with Asp-93 and Glu-241 in human eosinophil peroxidase. The ester with Asp-93 is only partially formed in vivo. *J. Biol. Chem.* 274, 16953–16958.
- (27) Soudi, M., Paumann-Page, M., Delporte, C., Pirker, K. F., Bellei, M., Edenhofer, E., Stadlmayr, G., Battistuzzi, G., Zouaoui Boudjeltia, K., Furtmüller, P. G., Van Antwerpen, P., and Obinger, C. (2015) Multidomain human peroxidase I is a highly glycosylated and stable homotrimeric high-spin ferric peroxidase. *J. Biol. Chem.* 290, 10876–10890.
- (28) Paumann-Page, M., Katz, R. S., Bellei, M., Schwartz, I., Edenhofer, E., Sevcnikar, B., Soudi, M., Hofbauer, S., Battistuzzi, G., Furtmüller, P. G., and Obinger, C. (2017) Kinetics of interconversion of redox intermediates of truncated human peroxidase I mediated by hydrogen peroxide, bromide, iodide and thiocyanate. *J. Biol. Chem.* 292, 4583–4592.
- (29) Colas, C., and Ortiz de Montellano, P. R. (2004) Horseradish peroxidase mutants that autocatalytically modify their prosthetic heme group: insights into mammalian peroxidase heme-protein covalent bonds. *J. Biol. Chem.* 279, 24131–24140.
- (30) Battistuzzi, G., Bellei, M., Zederbauer, M., Furtmüller, P. G., Sola, M., and Obinger, C. (2006) Redox thermodynamics of the Fe(III)/Fe(II) Couple of human myeloperoxidase in its high-spin and low-spin forms. *Biochemistry* 45, 12750–12755.
- (31) Battistuzzi, G., Bellei, M., Vlasits, J., Banerjee, S., Furtmüller, P. G., Sola, M., and Obinger, C. (2010) Redox thermodynamics of lactoperoxidase and eosinophil peroxidase. *Arch. Biochem. Biophys.* 494, 72–77.
- (32) Furtmüller, P. G., Arnhold, J., Jantschko, W., Zederbauer, M., Jakopitsch, C., and Obinger, C. (2005) Standard reduction potentials of all couples of the peroxidase cycle of lactoperoxidase. *J. Inorg. Biochem.* 99, 1220–1229.
- (33) Huang, L., and Ortiz de Montellano, P. R. (2006) Heme-protein covalent bonds in peroxidases and resistance to heme modification during halide oxidation. *Arch. Biochem. Biophys.* 446, 77–83.
- (34) Huang, L., Wojciechowski, G., and Ortiz de Montellano, P. R. (2006) Role of heme-protein covalent bonds in mammalian peroxidases. Protection of the heme by a single engineered heme-protein link in horseradish peroxidase. *J. Biol. Chem.* 281, 18983–18988.
- (35) Furtmüller, P. G., Burner, U., and Obinger, C. (1998) Reaction of human myeloperoxidase compound I with chloride, bromide, iodide, and thiocyanate. *Biochemistry* 37, 17923–17930.
- (36) Furtmüller, P. G., Jantschko, W., Regelsberger, G., Jakopitsch, C., Arnhold, J., and Obinger, C. (2002) Reaction of lactoperoxidase compound I with halides and thiocyanate. *Biochemistry* 41, 11895–11900.
- (37) Furtmüller, P. G., Burner, U., Regelsberger, G., and Obinger, C. (2000) Spectral and kinetic studies on the formation of eosinophil peroxidase compound I and its reaction with halides and thiocyanate. *Biochemistry* 39, 15578–15584.
- (38) Blair-Johnson, M., Fiedler, T., and Fenna, R. (2001) Human myeloperoxidase: structure of a cyanide complex and its interaction with bromide and thiocyanate substrates at 1.9 Å resolution. *Biochemistry* 40, 13990–13997.
- (39) Grishkovskaya, I., Paumann-Page, M., Tscheliessnig, R., Hofbauer, S., Stampfer, J., Soudi, M., Sevcnikar, B., Oostenbrink, C., Furtmüller, P. G., Djinović-Carugo, K., Nauseef, W. M., and Obinger, C. (2017) Structure of human promyeloperoxidase (proMPO) and the role of the propeptide for processing and maturation. *J. Biol. Chem.* 292, 8244–8261.
- (40) Singh, P. K., Sirohi, H. V., Iqbal, N., Tiwari, P., Kaur, P., Sharma, S., and Singh, T. P. (2017) Structure of bovine lactoperoxidase with a partially linked heme moiety at 1.98 Å resolution. *Biochim. Biophys. Acta, Proteins Proteomics* 1865, 329–335.
- (41) Zederbauer, M., Jantschko, W., Neugschwandtner, K., Jakopitsch, C., Moguilevsky, N., Obinger, C., and Furtmüller, P. G. (2005) Role of covalent glutamic acid 242-heme linkage in the formation and reactivity of redox intermediates of human myeloperoxidase. *Biochemistry* 44, 6482–6491.
- (42) Zederbauer, M., Furtmüller, P. G., Bellei, M., Stampfer, J., Jakopitsch, C., Battistuzzi, G., Moguilevsky, N., and Obinger, C. (2007) Disruption of the aspartate to heme ester linkage in human myeloperoxidase: impact on ligand binding, redox chemistry, and interconversion of redox intermediates. *J. Biol. Chem.* 282, 17041–17052.

SUPPLEMENTAL INFORMATION

Posttranslational Modification of Heme *b* in a Bacterial Peroxidase: The Role of Heme to Protein Ester Bonds in Ligand Binding and Catalysis

**Andrea Nicolussi^[1], Markus Auer^[1], Julia Weissensteiner^[1], Georg Schütz^[1], Sonja Katz^[1],
Daniel Maresch^[1], Stefan Hofbauer^[1], Marzia Bellei^[2], Gianantonio Battistuzzi^[3], Paul G.
Furtmüller^[1] and Christian Obinger^{[1]*}**

*[1] Department of Chemistry, Division of Biochemistry, Vienna Institute of BioTechnology,
BOKU – University of Natural Resources and Life Sciences, Muthgasse 18, A-1190 Vienna,
Austria*

*[2] Department of Life Sciences, University of Modena and Reggio Emilia, via Campi 103,
41125 Modena, Italy*

*[3] Department of Chemistry and Geology, University of Modena and Reggio Emilia, via Campi
103, 41125 Modena, Italy*

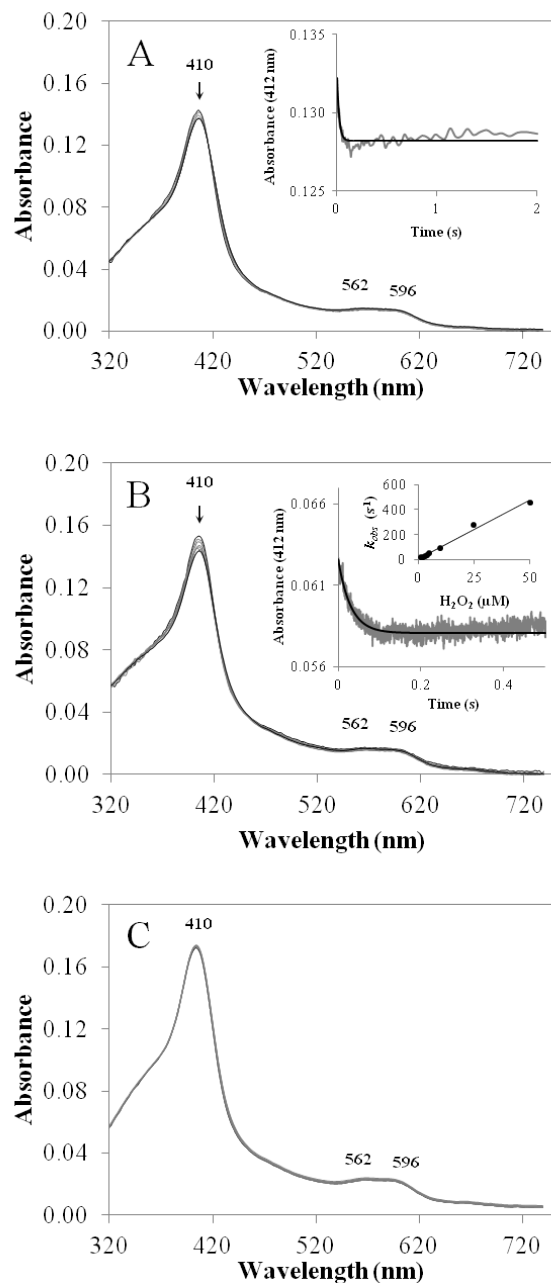
SUPPLEMENTAL MATERIAL

Table S1. List of primers. For construction of the double mutant D109A/E238A, two subsequent site-directed mutagenesis steps were performed, using the primers of both single mutants.

Mutant	Primer	Sequence
D109A	forward	GTGGGGTCAGTTTATTGCGCACGACATGGATTTGACGCCG
	reverse	CGGCGTCAAATCCATGTTCGTGCGCAATAAACTGACCCAC
E238A	forward	GTGCGTGCAAATGCGCAGGTTGGCCTGACC
	reverse	GGTCAGGCCAACCTGCGCATTTCACGCAC

Table S2. Conditions and delay times for pre-steady state kinetics followed by a stopped flow spectrophotometer in the sequential mixing mode.

Mutant	Excess H ₂ O ₂	Delay time (ms)
LspPOX	2x	400
LspPOX (PTM)	2x	300
D109A	2x	500
D109A (PTM)	equimolar	300
E238A	equimolar	100
E238A (PTM)	equimolar	100
D109A/E238A	2x	100
D109A/E238A (PTM)	2x	100



Supplemental Figure S1. Reaction of ferric D109A/E238A with cyanide and hydrogen peroxide and reduction of D109A/E238A Compound I with bromide. (A) Spectral transition during reaction of 2 μ M D109A/E238A with 100 μ M cyanide measured in conventional stopped-flow mode. Inset: Typical time trace at 412 nm upon reaction of 2 μ M protein with 50 μ M cyanide (single exponential fit). (B) Spectral changes upon reaction of 2 μ M D109A/E238A with 4 μ M H_2O_2 measured in the conventional stopped-flow mode. Inset 1: Typical time trace at 412 nm upon reaction of 1 μ M enzyme with 3 μ M H_2O_2 . Inset 2: Linear dependence of k_{obs} from H_2O_2 concentrations. The apparent bimolecular rate constant k_{app} was obtained from the slope of the regression line. (C) Spectral transition after adding 200 μ M bromide to 2 μ M D109A/E238A Compound I in the sequential stopped-flow mode.

S2

Secreted Heme Peroxidase from *Dictyostelium discoideum*: Insights into Catalysis, Structure and Biological Role

Nicolussi, A., Dunn, J. D., Mlynek, G., Bellei, M., Zamocky, M., Battistuzzi, G., Djinović-Carugo, K., Furtmüller, P. G., Soldati, T., and Obinger, C.

Research article

Journal of Biological Chemistry (2017) accepted on December 14th, 2017

doi: 10.1074/jbc.RA117.000463

Secreted Heme Peroxidase from *Dictyostelium discoideum*: Insights into Catalysis, Structure and Biological Role

Andrea Nicolussi^[1], Joe Dan Dunn^[2], Georg Mlynek^[3], Marzia Bellei^[4], Marcel Zamocky^[1,5],
Gianantonio Battistuzzi^[6], Kristina Djinović-Carugo^[3,7], Paul G. Furtmüller^[1],
Thierry Soldati^[2], and Christian Obinger^{[1]*}

[1] Department of Chemistry, Division of Biochemistry, BOKU - University of Natural Resources and Life Sciences, 1190 Vienna, Austria; [2] Department of Biochemistry, Faculty of Science, University of Geneva, 1211 Genève, Switzerland; [3] Department for Structural and Computational Biology, Max F. Perutz Laboratories, University of Vienna, 1030 Vienna, Austria; [4] Department of Life Sciences, University of Modena and Reggio Emilia, via Campi 103, 41125 Modena, Italy; [5] Institute of Molecular Biology, Slovak Academy of Sciences, 84551 Bratislava, Slovakia; [6] Department of Chemistry and Geology, University of Modena and Reggio Emilia, 41125 Modena, Italy; [7] Department of Biochemistry, Faculty of Chemistry and Chemical Technology, University of Ljubljana, 1000 Ljubljana, Slovenia

Running title: Secreted heme peroxidase from *Dictyostelium discoideum*

*Author to whom correspondence should be addressed: Christian Obinger. Phone: +43-1-47654-77273; fax: +43-1-47654-77059, email: christian.obinger@boku.ac.at

Keywords: Heme peroxidase, *Dictyostelium discoideum*, modified heme, halide oxidation, antibacterial activity, fruiting body.

ABSTRACT

Oxidation of halides and thiocyanate by heme peroxidases to antimicrobial oxidants is an important cornerstone in the innate immune system of mammals. Interestingly, phylogenetic and physiological studies suggest that homologous peroxidases are already present in mycetozoan eukaryotes such as *Dictyostelium discoideum*. This social amoeba kills bacteria *via* phagocytosis for nutrient acquisition at its single-cell stage and for antibacterial defense at its multicellular stages. Here we demonstrate that peroxidase A from *D. discoideum* (DdPoxA) is a stable, monomeric, glycosylated and secreted heme peroxidase with homology to mammalian peroxidases. The first crystal structure (2.5 Å resolution) of a mycetozoan peroxidase of this superfamily shows the presence of a

posttranslationally-modified heme with one single covalent ester bond between the 1-methyl heme substituent and E236. The metalloprotein follows the halogenation cycle, whereby Compound I oxidizes iodide and thiocyanate at high ($> 10^8 \text{ M}^{-1} \text{ s}^{-1}$) and bromide at very low rates. It is demonstrated that DdPoxA is upregulated and likely secreted at late multicellular development stages of *D. discoideum* when migrating slugs differentiate into fruiting bodies that contain persistent spores on top of a cellular stalk. Expression of DdPoxA is shown to restrict bacterial contamination of fruiting bodies. Structure and function of DdPoxA are compared to evolutionary related mammalian peroxidases in the context of non specific immune defense.

INTRODUCTION

For more than 70 years, *Dictyostelium discoideum* has been used as a model organism for various fundamental biological processes such as phagocytosis, autophagy, cell aggregation or cell communication (1, 2, 3). As a single cellular amoeba, *D. discoideum* lives as a professional phagocyte, feeding on bacteria. In its natural habitat, *D. discoideum* is able to engulf, kill and digest microorganisms at a rate of at least one per minute (2). Upon starvation, it undergoes a program of multicellular development, leading to differentiation into fruiting bodies containing persistent spores (4, 5). Both the single-celled amoebae and the multicellular aggregates have developed antibacterial defense mechanisms that exhibit many parallels to mammalian innate immune responses including phagocytosis by many types of white blood cells. *D. discoideum* as a model system has shed light on the conserved molecular mechanisms of phagocytosis and the evolution of innate immune responses (2).

Sequencing and annotation of the genome of *D. discoideum* (Dd) revealed the presence of three peroxidases, namely one representative of the peroxiredoxin family (i.e. peroxiredoxin-4, prdx4) and two heme peroxidases, namely DdPoxA and DdPoxB from two different superfamilies (6, 7). DdPoxB belongs to Class B of the family of so-called dye-decolorizing peroxidases (8), whereas DdPoxA is a member of the peroxidase-cyclooxygenase superfamily (7, 9). Most interestingly, DdPoxA shares homology to mammalian peroxidases, which are important players in the mammalian innate immune response (9).

The peroxidase-cyclooxygenase superfamily has been shown to be comprised of seven families (7, 9). Family 1 is composed of chordata peroxidases including thyroid peroxidase, lactoperoxidase (LPO), eosinophil peroxidase (EPO) and myeloperoxidase (MPO). LPO, EPO and MPO play an

antimicrobial role by catalyzing the production of reactive oxidants, e.g. hypohalous acids or hypothiocyanate (10, 11). LPO is secreted from mammary, salivary, and other mucosal glands, EPO is released by eosinophils and MPO is secreted into the phagolysosome of phagocytosing neutrophils upon degranulation in order to kill engulfed pathogens such as bacteria (12, 13, 14).

Phylogenetic analysis demonstrated that DdPoxA belongs to Family 6 of this heme peroxidase superfamily, shares a striking sequence similarity to the mammalian heme peroxidases, and has a signal peptide for secretion (7). The substantial similarity of the molecular mechanism(s) of phagocytosis and bacterial killing for food acquisition in *D. discoideum* and of the antimicrobial activity of neutrophils, monocytes or macrophages (15, 16) prompted us to investigate the biochemistry and physiology of DdPoxA.

Here, we present the biochemical characterization and the first crystal structure of DdPoxA and demonstrate that the overall structures and heme cavity architecture of mammalian peroxidases were already established very early in evolution. Similar to Family 1 peroxidases, the heme of DdPoxA is posttranslationally modified by an autocatalytic process. In contrast to the mammalian enzymes (17, 18, 19), only one heme protein ester bond is found, which is formed between E236 and the 1-methyl substituent of the porphyrin ring. The metalloenzyme is shown to follow the halogenation cycle and to catalyze the efficient two-electron oxidation of iodide and thiocyanate. Nevertheless, DdPoxA is a poor oxidizer of bromide and cannot mediate the oxidation of chloride. The presented *in-vivo* investigations include a detailed expression pattern of *DdpoxA* throughout the development cycle of *D. discoideum* at the protein level together with comparative cell development studies on wild-type *D. discoideum* and the *DdpoxA* knockout mutant

($\Delta DdpoxA$). It is demonstrated that the heme enzyme supports maintenance of sterility of the slug and the subsequently produced fruiting bodies, which suggests a role in antibacterial defense of the multicellular aggregate.

RESULTS

Recombinant DdPoxA is a Stable, Monomeric and Glycosylated Heme Peroxidase. Recombinant DdPoxA was successfully produced with an N-terminal His₆-tag in the *Pichia pastoris* BG11 ($\Delta AOX1$) strain. The secreted protein was purified by a two-step ammonium sulfate precipitation and, after resuspension, by affinity chromatography. The yield was found to be ~50 mg/L of *P. pastoris* supernatant and the purity number (RZ, $A_{\text{Soret}}/A_{280\text{nm}}$) 1.1 - 1.2 indicating 90-95% heme occupancy. Figure 1A depicts the UV-vis spectrum of ferric DdPoxA with the Soret maximum at 416 nm, Q-bands at 541 and 576 nm, and the charge transfer band at 644 nm (black spectrum).

The secreted glycosylated peroxidase has three N-glycosylation sites at positions N62, N131 and N338 as predicted by the online tool N-Glycosite (20). Analysis of the protein by SDS-PAGE and Western blot showed hyperglycosylation which is typical for recombinant protein expressed in *P. pastoris* (not shown). Thus, deglycosylation of recombinant DdPoxA by Endo H_f glucosidase was performed, followed by SEC purification. Deglycosylation had no impact on the UV-vis and ECD spectral features in the far-UV, near-UV and visible range, clearly suggesting that the overall and heme cavity architecture were not affected (compare black and grey spectra in Figures 1A-C). Between pH 5.0 and pH 9.0 the spectral features of DdPoxA remained unchanged (not shown).

In the homologous lactoperoxidase (LPO) (orange spectrum in Figures 1A-C) the Soret band is blue-shifted as is evident by the

respective UV-vis (412 nm) and ECD (minimum at 406 nm) spectra, which clearly suggests differences in the heme cavity architecture compared to DdPoxA. It is well known that LPO has two heme to protein ester bonds derived from a hydrogen peroxide-mediated posttranslational modification (21, 22). The involved acidic amino acids (D225 and E375, goat LPO numbering) are fully conserved in Family 1 peroxidases (Supplemental Figure S1). Interestingly, the sequence alignment shown in Supplemental Figure S1 suggests that DdPoxA has only one covalent link between the 1-methyl substituent of the prosthetic group and E236, because the DdPoxA residue corresponding to D225 of LPO is an isoleucine.

Differences in the active site architecture were also reflected by spectroelectrochemical investigations of DdPoxA at pH 7.0. Upon reduction of ferric to ferrous DdPoxA its Soret peak shifts from 416 to 428 nm. Figure 1D shows a representative family of spectra at different applied potentials in the OTTLE cell. The calculated reduction potential E° for the Fe(III)/Fe(II) couple, determined from the corresponding Nernst plot (inset to Figure 1D), was calculated to be -0.276 ± 0.010 V, which is significantly more negative compared to LPO (-0.176 V) (23).

Importantly, incubation of recombinant DdPoxA with low micromolar hydrogen peroxide altered neither its UV-vis and ECD spectral features nor the standard reduction potential (not shown). This suggests that the autocatalytic posttranslational modification of the heme group (24) was already established during recombinant protein production in the methylotrophic yeast. By contrast, for other members of this heme peroxidase superfamily addition of excess H₂O₂ was necessary to complete the posttranslational modification, which was reflected by changes in spectral and redox properties (25, 26, 27, 28).

Next, we probed the presence of the proposed covalent heme to protein ester bond in deglycosylated DdPoxA by mass spectrometry (Figure 2A). The resulting chromatogram shows four major peaks, whereby peak 1 (60583.7 Da) was assigned to DdPoxA with three N-acetyl-D-glucosamines (GlcNAcs) and a covalently bound heme. Peaks 2 and 3 in the chromatogram (60745.7 Da and 60906.9 Da) represent DdPoxA carrying one and two additional hexoses (162 Da each). Peptide mapping revealed that these hexoses derive from single O-glycosylations on positions T133 and T142, which were not cleaved during deglycosylation (data not shown). The minor peak 4 (60196 Da) was assigned to a degradation product lacking four histidines from the N-terminal His₆-tag. Most importantly, no peak could be assigned to protein without covalently bound heme.

The presence of a covalently bound heme in DdPoxA was further confirmed by SDS-PAGE and visualization of the blotted proteins by enhanced chemiluminescence. Note that unbound heme is lost during SDS-PAGE and Western blotting. Figure 2B compares LPO, DdPoxA and horseradish peroxidase (HRP). The latter carries non-covalently bound heme *b* at the active site. It is clearly demonstrated that both LPO and DdPoxA but not HRP exhibited chemiluminescence at the respective protein bands, demonstrating covalent heme attachment.

Further, we probed the oligomeric state of deglycosylated DdPoxA by SEC-MALS. Figure 2C depicts a sharp peak at a retention time at 20.3 min in the corresponding chromatogram. By using MALS an average molar mass of 63.4 kDa was calculated, which is similar to the theoretical mass (60.7 kDa) and suggests the presence of a monomer.

Finally, we investigated the thermal stability of DdPoxA using differential scanning calorimetry and temperature-dependent ECD experiments (Figure 3). In the DSC experiment, ferric glycosylated DdPoxA

showed two independent unfolding events with T_m values of 71.1 °C and 80.4 °C, respectively, at pH 7.0 (Figure 3A). The thermal stability rapidly decreases at alkaline pH, whereas stability is retained in the acidic region until pH 5.0 (Figure 3B).

Complementary temperature-dependent ECD measurements of glycosylated DdPoxA at pH 7.0 showed a mid-point transition of 62 °C in the far-UV at 208 nm reflecting unfolding of the secondary structure (Figure 3C). The overall secondary structure of deglycosylated DdPoxA and LPO were slightly less stable ($T_m = 59.6$ °C). In the visible region at 408 nm, glycosylated DdPoxA showed a T_m value of 74.3 °C suggesting that the second endotherm in the DSC thermogram reflects unfolding of the heme cavity (Figure 3D). The corresponding T_m values of deglycosylated DdPoxA and LPO were found to be at 68.3 and 75.1 °C, respectively.

DdPoxA Displays High Structural Similarity to Mammalian Peroxidases but Unusual Posttranslational Heme Modification. Crystal structures of deglycosylated DdPoxA (space group P 3₁ 2 1) comprises two DdPoxA molecules per asymmetric unit (RMSD value between the two chains: 0.54 Å - calculated over 508 C_α atoms, pdb accession code 6ERC). The structure was solved to 2.5 Å resolution by molecular replacement using the balbes webserver (29). Figure 4A shows the overall largely α -helical structural organization of DdPoxA. Only three small antiparallel β -strands (residues F43-P46, residues A141-E143, residues Y160-N164) are present. The protein is comprised of 21 α -helices of varying length. The central core of the molecule consists of five long α -helices (H2, H6, H7, H8 and H13) with a covalently attached heme group. A very similar architecture is found in LPO (core helices are H2, H5, H6, H8, H12) (RMSD value between

the chain A of DdPoxA and goat LPO (pdb code 2R5L) is 1.61 Å calculated over 444 C α atoms, z-score is 13.4) (22). The conserved distal residues Q97 and H101 are found in helix 2, while the proximal H325 belongs to helix 8 and the proximal N403 and R406 are part of helix 13. Alike in LPO, the core helices form triangles (H6, H7, H8 in DdPoxA and H5, H6, H8 in LPO), whereby the heme group is located between helix 2 and 8 (22).

The heme environment of DdPoxA shows a striking sequence similarity to LPO (Supplemental Figure S1). The important catalytic residues on the distal heme site (H101, Q97, R233) are fully conserved, including E236 that forms an ester bond with the 1-methyl substituent of the heme porphyrin ring (Figure 4B and Supplemental Figure S2). However, DdPoxA lacks the covalent ester bond that is formed between the heme and the distal aspartate in LPO, since the corresponding residue in DdPoxA is an isoleucine. The position of the distal Ca²⁺ binding site is conserved; however, different residues are involved in binding of the ion. In LPO, the Ca²⁺ binding site consists of the residues D, D, S, Y and F, while in DdPoxA the ion is coordinated by N102, G167, Y169, D171 and N173. The proximal triad H325, N403 and R406 is fully conserved between the two enzymes (Figures 4C and 4D).

The polypeptide chain of DdPoxA contains eight cysteines, six of which are involved in disulfide bridges (C120-C128, C146-C159 and C277-C505) (Figure 4A). In comparison, LPO has 15 cysteine residues, forming seven intramolecular disulfide bridges. None of the disulfide bridges are conserved between DdPoxA and LPO. DdPoxA contains three N-glycosylation sites (N62, N131, N338) which are all occupied by complex sugar moieties in the recombinant protein. However, in the crystal structure, only one GlcNAc is left on each N-glycosylation site due to the deglycosylation

procedure (see also mass spectrometric analysis). In comparison, LPO shows four N-glycosylation sites, and none of them is conserved between the two proteins.

Approximate bottlenecks of the substrate channel were determined by tunnel calculations using CAVER 3.0. The most important channels of both, DdPoxA and goat LPO, are given by throughput-values of 0.75 and 0.79, respectively (throughput-values range from 0 to 1; the higher the value, the greater the probability that the tunnel is functionally relevant). The bottleneck radii 1.19 Å (DdPoxA) and 1.22 Å (LPO) are very similar, but their length differs significantly with 8.61 Å (DdPoxA) compared to 4.85 Å (LPO) (Figure 4E).

DdPoxA Compound I is an Efficient Oxidant of Iodide and Thiocyanate. Finally, we probed the accessibility and binding kinetics of cyanide to the heme cavity of ferric DdPoxA. Upon cyanide binding, the high-spin ($S = 5/2$) ferric protein is converted into the low-spin ($S = 1/2$) thereby shifting the Soret maximum from 416 nm to 425 nm with a clear isosbestic point at 420 nm. In the visible range, a typical low-spin peak at 541 nm arose, while the peaks at 576 nm and 644 nm disappeared (Figure 5A). Plotting the single exponentially fitted pseudo-first order rate constants (k_{obs}) versus cyanide concentration yielded an apparent second-order dissociation rate constant (k_{on}) of $3.3 \times 10^5 \text{ M}^{-1} \text{ s}^{-1}$ ($K_{\text{D}} = k_{\text{off}}/k_{\text{on}} = 3.7 \text{ }\mu\text{M}$), which was approximately five-fold lower than for MPO ($k_{\text{on}} = 1.6 \times 10^6 \text{ M}^{-1} \text{ s}^{-1}$, $K_{\text{D}} = 1.9 \text{ }\mu\text{M}$) and LPO ($k_{\text{on}} = 1.3 \times 10^6 \text{ M}^{-1} \text{ s}^{-1}$, $K_{\text{D}} = 23 \text{ }\mu\text{M}$) (17, 30, 31, 32). At pH 5.0 cyanide binding to ferric DdPoxA decreased ($k_{\text{on}} = 8.9 \times 10^4 \text{ M}^{-1} \text{ s}^{-1}$ and $K_{\text{D}} = k_{\text{off}}/k_{\text{on}} = 10.1 \text{ }\mu\text{M}$).

Next, we tested the reaction of ferric DdPoxA with H₂O₂. Formation of Compound I was characterized by a decrease of the Soret maximum and a shift to 412 nm, and the formation of typical peaks in the visible range at 604 nm and 660 nm, while the peak at 541

nm vanished (Figure 5B). Full hypochromicity of the Soret peak (46%) was obtained using a 2.5-fold stoichiometric excess of H_2O_2 . The reaction showed a biphasic behavior with the fast reaction being responsible for ~85% of absorbance change at 412 nm. The apparent bimolecular rate constant was calculated to be $3.2 \times 10^6 \text{ M}^{-1} \text{ s}^{-1}$, which is approximately 5-times slower compared to MPO and LPO ($k_{\text{app}} = 1.1 - 1.4 \times 10^7 \text{ M}^{-1} \text{ s}^{-1}$) (29). Similar to cyanide binding, the rate of Compound I formation decreased at pH 5.0 ($k_{\text{app}} = 5.9 \times 10^5 \text{ M}^{-1} \text{ s}^{-1}$).

Further, we probed the reaction of the preformed DdPoxA Compound I with the two-electron donors chloride, bromide, iodide and the pseudohalide thiocyanate (X^-). Chloride was unable to reduce Compound I while bromide is a very poor electron donor with k_{app} being $15 \text{ M}^{-1} \text{ s}^{-1}$ (pH 7.0) and $13 \text{ M}^{-1} \text{ s}^{-1}$ (pH 5.0) (Figure 5C). However, oxidation of iodide and thiocyanate by DdPoxA Compound I is extremely efficient ($k_{\text{app}} > 10^8 \text{ M}^{-1} \text{ s}^{-1}$ at pH 7.0). Similar values have been reported for LPO, whereas MPO shows a 10-fold lower oxidation capacity for iodide and thiocyanate ($k_{\text{app}} \sim 10^7 \text{ M}^{-1} \text{ s}^{-1}$) (30). At pH 5.0, oxidation of thiocyanate is also extremely fast ($k_{\text{app}} > 10^8 \text{ M}^{-1} \text{ s}^{-1}$), whereas iodide oxidation at pH 5.0 is drastically impaired ($7.4 \times 10^3 \text{ M}^{-1} \text{ s}^{-1}$).

DdPoxA is Expressed at Multicellular Stages and Supports Fruiting Body Sterility.

One remarkable characteristic of *D. discoideum* is its ability to shift from single-cells to a multi-cellular stage in response to starvation. Starting from cell aggregation towards a cAMP signal, a multicellular aggregate is formed containing up to 100,000 cells. Subsequently, a migrating slug is formed that later culminates into a fruiting body, which comprises a spore containing structure, the sorus, on top of a cellular stalk (5). Since the proteome and the morphology of the cells significantly change upon development, it is crucial to know the

expression pattern of the investigated protein throughout the developmental cycle. Figure 6A shows a simplified scheme of the development cycle of *D. discoideum*. Formerly published open source RNAseq data (33, 34) on the *D. discoideum* laboratory strain AX4 indicated that expression of DdPoxA was upregulated at late development stages, starting approximately from 12 hours after initiation of starvation (Figure 6B). To confirm these findings, we let *D. discoideum* wild-type AX2 and $\Delta DdpoxA$ cells undergo the development cycle and detected the expression of DdPoxA by Western blotting with a polyclonal antibody against the recombinantly produced DdPoxA (Figure 6C). The bands at approximately 60 kDa confirmed the RNAseq data and clearly showed that the expression of DdPoxA was upregulated at late development stages, approximately 14 h after the initiation of starvation (left panel). A GFP-tagged version of DdPoxA serves as positive control (right panel). The negative control $\Delta DdpoxA$ showed no expression at all (right panel).

As outlined above, analysis of the polypeptide sequence suggested the existence of a signal peptide for secretion into the extracellular space. Fluorescence microscopy of a *D. discoideum* population expressing a GFP-tagged version of DdPoxA indicated that the tagged peroxidase co-localizes with the ER marker PDI (arrows Figure 6D). The additional juxtannuclear localization (arrowheads Figure 6D) is typical of the Golgi apparatus and/or the recycling endosomes (35, 36), suggesting that DdPoxA is most probably present in the secretory pathway.

Since DdPoxA expression was not detected in the vegetative phagocytosing amoebae, the initial hypothesis of its MPO-like function had to be revised. Subsequently we focused on elucidating the putative roles of this peroxidase at the late development stages. We investigated the effects of the

$\Delta DdpoxA$ knockout on the development cycle of *D. discoideum* in comparison to the wild-type AX2 and the $\Delta noxABC$ knockout strains. It has been shown in previous studies that the knockout of the three *nox* genes (each encoding a homolog of gp91^{phox}, the catalytic subunit of NADPH oxidases (NOX)) leads to a deficiency in immune defense at the slug and sorus stages (37, 38). NOXs are crucial enzymes producing reactive oxygen species during phagocytosis or pathogen attack (37). In contrast to DdPoxA, the NOXs are not secreted but membrane bound. RNAseq detection has shown that NoxB and NoxC are also upregulated during cell development, while NoxA is predominantly expressed in the amoeboid stage (33, 34). To elucidate the impact of DdPoxA and the NOX enzymes during development, a defined concentration of *D. discoideum* cells (1×10^6 / mL) was plated on non-nutrient agar plates to induce starvation. Time-dependent morphological changes were documented using a stereoscope. Comparison of the $\Delta DdpoxA$ to the AX2 wild-type and the $\Delta noxABC$ mutant did not show any differences concerning cell development, indicating that DdPoxA was not essential for this process (Supplemental Figure S3). Further, we demonstrated that there was no significant difference in the amount of produced fruiting bodies or spores between the three investigated variants (Figure 7A-B).

Finally, we probed the effect of the $\Delta DdpoxA$ knockout on the sterility of the sori in comparison to the AX2 wild-type and the $\Delta noxABC$ knockout mutant. For this, we cultivated *D. discoideum* cells on a lawn of *Klebsiella aerogenes* as a food source. After consumption of the bacteria, *D. discoideum* cells started the multicellular life cycle and formed fruiting bodies. Subsequently, we analyzed the sori of those fruiting bodies for the presence of live bacteria by plating them on fresh agar plates (Figure 7C). After investigating a significant number of sori ($N \geq$

125 for each mutant), we demonstrated that both $\Delta DdpoxA$ as well as $\Delta noxABC$, showed a higher percentage of contaminated sori than the AX2 wild-type strain (43% and 52%, respectively, compared to 15% for the wild-type). Further, we quantified the number of remaining bacteria in the sori. This was accomplished by resuspending a defined number of sori in Soerensen medium and plating the suspension on fresh selective agar plates. We found that sori from $\Delta DdpoxA$ and $\Delta noxABC$ strains contained twice as many contaminating bacteria as the wild-type AX2 (Figure 7D). Hence, it was clearly shown that both mutants have significant deficiencies in keeping the slug and the sori sterile upon cell development.

DISCUSSION

Phylogenetic reconstruction of the main evolutionary lines of the mammalian heme peroxidases such as lactoperoxidase or myeloperoxidase revealed the presence of novel bacterial and early eukaryotic representatives within Family 6 of the peroxidase-cyclooxygenase superfamily (7, 9). This work presents the first comprehensive biochemical study of an antibacterial peroxidase expressed in an organism that branched from the evolution tree close to the emergence of multicellularity and metazoans. We focused on DdPoxA because *D. discoideum* is a social amoeba that can switch from a single-cell to a multi-cellular lifestyle under conditions of starvation. Moreover, DdPoxA is a typical representative for all related heme peroxidases from the whole genus *Dictyostelium* that already counts more than 80 distinct species (NCBI Taxonomy Database).

At the single cell stage, *D. discoideum* feeds on bacteria ingested by phagocytosis, a process that closely resembles bacterial killing within the neutrophil phagosome of vertebrates. In the absence of a food source,

starting from single cell streams that chemotax towards a cAMP signal, a multicellular migrating slug is formed that, finally, differentiates in fruiting bodies containing persistent spores (5). At these late development stages DdPoxA is shown to be upregulated (Figure 7C). These findings are supported by published RNAseq data on a slightly different *D. discoideum* laboratory strain (AX4) (33, 34).

Knockout of the *DdpxxA* gene had no observable impact on cell development, cell communication and aggregation, formation of the stalk or the fruiting body. However, we showed that knockout of DdPoxA significantly increased the bacterial contamination of the sori in comparison to the wild-type strain. This impact is very similar to the one already reported for a *D. discoideum* mutant lacking functional NOX (38, 39). These findings suggest that DdPoxA exhibits antibacterial activity that depends on H₂O₂ derived from dismutation of superoxide released by the NADPH oxidase(s).

Antibacterial activity requires DdPoxA secretion at the slug and fruiting body state as well as production of oxidants. A respective signal peptide translocates the nascent polypeptide chain to the endoplasmatic reticulum (ER). In the ER core glycosylation occurs, the heme group is inserted and, most probably, posttranslationally modified as recently demonstrated for human promyelo-peroxidase (40). Localization of GFP-tagged DdPoxA in the ER, the Golgi apparatus and recycling endosomes clearly underlines that the likely glycosylated peroxidase follows the secretory pathway.

Similar to secreted mammalian peroxidases involved in antimicrobial activity (31, 41) DdPoxA exhibits a high thermal stability ($T_m > 70$ °C) in the pH range 5.0-7.0 which guarantees conformational stability under harsh conditions such as the one encountered in the soil environment of the amoeba.

Mammalian peroxidases and DdPoxA share a similar overall fold. The arrangement of the 21 α -helices and especially of the core helices, which provide the heme binding ligands and catalytic residues, are fully conserved. Nevertheless the number and localization of the disulfide bridges and the N-glycosylation sites, the nature of ligands of the distal Ca²⁺-binding site as well as the length of the substrate channel are different between DdPoxA and mammalian peroxidases such as LPO.

As already demonstrated for chordata (Family 1) peroxidases (18), peroxidasin 1 (hsPxd01, Family 2) (29) and a bacterial enzyme (Family 6) (27, 28), the prosthetic group of DdPoxA is posttranslationally modified by an auto-catalytic radical mechanism that depends on hydrogen peroxide. However, DdPoxA is unique in having only one covalent ester bond between the hydroxymethyl group on pyrrole ring A and E236, whereas all other representatives studied so far have an additional ester bond between a conserved aspartate residue and the hydroxymethyl group of pyrrole ring C. In the case of DdPoxA this acidic amino acid is replaced by I100. All other amino acids of structural and functional relevance at the heme cavity are fully conserved in DdPoxA, including the proximal (H325-N403-R406) and distal (Q97-H101-R233) triads. However, due to the lack of the second ester bond at pyrrole ring C the stretch Q97-H101 should be less constrained compared to LPO.

As a consequence the spectral and redox properties of DdPoxA are different from Family 1 proteins. The standard reduction potential of the Fe(III)/Fe(II) couple of DdPoxA is significantly more negative than that of LPO. Within the peroxidase-cyclooxygenase superfamily there is a clear correlation between the number of covalent ester bonds and E° [Fe(III)/Fe(II)] values with E° (one ester bond, e.g. DdPoxA: -0.276 V) < E° (two ester bonds, e.g. LPO: -0.183 V;

EPO: -0.176 V; LspPOX: -0.158 V; hsPxd01, -0.128 V) < E° (two ester bonds, one sulfonium ion linkage, MPO: +0.005 V) (27, 28, 43, 44, 45).

Closely related with the redox properties of these peroxidases is their capacity to oxidize halides by the redox intermediate Compound I. Whereas the kinetics of the two-electron oxidation of the ferric peroxidases to Compound I by hydrogen peroxide is typically very fast ($3.2 \times 10^6 \text{ M}^{-1} \text{ s}^{-1}$ in case of DdPoxA) and does not depend on the posttranslational modification of the prosthetic group (21, 30), the thermodynamics of the two-electron reduction of Compound I by halides and thiocyanate strongly depends on the presence of heme to protein bonds. Only MPO is able to oxidize chloride [E° (HOCl/Cl⁻, H₂O) = 1.28 V at pH 7.0] at reasonable rates (46, 47). Bromide oxidation [E° (HOBr/Br⁻, H₂O) = 1.13 V at pH 7.0] has been demonstrated for EPO (48), LspPOX (27) and hsPxd01 (28). Oxidation of iodide [E° (HOI/I⁻, H₂O) = 0.78 V at pH 7.0] and thiocyanate [E° (HOSCN/SCN⁻, H₂O) = 0.56 V at pH 7.0] (46) is thermodynamically less challenging and thus typically is performed at high rates by Compound I of all peroxidases of this superfamily. This applies also to DdPoxA that is unable to produce hypochlorous and hypobromous acid but oxidizes iodide and thiocyanate extremely efficiently ($> 10^8 \text{ M}^{-1} \text{ s}^{-1}$).

This poses the question about the relation of this enzymatic activity and the role of DdPoxA in bacterial killing at the slug and fruiting body stage. It has been demonstrated by Klebanoff already in 1967 (49) that human myeloperoxidase, iodide, and H₂O₂ have a bactericidal effect on *E. coli* and that this effect corresponded to the iodination of the bacteria. Hypothiocyanous acid (HOSCN) is well known to be a potent antimicrobial species, being formed by LPO in human secretory mucosa, including the oral cavity, airway and alimentary tract, thereby

regulating the resident and transient flora as part of innate immunity (50). HOSCN is a weaker, more selective oxidant than HOCl or HOBr that reacts at biologically relevant rates with cysteine and/or selenocysteine residues of proteins and peptides and thus is responsible for arresting the spread of pathogens (51). Thus the high rate of oxidation of iodide and thiocyanate by DdPoxA suggests a comparable antibacterial function in *D. discoideum* as described for mammalian peroxidases like LPO. Both thiocyanate and iodide are known to be found in the soil. Thiocyanate, for example, is known to be both secreted and utilized by various soil organisms as nitrogen source (52), whereas iodide is reported as the most prevalent form of iodine in soil and rivers (53).

Summing up, in this report we present the first structural and functional characterization of a heme peroxidase with one heme to protein ester bond. Its high efficiency in H₂O₂-dependent iodide and thiocyanate oxidation and its expression at multi-cellular lifestyle of *D. discoideum* together with its antibacterial activity, suggest that this secreted and highly stable glycoprotein acts in the first line defense of the fruiting bodies containing spores against bacteria.

EXPERIMENTAL PROCEDURES

Materials and Reagents. Chemicals and enzymes were purchased from following sources: the synthetic gene coding for DdPoxA and the expression vector were ordered from ATUM (Menlo Park, California). Restriction enzymes and Endo H_f glucosidase were from New England Biolabs. Zeocin was purchased from Fisher Scientific. *Pichia pastoris* strain (BG11 with deleted AOX1 ORF) was purchased from bisy e.U. (Hofstätten, Austria). Chelating Sepharose Fast Flow column was from Amersham

Biosciences; size exclusion chromatography (SEC) column (HiLoad 16/600 Superdex 200 pg, prep grade) was purchased from GE Healthcare. Centripreps-30 were from Amicon, PD10 desalting columns from Sigma-Aldrich and Whatman filter papers from GE Healthcare. Polyclonal antibodies against the recombinant DdPoxA raised in rabbits and purified by Protein A Sepharose chromatography were ordered from Seramun Diagnostica GmbH (Heidesee, Germany). All other chemicals were purchased from Sigma-Aldrich at highest available grade.

Cloning, Expression, and Purification.

The gene coding for DdPoxA (Uniprot accession code Q6TMK4) was synthesized with an additional N-terminal hexa-histidine tag (His₆-tag) and codon optimized for expression in *Pichia pastoris* at DNA 2.0. The signal peptide prediction server SignalP 4.1 (54) was used to identify the secretion signal, which was subsequently removed. The gene was cloned into the pJ912 shuttle vector carrying a zeocin resistance and the alpha-factor from *Saccharomyces cerevisiae* as signal sequence for secretion into the extracellular space. The plasmid was transferred into electrocompetent *E. coli* Top 10 cells for amplification. The purified plasmid was linearized using the restriction enzyme SwaI and transformed into the *P. pastoris* BG11 expression strain by electroporation (BioRad Electroporator with VWR cuvettes, option “Fungi Sc2”). Transformants were selected on YPD plates (10 g/L yeast extract, 20 g/L peptone, 10 g/L glucose, 15 g/L agar) supplemented with zeocin (100 mg/L). The transformed *P. pastoris* BG11 cells were initially cultivated in YP medium supplemented with 1% glycerol at 28 °C and 180 rpm overnight. Subsequently, 10 mL aliquots of these precultures were further used to inoculate 200 mL of fresh YP-glycerol medium supplemented with biotin solution (final concentration 4 mg/L) in baffled shaken flasks

and incubated at 28 °C and 180 rpm. After complete glycerol consumption (~24 hours), protein expression was induced by adding methanol to 0.5% final concentration. Expression proceeded for further 24 hours at 25 °C and 180 rpm. Subsequently, methanol was added to 1% final concentration. Hemin solution (10 μM final concentration, pH 9 - 10) was added shortly after addition of methanol and incubation was continued. After 24 hours, methanol was added once more to 1% final concentration. Four hours after last addition of methanol, the supernatant was separated from the cells by centrifugation (3000 × g, 10 min, 4 °C). The supernatant was stored at -30 °C until further purification.

Recombinant DdPoxA was purified from the *P. pastoris* cell supernatant by metal chelate affinity chromatography using the N-terminal His₆-tag. First, proteins were precipitated using ammonium sulfate in two steps. In the first step, 170 g/L ammonium sulfate (31% saturation) was added stepwise at 4 °C to the cell supernatant. Subsequent centrifugation (45000 × g, 20 min, 4 °C) led to precipitation of host proteins. In the second step, 343 g/L ammonium sulfate (82% final saturation) was added stepwise at 4 °C to the remaining supernatant and the recombinant protein was precipitated by centrifugation (45000 × g, 20 min, 4 °C). The pellet was dissolved in binding buffer (67 mM phosphate buffer supplemented with 20 mM imidazole and 0.5 M NaCl, pH 7.2, 50 mL/L of *P. pastoris* cell culture) for subsequent purification by metal chelate affinity chromatography. The column was loaded with Ni²⁺ ions and equilibrated with three column volumes of binding buffer. The protein solution was loaded on the column, followed by extensive washing (six column volumes) with binding buffer. A linear gradient from 20 - 250 mM imidazole was used for elution and 1.5 mL fractions were collected. The fractions were investigated by SDS-PAGE and UV-vis spectroscopy and the purest fractions were

concentrated (Amicon centrifugal filters, 30 kDa cutoff), desalted using PD10 columns and stored in 10 mM phosphate buffer, pH 7.0, at -80 °C.

UV-vis and Electronic Circular Dichroism Spectroscopy. UV-vis spectra were recorded using a Hitachi U-3900 spectrophotometer from 200 - 800 nm at 25 °C in 10 mM phosphate buffer, pH 7.0. The molar extinction coefficient of DdPoxA has been determined by the method of Bradford and shows a value of 84,950 M⁻¹ cm⁻¹ at 416 nm (55). It was used for all calculations of protein concentrations of DdPoxA.

Electronic Circular Dichroism (ECD) measurements were performed with Chirascan (Applied Photophysics) that allowed simultaneous measurement of UV-vis and ECD spectra at defined temperature using a Peltier temperature control unit. The machine was flushed with nitrogen with a flow rate of 5 L/min before and throughout the measurements. For probing the overall secondary structure composition in the far-UV region (180 - 260 nm), the path length of the cuvette was 1 mm, bandwidth 3 nm and scan time 10 s per point. Concentration of DdPoxA was 0.5 mg/mL in 10 mM phosphate buffer, pH 7.0. For unfolding studies changes in the ellipticity at 208 nm were followed between 25 - 95 °C (1 °C increase per min). To obtain information about tertiary structure and heme insertion the ECD spectrum at 25 °C was recorded in the near-UV and visible region (250 - 470 nm) with the path length and spectral bandwidth set to 10 mm and 1 nm, respectively. For studying unfolding of the heme cavity the ellipticity was monitored at the Soret minimum at 408 nm between 25 and 95 °C (1 °C increase per min).

Size-exclusion chromatography combined with multi-angle light scattering. Protein purity and the oligomeric state of the recombinantly produced DdPoxA was determined by size-exclusion chromatography (SEC) combined with multi-angle light

scattering (MALS). Measurements were performed on an LC20 prominence HPLC system equipped with the refractive index detector RID-10A, the photodiode array detector SPD-M20A (all from Shimadzu) and a MALS Heleos Dawn8+ plus QELS detector (Wyatt Technology). The column (Superdex 200 10/300 GL, GE Healthcare) was equilibrated with Dulbecco PBS plus 200 mM NaCl, pH 7.2, as running buffer. Experiments were carried out at a flow rate of 0.75 mL/min at 25 °C and analyzed using the ASTRA 6 software (Wyatt Technology). Accuracy of molar mass determination was verified by measuring a sample containing bovine serum albumin. The protein (25 µg per analysis) was centrifuged (17 000 × g, 10 min, 20 °C) and filtered (0.1 µm Ultrafree-MC filter from Merck Millipore) before applying to the column.

Spectroelectrochemistry. The standard reduction potential E° of the Fe(III)/Fe(II) couple of the heme protein was measured using a homemade OTTLE cell (optically transparent thin layer spectroelectrochemical cell) in a three-electrode configuration. The setup was composed of a gold mini-grid working electrode (Buckbee-Mears), an Ag/AgCl/KCl_{sat} micro-reference electrode, separated from the working solution by a Vycor set, and a platinum wire as counter-electrode. The reference electrode was calibrated against a saturated calomel electrode (Hg₂Cl₂) before each set of measurements. The potentials were applied using a potentiostat/galvanostat (Amel model 2053). UV-vis spectra were recorded using a Varian Cary C50 spectrophotometer, flushed with Argon. The obtained potentials were referenced to the standard hydrogen electrode. Spectroelectrochemical titrations were carried out using samples containing 10 µM DdPoxA in 100 mM phosphate buffer, pH 7.0, and 100 mM NaCl, at 25 °C. 100 µM methyl viologen and 2 µM lumiflavin 3-acetate, methylene

blue, phenazine methosulfate, and indigo disulfonate were used as redox mediators.

Differential Scanning Calorimetry. Differential scanning calorimetry (DSC) measurements were conducted using a VP-DSC microcalorimeter (MicroCal) controlled by the VP-viewer program and equipped with a 137 μ L cell and an autosampler for 96 well plates. Samples were measured with a concentration of 10 μ M in 50 mM phosphate buffer, pH 7.0. The heating scan rate was 60 $^{\circ}$ C/h and the cell pressure was constant at 4.1 bar, the temperature range was programmed from 20 - 100 $^{\circ}$ C. Data analysis was performed using the MicroCal Origin7 software. Raw DSC data were baseline-corrected with buffer and normalized for the applied protein concentration. The resulting endotherms were fitted by a non two-state transition model.

SDS-PAGE and Enhanced Chemilumi-nescence (ECL). Protein separation by SDS-PAGE was carried out using Mini Protean TGX Gels (Bio-Rad) in Tris-Glycin-SDS running buffer (Bio-Rad) at 250 V. The gels were stained with Coomassie Brilliant Blue staining solution with Precision Plus Protein (All blue) as prestained ladder (Bio-Rad). The iBlot Dry Blotting System (Invitrogen) with nitrocellulose membranes was used for immobilizing proteins on nitrocellulose membranes (iBlot Gel Transfer Stacks, Nitrocellulose mini). Enhanced chemilumi-nescence was performed using the Bio-Rad ChemiDoc XRS+ Imaging System. The blotted membrane was incubated with Clarity Western ECL Substrate, applying an exposure time between 1 and 20 s (depending on sample concentration). Note that non-covalently bound heme is lost during gel electrophoresis. The ECL detection reagent relies on the hydrogen peroxide-mediated oxidation of luminol to the light-emitting 3-aminophthalate in the presence of a catalyst like heme.

Mass spectrometry. Prior to mass spectrometric analysis (MS), deglycosylation of purified DdPoxA was conducted using the glucosidase Endo Hf overnight at 37 $^{\circ}$ C and 180 rpm. Deglycosylated protein was further purified by size exclusion chromatography (SEC) on a HiLoad 16/600 Superdex 200 pg (prep grade) column, equilibrated with 50 mM phosphate buffer, pH 7.0. The eluted protein solution was concentrated and stored at -80 $^{\circ}$ C.

To detect the mass of the deglycosylated protein, intact protein mass spectrometry analysis was performed. In detail, 2.5 μ g of deglycosylated DdPoxA were analyzed using a Dionex Ultimate 3000 system directly linked to a QTOF instrument (maXis 4G ETD, Bruker) equipped with the standard ESI source in the positive ion mode. Data were recorded within a range from 400 - 3800 m/z. The instrument was calibrated using the ESI calibration mixture (Agilent). For protein separation, a Thermo ProSwift™ RP-4H analytical separation column (250 * 0.200 mm) was used. A gradient from 80% solvent A and 20% solvent B (Solvent A: 0.05% trifluoroacetic acid (TFA), B: 80.00% acetonitrile, 19.95% H₂O and 0.05% TFA) to 65% B in 20 min was applied, followed by a 15 min gradient from 65% to 95% B, at a flow rate of 8 μ L/min and at 65 $^{\circ}$ C. The obtained data was processed using Data Analysis 4.0 (Bruker) and the obtained spectrum was deconvoluted by MaxEnt (Maximum Entropy Method, low mass: 40000, high mass: 200000, instrument resolving power 100000).

Crystallization, X-ray data collection, structure determination and refinement. Crystallization experiments were performed using the sitting drop vapor diffusion method in SWISSCI MRC three-well crystallization plates (Molecular Dimensions, Newmarket, UK). Crystallization drops were set using a mosquito crystallization robot (TTP Labtech, GB). The reservoir was filled with 40 μ L precipitant solution. In the sample wells,

ratios of 100:150 nL, 150:150 nL, and 200:150 nL protein to precipitant were dispensed. Protein concentration was 10 mg/mL in 10 mM phosphate buffer, pH 7.0. Commercially available crystallization screens were used for initial screening. Crystallization plates were stored in a Formulatrix RI-1000 imaging device at 22 °C. Successful hits were obtained using the JCSG-plusTM from Molecular Dimensions. Initial screening conditions were optimized for growth of larger crystals, yielding final conditions as follows: 0.2 M BIS-TRIS, pH 5.5, 0.2 M MgSO₄, 23.2% PEG 3350.

The crystal was soaked with mother liquor supplemented with 20% 2-methyl-2,4-pentanediol (MPD), harvested using a cryo-loop, and flash-vitrified in liquid nitrogen. Datasets were collected at beam-line ID29 (56) of European Synchrotron Radiation Facility (ESRF, Grenoble, France) at 100 K using a DECTRIS PILATUS 6M detector.

The dataset was processed with XDS and symmetry equivalent reflections merged with XDSCONV (57). Intensities were not converted to amplitudes. Initially the high-resolution cutoff was 2.31 Å (CC1/2=0.23) (58). The phase problem was solved by molecular replacement using balbes (29). The model was further improved by iterative cycles of manual model building using COOT (59) and maximum likelihood refinement using PHENIX-Refine (60). PHENIX-Refine converted intensities into amplitudes using the French and Wilson algorithm (61). The final high-resolution cutoff was based on performing paired refinement using the PDB_REDO webservice (62). Final stages of refinement included Translation Liberation Screw (TLS) parameters, isotropic B-factor model, automated addition of hydrogens and water molecules, optimization of X-ray/ADP weight, and optimization of X-ray/stereochemistry weight. The model was validated with MolProbity (63). Figures were prepared with PyMOL Molecular Graphics

System (Version 1.3, Schrödinger, LLC). Atomic coordinates have been deposited in the Protein Data Bank under accession code 6ERC. OMIT maps were calculated by removing the heme followed by refinement in phenix.refine (59). FEM maps were calculated using the feature-enhanced map tool in PHENIX (59).

RMSD values and Z-scores were calculated using the PDBe Fold v2.59 server with a lowest acceptable match of 70% (64). CAVER (65) was used to detect putative substrate channels of DdPoxA and goat LPO (pdb-code: 2R5L). For calculation of the characteristics of the channels, the heme iron was set as a starting point for both proteins. Channels were calculated with the following settings: minimum probe radius: 0.9 Å; shell depth: 4 Å; shell radius: 3 Å; clustering threshold: 3.5; number of approximating balls: 12; input atoms: 20 amino acids.

Stopped-flow Spectroscopy. Pre-steady-state kinetic experiments were performed to study the relevant redox intermediates of DdPoxA. The experiments were carried out with a stopped-flow apparatus (model SX-18MV and Pi-star-180, Applied Photophysics) in the conventional or sequential mode. The optical quartz cell with a path length of 10 mm had a volume of 20 µl. The dead time of both stopped-flow machines was 1.0 ms. The spectra were followed with the photodiode array detector, and the single wavelength time traces were recorded using a photomultiplier detector (Applied Photophysics). All measurements were performed at 25 °C in triplicates.

Binding of cyanide and reaction with hydrogen peroxide were performed in the conventional stopped-flow mode. The first syringe contained 2 - 4 µM protein solution in 50 mM phosphate buffer, pH 7.0, the second syringe contained cyanide or hydrogen peroxide solutions in varying concentrations. Rates of cyanide binding and Compound I formation were obtained by single or double

exponential fitting of the time traces at 412 nm. Pseudo-first-order rate constants, k_{obs} , were used to calculate the apparent bimolecular binding constant (k_{on}) by plotting k_{obs} values *versus* cyanide concentration. From the x-intercept of this plot k_{off} , the dissociation rate constant, was estimated, enabling calculation of the dissociation constant $K_{\text{D}} = k_{\text{off}}/k_{\text{on}}$.

For determination of Compound I formation, the obtained pseudo-first-order rate constants (k_{obs}) were used to calculate the apparent bimolecular rate constant (k_{app}) from the slope of the plot of k_{obs} values *versus* hydrogen peroxide concentration. Multi-mixing, sequential stopped-flow spectroscopy was performed to monitor the reduction of DdPoxA Compound I using the two-electron donors Cl^- , Br^- , I^- and SCN^- . A solution containing 4 - 8 μM DdPoxA was premixed with a 2.5 molar excess of hydrogen peroxide in the aging loop for 400 ms to form Compound I.

***Dictyostelium discoideum* and *Klebsiella aerogenes* cell culture.** The *D. discoideum* laboratory strain AX2 and the mutant strains ΔDdpoxA and ΔnoxABC (38) were cultivated axenically in 10 cm Petri dishes in HL5c medium (5 g/L peptone, 5 g/L thiotone E peptone, 10 g/L glucose, 5 g/L yeast extract, 0.35 g/L $\text{Na}_2\text{HPO}_4 \cdot 7\text{H}_2\text{O}$, 0.35 g/L KH_2PO_4 , 0.05 g dihydrostreptomycin-sulfate, pH 6.5) supplemented with 50 U/mL penicillin and 50 mg/mL streptomycin (Pen/Strep) at 22 °C. The exponentially growing cells were harvested at about 80% confluence for experiments. To obtain higher cell numbers, *D. discoideum* was transferred into shaking flasks with HL5c medium (plus Pen/Strep) at 22 °C, and cells were harvested with a maximal density of 5×10^6 /mL. The avirulent laboratory wild-type strain of *K. aerogenes* was cultured overnight in LB medium (10 g/L peptone, 5 g/L yeast extract, 5 g/L NaCl, pH 7.0) without antibiotics at 37 °C and 180 rpm.

Expression of DdPoxA during cell development. *D. discoideum* cells were grown in shaking culture in HL5c medium (+ Pen/Strep), harvested by centrifugation (1600 rpm, 4 °C, 4 min) and washed three times by resuspending the pellet in 0.5 volume of cold, sterile development buffer (5 mM Na_2HPO_4 , 5 mM KH_2PO_4 , 1 mM CaCl_2 , 2 mM MgCl_2). For each required time point, 2×10^8 cells were resuspended in 2 mL cold development buffer and one aliquot was frozen as time point zero. For each time point, one 10 cm Petri dish was prepared with three Whatman #3 filter papers and one Whatman #50 on top. The filter papers were soaked with 5 mL development buffer, remaining air bubbles were removed with a sterile spreader and any excess liquid was aspirated. The cell suspensions were slowly distributed over the filter. Cells were incubated at 22 °C in a humid box. For cell harvesting, the #50 filter paper was placed in a Falcon tube, 20 mL cold development buffer was added and mixed to remove cells from the filter. The cell suspension was centrifuged (1600 rpm, 4 °C, 4 min) and frozen (66). Subsequently, *D. discoideum* cells were thawed by immediately adding 400 μL lysis buffer to the pellet. Cells lysis was carried out by sonication (micro tip, 3×20 sec per sample, 50% duty cycle) and cell debris was centrifuged (13000 rpm, 4 °C, 15 min). Protein concentration was determined by Nanodrop using the formula for DNA contaminated protein samples: $c(\text{mg/mL}) = 1.55 \times (A_{280}) - 0.76 \times (A_{260})$. Samples were diluted to a concentration of 10 mg/mL in hot SDS-PAGE sample buffer for gel electrophoresis. Protein separation by SDS-PAGE was carried out using 8% acrylamide gels at 150 V. The separated proteins were blotted on nitrocellulose membranes (120 V, 4 °C, 90 min), and stained with Ponceau S to verify that the total amount of protein is constant in all samples. After washing the membrane with PBS-T, the blotted proteins were blocked with Blotting-

Grade Blocker (BioRad) and detected with an anti-DdPoxA as primary antibody and an anti-rabbit antibody conjugated to HRP as secondary antibody. As a positive control, the blot was stripped and incubated again with anti-Actin antibody as primary antibody and anti-mouse conjugated with HRP as secondary antibody. Band development was carried out with the Clarity Western ECL Substrate (BioRad).

Comparative development of *D. discoideum*. *D. discoideum* wild-type (AX2), Δ DdPoxA and Δ noxABC were grown in HL5c medium (+ Pen/Strep) to a maximal cell density of 5×10^6 /mL. Cells were centrifuged (1600 rpm, 4 °C, 4 min) and washed three times with Soerensen medium (2 g/L KH_2PO_4 , 0.29 g/L Na_2HPO_4 , pH 6.0). Drops of *D. discoideum* cells with a known concentration (1×10^6 /mL) were plated on Soerensen agar plates (2 g/L KH_2PO_4 , 0.29 g/L Na_2HPO_4 , pH 6.0, 15 g/L agar) and incubated at 22 °C in a humid box. Pictures were taken with a stereoscope at desired time points during development.

Investigation of fruiting body sterility. 0.2 mL overnight culture of *K. aerogenes* in LB medium was mixed with 8×10^4 *D. discoideum* cells. The cell mixture was plated on SM/2 agar plates (5 g/L glucose, 5 g/L bacto peptone, 0.5 g/L yeast extract, 1 g/L $\text{MgSO}_4 \times 7\text{H}_2\text{O}$, 1 g/L Na_2HPO_4 , 2.2 g/L KH_2PO_4 , 15 g/L agar) and incubated 3 - 4 days at 22 °C upside down in a humid box, until *D. discoideum* cells have formed fruiting bodies. To investigate the contamination of individual fruiting bodies, single sori were picked up carefully with sterile pipette tips and transferred to a new SM/2 agar plate. The plates were incubated over night at 37 °C (a temperature that fully restricts *D. discoideum* growth) to grow residual *K. aerogenes* cells and the number of contaminated fruiting bodies was counted. To quantify the number of residual bacteria, 25 fruiting bodies were taken up with sterile pipette tips and dissolved

in 500 μL Soerensen medium. 50 μL of the suspension were plated on new SM/2 agar plates. The plates were incubated at 37 °C overnight to grow *K. aerogenes* cells and the number of bacterial colonies was counted. The experiment was carried out in biological triplicate.

Determination of number of spores and fruiting bodies. 10 fruiting bodies of each, *D. discoideum* wild-type (AX2) and the mutants Δ DdPoxA and Δ noxABC, were randomly picked and resuspended in 100 μL Soerensen medium. The number of spores in the solution was determined using a hemocytometer. Number of produced fruiting bodies was determined by counting fruiting bodies in the comparative development experiment (see above).

Cloning, Expression, and localization of DdPoxA-GFP. The *poxA* CDS was PCR-amplified with forward primer *poxA*-FL-F (ttgatctaaaaATGCGATTAAATTTAATATCGTTTTTTAT AATATTAC), which contains a BglII site, and reverse primer *poxA*-FL-R (tttactagtTTTTCTAAAAACATTTGGTTGAACATAACCAATAT), which contains a SpeI site, from cDNA generated from *D. discoideum* cells undergoing development. The PCR product was cloned into pJET1.2 using the CloneJET PCR Cloning Kit (ThermoFisher) and sequenced. The *poxA*-containing fragment was excised by sequential digestion with SpeI and BglII, gel-extracted, and ligated into pDM323 (67), also cut with SpeI and BglII, upstream of *gfp* to create a *poxA-gfp* fusion. Amoeba stage *D. discoideum* cells were transfected with the resulting plasmid and selected with 5 $\mu\text{g}/\text{ml}$ G418. PoxA-GFP expressing cells were seeded on glass coverslips and fixed in ultracold methanol (68). After blocking with PBS/0.3% gelatin, cells were stained with rabbit anti-GFP (MBL), a cocktail of four mouse monoclonal antibodies recognizing protein disulphide isomerase (PDI) (69), rat

anti-rabbit antibody labelled with AlexaFluor 488 (ThermoFisher), and rat anti-mouse antibody labelled with AlexFluor 594 (ThermoFisher). Nuclei were stained with DAPI, and coverslips were mounted on

microscope slides with ProLong Gold antifade reagent (ThermoFisher). Images were taken with a Axio Imager Z1m (Zeiss) and processed using ImageJ.

ACKNOWLEDGEMENTS

This project was supported by the Austrian Science Fund, FWF [Doctoral Program BioToP - Molecular Technology of Proteins (W1224)]. The TS laboratory is supported by multiple grants from the Swiss National Science Foundation, and TS is a member of iGE3 (www.ige3.unige.ch) as well as of the COST Actions BM1203 EU-ROS and CA15138 TRANSAUTOPHAGY. We thank Xhuezhi Zhang for creating the $\Delta DdpoxA$ knockout mutant. GM was in part supported by Federal Ministry of Economy, Family and Youth through the initiative “Laura Bassi Centres of Expertise”, funding the Center of Optimized Structural Studies, N°253275. We thank Daniel Maresch for performing the mass spectrometry measurements. We thank Cristina Bosmani, Louise Lefrançois, Ana Teresa López Jiménez, Lyudmil Raykov, Elena Cardenal-Muñoz, Florence Leuba, Nabil Hanna and Caroline Barisch for help in lab work and discussions.

CONFLICT OF INTEREST

The authors declare that they have no conflict of interest with the contents of this work.

AUTHOR CONTRIBUTIONS

CO and PGF conceived and coordinated the study. AN and CO wrote the paper. AN performed *in vitro* protein production, purification and data collection. AN and JDD performed *in-vivo* experiments and data collection. JDD and TS coordinated and supervised the *in vivo* studies, reviewed and edited the manuscript. DM performed mass spectrometric measurements. GM and KDC were responsible for structural studies including crystallization, structure determination, refinement and analysis. MZ supervised recombinant protein expression and purification. AN, MB and GB conducted and analyzed spectroelectrochemical measurements.

FOOTNOTES

The refined coordinates and structure factors have been deposited in the RCSB Protein Data Bank under the accession code 6ERC.

Abbreviations: AX2, *Dictyostelium discoideum* wild-type laboratory strain; DdPoxA, peroxidase from *Dictyostelium discoideum*; $\Delta DdpoxA$, *Dictyostelium discoideum* knockout strain lacking DdPoxA; DSC, differential scanning calorimetry; ECD, electronic circular dichroism; EPO, eosinophil peroxidase; hsPxd01, human peroxidase 1; HOX, hypohalous acid; LPO, lactoperoxidase; LspPOX; peroxidase from the cyanobacterium *Lyngbya* sp. PCC 8106; MALS, multi-angle light scattering; MPO, myeloperoxidase; GlcNAc, N-acetyl-D-glucosamine; ER, endoplasmic reticulum; $\Delta noxABC$, *Dictyostelium discoideum* knockout strain lacking the NoxA, B and C, homologs of Nox2/gp91^{phox}, the catalytic subunit of NOX; NOX, NADPH oxidase; SEC, size-exclusion chromatography; ROS, reactive oxygen species; TPO, thyroid peroxidase; X⁻, halide.

REFERENCES

1. Annesley, S. J., and Fisher, P. R. (2009) *Dictyostelium discoideum* - A model for many reasons. *Mol. Cell. Biochem.* **329**, 73-91
2. Cosson, P., and Soldati, T. (2008) Eat, kill or die: when amoeba meets bacteria. *Curr. Opin. Microbiol.* **11**, 271-276
3. Romeralo, M., Escalante, R., and Baldauf, S. L. (2012) Evolution and diversity of dictyostelid social amoebae. *Protist* **163**, 327-343
4. Li, S. I., and Purugganan, M. D. (2011) The cooperative amoeba: *Dictyostelium* as a model for social evolution. *Trends Genet.* **27**, 48-54
5. Williams, J. G. (2010) *Dictyostelium* finds new roles to model. *Genetics.* **185**, 717-726
6. Eichinger, L., Pachebat, J. A., Glöckner, G., Rajandream, M. A., Sugang, R., Berriman, M., Song, J., Olsen, R., Szafranki, K., Xu, Q., Tunggal, B., Kummerfeld, S., Madera, M., Konfortov B. A., Rivero F., Bankier, A. T., Lehmann R., Hamlin N., Davies, R., Gaudet, P., Fey, P., Pilcher K., Chen, G., Saunders, D., Sodergren, E., Davis, P., Kerhornou, A., Nie, X., Hall, N., Anjard, C., Hemphill, L., Bason N., Farbrother, P., Desany, B., Just E., Morio T., Rost, R., Churcher, C., Cooper, J., Haydock, S., van Driessche, N., Cronin, A., Goodhead, I., Muzny, D., Mourier, T., Pain, A., Lu, M., Harper, D., Lindsay, R., Hauser, H., James, K., Quiles, M., Madan Babu, M., Saito, T., Buchrieser, C., Wardroper, A., Felder, M., Thangavelu, M., Johnson, D., Knights, A., Loulseged, H., Mungall, K., Oliver, K., Price, C., Quail, M. A., Urushihara, H., Hernandez, J., Rabinowitsch, E., Steffen, D., Sanders, M., Ma, J., Kohara, Y., Sharp, S., Simmonds, M., Spiegler, S., Tivey, A., Sugano, S., White, B., Walker, D., Woodward, J., Winckler, T., Tanaka, Y., Shaulsky, G., Schleicher, M., Weinstock, G., Rosenthal, A., Cox, E. C., Chisholm R. L., Gibbs, R., Loomis, W. F., Platzer, M., Kay, R. R., Williams, J., Dear, P. H., Noegel, A. A., Barrell, B., and Kuspa, A. (2005) The genome of the social amoeba *Dictyostelium discoideum*. *Nature* **435**, 43-57
7. Zamocky, M., Hofbauer, S., Schaffner, I., Gasselhuber, B., Nicolussi, A., Soudi, M., Pirker, K. F., Furtmüller, P. G., and Obinger, C. (2015) Independent evolution of four heme peroxidase superfamilies. *Arch. Biochem. Biophys.* **574**, 108-119
8. Hofbauer, S., Schaffner, I., Furtmüller, P. G., and Obinger, C. (2014) Chlorite dismutases - a heme enzyme family for use in bioremediation and generation of molecular oxygen. *Biotechnol. J.* **9**, 461-473
9. Zamocky, M., Jakopitsch, C., Furtmüller, P. G., Dunand, C., and Obinger, C. (2008) The peroxidase-cyclooxygenase superfamily. Reconstructed evolution of critical enzymes of the innate immune system. *Proteins* **71**, 589-605
10. Klebanoff, S. J., Kettle, A. J., Rosen, H., Winterbourn, C. C., and Nauseef, W. M. (2013) Myeloperoxidase: a front-line defender against phagocytosed microorganisms. *J. Leukoc. Biol.* **93**, 185-196
11. Bafort, F., Parisi, O., Perraudin, J. P., and Jijakli, M. H. (2014) Mode of action of lactoperoxidase as related to its antimicrobial activity: a review. *Enzyme Res.* **2014**, Article ID 517164
12. Nauseef, W. M. (2014) Myeloperoxidase in human neutrophil host defence. *Cell Microbiol.* **16**, 1146-1155
13. Ihalin, R., Loimaranta, V., and Tenovuo, J. (2006) Origin, structure, and biological activities of peroxidases in human saliva. *Arch. Biochem. Biophys.* **445**, 261-268
14. Malik, A., and Batra, J. K. (2012) Antimicrobial activity of human eosinophil granule proteins: involvement in host defence against pathogens. *Crit. Rev. Microbiol.* **38**, 168-181
15. Desjardins M., Houde, M., and Gagnon, E. (2005) Phagocytosis: the convoluted way from nutrition to adaptive immunity. *Immunol. Rev.* **207**, 158-165
16. Cosson, P., and Lima, W. C. (2014) Intracellular killing of bacteria: Is *Dictyostelium* a model macrophage or an alien? *Cell. Microbiol.* **16**, 816-823

17. Furtmüller, P. G., Zederbauer, M., Jantschko, W., Helm, J., Bogner, M., Jakopitsch, C., and Obinger, C. (2006) Active site structure and catalytic mechanisms of human peroxidases. *Arch. Biochem. Biophys.* **445**, 199-213
18. Zederbauer, M., Furtmüller, P. G., Brogioni, S., Jakopitsch, C., Smulevich, G., and Obinger, C. (2007) Heme to protein linkages in mammalian peroxidases: impact on spectroscopic, redox and catalytic properties. *Nat. Prod. Rep.* **24**, 571–584
19. Lin, Y. W. (2015) The broad diversity of heme-protein cross-links: an overview. *Biochim. Biophys. Acta* **1854**, 844-859
20. Zhang, M., Gaschen, B., Blay, W., Foley, B., Naigwood, N., Kuiken, C., and Korber, B. (2004) Tracking global patterns of N-linked glycosylation site variation in highly variable viral glycoproteins: HIV, SIV, and HCV envelopes and influenza hemagglutinin. *Glycobiology* **14**, 1229-1246
21. Zederbauer, M., Furtmüller, P. G., Brogioni, S., Jakopitsch, C., Smulevich, G., and Obinger, C. (2007) Heme to protein linkages in mammalian peroxidases: impact on spectroscopic, redox and catalytic properties. *Nat. Prod. Rep.* **24**, 571–584
22. Singh, A. K., Singh, N., Sharma, S., Singh, S. B., Kaur, P., Bhushan, A., Srinivasan, A., and Singh, T. P. (2008) Crystal structure of lactoperoxidase at 2.4 Å resolution. *J. Mol. Biol.* **376**, 1060-1075
23. Battistuzzi, G., Bellei, M., Vlasits, J., Banerjee, S., Furtmüller, P. G., Sola, M., and Obinger, C. (2010) Redox thermodynamics of lactoperoxidase and eosinophil peroxidase. *Arch. Biochem. Biophys.* **494**, 72-77
24. Ortiz de Montellano, P. R. (2016) Heme peroxidases: selfprocessing of peroxidases (Raven, E., and Dunford, B., Eds) RSC Metallobiology Series No. 4, pp 3–30, The Royal Society of Chemistry, Cambridge, U.K.
25. Auer, M., Gruber, C., Bellei, M., Pirker, K. F., Zamocky, M., Kroiss, D., Teufer, S. A., Hofbauer, S., Soudi, M., Battistuzzi, G., Furtmüller, P. G., and Obinger, C. (2013) A stable bacterial peroxidase with novel halogenating activity and an autocatalytically linked heme prosthetic group. *J. Biol. Chem.* **288**, 27181-27199
26. Auer, M., Nicolussi, A., Schütz, G., Furtmüller, P. G., and Obinger, C. (2014) How covalent heme to protein bonds influence the formation and reactivity of redox intermediates of a bacterial peroxidase. *J. Biol. Chem.* **289**, 31480-31491
27. Nicolussi, A., Auer, M., Weissensteiner, J., Schütz, G., Katz, S., Maresch, D., Hofbauer, S., Bellei, M., Battistuzzi, G., Furtmüller, P. G., and Obinger, C. (2017) Posttranslational modification of heme *b* in a bacterial peroxidase: The role of heme to protein bonds in ligand binding and catalysis. *Biochemistry* **56**, 4525-4538
28. Paumann-Page, M., Katz, R. S., Bellei, M., Schwartz, I., Edenhofer, E., Sevcnikar, B., Soudi, M., Hofbauer, S., Battistuzzi, G., Furtmüller, P. G., Obinger, C. (2017) Pre-steady-state kinetics reveal the substrate specificity and mechanism of halide oxidation of truncated human peroxidase 1. *J. Biol. Chem.* **292**, 4583-4592
29. Long, F., Vagin, A. A., Young, P., and Murshudov, G. N. (2008) BALBES: a molecular-replacement pipeline. *Acta Crystallogr. D Biol Crystallogr.* **64**, 125-32
30. Furtmüller, P. G., Janschko, W., Zederbauer, M., Jakopitsch, C., Arnhold, J., and Obinger, C. (2004) Kinetics of interconversion of redox intermediates of lactoperoxidase, eosinophil peroxidase and myeloperoxidase. *Jpn. J. Inf. Dis.* **57**, 30-31
31. Banerjee, S., Furtmüller, P. G., and Obinger, C. (2011) Bovine lactoperoxidase – a versatile one- and two-electron catalyst of high structural and thermal stability. *Biotechnol. J.* **6**, 231-243
32. Sharma, S., Singh, A. K., Kaushik, S., Sinha, M., Singh, R. P., Sharma, P., Sirohi, H., Kaur, P., and Singh T. P. (2013) Lactoperoxidase: structural insights into the function, ligand binding and inhibition. *Int. J. Biochem. Mol. Biol.* **4**, 108-128
33. Stajdohar, M., Jeran, L., Kokosar, J., Blenkus, D., Janez, T., Kuspa, A., Shaulsky, G., and Zupan, B. (2015) dictyExpress: visual analytics of NGS gene expression in *Dictyostelium*, February 26, [https://www.dictyexpress.org]

34. Parikh A., Miranda, E. R., Katoh-Kurasawa M., Fuller, D., Rot, G., Zagar, L., Curk, T., Sucgang, R., Chen, R., Zupan, B., Loomis, W. F., Kuspa, A., and Shaulsky, G. (2010) Conserved developmental transcriptomes in evolutionary divergent species. *Genome Biol.*, **11**, R35
35. Leiba, J., Sabra, A., Bodinier, R., Marchetti, A., Lima, W. C., Melotti, A., Perrin, J., Burdet, F., Pagni, M., Soldati, T., Lelong, E., and Cosson, P. (2017) Vps13F links bacterial recognition and intracellular killing in *Dictyostelium*. *Cell. Microbiol.* **19**, e12722
36. Buckley, C. M., Gopaldass, N., Bosmani, C., Johnston, S. A., Soldati, T., Insall, R. H., and King, J. S. (2016) WASH drives early recycling from macropinosomes and phagosomes to maintain surface phagocytic receptors. *Proc. Natl. Acad. Sci. USA*, **4**, E5902-E5915
37. Aguirre, J. and Lambeth, J. D. (2010) Nox enzymes from fungus to fly to fish and what they tell us about Nox function in mammals. *Free Radic. Biol. Med.* **49**, 1342–1353
38. Zhang, X., Zhuchenko, O., Kuspa, A., and Soldati, T. (2016) Social amoebae trap and kill bacteria by casting DNA nets. *Nat. Commun.* **7**, 10938
39. Zhang, X., and Soldati, T. (2016) Of Amoeba and Men: Extracellular DNA traps as an ancient cell-intrinsic defense mechanism. *Front. Immunol.* **7**, Article 269
40. Grishkovskaya, I., Paumann-Page, M., Tscheliessnig, R., Stampler, J., Hofbauer, S., Soudi, M., Sevcnikar, B., Oostenbrink, C., Furtmüller, P. G., Djinović-Carugo, K., Nauseef, W. M., and Obinger, C. (2017) Structure of human promyeloperoxidase (proMPO) and the role of the propeptide in processing and maturation. *J. Biol. Chem.* **292**, 8244-8261
41. Banerjee, S., Stampler, J., Furtmüller, P. G., and Obinger, C. (2011) Conformational and thermal stability of mature dimeric human myeloperoxidase and a recombinant monomeric form from CHO cells. *Biochim. Biophys. Acta* **1814**, 375-87.
42. Carpena, X., Vidossich, P., Schroettner, K., Calisto, B. M., Banerjee, S., Stampler, J., Soudi, M., Furtmüller, P. G., Rovira, C., Fita, I., and Obinger, C. (2009) Essential role of proximal histidine-asparagine interaction in mammalian peroxidases. *J. Biol. Chem.* **284**, 25929-25937
43. Battistuzzi, G., Bellei, M., Zederbauer, M., Furtmüller, P. G., Sola, M., and Obinger, C (2006) Redox thermodynamics of the Fe(III)/Fe(II) couple of human myeloperoxidase in its high-spin and low-spin forms. *Biochemistry* **45**, 12750-12755
44. Battistuzzi, G., Bellei, M., Bortolotti, C. A., and Sola, M. (2010) Redox properties of heme peroxidases. *Arch. Biochem. Biophys.* **500**, 21-36
45. Battistuzzi, G., Stampler, J., Bellei, M., Vlasits, J., Soudi, M., Furtmüller, P. G., and Obinger, C. (2011) Influence of the covalent heme-protein bonds on the redox thermodynamics of human myeloperoxidase. *Biochemistry* **50**, 7987-7994
46. Arnhold, J., Monzani, E., Furtmüller, P. G., Zederbauer, M., Casella, L., and Obinger, C. (2006) Kinetics and thermodynamics of halide and nitrite oxidation by heme peroxidases. *Eur. J. Inorg. Chem.* **2006**, 3801–3811.
47. Furtmüller, P. G., Burner, U., and Obinger, C. (1998) Reaction of myeloperoxidase compound I with chloride, bromide, iodide, and thiocyanate. *Biochemistry* **37**, 17923-17930
48. Furtmüller, P. G., Burner, U., Regelsberger, G., and Obinger, C. (2000) Spectral and kinetic studies on the formation of eosinophil peroxidase compound I and its reactions with halides and thiocyanate. *Biochemistry* **39**, 15578-84
49. Klebanoff, S.J. (1967) Iodination of bacteria: a bactericidal mechanism. *J. Exp. Med.* **126**, 1063-1078
50. Chandler, J. D., and Day, B.J. (2015) Biochemical mechanisms and therapeutic potential of pseudohalide thiocyanate in human health. *Free Radic. Res.* **49**, 695-710

51. Skaff, O., Pattison, D. I., and Davies, M. J. (2009) Hypothiocyanous acid reactivity with low-molecular mass and protein thiols: absolute rate constants and assessment of biological relevance. *Biochem. J.*, **422**, 111-117
52. Betts, P. M., Rinder, D. F., and Fleeker, J. R. (1979) Thiocyanate utilization by an Arthrobacter. *Can. J. Microbiol.* **25**, 1277-1282
53. Shetaya, W. H., Young, S. D., Watts, M. J., Ander, E. L., and Bailey, E. H. (2012) Iodine dynamics in soils. *Geochim. Cosmochim. Acta* **77**, 457-473
54. Petersen, T. N., Brunak, S., von Heijne, G., and Nielsen, H (2011) SignalP 4.0: discriminating signal peptides from transmembrane regions. *Nature Methods* **8**, 785-786
55. Bradford, M. M. (1976) A rapid and sensitive method for the quantification of microgram quantities of protein utilizing the principle of protein-dye binding. *Anal. Biochem.* **72**, 248-254
56. de Sanctis D., Beteva A., Caserotto H., Dobias F., Gabadinho J., Giraud T., Gobbo A., Guijarro M., Lentini M., Lavault, B., Mairs, T., McSweeney, S., Petitdemange, S., Rey-Bakaikoa, V., Surr, J., Theveneau, P., Leonard, G. A., and Mueller-Dieckmann, C. (2012) ID29: a high-intensity highly automated ESRF beamline for macromolecular crystallography experiments exploiting anomalous scattering. *J. Synchrotron Radiat.* **19**, 455-461
57. Kabsch W. (2010) XDS. *Acta Crystallogr D. Biol. Crystallogr.* **66**, 125-132
58. Karplus P. A., and Diederichs K. (2012) Linking crystallographic model and data quality. *Science* **336**, 1030-1033
59. Emsley P., Lohkamp B., Scott W. G., and Cowtan, K. (2010) Features and development of Coot. *Acta Crystallogr. D. Biol. Crystallogr.* **66**, 486-501
60. Adams P. D., Afonine P. V., Bunkóczi G., Chen V.B., Davis I. W., Echols N., Headd J. J., Hung L. W., Kapral G. J., Grosse-Kunstleve R. W., McCoy, A. J., Moriarty, N. W., Oeffner, R., Read, R. J., Richardson, D. C., Richardson, J. S., Terwilliger, T. C., and Zwart, P. H. (2010) PHENIX: a comprehensive Python-based system for macromolecular structure solution. *Acta Crystallogr. D. Biol. Crystallogr.* **66**, 213-221
61. French S., and Wilson K. (1978) On the treatment of negative intensity observations. *Acta Crystallogr. A* **34**, 517-525
62. Joosten, R. P., Salzemann, J., Bloch, V., Stockinger, H., Berglund, A. C., Blanchet, C., Bongcam-Rudloff, E., Combet, C., Da Costa, A. L., Deleage, G., Diarena, M., Fabbretti, R., Fettahi, G., Flegel, V., Gisel, A., Kasam, V., Kervinen, T., Korpelainen, E., Mattila, K., Pagni, M., Reichstadt, M., Breton, V., Tickle, I. J. and Vriend, G (2009) PDB_REDO: automated re-refinement of X-ray structure models in the PDB. *J. Appl. Crystallogr.* **42**, 376-384
63. Davis I. W., Murray L. W., Richardson J. S., and Richardson D. C. (2004) MOLPROBITY: structure validation and all-atom contact analysis for nucleic acids and their complexes. *Nucleic Acids Res.* **32**, W615-W619
64. Krissinel, E., and Henrick, K. (2004). Secondary-structure matching (SSM), a new tool for fast protein structure alignment in three dimensions. *Acta Cryst. D Biol Crystallogr.* **60**, 2256-2268.
65. Chovancova, E., Pavelka, A., Benes, P., Strnad, O., Brezovsky, J., Kozlikova, B., Gora, A., Sustr, V., Klvana, M., Medek, P., Biedermannova, L., Sochor, J., and Damborsky, J. (2012) CAVER 3.0: a tool for the analysis of transport pathways in dynamic protein structures. *PLoS Comput. Biol.* **8**, e1002708
66. Fey, P., Kowal, A.S., Gaudet, P., Pilcher, K. E., and Chisholm, R. L. (2007) Protocols for growth and development of *Dictyostelium discoideum*. *Nat. Protoc.* **2**, 1307-1316

67. Veltman, D. M., Akar, G., Bosgraaf, L., and Van Haastert, P. J. (2009) A new set of small, extrachromosomal expression vectors for *Dictyostelium discoideum*. *Plasmid* **61**, 110-118
68. Hagedorn, M., Neuhaus, E. M., and Soldati, T. (2006) Optimized fixation and immunofluorescence staining methods for Dictyostelium cells. *Methods Mol. Biol.* **346**, 327-338
69. Monnat, J., Hacker, U., Geissler, H., Rauchenberger, R., Neuhaus, E. M., Maniak, M., and Soldati, T. (1997) Dictyostelium discoideum protein disulfide isomerase, an endoplasmatic reticulum resident enzyme lacking a KDEL-type retrieval signal. *FEBS Lett.* **418**, 357-362

TABLES

Table 1. Data collection and refinement statistics.

	DdPoxA (6ERC)
Data collection	
Wavelength (nm)	1.072
Resolution range (Å)	48.67 - 2.5 (2.589 - 2.5) ^a
Space group	P 3 ₁ 2 1
Unit cell (Å)	128.253, 128.253, 146.015, 90, 90, 120
Total reflections	485020 (46671)
Unique reflections	48501 (4813)
Multiplicity	10.0 (9.7)
Completeness (%)	99.90 (99.98)
Mean <i>I</i> /sigma (<i>I</i>)	7.64 (0.60)
Wilson B-factor (Å ²)	55.76
Refinement	
R-merge (%)	0.3149 (4.14)
R-meas (%)	0.3319 (4.372)
R-pim (%)	0.1043 (1.395)
CC1/2	0.995 (0.298)
CC*	0.999 (0.678)
Reflections used in refinement	48462 (4812)
Reflections used for <i>R</i> -free	1189 (113)
<i>R</i> -work	0.2311 (0.3814)
<i>R</i> -free	0.2594 (0.3385)
CC (work)	0.954 (0.527)
CC (free)	0.928 (0.440)
No. of non-hydrogen atoms	8586
No. of atoms macromolecules	8240
No. of atoms ligands	182
No. of atoms solvent	164
Protein residues	1022
RMS (bonds) (Å)	0.005
RMS (angles) (°)	0.8
Ramachandran favored (%)	96.37
Ramachandran allowed (%)	3.63
Ramachandran outliers (%)	0
Rotamer outliers (%)	0.11
Clashscore	1.51
Average B-factor (Å ²)	64.84
Macromolecules (Å ²)	65.41
Ligands (Å ²)	54.96
Solvent (Å ²)	47.02
Number of TLS groups	2

^a Values in parentheses represent the highest resolution shell.

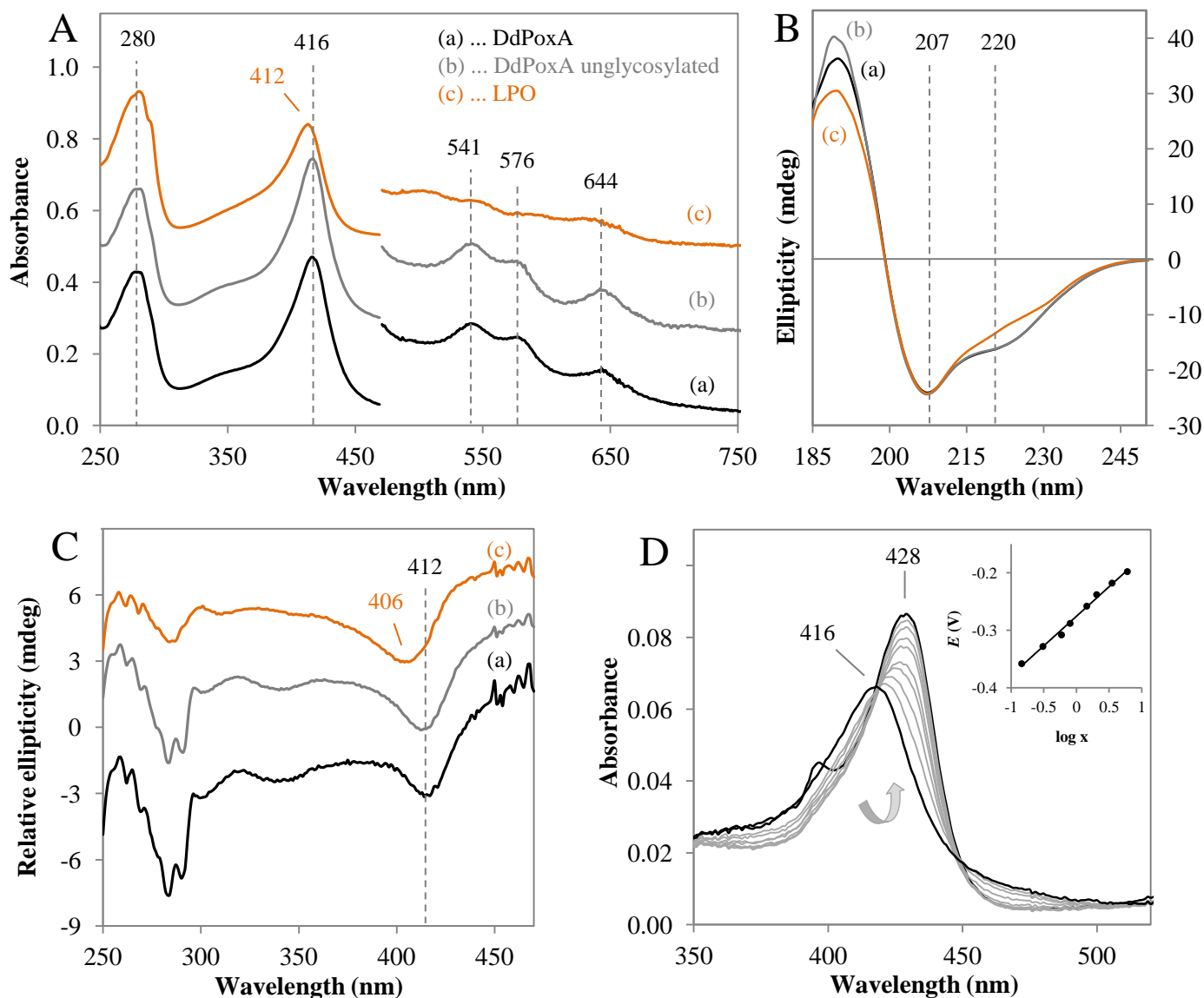


Figure 1. UV-vis, ECD spectra and reduction potential of DdPoxA. (A) UV-vis spectra of purified DdPoxA and LPO were recorded using 5 μM protein in 50 mM phosphate buffer at pH 7.0. The wavelength range from 480 - 750 nm is expanded by a factor of five for better visibility. (B) Electronic circular dichroism spectra of DdPoxA in the far-UV region from 185 - 250 nm at 25 $^{\circ}\text{C}$. Concentration of DdPoxA was 0.5 mg/mL in 10 mM phosphate buffer, pH 7.0. The path length was 1 mm, with a bandwidth of 3 nm, using a scan time of 10 sec per point. (C) Electronic circular dichroism spectra of 10 μM DdPoxA and LPO in 50 mM phosphate buffer, pH 7.0 in the visible region from 300 - 470 nm at 25 $^{\circ}\text{C}$. The path length was 10 mm, the spectral bandwidth was 1 nm, and the scan time was 10 s per point. (D) Electronic absorption spectra of DdPoxA at different applied potentials, whereby black line represent fully oxidized ($A_{\lambda_{\text{ox}}}^{\text{Max}}$ at 416 nm) and red line shows fully reduced form ($A_{\lambda_{\text{red}}}^{\text{Max}}$ at 428 nm). Arrow indicates the transition from oxidized to reduced form. Titration was performed with 10 μM protein in 100 mM potassium phosphate buffer pH 7.0 containing 100 mM NaCl at 25 $^{\circ}\text{C}$. Inset: Corresponding Nernst plot, whereby X represents $(A_{428\text{nm}}^{\text{Max}} - A_{428\text{nm}})/(A_{410\text{nm}}^{\text{Max}} - A_{410\text{nm}})$.

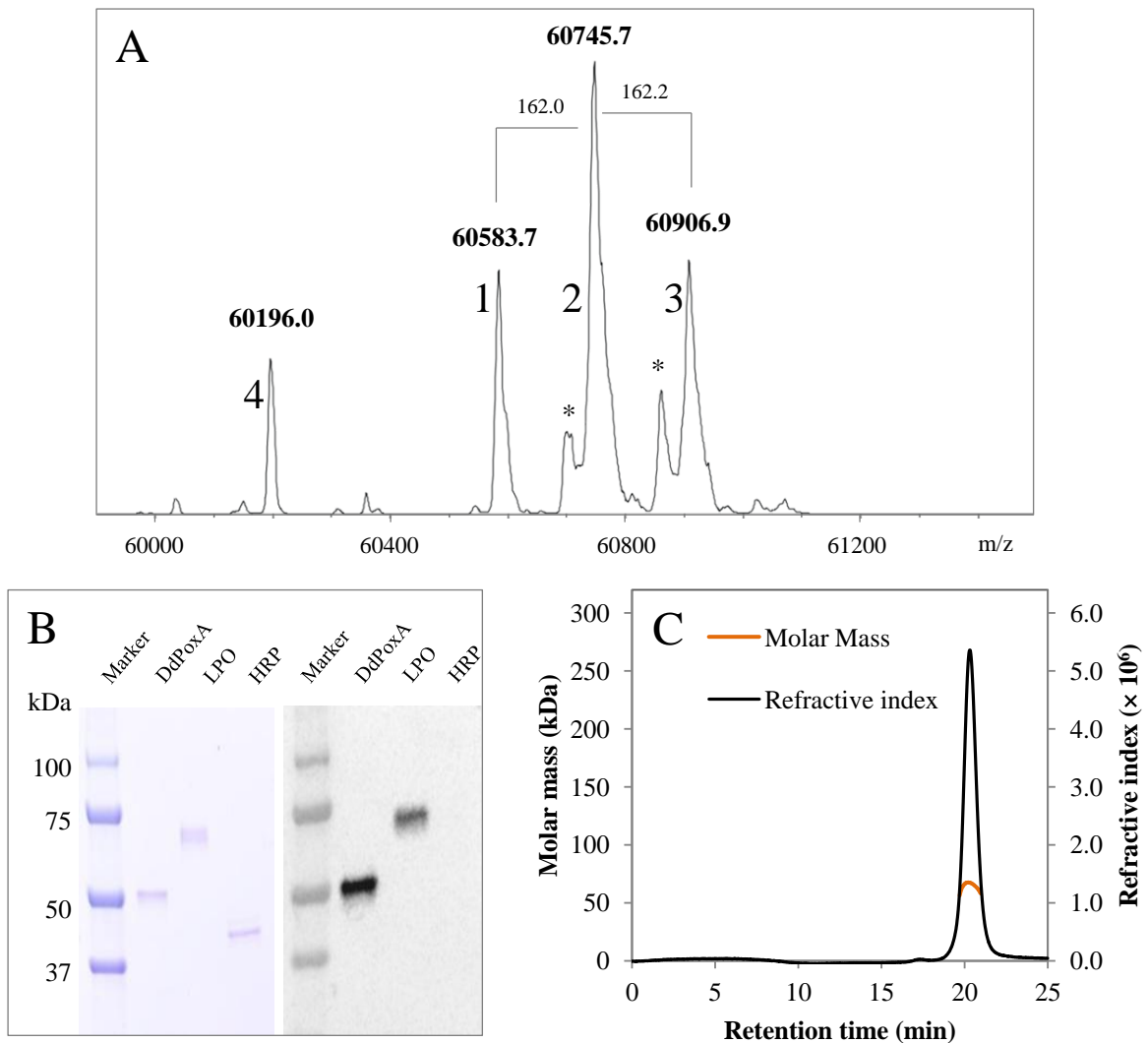


Figure 2. Evidence of covalently bound heme and analysis of oligomeric state. (A) For intact mass spectrometry, 2.5 μg DdPoxA in 10 mM phosphate buffer pH 7.0, was directly injected to the LC-MS system and analysed by a QTOF instrument equipped with the standard ESI source in the positive ion mode. Asterisks represent nonspecific adducts caused by TFA. (B) SDS-PAGE (left panel) and detection of covalently bound heme by ECL (right panel) of 0.3 μg of deglycosylated DdPoxA (lane 1), lactoperoxidase (lane 2) and horseradish peroxidase (lane 3). (C) Presentation of MALS analysis showing refractive index (RI, black line) detection. The orange line shows the distribution of molar masses in the analysed protein solution.

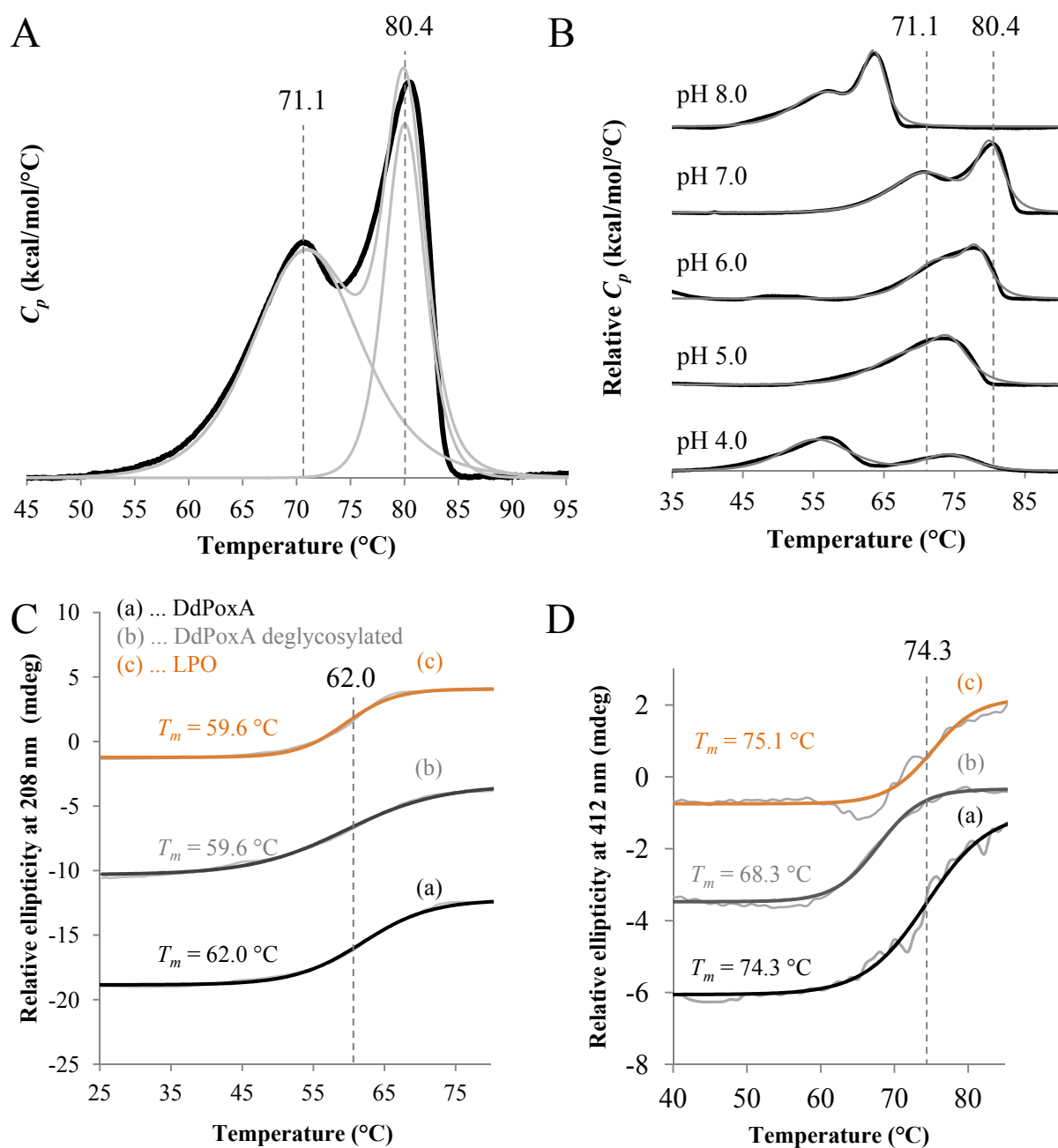


Figure 3. Investigation of thermal and conformational stability of DdPoxA. Normalized DSC thermograms of DdPoxA at pH 7.0 (A) and pH 4.0 – 8.0 (B) after baseline correction. Measurements were performed with 5 μ M protein in 100 mM phosphate buffer, using a heat rate of 60 °C/h. The obtained thermograms are shown as bold black lines and the corresponding fitted non-two state transition peaks are depicted as thin grey lines. Vertical lines have been inserted for presentation of respective melting temperatures at pH 7.0. (C) Temperature-mediated unfolding of DdPoxA was monitored by electronic circular dichroism at 208 nm, following the melting of α -helical structures in 100 mM phosphate buffer, pH 7.0. (D) Temperature-mediated unfolding of DdPoxA monitored by electronic circular dichroism at 412 nm in 100 mM phosphate buffer, pH 7.0, showing the unfolding of the heme cavity.

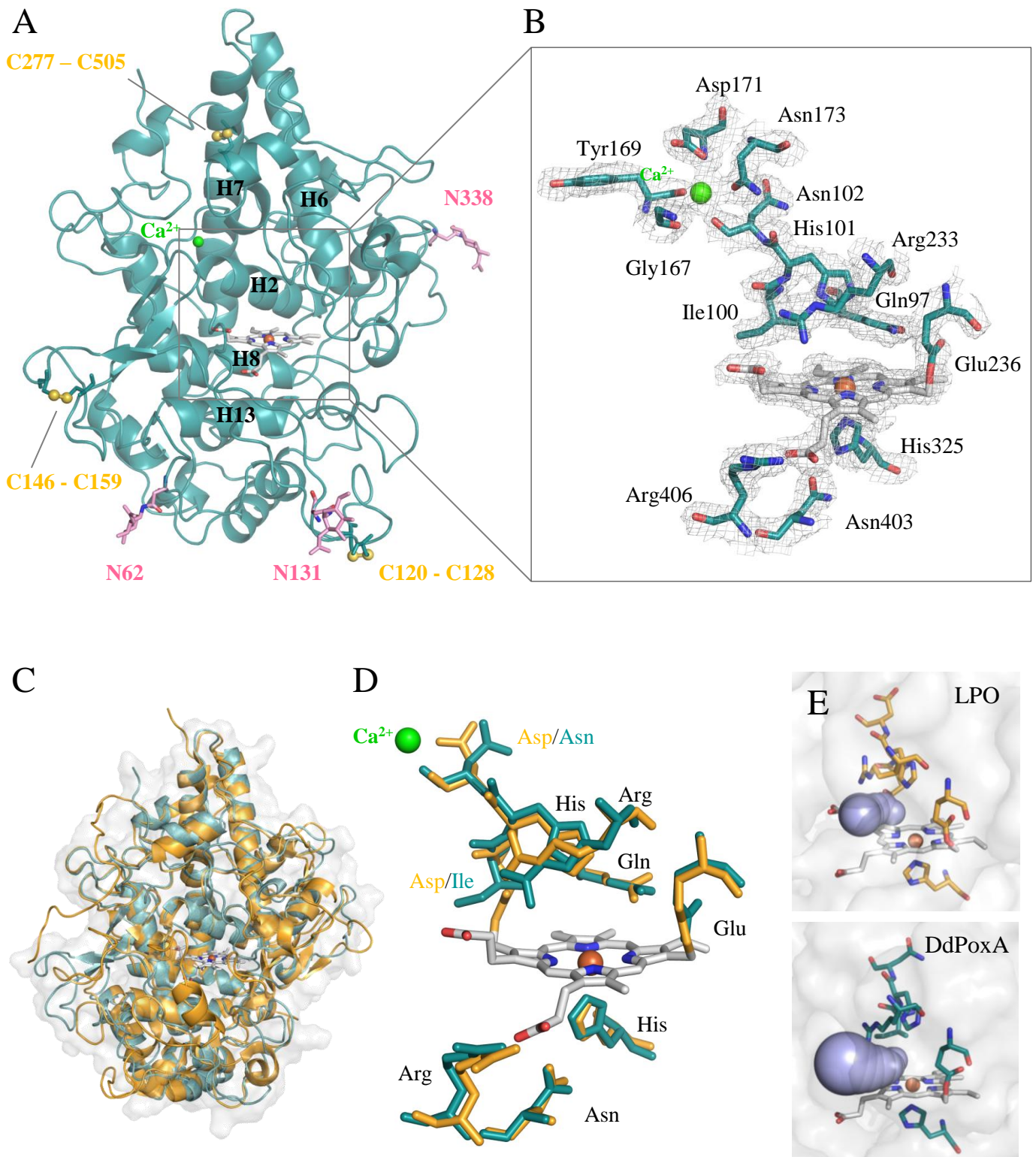


Figure 4. Structural investigation of DdPoxA. (A) Crystal structure of recombinant DdPoxA (in teal, pdb accession code 6ERC). Chain A of the asymmetric unit was used for preparation of figures. The three disulfide bridges are depicted in yellow. The three N-glycosylation sites with one attached GlcNAc are shown in pink, the distal Ca^{2+} ion is highlighted in green. (B) Close-up of the active site and the Ca^{2+} binding site of DdPoxA including a 2.5 Å resolution FEM map contoured at 1 σ (grey). (C) Overlay of the secondary structures of DdPoxA (teal) and goat LPO (yellow, pdb accession code 2R5L). (D) Active site overlay of DdPoxA (teal) and goat LPO (yellow). (E) Accessibility of substrate channels of LPO (yellow) and DdPoxA (teal) with the highest calculated probabilities. Substrate channels are depicted in violet. Distances and bottlenecks were calculated with CAVER 3.0.

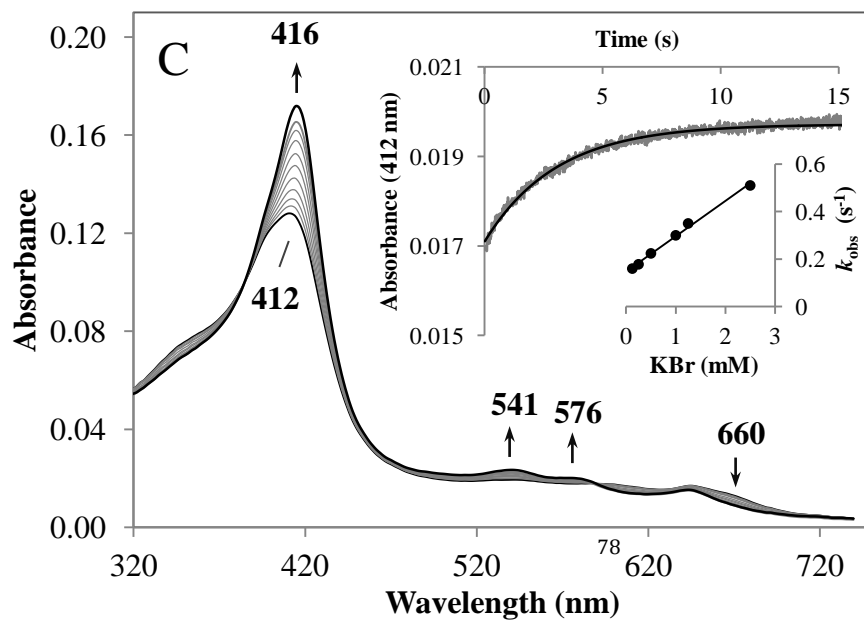
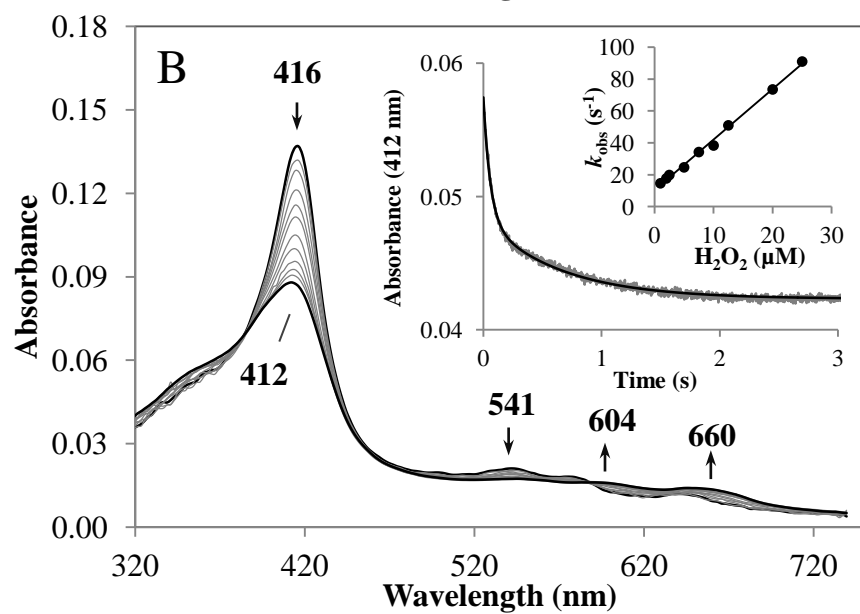
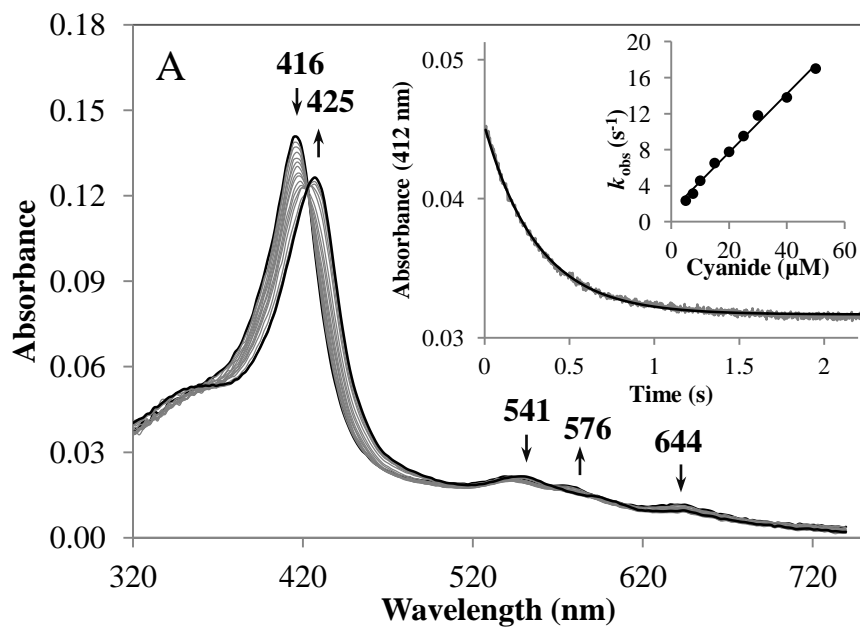


Figure 5. Reaction of ferric DdPoxA with cyanide and H₂O₂, and reaction of Compound I with bromide. (A) Spectral transition upon binding of 500 μM cyanide to 2 μM DdPoxA, measured in conventional stopped-flow mode. The first spectrum shows the ferric protein in its high-spin state (absorbance maximum at 416 nm), the second spectrum was recorded after 5 ms of mixing and the following spectra show the formation of the DdPoxA-cyanide low-spin complex (absorbance maximum at 425 nm). Arrows indicate directions of spectral changes. All measurements were performed in 50 mM phosphate buffer pH 7.0 at 25 °C. Inset 1: Typical time trace at 412 nm upon reaction of 1 μM protein with 7.5 μM cyanide (single exponentially fitted). Inset 2: Linear dependence of k_{obs} from cyanide concentrations. The apparent association rate constant k_{on} was obtained from the slope and the apparent dissociation rate constant k_{off} was calculated from the intercept. The dissociation constant K_{D} is determined by the ratio of $k_{\text{off}}/k_{\text{on}}$. (B) Spectral changes during reaction of 2 μM DdPoxA with 5 μM H₂O₂ measured in the conventional stopped-flow mode. The first spectrum shows the ferric protein, the second spectrum was recorded 1 ms after mixing and the subsequent spectra display the transition to Compound I. Inset 1: Typical time trace at a wavelength of 412 nm upon reaction of 0.5 μM DdPoxA with 2 μM H₂O₂, fitted as a double exponential function. Inset 2: Linear dependence of k_{obs} from H₂O₂ concentrations. The apparent bimolecular rate constant k_{app} obtained from the slopes of the regression lines. (C) Spectral transition upon adding 5 mM bromide to 2 μM DdPoxA Compound I in the sequential stopped-flow mode. Compound I was preformed using 5 μM hydrogen peroxide. After a delay time of 400 ms, the first spectrum was recorded 4.9 s after mixing. Subsequent spectra show the reduction of Compound I. Inset 1: Typical time trace at 412 nm of 0.5 μM Compound I with 5 mM bromide (single exponential fit). Inset 2: Linear dependence of the pseudo first order constant k_{obs} from bromide concentrations.

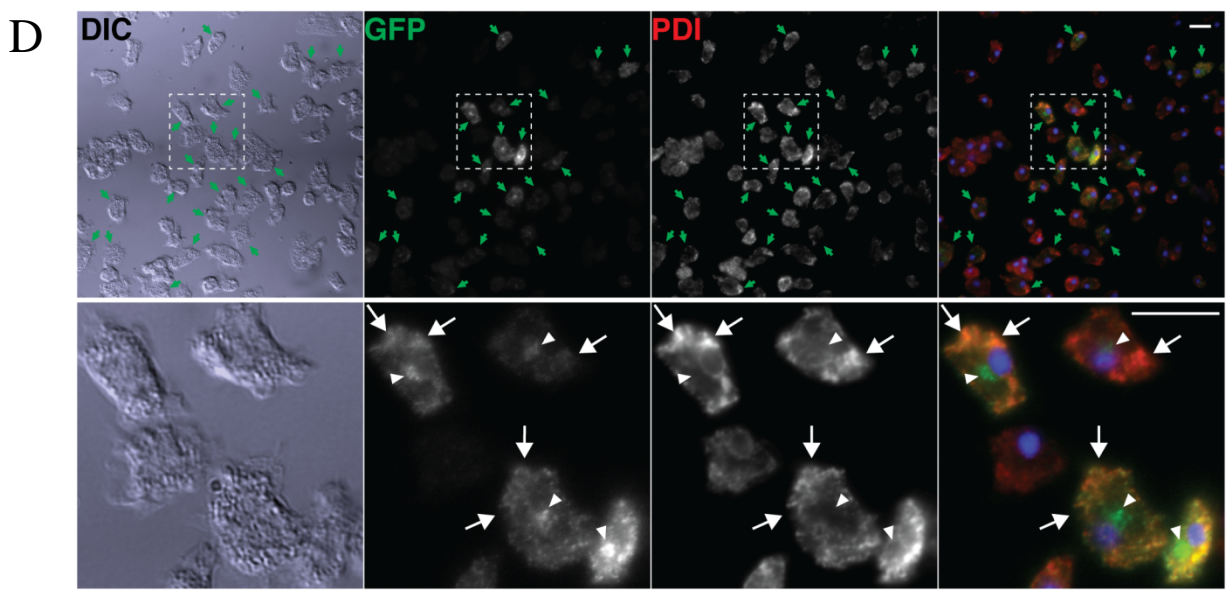
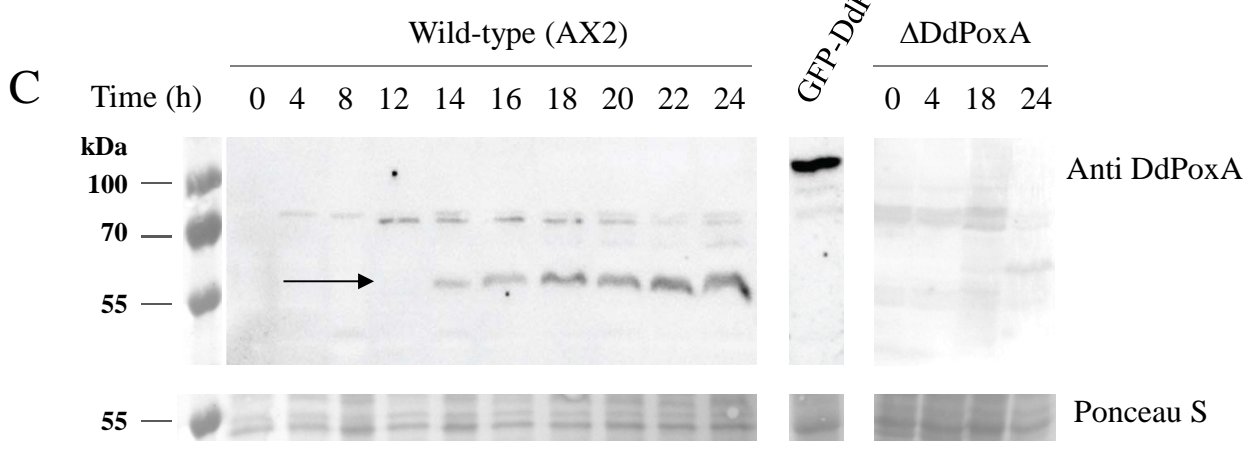
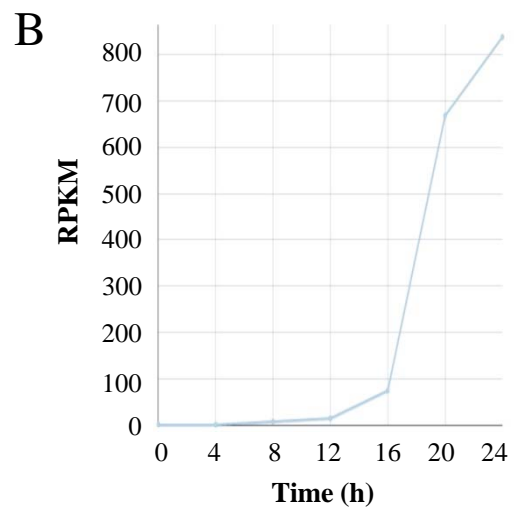
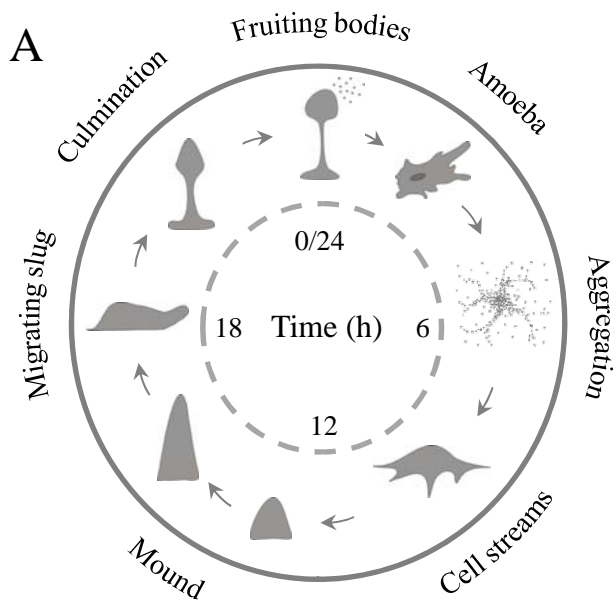


Figure 6. Expression pattern of DdPoxA in *D. discoideum*. (A) Schematic time course of *D. discoideum* development upon starvation in a time range of 24 hours. (B) Open source RNAseq detection of DdPoxA throughout the development cycle of *D. discoideum* AX4 wild-type, whereby RPKM represent reads per million mapped reads. Data extracted using dictyExpress. (C) Ponceau S staining and Western blot of *D. discoideum* wild-type (AX2) and $\Delta DdpoxA$ cell lysates at different time points of development (0-24 hours after start of starvation). Ponceau S staining and Western blot detected by anti-Actin indicate loading of equal protein concentration. Anti-DdPoxA staining shows expression profile of DdPoxA upon cell development. (D) Fluorescence microscopy analysis of DdPoxA localization. A heterogeneous population of *D. discoideum* expressing a GFP-tagged version of DdPoxA was fixed and stained with antibodies against GFP (green) and PDI (red), a marker for the endoplasmic reticulum. Nuclei were stained with DAPI (blue). Scale bars represent 10 μm . In the upper panel, green arrows mark cells expressing PoxA-GFP, and the box delineates the area magnified in the lower panel, in which white arrows indicate co-localization in the ER and white arrowheads indicate a Golgi-like staining pattern.

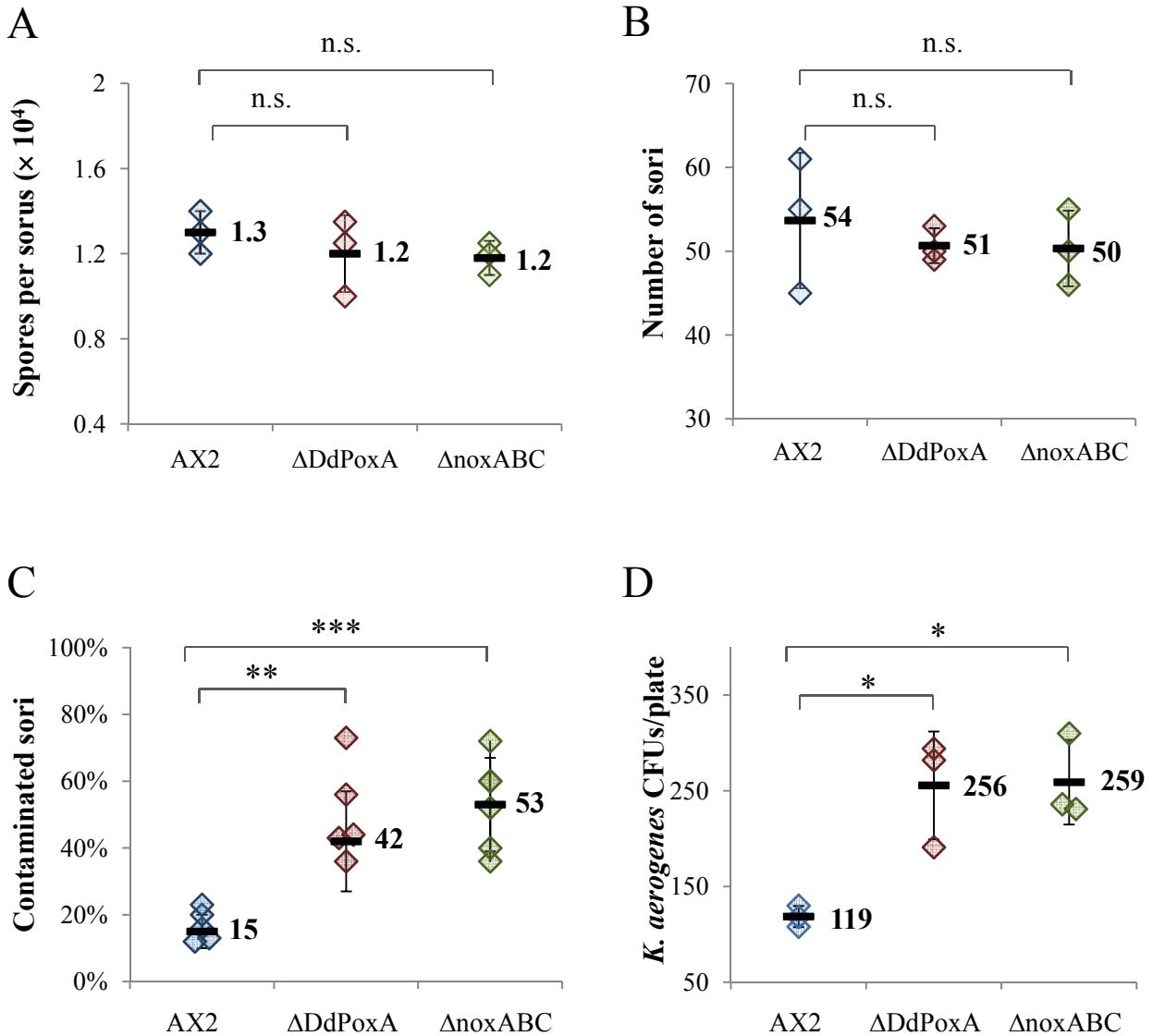


Figure 7. Influence of DdPoxA on fruiting body sterility of *D. discoideum*. Comparison of *D. discoideum* wild-type (AX2), Δ DdPoxA and Δ noxABC mutants regarding production of spores (A) and fruiting bodies (B). Numbers in the graph (A) refer to the average number of spores in one fruiting body. Significance of data was analysed by using a t-test with a p-value cutoff of 0.05. P-values are indicated as follows: n.s., not significant ($p > 0.05$); *, $p \leq 0.05$; **, $p \leq 0.01$; ***, $p \leq 0.001$. Numbers in graph (B) are counted fruiting bodies from drops of developed *D. discoideum* cells with an initial cell density of 1×10^6 cells per drop. Both experiments were carried out in biological triplicates. (C) Contamination of fruiting bodies from *D. discoideum* wild-type (AX2), Δ DdPoxA and Δ noxABC. Cells were grown on a lawn of *K. aerogenes*, cell development started upon consumption of edible bacteria. N = 125 examined fruiting bodies for AX2 and Δ DdPoxA and 150 fruiting bodies for Δ noxABC in at least five biological replicates. (D) Number of CFUs of *K. aerogenes* in fruiting body suspensions from *D. discoideum* wild-type (AX2), Δ DdPoxA and Δ noxABC. The experiment was carried out in biological triplicates.

SUPPLEMENTAL INFORMATION

Secreted Heme Peroxidase from *Dictyostelium discoideum*: Insights into Catalysis, Structure and Biological Role

Andrea Nicolussi^[1], Joe Dan Dunn^[2], Georg Mlynek^[3], Marzia Bellei^[4], Marcel Zamocky^[1,5], Gianantonio Battistuzzi^[6], Kristina Djinović-Carugo^[3,7], Paul G. Furtmüller^[1], Thierry Soldati^[2], and Christian Obinger^[1]*

[1] Department of Chemistry, Division of Biochemistry, BOKU - University of Natural Resources and Life Sciences, 1190 Vienna, Austria;

[2] Department of Biochemistry, Faculty of Science, University of Geneva, 1211 Genève, Switzerland;

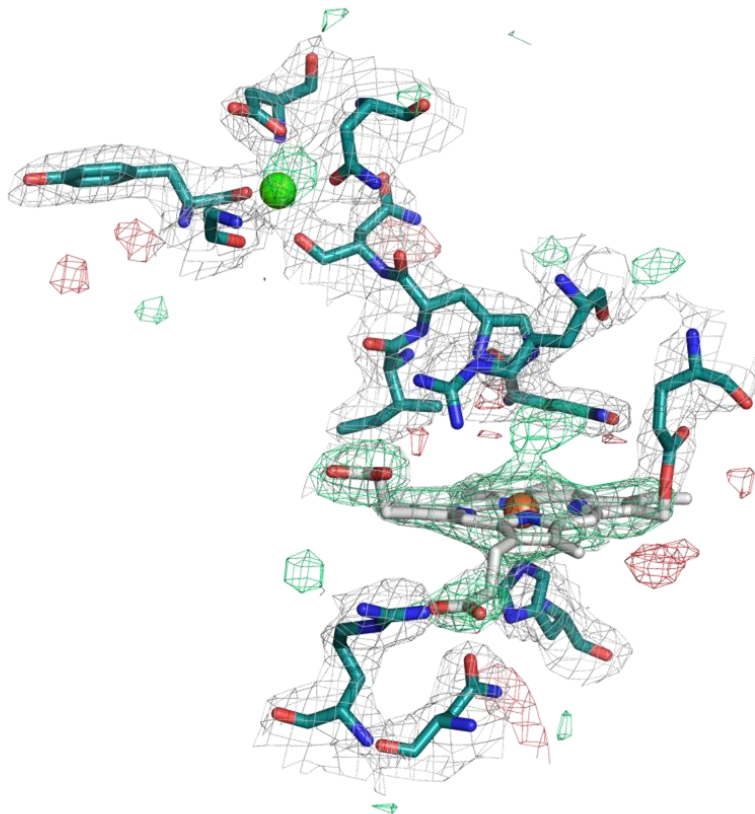
[3] Department for Structural and Computational Biology, Max F. Perutz Laboratories, University of Vienna, 1030 Vienna, Austria;

[4] Department of Life Sciences, University of Modena and Reggio Emilia, via Campi 103, 41125 Modena, Italy;

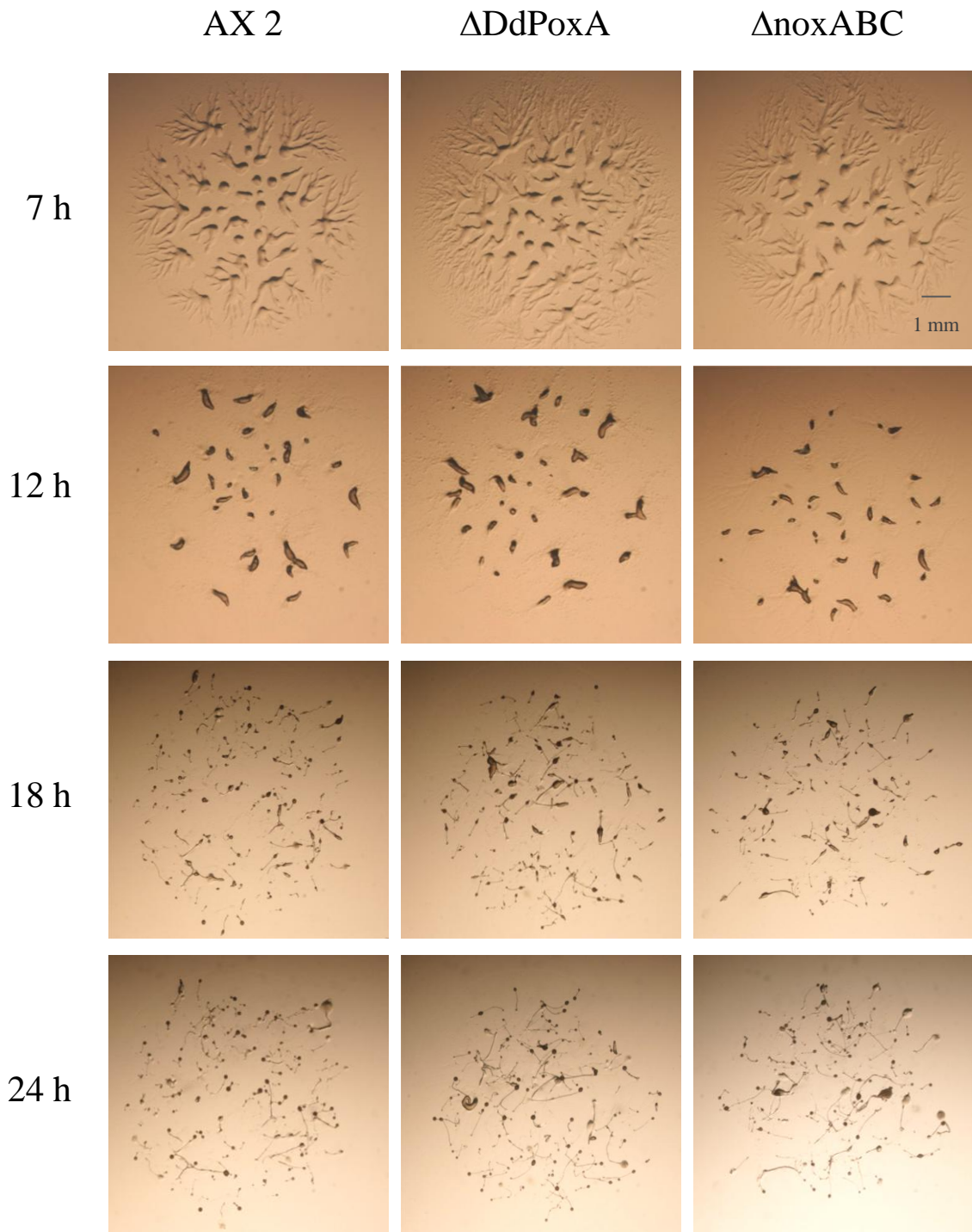
[5] Institute of Molecular Biology, Slovak Academy of Sciences, 84551 Bratislava, Slovakia;

[6] Department of Chemistry and Geology, University of Modena and Reggio Emilia, 41125 Modena, Italy;

[7] Department of Biochemistry, Faculty of Chemistry and Chemical Technology, University of Ljubljana, 1000 Ljubljana, Slovenia



Supplemental Figure S2. OMIT map of DdPoxA active site structure. OMIT map (A) of the active site structure of DdPoxA. The 2.5 Å resolution mF_o-DF_c maps contoured at $\pm 3 \sigma$ positive (green) and negative (red) and $2mF_o-DF_c$ maximum-likelihood omit map contoured at 1σ (grey) are shown. Maps were calculated for a refined model with the heme atoms omitted.



Supplemental Figure S3. Comparative cell development. Representative images of *D. discoideum* wild-type (AX2), Δ DdPoxA and Δ noxABC mutants throughout the development cycle (7, 12, 18 and 24 h after start of starvation) recorded using a stereomicroscope. Cell density in all images is 1×10^6 cells per drop.

Conclusion

In contrast to former studies that mainly focused on human or vertebrate peroxidases, this thesis aimed on investigating two ancestral, non-mammalian representatives of the peroxidase-cyclooxygenase superfamily. Phylogenetic reconstruction of this superfamily provided the basis of the project by revealing the presence of bacterial and ancient eukaryotic peroxidases with homology to mammalian counterparts.¹ This work focused on the LspPOX from the cyanobacterium *Lyngbya* sp. PCC 8106 and DdPoxA from the social amoeba *Dictyostelium discoideum*. While LspPOX has already been studied earlier^{2,3}, DdPoxA is a novel subject of research. Both of these heme enzymes belong to Family 6 (i.e. peroxidockerins) of the peroxidase-cyclooxygenase superfamily⁴ and share a high sequence similarity with the mammalian peroxidases, especially lactoperoxidase (47% amino acid similarity for LspPOX and 58% for DdPoxA). However, a detailed investigation of the structure-function relationships in the active site of vertebrate peroxidases such as MPO, LPO, EPO (Family 1) or peroxidasin 1 (Family 2) has been hampered by the fact that their recombinant production was limited to mammalian or insect cell cultures with small yields. In contrast, LspPOX and DdPoxA can be produced recombinantly in satisfying amounts in *E. coli* and *P. pastoris* and therefore allowed for a comprehensive biochemical and biophysical characterization as well as the production of site-directed mutants and X-ray crystallization experiments.

Wild-type LspPOX has been described in previous publications.^{2,3} However, the impact of each covalent heme to protein bond has not been studied in detail. Hence, three mutants of LspPOX were produced and investigated, having the acidic amino acids (Glu and Asp) in the active site exchanged by alanine (D109A, E238A and the double mutant D109A/E238A). We demonstrated that this enzyme is a perfect model peroxidase for the mammalian counterparts with almost 100% amino acid identity to LPO regarding the catalytic residues in the active site. For the first time, we were able to produce heme-free apo-proteins of the wild-type and the mutants that could be reconstituted with hemin to the corresponding heme *b* holoprotein. The autocatalytic formation of the heme to protein bonds was facilitated by incubating the holoenzymes with hydrogen peroxide. Thus we were able to study the consequences of the posttranslationally modified heme that is characteristic for several members of the peroxidase-cyclooxygenase superfamily.

In addition, recent sequencing of the genome of *D. discoideum* combined with phylogenetic reconstructions revealed the presence of a homologous heme peroxidase in *D. discoideum* (DdPoxA).^{4,5} Also DdPoxA shows homology to the vertebrate peroxidases, even though their last common ancestor lived approximately one billion years ago.⁶ It also exhibits a high sequence

similarity to the prokaryotic LspPOX (55% amino acid sequence similarity). The fully sequenced genome and the enormous knowledge about *D. discoideum* as a cell culture emphasized our idea to investigate this enzyme also *in vivo*. Hence, the two selected model proteins were investigated in a comprehensive biophysical and biochemical study and the results are discussed with respect to the well-investigated mammalian peroxidases with a primary focus on catalysis and structural features.

X-ray structures have been solved from mammalian MPO and LPO to different resolutions and in combination with various ligands.⁷⁻⁹ While the crystal structure of human MPO was solved already in 1995¹⁰, the only structures available from LPO derive from other vertebrates (e.g. goat, bovine, buffalo). The presence of covalent heme to protein ester bonds has been proven by these X-ray structures, nevertheless no structural data of active site mutants of these metalloenzymes is available. Although we did not solve the X-ray crystal structure of LspPOX or the mutants, we demonstrated by mass spectrometry that the covalent heme attachments at each site (Asp or Glu) can be formed individually and independently from each other. Further, the introduced mutations do not affect the overall secondary structure of the polypeptide chain, but have a severe impact on the architecture of the heme cavity.¹¹

In case of DdPoxA, chemiluminescent detection and mass spectrometry provided first evidence that the heme is covalently attached to the protein matrix.¹² However, sequence alignments with the mammalian counterparts revealed that there is only one acidic amino acid (Glu236) in the active site that could possibly form a heme to protein ester bond. The second acidic amino acid in DdPoxA that forms a covalent ester linkage in MPO or LPO (Asp) is replaced by an isoleucine. Finally, the X-ray crystal structure of DdPoxA was solved to a resolution of 2.5 Å and for the first time allowed for structural analysis of a non-vertebrate peroxidase from the peroxidase-cyclooxygenase superfamily (pdb accession code 6ERC). The overall, mainly α -helical secondary structure and especially the architecture of the five core helices is conserved between DdPoxA and the homologous goat LPO (pdb accession code 2R5L).¹³ However, neither the glycosylation sites nor the disulfide bridges are conserved between the two enzymes. Zooming into the active site of DdPoxA confirmed the presence of one covalent ester linkage between the conserved Glu236 and the 1-methyl substituent of the heme group, which is established to full extent. This completeness has not been observed in any other homologous peroxidase yet. In fact, a recently published crystal structure of bovine LPO revealed that the bond between the distal glutamate and the heme group is only partially formed¹³, whereas the aspartate linkage is formed entirely. These findings underline

the importance of the DdPoxA crystal structure for understanding the structure-function relationships and distinctions of the peroxidase-cyclooxygenase superfamily.

It has been reported previously that the presence of covalent heme to protein ester linkages has a severe impact on the planarity of the heme group. The covalent bonds lead to a distortion of the heme causing a bow-shaped structure of the porphyrin ring. Subsequently this bending leads to a decreased electron density at the heme iron, thereby increasing the reduction potential of the iron center.¹⁴⁻¹⁶ We probed the redox properties of the Fe(III)/Fe(II) couples of LspPOX as well as DdPoxA spectroelectrochemically using an OTTLE cell. However, determination of reliable values for wild-type LspPOX and the D109A mutant was not possible due to the fact that two different species were present in the samples. Most probably this heterogeneity derived from the presence of molecules with bound heme group as well as non-covalently linked heme *b* species. Nevertheless, we could see a trend in the values, whereby the deletion of the ester linkages significantly decreased the standard reduction potential of the Fe(III)/Fe(II) couples, ranging from $E^{\circ'} = -158$ mV (wild-type LspPOX) to $E^{\circ'} = -227$ mV (double mutant D109A/E238A).¹¹ The standard reduction potential of the Fe(III)/Fe(II) couple of DdPoxA was found to be rather low compared to the mammalian peroxidases ($E^{\circ'} = -0.276$ V).¹² These values confirm the hierarchy that has been proposed for the mammalian peroxidases, whereby the standard reduction potential increases with the number of covalent heme to protein ester bonds. The hierarchy was reported as follows: MPO: +5 mV (three covalent linkages) > wild-type LspPOX: -158 mV > LPO: -176 mV > human peroxidase 1: -128 mV > EPO: -126 mV (two covalent linkages each) > DdPoxA: -276 mV (one covalent linkage) > horseradish peroxidase: -306 mV (non-covalently linked heme *b*).¹⁷⁻²⁰

According to these differences in the standard reduction potentials, also the catalytic properties of peroxidases change upon formation of the covalent heme to protein bonds. Formation of Compound I seems to be not affected by these posttranslational modifications and shows a rate of approximately $1 - 5 \times 10^7$ M⁻¹ s⁻¹ for all investigated peroxidases of the peroxidase-cyclooxygenase superfamily. Similar values were also found for LspPOX as well as DdPoxA. The halogenation reaction, however, is greatly dependent on the presence of heme to protein bonds as a high reduction potential is needed to oxidize halides like bromide or chloride. This has been shown in detail for LspPOX, where the halogenation activity is drastically altered by the active site mutations described above. Exchange of E238 to alanine resulted in enzymatic features similar to the wild-type enzyme, while the mutant D109A exhibited significantly reduced reaction rates for all investigated oxidation reactions. Nevertheless, upon formation of the covalent bond of the

remaining acidic amino acid (Glu) by incubation with H₂O₂, the D109A mutant exhibited wild-type-like features, including a very efficient oxidation of bromide to hypobromous acid. The double mutant D109A/E238A showed no reactivity at all, except a neglectable spectral change upon formation of the Compound I.¹¹

Investigation of the redox intermediates of DdPoxA revealed that DdPoxA Compound I is also not able to oxidize chloride, and bromide only to a very small extent. Nevertheless it exhibits extraordinary high reaction rates with iodide and the pseudohalide thiocyanate ($> 10^8 \text{ M}^{-1} \text{ s}^{-1}$), suggesting these one-electron donors as the *in vivo* substrates¹² and HOI and HOSCN as primary oxidation products. Both of these (pseudo-)halides are found in steady-state equilibria in soil, the natural habitat of *D. discoideum*. Thiocyanate (SCN⁻) is secreted and utilized by many organisms as a nitrogen source, and it has been shown to be a suitable substrate for the vertebrate peroxidases LPO, EPO and MPO. The oxidation product - HOSCN - is a more selective and less reactive molecule than other hypohalous acids, such as HOCl or HOBr.²¹ Iodide on the other hand is the most prevalent form of iodine-species in soil and river water, being in a constant balance with iodine and iodate.²² The bactericidal effect of ionization of bacteria such as *E. coli* has been described already in 1967.²³

However, MPO is still the only known peroxidase which is able to oxidize chloride to hypochlorous acid due to its extraordinarily high reduction potential of the Fe(III)/Fe(II) couple.^{14,24} Hypobromous acid is known to be produced by the mammalian peroxidases MPO, LPO, EPO and peroxidasin 1.^{16,19,25} On the other hand, iodide and the pseudohalide thiocyanate have a rather low reduction potential and can therefore be oxidized even by peroxidases with very low reduction potential (e.g. HRP).^{20,26}

Apart from analyzing the recombinant DdPoxA, we also aimed at elucidating the physiological role of the peroxidase in *D. discoideum*. Initially we suggested a function of DdPoxA in phagocytosis, analogous to myeloperoxidase in neutrophil leukocytes, where engulfed pathogens are killed by producing highly oxidizing hypochlorous acid.²⁷ However, contrary to this theory, DdPoxA is not expressed in vegetative cells but is upregulated only in later stages of cell development.¹² Therefore, the hypothesis of a MPO-like function of DdPoxA during phagocytosis had to be revised as phagocytosis is (nearly) exclusively found in the amoeboid, single celled stage of *D. discoideum*.²⁸ We demonstrated that a GFP-tagged version of DdPoxA in *D. discoideum* is present in the endoplasmic reticulum, suggesting that it passes the secretion pathway and very likely is secreted into the extracellular space. The prediction of a signal peptide in the DdPoxA

sequence further supports our theory that DdPoxA is secreted by the multicellular aggregates of *D. discoideum* as an antibacterial agent. Investigations on the cell development cycle of wild-type *D. discoideum* and the $\Delta DdpoxA$ knockout mutant revealed that the knockout mutant is neither impaired in cell development, nor in production of spores or fruiting bodies. Hence, expression of the peroxidase has no observable impact on the cellular development. Nevertheless the $\Delta DdpoxA$ knockout mutant shows significantly higher numbers of contaminated fruiting bodies, suggesting a decreased antibacterial - or at least bacteriostatic - effect in absence of the peroxidase.¹²

Summing up, two representatives of a yet insufficiently studied family within the peroxidase-cyclooxygenase superfamily were investigated in this thesis. For both enzymes, we could provide evidence for covalent heme to protein ester linkages formed by acidic amino acids on the distal heme site and methyl substituents of the porphyrin ring. The same covalent attachment of the prosthetic group is also found in the well-investigated mammalian peroxidases and is crucial for their catalytic activity, especially for the oxidation of halides or pseudohalides to their corresponding (pseudo-)hypohalous acids.^{19,24} The presence of homologous heme peroxidases in prokaryotes like cyanobacteria (LspPOX) and ancient eukaryotes such as *D. discoideum* (DdPoxA) demonstrates that immune defense mechanisms driven by reactive oxygen species are not an invention of the innate immunity of mammals, but seem to be evolutionary old processes that could possibly be found as well in other ancient organisms.

References

1. Zamocky, M., Jakopitsch, C., Furtmüller, P. G., Dunand, C., and Obinger, C. (2008) The peroxidase-cyclooxygenase superfamily. Reconstructed evolution of critical enzymes of the innate immune system. *Proteins* **71**, 589-605.
2. Auer, M., Gruber, C., Bellei, M., Pirker, K.F., Zamocky, M., Kroiss, D., Teufer, A. S., Hofbauer, S., Soudi, M., Battistuzzi, G., Furtmüller, P. G., and Obinger, C. (2013) A stable bacterial peroxidase with novel halogenating activity and an autocatalytically linked heme prosthetic group. *J Biol Chem* **288**, 27181–27199.
3. Auer, M., Nicolussi, A., Schütz, G., Furtmüller, P. G., and Obinger, C. (2014) How covalent heme to protein bonds influence the formation and reactivity of redox intermediates of a bacterial peroxidase. *J Biol Chem* **289**, 31480–31491.
4. Zamocky, M., Hofbauer, S., Schaffner, I., Gasselhuber, B., Nicolussi, A., Soudi, M., Pirker, K. F., Furtmüller, P. G., and Obinger, C. (2015) Independent evolution of four heme peroxidase superfamilies. *Arch Biochem Biophys* **574**, 108-19.
5. Eichinger, L., Pachebat, J. A., Glöckner, G., Rajandream, M. A., Sucgang, R., Berriman, M., Song, J, Olsen, R., Szafranki, K., Xu, Q., Tunggal, B., Kummerfeld, S., Madera, M., Konfortov B. A., Rivero F., Bankier, A. T., Lehmann R., Hamlin N., Davies, R., Gaudet, P., Fey, P., Pilcher K., Chen, G., Saunders, D., Sodergren, E., Davis, P., Kerhornou, A., Nie, X., Hall, N., Anjard, C., Hemphill, L., Bason N., Farbrother, P., Desany, B., Just E., Morio T., Rost, R., Churcher, C., Cooper, J., Haydock, S., van Driessche, N., Cronin, A., Goodhead, I., Muzny, D., Mourier, T., Pain, A., Lu, M., Harper, D., Lindsay, R., Hauser, H., James, K., Quiles, M., Madan Babu, M., Saito, T., Buchrieser, C., Wardroper, A., Felder, M., Thangavelu, M., Johnson, D., Knights, A., Loulseged, H., Mungall, K., Oliver, K., Price, C., Quail, M. A., Urushihara, H., Hernandez, J., Rabbino-witsch, E., Steffen, D., Sanders, M., Ma, J., Kohara, Y., Sharp, S., Simmonds, M., Spiegler, S., Tivey, A., Sugano, S., White, B., Walker, D., Woodward, J., Winckler, T., Tanaka, Y., Shaulsky, G., Schleicher, M., Weinstock, G., Rosenthal, A., Cox, E. C., Chisholm R. L., Gibbs, R., Loomis, W. F., Platzer, M., Kay, R. R., Williams, J., Dear, P. H., Noegel, A. A., Barrell, B., and Kuspa, A. (2005) The genome of the social amoeba *Dictyostelium discoideum*. *Nature* **435**, 43-57.
6. Boulais, J., Trost, M., Landry, C. R., Dieckmann, R., Levy, E. D., Soldati, T., Michnick, S. W., Thibault, P., and Desjardins, M. (2010) Molecular characterization of the evolution of phagosomes. *Mol Syst Biol* **6**, Article number 423.
7. Singh, A. K., Singh, N., Sharma, S., Singh, S. B., Kaur, P., Bhushan, A., Srinivasan, A., and Singh, T. P. (2008) Crystal structure of lactoperoxidase at 2.4 Å resolution. *J Mol Biol* **376**, 1060-1075.
8. Carpena, X., Vidossich, P., Schroettner, K., Calisto, B. M., Banerjee, S., Stampler, J., Soudi, M., Furtmüller, P. G., Rovira, C., Fita, I., and Obinger, C. (2009) Essential role of proximal histidine-asparagine interaction in mammalian peroxidases. *J Biol Chem* **284**, 25929-25937.
9. Grishkovskaya, I., Paumann-Page, M., Tscheliessnig, R., Stampler, J., Hofbauer, S., Soudi, M., Sevcnikar, B., Oostenbrink, C., Furtmüller, P. G., Djinovic-Carugo, K., Nauseef, W. M., and Obinger, C. (2017) Structure of human promyeloperoxidase (proMPO) and the role of the propeptide on processing and maturation. *J Biol Chem* **292**, 8244-8261.
10. Fenna, R., Zeng, J., and Davey, C. (1995) Structure of the green heme in myeloperoxidase. *Arch Biochem Biophys* **316**, 653-656.
11. Nicolussi, A., Auer, M., Weissensteiner, J., Schütz, G., Katz, S., Maresch, D., Hobauer, S., Bellei, M., Battistuzzi, G., Furtmüller, P. G., and Obinger, C. (2017) Posttranslational modification of heme *b* in a bacterial peroxidase: the role of heme to protein ester bonds in ligand binding and catalysis. *Biochemistry* **56**, 4525-38.

12. Nicolussi, A., Dunn, J. D., Mlynek, G., Bellei, M., Zamocky, M., Battistuzzi, G., Djinović-Carugo, K., Furtmüller, P. G., Soldati, T., and Obinger, C. (2017) Secreted Heme Peroxidase from *Dictyostelium discoideum*: Insights into Catalysis, Structure and Biological Role. *J Biol Chem*, accepted on December 14th.
13. Singh, P. K., Sirohi, H. V., Iqbal, N., Tiwari, P., Kaur, P., Sharma, S., and Singh, T. P. (2017) Structure of bovine lactoperoxidase with a partially linked heme moiety at 1.98 Å resolution. *Biochim Biophys Acta* **1865**, 329-335.
14. Battistuzzi, G., Bellei, M., Zederbauer, M., Furtmüller, P. G., Sola, M., and Obinger, C. (2006) Redox thermodynamics of the Fe(III)/Fe(II) couple of human myeloperoxidase in its high-spin and low-spin forms. *Biochemistry* **45**, 12750-12755.
15. Battistuzzi, G., Bellei, M., Bortolotti, C. A., and Sola, M. (2010) Redox properties of heme peroxidases. *Arch Biochem Biophys* **500**, 21-36.
16. Furtmüller, P. G., Zederbauer, M., Jantschko, W., Helm, J., Bogner, M., Jakopitsch, C., and Obinger, C. (2006) Active site structure and catalytic mechanisms of human peroxidases. *Arch Biochem Biophys* **445**, 199-213.
17. Battistuzzi, G., Stampfer, J., Bellei, J., Vlasits, J., Soudi, M., Furtmüller, P. G., and Obinger, C. (2012) Influence of the covalent heme-protein bonds on the redox thermodynamics of human myeloperoxidase. *Biochemistry* **50**, 7887-7994.
18. Battistuzzi, G., Bellei, M., Vlasits, J., Banerjee, S., Furtmüller, P. G., Sola, M., and Obinger, C. (2010) Redox thermodynamics of lactoperoxidase and eosinophil peroxidase. *Arch. Biochem. Biophys.* **494**, 72-77.
19. Paumann-Page, M., Katz, R. S., Bellei, M., Schwartz, I., Edenhofer, E., Sevcnikar, B., Soudi, M., Hofbauer, S., Battistuzzi, G., Furtmüller, P. G., and Obinger, C. (2017) Pre-steady-state kinetics reveal the substrate specificity and mechanism of halide oxidation of truncated human peroxidase 1. *J Biol Chem* **292**, 4583-4592.
20. Battistuzzi, G., Borsari, M., Ranieri, J., and Sola, M. (2001) Redox thermodynamics of the Fe³⁺/Fe²⁺ couple in horseradish peroxidase and its cyanide complex. *J Am Chem Soc* **124**, 26-27.
21. Skaff, O., Pattison, D. I., and Davies, M. J. (2009) Hypothiocyanous acid reactivity with low-molecular mass and protein thiols: absolute rate constants and assessment of biological relevance. *Biochem J*, **422**, 111-117.
22. Shetaya, W. H., Young, S. D., Watts, M. J., Ander, E. L., and Bailey, E. H. (2012) Iodine dynamics in soils. *Geochim Cosmochim Acta* **77**, 457-473.
23. Klebanoff, S. J. (1967) Iodination of bacteria: a bactericidal mechanism. *J Exp Med* **126**, 1063-1078.
24. Zederbauer, M., Furtmüller, P. G., Brogioni, S., Jakopitsch, C., Smulevich, G., and Obinger, C. (2007) Heme to protein linkages in mammalian peroxidases: impact on spectroscopic, redox and catalytic properties. *Nat Prod Rep* **24**, 571-584.
25. Spalteholz, H., Panasenko, O. M., and Arnhold, J. (2006) Formation of reactive halide species by myeloperoxidase and eosinophil peroxidase. *Arch Biochem Biophys* **445**, 225-234.
26. Adak, S., Mazumdar, A., and Banerjee, R. K. (1997) Low catalytic turnover of horseradish peroxidase in thiocyanate oxidation. *J Biol Chem* **272**, 11049-11056.
27. Klebanoff, S. J., Kettle, A. J., Rosen, H., Winterbourn, C. C., and Nauseef, W. M. (2012) Myeloperoxidase: a front-line defender against phagocytosed microorganisms. *J Leukoc Biol* **93**, 185-196.
28. Zhang, X., Zhuchenko, O., Kuspa, A., and Soldati, T. (2015) Social amoebae trap and kill bacteria by casting DNA nets. *Nat Commun* **7**: 10938.

APPENDICES

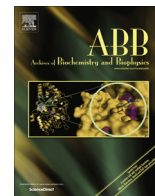
Independent Evolution of Four Heme Peroxidase Superfamilies

Zamocky, M., Hofbauer, S., Schaffner, I., Gasselhuber, B., **Nicolussi, A.**, Soudi, M.,
Pirker, K. F., Furtmüller, P. G., and Obinger, C.

Research article

Archives of Biochemistry and Biophysics (2015) **574**, 108-119.

doi: 10.1016/j.abb.2014.12.025



Independent evolution of four heme peroxidase superfamilies



Marcel Zámocký^{a,b,*}, Stefan Hofbauer^{a,c}, Irene Schaffner^a, Bernhard Gasselhuber^a, Andrea Nicolussi^a, Monika Soudi^a, Katharina F. Pirker^a, Paul G. Furtmüller^a, Christian Obinger^a

^a Department of Chemistry, Division of Biochemistry, VIBT – Vienna Institute of BioTechnology, University of Natural Resources and Life Sciences, Muthgasse 18, A-1190 Vienna, Austria

^b Institute of Molecular Biology, Slovak Academy of Sciences, Dúbravská cesta 21, SK-84551 Bratislava, Slovakia

^c Department for Structural and Computational Biology, Max F. Perutz Laboratories, University of Vienna, A-1030 Vienna, Austria

ARTICLE INFO

Article history:

Received 26 November 2014

and in revised form 23 December 2014

Available online 7 January 2015

Keywords:

Heme peroxidase

Peroxidase–catalase superfamily

Peroxidase–cyclooxygenase superfamily

Peroxidase–chlorite dismutase superfamily

Peroxidase–peroxygenase superfamily

ABSTRACT

Four heme peroxidase superfamilies (peroxidase–catalase, peroxidase–cyclooxygenase, peroxidase–chlorite dismutase and peroxidase–peroxygenase superfamily) arose independently during evolution, which differ in overall fold, active site architecture and enzymatic activities. The redox cofactor is heme *b* or posttranslationally modified heme that is ligated by either histidine or cysteine. Heme peroxidases are found in all kingdoms of life and typically catalyze the one- and two-electron oxidation of a myriad of organic and inorganic substrates. In addition to this *peroxidatic* activity distinct (sub)families show pronounced catalase, cyclooxygenase, chlorite dismutase or peroxygenase activities. Here we describe the phylogeny of these four superfamilies and present the most important sequence signatures and active site architectures. The classification of families is described as well as important turning points in evolution. We show that at least three heme peroxidase superfamilies have ancient prokaryotic roots with several alternative ways of divergent evolution. In later evolutionary steps, they almost always produced highly evolved and specialized clades of peroxidases in eukaryotic kingdoms with a significant portion of such genes involved in coding various fusion proteins with novel physiological functions.

© 2015 The Authors. Published by Elsevier Inc. This is an open access article under the CC BY license (<http://creativecommons.org/licenses/by/4.0/>).

Introduction

Heme peroxidases use heme *b* or posttranslationally modified heme as redox cofactor to catalyze the hydrogen peroxide-mediated one- and two-electron oxidation of a myriad of molecules including aromatic molecules (e.g., coniferyl alcohol or tyrosine), cations (e.g., Mn²⁺), anions (e.g., ascorbate or halides) or even proteins (e.g., cytochrome *c*). During turnover H₂O₂ is reduced to water and one-electron donors (AH₂) are oxidized to the respective radicals (·AH) (Reaction 1) whereas two-electron donors like halides (X[−]) are oxidized to the corresponding hypohalous acids (HOX)

(Reaction 2). Besides these *peroxidatic* reactions very few heme peroxidases also show a reasonable *catalatic* reaction (Reaction 3) and use a second hydrogen peroxide molecule as two-electron donor thereby releasing dioxygen. One additional activity catalyzed by a special group of heme peroxidases is the peroxygenation reaction, i.e., the (selective) introduction of peroxide-derived oxygen functionalities into organic molecules (Reaction 4).



In the last decade – due to the application of powerful sequencing techniques – an ever increasing amount of protein sequences (including numerous heme peroxidases) were automatically assigned to related protein families due to typical conserved motifs [1]. However, critical analysis shows that these annotations often need corrections based on the knowledge of the relationship between sequence, structure and function of the respective protein

Abbreviations: APx, ascorbate peroxidase; CcP, cytochrome *c* peroxidase; ClD, chlorite dismutase; DyP, dye-decolorizing peroxidase; EPO, eosinophil peroxidase; HGT, horizontal gene transfer; HRP, horseradish peroxidase; KatG, catalase–peroxidase; LDS, linoleate diol synthase; LPO, lactoperoxidase; LspPOX, *Lyngbya* peroxidase; ML, maximum likelihood method; MnP, manganese peroxidase; MPO, myeloperoxidase; PERCAL, calcium binding motif; PDB, Protein Data Bank; Pfam, protein families database; SCOP, structural classification of proteins; TPO, thyroid peroxidase; WSC, cell-wall integrity & stress response component.

* Corresponding author at: Department of Chemistry, Division of Biochemistry, VIBT – Vienna Institute of BioTechnology, University of Natural Resources and Life Sciences, Muthgasse 18, A-1190 Vienna, Austria. Fax: +43 1 47654 6059.

E-mail address: marcel.zamocky@boku.ac.at (M. Zámocký).

<http://dx.doi.org/10.1016/j.abb.2014.12.025>

0003-9861/© 2015 The Authors. Published by Elsevier Inc.

This is an open access article under the CC BY license (<http://creativecommons.org/licenses/by/4.0/>).

family. An important aspect of sorting structural superfamilies is to classify the numerous sequences according to their phylogenetic relationships [2,3] and to identify turning points and evolutionary hybrids. Moreover, interesting newly discovered evolutionary clades frequently with yet unknown function and mostly marginal but important sequence variations can be selected for further structural and kinetic studies.

This review demonstrates the independent evolution of four heme peroxidase superfamilies, namely of the (1) peroxidase–catalase superfamily, (2) peroxidase–cyclooxygenase superfamily, (3) peroxidase–chlorite dismutase superfamily and the (4) peroxidase–peroxygenase superfamily. We present an update of their reconstructed phylogeny and introduce their representative sequence signatures and essential amino acids in the heme cavity. From Fig. 1 it is obvious that each superfamily possesses a peculiar fold of the heme peroxidase domain that evolved independently with respect to other peroxidase superfamilies. It is further demonstrated that these ubiquitous oxidoreductases are present in all kingdoms of life. This strongly underlines the necessity to use the nomenclature suggested before (e.g., in [4] and not to talk about bacterial or plant or animal heme peroxidases as is still widespread in the literature and some databases). The denomination of the peroxidase superfamilies should reflect the characteristic enzymatic activities rather than their origin. The criteria for the definition of a peroxidase superfamily were presented already in [4] and here they are systematically applied on all four above listed heme peroxidase superfamilies that are further divided in particular families and subfamilies.

Peroxidase–catalase superfamily

The peroxidase–catalase superfamily previously known as the “superfamily of bacterial, fungal and plant heme peroxidases” [5] is currently the most abundant peroxidase superfamily present in various gene and protein databases. Representatives of this superfamily were detected not only in the domains of Bacteria, Archaea, eukaryotic kingdoms of Fungi and Plantae but besides numerous Protozoa and Chromista species also within Metazoan kingdom [6]. In Pfam database (<http://pfam.xfam.org>) this universally distributed superfamily is annotated as PF00141.

Here we have selected 500 representative full-length sequences that were used for an updated phylogenetic reconstruction based on the maximum likelihood (ML) method. Fig. 2 shows the occurrence of three well separated families already defined by K. Welinder in 1992 as distinct structural classes Class I, II and III [5]. We suggest to use for them the term *families* in analogy with all other heme peroxidase superfamilies (see below). Novel clades representing hybrid enzymes between the previously defined classes are well distinguishable in this reconstruction. Fig. 3 shows the typical sequence signatures of this superfamily that includes the distal amino acid triad Arg-Trp/Phe-His within the sequence –X-R-XX-W/F-H-X- and the proximal triad His-Trp/Phe-Asp (these amino acids are not neighbored in the primary sequence). The typical overall globular fold of representatives of this superfamily consists of twelve α -helices and was already acquired from the beginning. It was only slightly modified in the later steps of ongoing divergent evolution. Generally, the level of structural conservation is higher than the conservation of amino acid sequences [7].

Family I was previously defined to contain intracellular bacterial catalase–peroxidases [8,9], cytosolic, chloroplastic and peroxisomal ascorbate peroxidases [10] and mitochondrial (membrane bound) cytochrome *c* peroxidases [11,12]. Catalase–peroxidases are the only representatives of this superfamily with a high *catalytic* activity according to Reaction 3 [13] besides a peroxidatic activity. Ascorbate and cytochrome *c* peroxidases are typical

monofunctional peroxidases (i.e., cannot catalyze Reaction 3) that follow Reaction 1 with either ascorbate or cytochrome *c* as one electron donor (AH₂). The main function of Family I peroxidases seems to be scavenging of excess H₂O₂.

Family I is the most divergent one among the three structural classes. It contains eukaryotic intracellular [14,15] or even peroxisomal [16] as well as extracellular [17] catalase–peroxidases and also putative cytochrome *c* peroxidases from Choanoflagellida predecessors of fungi and animals [6]. Moreover, hybrid-type A heme peroxidases were shown to belong to Family I [7]. Their biochemical properties are between those of monofunctional APxs and CcPs [18,19], thus they represent an important turning point from ancient bifunctional catalase–peroxidases towards monofunctional specialization within this large superfamily (Fig. 2).

A peculiar minor descendant clade containing yet putative secreted ascorbate peroxidases from Unikonts/Metazoan lineages represents another evolutionary turning point (Fig. 2). A majority of further evolutionary descendants of this clade were verified as extracellular secreted proteins [6]. Among Family II sequences well known and intensively investigated lignin, manganese, versatile and generic peroxidases are found. Their main function seems to be the degradation of lignin-containing soil debris [20,21]. Recently, several novel clades with putative Family II members were detected also in various ascomycetous fungi unable to decay wood (Fig. 2). Thus, their physiological function and substrate specificity remain to be elucidated. Principally, they are able to catalyze Reactions 1 and 2.

The highest number of members are found in Family III that is comprised of numerous plant secretory peroxidases like horseradish peroxidase(s) (HRP) [e.g., 22] but also by a parallel abundant clade divided into “APx-related” yet putative algal and plant peroxidases [23] and hybrid-type B peroxidases that are present solely in the kingdom of fungi [6,7]. Sequence analysis has shown that most of these hybrid-type B peroxidases contain an additional C-terminal WSC sugar binding domain of unknown function. Family III peroxidases mainly follow Reaction 1. They are generally secreted into the cell wall or the apoplasmic compartment and the vacuole and play a role in the oxidation of lignin precursors, auxin and secondary metabolites [22].

Peroxidase–cyclooxygenase superfamily

The peroxidase–cyclooxygenase superfamily has Pfam accession PF03098 and its members are widely distributed among all domains of life [4]. Therefore, its (old) denomination as “animal heme-dependent peroxidases” is misleading but still present in some public databases. We have selected 400 representative sequences for an updated ML phylogenetic reconstruction (Fig. 4). The seven main families are well conserved in this update but some of them are presented as more abundant if compared with previous reconstructed phylogenies [24–26] that focused on particular (sub) families.

In contrast to the peroxidase–catalase superfamily, in many cases members of the peroxidase–cyclooxygenase superfamily are multidomain proteins with one heme peroxidase domain of predominantly α -helical fold with a central heme-containing core of five α -helices. Moreover, this superfamily is unique in having the prosthetic heme group posttranslationally modified [26,27]. The heme is covalently bound to the protein via two ester linkages formed by conserved Asp and Glu residues (Fig. 5A). In one representative (i.e., myeloperoxidase) a third heme to protein linkage is formed [28]. As a consequence of these modifications the heme is distorted and these peroxidases exhibit unique spectral and redox properties [29]. All representatives catalyze both Reactions 1 and 2 but with most members studied so far halide oxidation seems to be the dominating physiological enzymatic activity.

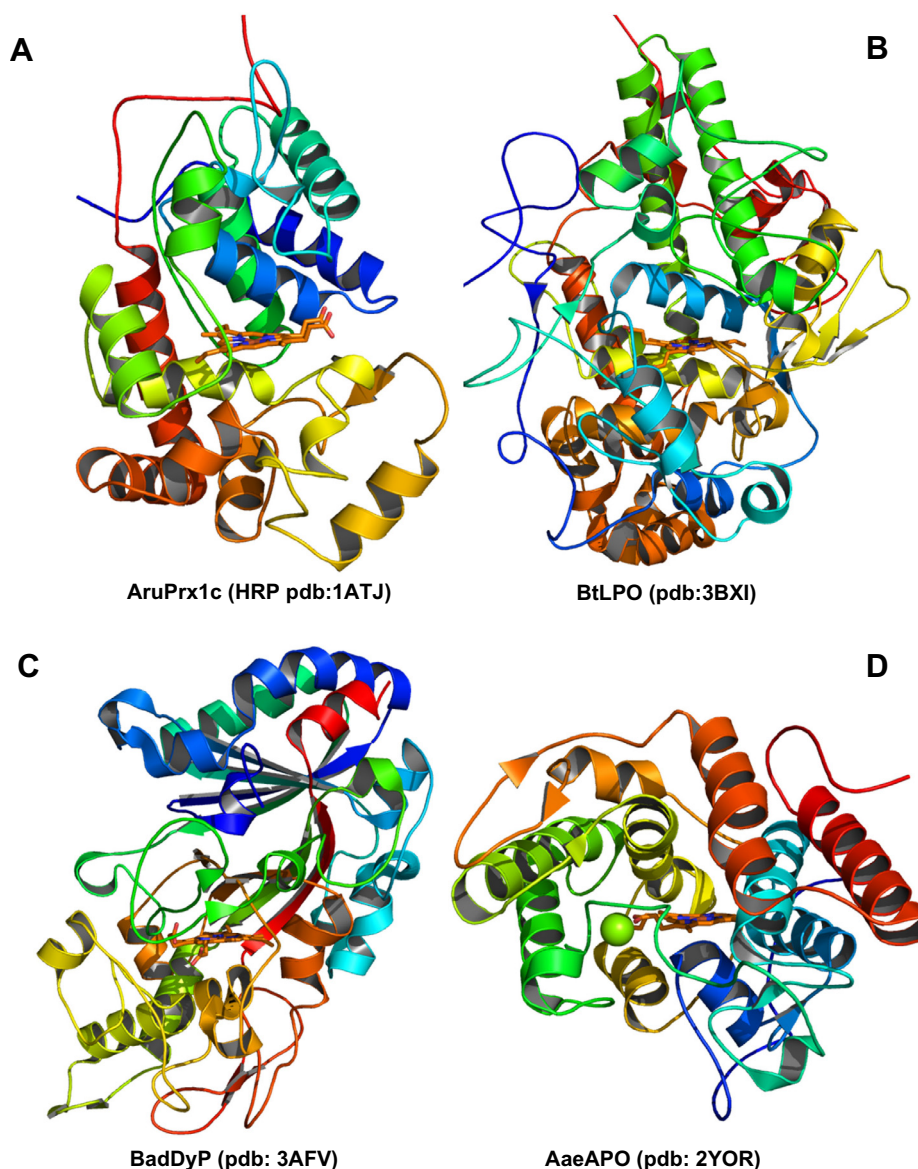


Fig. 1. Structural fold typical for the peroxidase domains of each presented heme peroxidase superfamily. Representative structures with prosthetic heme group are shown for a typical member of (A) the peroxidase–catalase superfamily, (B) the peroxidase–cyclooxygenase superfamily, (C) the peroxidase–chlorite dismutase superfamily and (D) the peroxidase–peroxygenase superfamily. Abbreviations of presented peroxidases correspond with PeroxiBase and they are also explained in [Supplem. Table 1](#).

Fig. 5A and **B** show the typical sequence signatures that allow the correct assignment of peroxidases to this superfamily. Except for families 4 and 7 the most typical sequence is **-X-G-Q-X-X-D-H-D-X-** which includes the distal catalytic histidine that is neighbored by two aspartates, the first being involved in ester bond formation and the second in Ca^{2+} -binding. The highly conserved glutamine seems to be involved in halide binding [30] (**Reaction 2**). **Fig. 5A** shows the active site of lactoperoxidase, which is a well studied member of family 1. Further typical distal residues include the catalytic arginine and a conserved glutamate that is involved in formation of the second ester bond. The typical sequence is **-X-R-X-X-E-X-** (**Fig. 5B**). The proximal ligand of peroxidases from the peroxidase–cyclooxygenase superfamily is a histidine hydrogen bonded to an asparagine (except Family 4 & 7) (**Fig. 5B**). Additionally, the calcium binding motif appears to be not fully conserved among the ancestral members (**Fig. 5**). It is conserved in families 1–3.

The ancestral clade of short bacterial peroxidases (i.e., family 5) is supposed to contain the oldest representatives of this superfamily (**Fig. 4**), namely the short peroxidases of cyanobacteria *Gloeobacter*

violaceus, *Rivularia* sp. and *Gloeocapsa* sp. which might represent (as molecular fossils) the early evolved heme peroxidases to cope with reactive oxygen species produced by ancient oxygenic photosynthesis [31]. From them, further proteobacterial and actinobacterial short peroxidases evolved (**Fig. 4**). Their closest descendant branch of long bacterial peroxidases represents a real turning point in the early phase of evolution within this superfamily. Possibly through several gene duplications and subsequent fusion events very large open reading frames (theoretically from 1600 up to 3300 amino acids) emerged in proteobacterial genomes. In such long ORFs, not only the peroxidase domains were duplicated (and fused) but also two different calcium binding motifs, namely PERCAL and hemolysin-type occur repeatedly [32]. Although the expression of such multi-domain proteins could not be verified yet, these long fusions were probably the basis for intensive further molecular evolution that proceeded in two quite different directions. The physiological role of Family 5 peroxidases that contains in the current reconstruction only putative sequences is completely unknown.

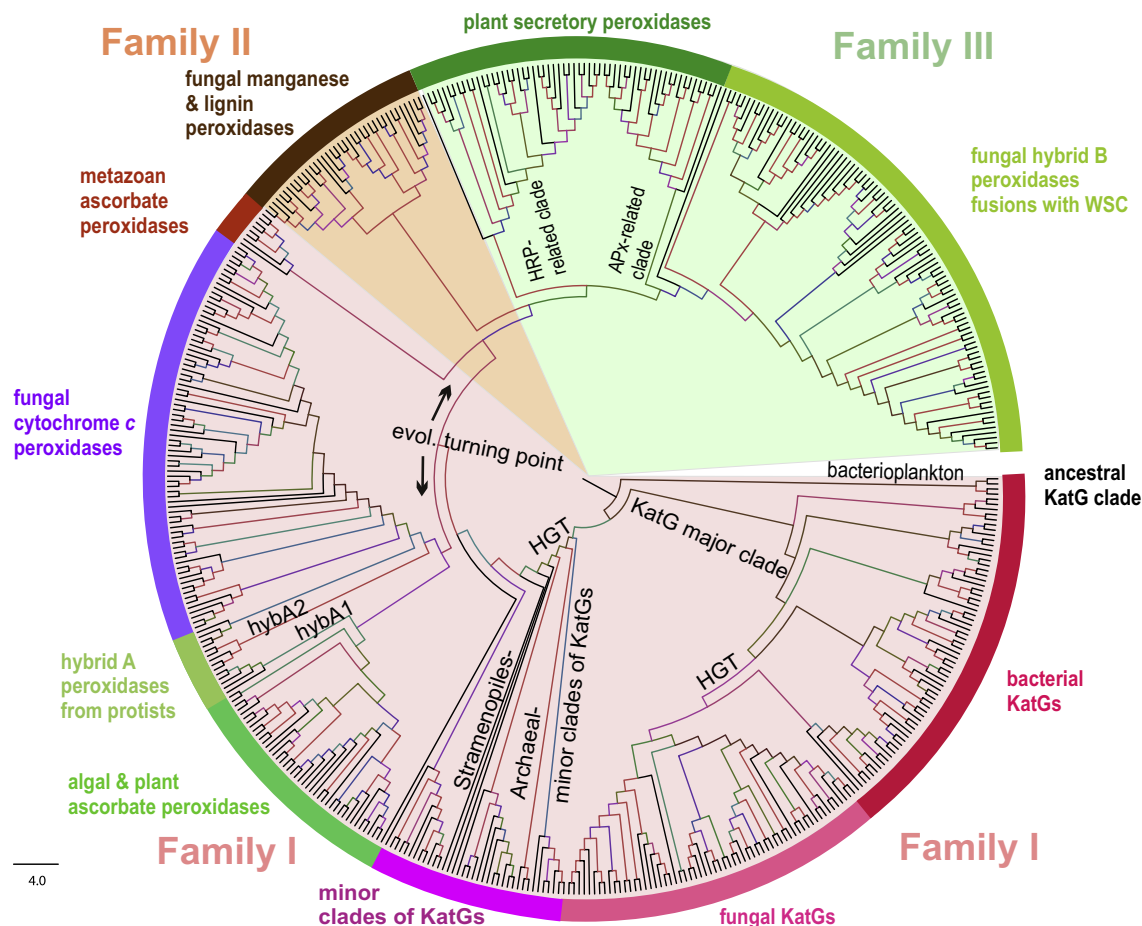


Fig. 2. Reconstructed phylogenetic tree of 500 members of the peroxidase-catalase superfamily. The evolutionary history was inferred by using the maximum likelihood method based on the Whelan & Goldman model implemented in MEGA 5 software [66]. Bootstrap values are presented as color branches based on the obtained ML output: red > 90, violet > 70, blue > 50 and green > 30. All three main families (based on previously defined structural classes I, II and III known from [5]) are highlighted on the perimeter. Important subfamilies including the two hybrid-types are also highlighted.

One evolutionary trend led to the emergence of the well known animal peroxidases like myeloperoxidase (MPO), eosinophil peroxidase (EPO), lactoperoxidase (LPO) and thyroid peroxidase (TPO) and started with bacterial peroxidockerins (Family 6). The cyanobacterial LspPOX is a typical representative of early stage in this direction and it was already investigated on protein level [26,33].

The second evolutionary direction leads towards bacterial and animal cyclooxygenases (Family 4) (Fig. 4). Although bacterial cyclooxygenases are still at the level of putative protein sequences, several cyclooxygenases from the animal phyla Cnidaria, Mollusca, Arthropoda and Chordata were already cloned and analyzed [34]. Multiple paralogs of this family have arisen from repeated gene duplication events and are separately regulated in each organism. A very important and peculiar branch of this family is presented by plant alpha dioxygenases that diverged early from cyclooxygenases (Fig. 4). Although they retained the conserved predominantly α -helical fold of this superfamily [35] slight structural modifications lead to decreased peroxidase activity whereas oxygenation of fatty acids to corresponding 2(R)-hydroperoxides is the main physiological activity of these enzymes [36]. In the opposite direction of this family evolution, we can observe a very abundant subfamily of fungal linoleate diol synthases (LDS) that apparently evolved from cyclooxygenases (Fig. 4). A few ascomycetous representatives were already purified and investigated [37,38] revealing a fusion of N-terminal peroxidase domain with C-terminal P450 domain. By studying the corresponding deletion mutants, the

regulation of LDS through protein kinase A mediated pathway was detected [38].

The alternative evolutionary trend leading from long peroxidins towards Families 3–1 occurred stepwise. First steps led over (already above mentioned) peroxidockerins (Family 6). It is important to note that evolutionary descendants of variable length emerged not only in eubacteria but can be also found in genomes of eukaryotic Amoebozoa, Heterolobosea and Chromalveolata (Fig. 4). This fact indicates that peroxidockerins were widely distributed among the early eukaryotic world but whether there was one or several HGTs from marine bacteria towards unicellular ancestral eukaryotes remains to be elucidated in the future research if more sequences of this Family 6 will be made available.

Dual oxidases (Family 7) were segregated from peroxidockerins at the level of primitive eukaryotes as stated before ([4] and Fig. 4). These multidomain oxidases have retained an extracellular peroxidase domain at the N-terminus followed by a transmembrane segment appended to an EF-hand calcium-binding cytosolic region and a cytosolic C-terminal enzymatic domain with homology to NADPH oxidase. The peroxidase domain is significantly mutated (proximal histidine is absent) and lost its peroxidase activity [39]. It was shown that dual oxidases generate H_2O_2 but the function of the modified peroxidase domain in this large multidomain protein remains obscure [40].

In a further step peroxinectins (Family 3) evolved. They were shown to exhibit cell adhesion function(s) and to be involved in

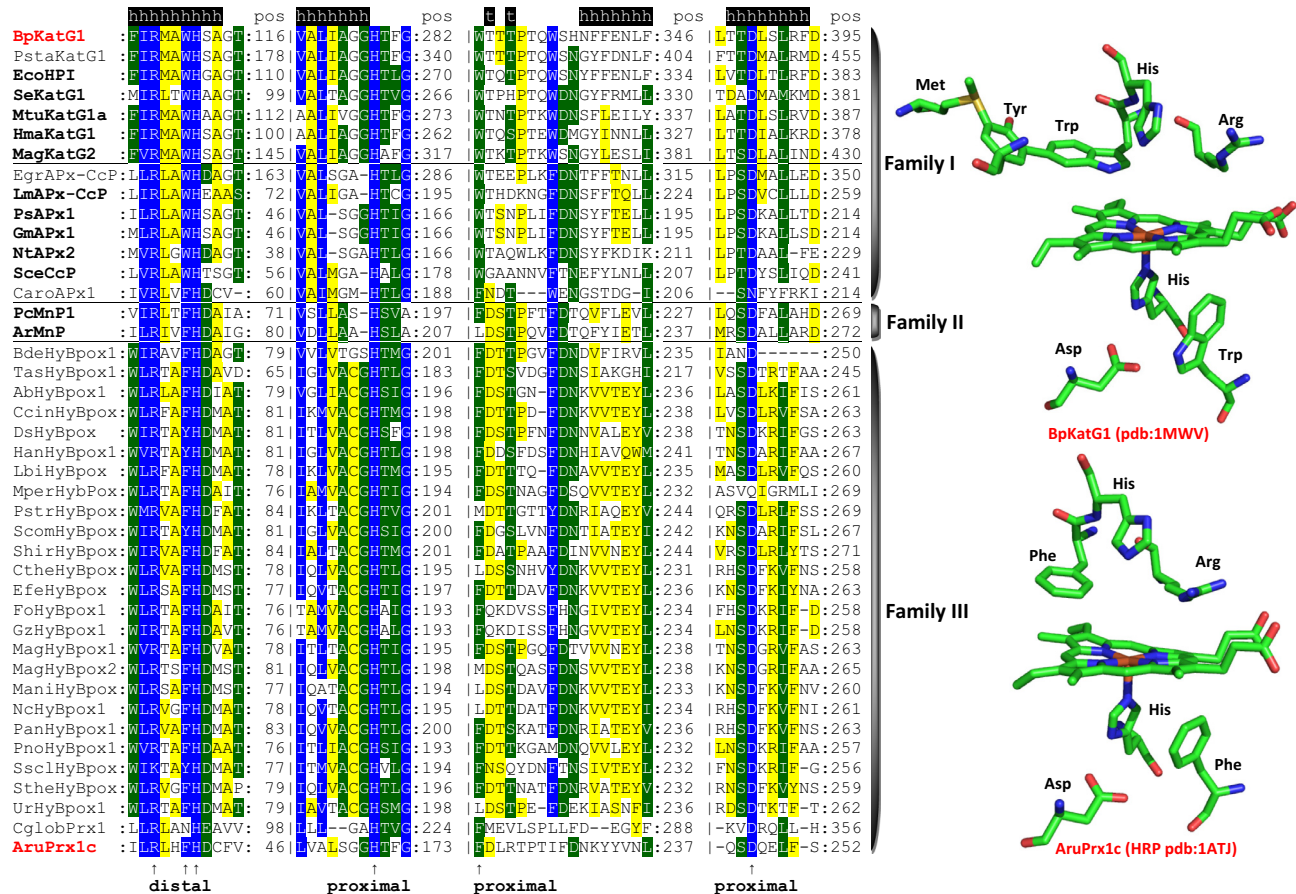


Fig. 3. Typical sequence patterns including distal and proximal triad found in all representatives of the peroxidase–catalase superfamily. In addition, the active site architectures of the Family I member, catalase–peroxidase from *Burkholderia pseudomallei* (BpKatG1) and the Family III protein horseradish peroxidase (AruPrx1c) is depicted. Note that BpKatG1 shows the unique KatG-typical distal side adduct that includes the distal tryptophan. Abbreviations of sequence names are explained in [Supplem. Table 1](#) and they correspond with the nomenclature of PeroxiBase (<http://peroxibase.toulouse.inra.fr>). Color scheme: blue highest sequence similarity (93% conservation), green moderate similarity (75%), yellow low similarity (33%). Secondary structure elements for BpKatG1 structure are given above the alignment.

invertebrate immune response by production of hypohalous acids according to [Reaction 2](#) [41]. In principle, they are also fusion proteins of a conserved heme peroxidase domain with an integrin-binding motif (i.e., KGD [41]) that probably co-evolved from the dockerin part of peroxidockerins together with the peroxidase domain. Peroxinectins are widely spread mainly among the Eumetazoan phyla arthropods and nematodes with occurrence of several paralogs in a single genome as result of frequent gene duplications.

Next evolutionary event led to division in peroxidasins (Family 2) and a sister family of Chordata peroxidases (Family 1). They diverged in several Chordata subfamilies including the separated subfamily of thyroid peroxidases, minor subfamilies of fish peroxidases and three closely connected subfamilies of mammalian lactoperoxidases (LPO), myeloperoxidases (MPO) and eosinophil peroxidases (EPO) (Fig. 4) that are major players in the innate immune system by the production of antimicrobial hypohalous acids [30]. The overall phylogenetic distribution of peroxidase orthologs in four mammalian monophyletic clades (i.e., subfamilies) is in accordance with the general evolution and speciation of these organisms with a positive selection detected at specific amino acid sites for slight functional shifts [42] with impact on innate immunity. Thyroid peroxidase (TPO) catalyzes the formation of thyroid hormones in mammals [43].

In contrast, we can observe a broad and rather abundant distribution of peroxidase isozymes in various Eumetazoan phyla (Fig. 4 and [25]). They were segregated in one minor subfamily of (yet putative) short peroxidasins and up to five distinct

subfamilies of long (multi-domain) peroxidasins where the peroxidase domain is fused N-terminally with domains of leucine-rich repeats and immunoglobulin type-C whereas C-terminally with von Willebrand factor C module. The subfamilies of long peroxidasins apparently evolved through many speciation events from Urochordata to Mammals [25]. The physiological function of peroxidasins was comprehensively studied only recently [44]. Besides expected (unspecific) antimicrobial activity through production of hypohalous acids (common with other chordata peroxidases) they play an important role in the biosynthesis of extracellular matrix. Human peroxidase 1 uses [Reaction 2](#) to catalyze specifically the essential formation of sulfilimine bonds in collagen IV thus being involved in the biosynthesis of the extracellular matrix [45]. Cross-linked collagen IV scaffold is essential for epithelial tissue genesis and stabilization. Systematic analysis showed that both collagen IV crosslink formation as well as tissue-specific peroxidase evolution probably arose at the point of divergence between Metazoan phyla Porifera and Cnidaria as evolutionary innovation for a specialized extracellular matrix–basement membrane of animal tissues [44].

Peroxidase–chlorite dismutase superfamily

This superfamily was first constituted by Goblirsch et al. [46] bringing together related sequences of three distinct protein families that share a common fold (however with low overall sequence

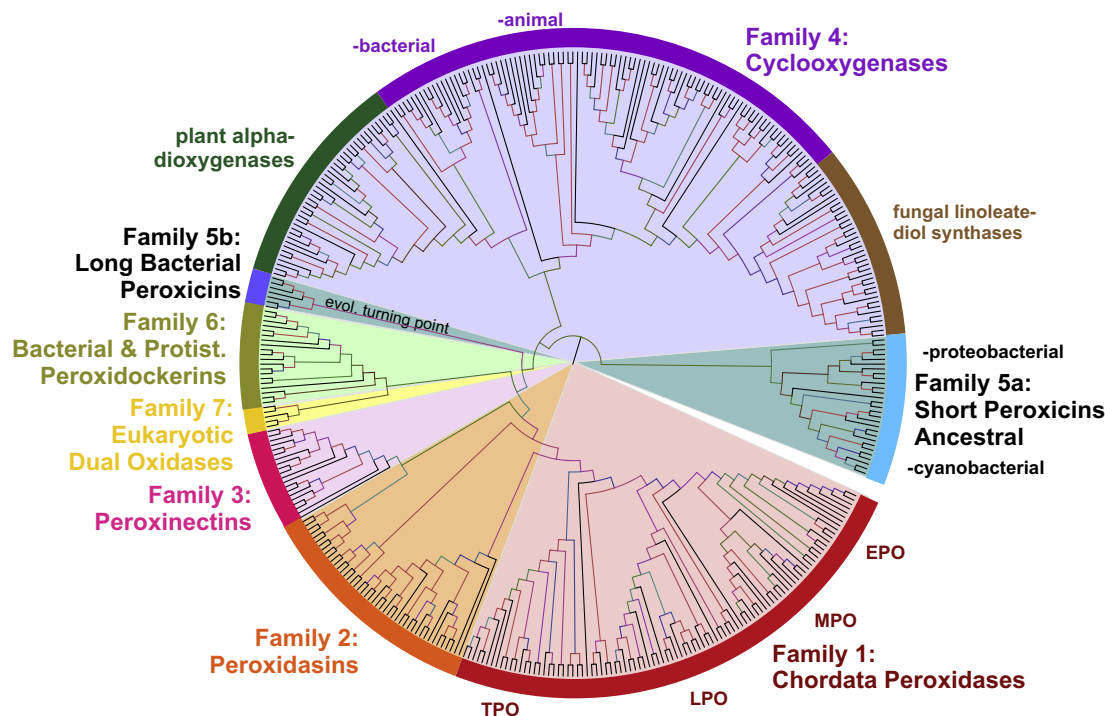


Fig. 4. Reconstructed phylogenetic tree of 400 members of the peroxidase–cyclooxygenase superfamily. The evolutionary history was inferred by using the maximum likelihood method based on the Whelan & Goldman model implemented in MEGA 5 software [66]. Bootstrap values are presented as a color branches based on the ML output: red > 90, violet > 70, blue > 50 and green > 30. All seven (numbered) families known from [4] are highlighted on the perimeter together with important subfamilies.

identity) and may possess essential and related functions in iron-dependent metabolism. A common heme-binding scaffold of so-called dye-decolorizing peroxidases (DyPs) with chlorite dismutases (Cld) and their evolutionary intermediates (i.e., deferochelatase/oxidases and Cld-like proteins) was the most important prerequisite for defining this novel superfamily of heme proteins (Fig. 6) [46]. Originally, this superfamily was designated as CDE (i.e., chlorite dismutase–DyP–EfeB) superfamily [46]. Updated phylogeny demonstrates that EfeB belongs to DyPs.

Fig. 7 depicts typical sequence patterns and heme cavity architectures of DyPs and Clds. The dye-decolorizing peroxidases and Clds show a fully conserved arginine at the distal heme site [47]. DyPs in addition have a catalytic aspartate, whereas in Cld-like proteins both residues are missing. In all members of the peroxidase–chlorite dismutase superfamily the proximal ligand is a histidine, which in Clds is hydrogen bonded to a glutamate, in DyPs to an aspartate. Another Cld-typical sequence pattern is **-X-I-P-V/I-K/R-K-X-** that includes proximal residues (Fig. 7).

Although the particular families possess two different accessions in Pfam, namely PF04261 (for DyP) and PF06778 (for Cld), they are classified in a common protein clan CL0032 (SCOP 54909) that comprises up to 18 member families, but most of them without the ability to bind the prosthetic heme group. It is important to note that in contrast to the two previously described heme peroxidase superfamilies, the peroxidase–chlorite dismutase family appears to cover only a small part of a very large dimeric α/β barrel structural superfamily (i.e., protein clan). The modification of such a fold to acquire the ability to bind the heme group and exploit it evolved probably only in one evolutionary event. The whole dimeric α/β barrel structural superfamily is outside of the scope of this issue.

DyP heme peroxidases are abundant not only in many bacterial phyla [48] but also among fungi. Recently a partial phylogeny focussing on 160 fungal sequences was reconstructed [20]. Further

phylogenies comprising also Cld sequences [46,49] revealed the extent and diversity of these peculiar heme peroxidases. Our updated phylogenetic reconstruction covering all taxonomical divisions is shown in Fig. 6. In principle, we can distinguish four DyP subfamilies known from previous classification [50,51], four Cld-like clades (i.e., subfamilies to be further resolved in the future) and two clades of functional Clds (Fig. 6). Dye-decolorizing peroxidases mainly follow Reaction 1 and exhibit a very broad substrate range. Originally, they were found to degrade bulky dyes and from these observations the denomination dye-decolorizing peroxidase derived. Functional Clds are able to degrade chlorite efficiently to chloride and O_2 , whereas Cld-like enzymes neither exhibit a peroxidase nor a chlorite degrading activity. Moreover, Cld-like proteins show a diminished affinity for the prosthetic group.

The ancestral clade of the whole superfamily is probably located in DyP-subfamily A, namely among sequences from thermophilic facultatively anaerobic bacteria of the division Firmicutes (Fig. 6). This would suggest ancient roots of the whole superfamily as thermophilic anaerobic bacilli are supposed to be of very old origin [52]. From this ancestral DyP-A subfamily the evolution led either to more sophisticated DyP-C and DyP-D subfamilies or in alternative direction towards shortened DyP-subfamily B and then further to subfamilies of Clds. DyP-type C & D subfamilies cluster together with a high bootstrap support but whereas DyP-C representatives are known from genomes of proteobacteria, actinobacteria and cyanobacteria, DyP-D members are only present among basidiomycetous and ascomycetous fungi. Thus, DyP-type D peroxidases from the fungal subkingdom of Dikarya apparently evolved via horizontal gene transfer (HGT) from cyanobacterial predecessors (see Fig. 6) that belong to the DyP-type C subfamily. Blast searches in genomes of ancestral (early diverging) fungi like *Mucor circinelloides* (a Zygomycete that contains also genes from the peroxidase–peroxygenase superfamily, see below) did not yield any output for DyP peroxidase genes. This supports the theory of

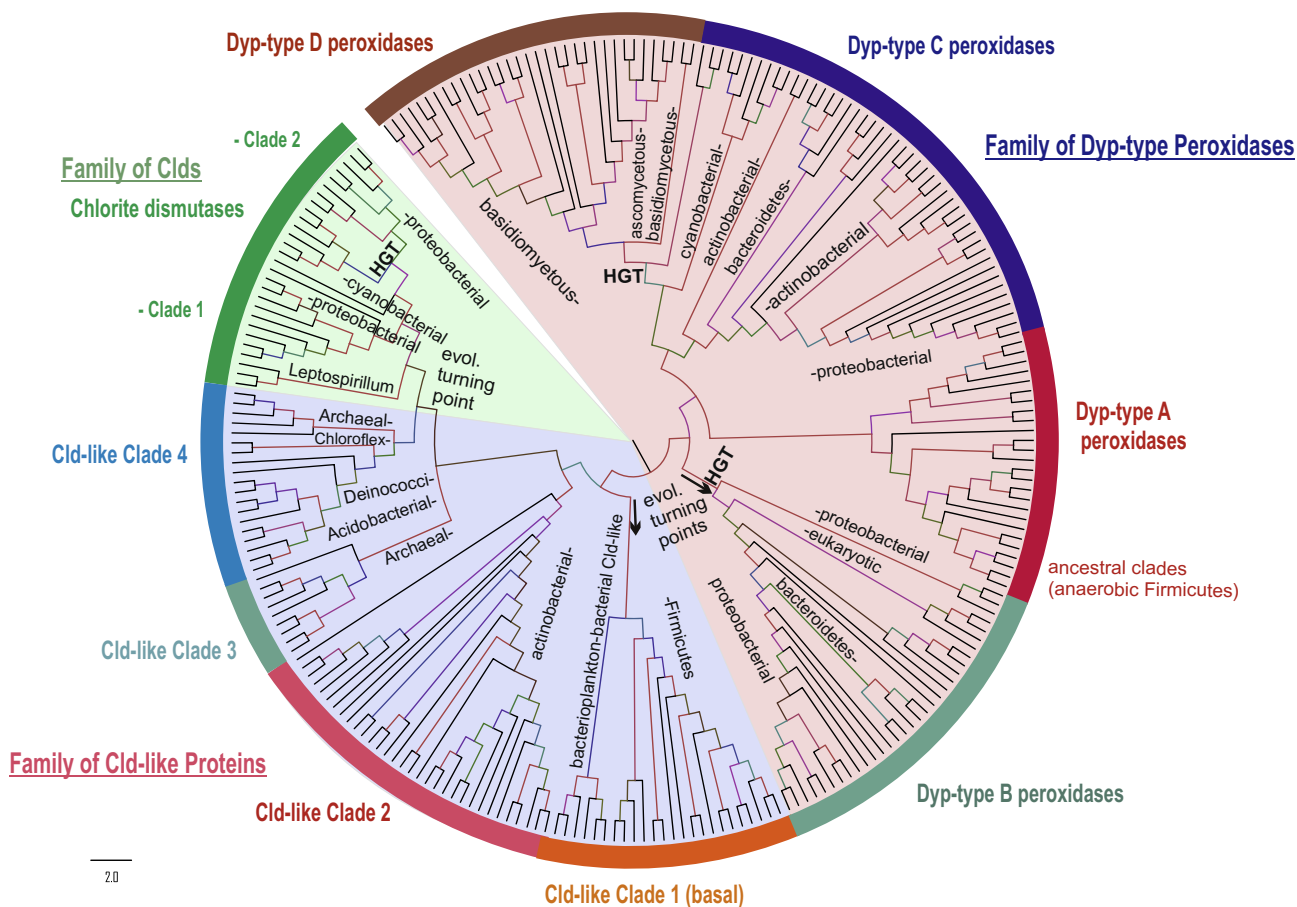


Fig. 6. Reconstructed phylogenetic tree of 250 members of the peroxidase–chlorite dismutase superfamily. The evolutionary history was inferred by using the maximum likelihood method based on the Whelan & Goldman model implemented in MEGA 5 software [66]. Bootstrap values are presented as color branches based on the ML output: red > 90, violet > 70, blue > 50 and green > 30. Three main families [chlorite dismutases (Clds), dye-decolorizing peroxidases (DyPs) and Cld-like proteins] known from [46,49] are highlighted on the perimeter. Important subfamilies (in some cases clades) are also shown.

HGT from autotrophic prokaryotes to heterotrophic eukaryotes. Anyway, upcoming new genomes of early diverging fungi must be also screened with blast in this respect. Their codon usage has to be analyzed and compared.

Fungal DyP sequences occur not only in subfamily D but also in subfamily B, where also several other sequences from lower eukaryotes like *Dictyostelium discoideum* or *Naegleria gruberi* DyP-peroxidases occur. Most of here presented protein sequences from this subfamily stem from Proteobacteria therefore also in subfamily B HGT events appeared probably several times during the evolution. Even more surprising is the occurrence of DyP-type B genes in the Trematode parasite *Schistosoma mansoni*. Also in this multicellular flatworm DyP genes were acquired by HGT from lower eukaryotes but their functionality must be proven experimentally. Thus it appears that subfamily B is the most divergent one of all four described DyP subfamilies leading to unique evolution of DyP peroxidases within Unicont genomes. Turning points in this superfamily's evolution lie unequivocally in this subfamily clades that besides several HGT events enabled also further evolution towards chlorite-dismutase like proteins.

Among four distinct Cld-like subfamilies (Fig. 6) the clade containing mainly Firmicutes representatives but also several archaeal sequences appears to be basal for further evolution towards functional chlorite dismutases. It is important to note that within archaeal genomes only Cld-like sequences were found yet but no sequences coding for DyPs. This underlines the hypothesis that Clds evolved in a later phase of the diversification from DyP B

subfamily (Fig. 6) via shortening of the gene. But as both DyPs and Clds are present as paralogs in genomes of extant Cyanobacteria, Firmicutes or Proteobacteria, Cld (or Cld-like) genes must have been transferred in mentioned bacteria by the means of secondary HGTs in later stages of this superfamily's evolution. The stepwise natural mutations in Cld-like clades finally led to two functional clades (i.e., subfamilies) of chlorite dismutases as probably the latest step of this long-term evolution. Whereas the physiological function of numerous putative Cld-like proteins is under discussion [58–60], the fully functional chlorite dismutases containing heme *b* prosthetic group are segregated in two distinct clades (6). Clade 1 is almost completely formed by proteobacterial pentamer or hexameric representatives whereas Clade 2 contains dimeric proteobacterial as well as numerous cyanobacterial enzymes. The N-terminus of Clade 2 proteins is truncated (Fig. 7) [49]. Some of them were investigated recently on protein level [53–57]. The question remains, however, whether removal of chlorite is indeed their native physiological function as higher concentrations of chlorite most likely occur in the environment just from anthropogenic actions of the last 50 years [46].

Observed conserved and variable patterns from the multiple sequence alignment support the above formulated phylogenetic hypothesis that Clds evolved from DyP-B peroxidases by partial deletions and modifications within the frequently but not stringently duplicated ancestral DyP-related gene. Some of the Cld-like clades that have lost the essential functional residues may represent “death-end products” of superfamily evolution (seen also in

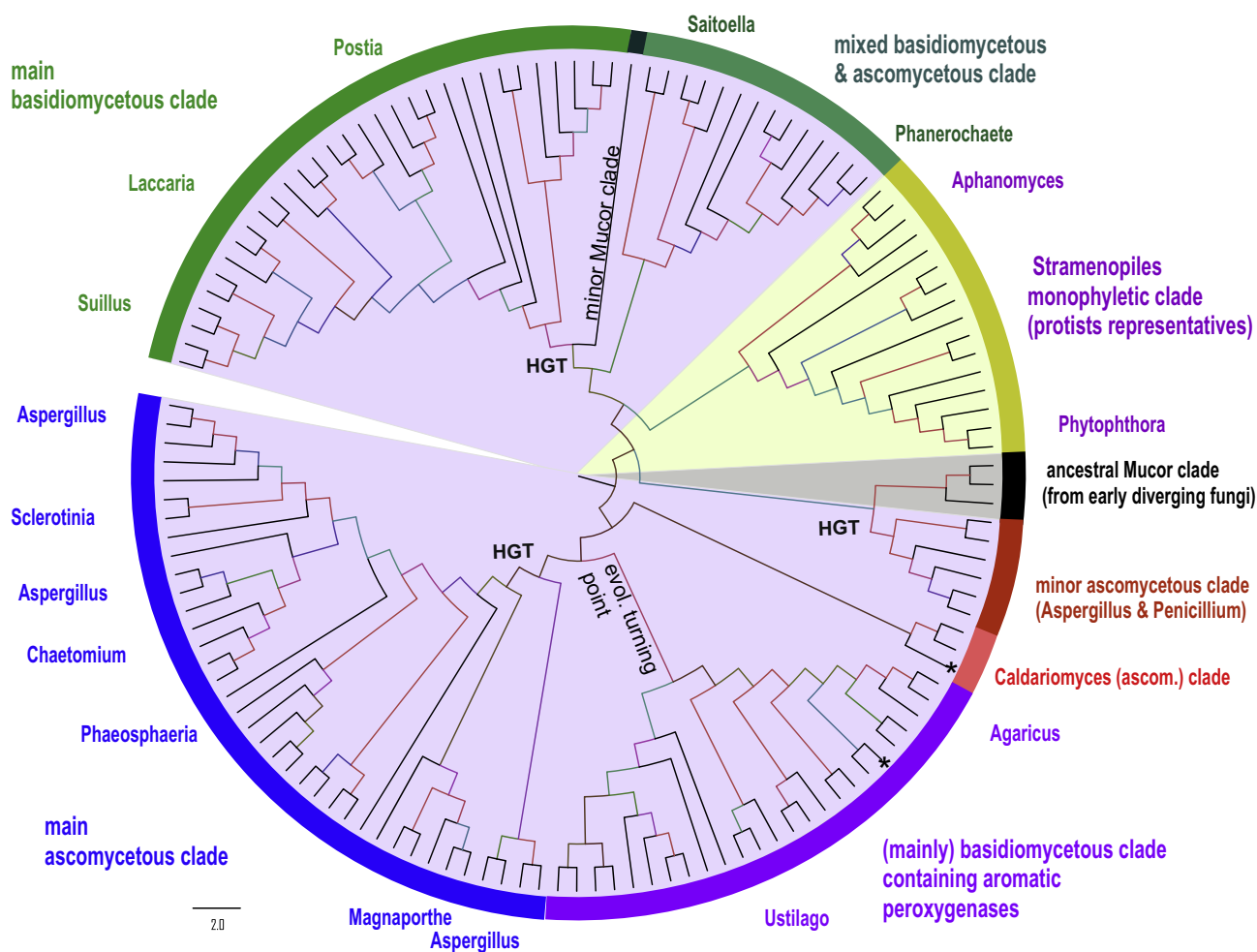


Fig. 8. Reconstructed phylogenetic tree of 136 members of the peroxidase–peroxygenase superfamily. The evolutionary history was inferred by using the maximum likelihood method based on the Whelan & Goldman model implemented in MEGA 5 software [66]. Bootstrap values are presented as color branches based on the ML output: red > 90, violet > 70, blue > 50 and green > 30. All main subfamilies (currently defined only as clades) are highlighted on the perimeter.

peroxidase–cyclooxygenase superfamily [4]) or they have acquired some new functions (e.g., in heme biosynthesis [58–60] that were different from the ancestral peroxidase activity.

Peroxidase–peroxygenase superfamily

This heme peroxidase superfamily is unique since its members can (besides typical *peroxidatic* activity) efficiently incorporate peroxide-derived oxygen into substrate molecules. Additionally their proximal heme ligand is cysteine instead of histidine (Fig. 9). In the literature several names are used for its members including heme-thiolate peroxidases (HTPs), unspecific peroxygenases (UPOs) or aromatic peroxygenases (APOs). For several decades chloroperoxidase from the ascomycetous fungus *Leptoxyphium* (*Caldariomyces*) *fumago* has been in the focus of research only. In the last decade other members of this superfamily (Pfam accession number PF01328) were found and started to be analyzed.

From the beginning of their discovery it was clear that these oxidoreductases differ from all previously known heme peroxidases and are functional hybrids between a “classical” heme peroxidase and a P450-monooxygenase [61]. These metalloproteins are secreted and highly glycosylated versatile enzymes that catalyze the oxidation of organic heteroatoms and inorganic halides, one-electron oxidations (Reactions 1 and 2) but also hydroxylations (Reaction 4), epoxidations and dealkylations [62–64].

Therefore, we suggest the denomination peroxidase–peroxygenase superfamily. Its members show a typical fold with ten α -helices and five very short β -sheets [61,65]. Currently, it is the smallest known heme peroxidase superfamily but its full phylogenomic extent still has to be discovered. This means that the particular families cannot be clearly defined yet and the current phylogenetic reconstruction (Fig. 8) comprises only division in main clades. A partial phylogeny was already reconstructed for isolates of forest floor samples [20] that focused predominantly on basidiomycetous sequences. Here, we show an updated phylogeny based on 136 representatively selected sequences that cover all organisms with already detected heme-thiolate peroxidase genes (Fig. 8) most of them still putative.

Typical conserved regions of members of this superfamily show the $-X-P-C-P-X-$ motif which includes the proximal heme ligand cysteine and the $-X-E-G-D-X-$ motif that contains three ligands involved in the binding of a cation (Fig. 9). Interestingly, the distal side, where the enzymatic reaction occurs, shows a surprising variability. In those representatives with an experimentally verified peroxidase and peroxygenase reaction an aspartate together with a basic amino acid is found (Fig. 9).

The ancestral clade appears to contain *Mucor* enzymes as representatives of genes from early diverging fungi of the division Zygomycota. This means that those genes were – in contrast with some other peroxidase subfamilies (e.g., Dyp-D or -B see above) – included in the genomes of ancestral, primitive fungi already from

- [3] G. Caetano-Anolles, M. Wang, D. Caetano-Anolles, J.E. Mittenthal, *Biochem. J.* 417 (2009) 621–637.
- [4] M. Zámocký, C. Jakopitsch, P.G. Furtmüller, C. Dunand, C. Obinger, *Proteins* 72 (2008) 589–605.
- [5] K.G. Welinder, *Curr. Opin. Struct. Biol.* 2 (1992) 388–393.
- [6] M. Zámocký, B. Gasselhuber, P.G. Furtmüller, C. Obinger, *Cell. Mol. Life Sci.* 71 (2014) 4681–4696.
- [7] M. Zámocký, P.G. Furtmüller, C. Obinger, *Arch. Biochem. Biophys.* 500 (2010) 45–57.
- [8] R. Singh, B. Wiseman, T. Deemagarn, V. Jha, J. Switala, P.C. Loewen, *Arch. Biochem. Biophys.* 471 (2008) 207–214.
- [9] M. Zámocký, *Eur. J. Biochem.* 271 (2004) 3297–3309.
- [10] F. Passardi, N. Bakalovic, F.K. Teixeira, M. Margis-Pinheiro, C. Penel, C. Dunand, *Genomics* 89 (2007) 567–579.
- [11] J.E. Erman, L.B. Vitello, *Biochim. Biophys. Acta* 1597 (2002) 193–200.
- [12] M. Zámocký, C. Dunand, *FEBS Lett.* 580 (2006) 6655–6664.
- [13] J. Vlasits, C. Jakopitsch, M. Bernroither, M. Zámocký, P.G. Furtmüller, C. Obinger, *Arch. Biochem. Biophys.* 500 (2010) 74–81.
- [14] M.W. Fraaije, H.P. Roubroeks, W.R. Hagen, W.J.H. van Berkel, *Eur. J. Biochem.* 235 (1996) 192–198.
- [15] L. Peraza, W. Hansberg, *Biol. Chem.* 383 (2002) 569–575.
- [16] M. Zámocký, G. Sekot, M. Bučková, J. Godočiková, C. Schäffer, M. Farkašová, C. Obinger, B. Polek, *Arch. Microbiol.* 195 (2013) 393–402.
- [17] M. Zámocký, E. Droghetti, M. Bellei, B. Gasselhuber, M. Pabst, P.G. Furtmüller, G. Battistuzzi, G. Smulevich, *Biochimie* 94 (2012) 673–683.
- [18] S. Adak, A.K. Datta, *Biochem. J.* 390 (2005) 465–474.
- [19] T. Ishikawa, N. Tajima, H. Nishikawa, J. Gao, M. Rapolu, H. Shibata, Y. Sawa, S. Shigeoka, *Biochem. J.* 426 (2010) 125–134.
- [20] D. Floudas, M. Binder, R. Riley, K. Barry, R.A. Blanchette, B. Henrissat, A.T. Martínez, R. Otiillar, J.W. Spatafora, J.S. Yadav, A. Aerts, I. Benoit, A. Boyd, A. Carlson, A. Copeland, P.M. Coutinho, R.P. de Vries, P. Ferreira, K. Findley, B. Foster, J. Gaskell, et al., *Science* 336 (2012) 1715–1719.
- [21] H. Kellner, P. Luis, M.J. Pecyna, F. Barbi, D. Kapturska, D. Krüger, D.R. Zak, R. Marmeisse, M. Vandenberg, M. Hofrichter, *PLoS One* 9 (2014) e95557.
- [22] C. Mathé, A. Barre, C. Jourda, C. Dunand, *Arch. Biochem. Biophys.* 500 (2010) 58–65.
- [23] F. Lazzarotto, F.K. Teixeira, S.B. Rosa, C. Dunand, C.L. Fernandes, A. de Vasconcelos Fontenele, J.A.G. Silveira, H. Verli, R. Margis, M. Margis-Pinheiro, *New Phytol* 191 (2011) 234–250.
- [24] S. Gui-Qin, Y. Quan-You, Z. Zhang, *Arch. Insect Biochem. Physiol.* 79 (2012) 87–103.
- [25] M. Soudi, M. Zámocký, C. Jakopitsch, P.G. Furtmüller, C. Obinger, *Chem. Biodivers.* (2012) 1776–1793.
- [26] M. Auer, C. Gruber, M. Bellei, K.F. Pirker, M. Zámocký, D. Kroiss, S.A. Teufer, S. Hofbauer, M. Soudi, G. Battistuzzi, P.G. Furtmüller, C. Obinger, *J. Biol. Chem.* 288 (2013) 27181–27199.
- [27] M. Zederbauer, P.G. Furtmüller, S. Brogioni, C. Jakopitsch, G. Smulevich, C. Obinger, *Nat. Prod. Rep.* 24 (2007) 571–584.
- [28] X. Carpena, P. Vidossich, K. Schroettner, B.M. Calisto, S. Banerjee, J. Stampler, M. Soudi, P.G. Furtmüller, C. Rovira, I. Fita, C. Obinger, *J. Biol. Chem.* 284 (2009) 25929–25937.
- [29] J. Arnhold, E. Monzani, P.G. Furtmüller, M. Zederbauer, L. Casella, *Eur. J. Inorg. Chem.* 19 (2006) 3801–3811.
- [30] P.G. Furtmüller, M. Zederbauer, W. Jantschko, J. Helm, M. Bogner, C. Jakopitsch, C. Obinger, *Arch. Biochem. Biophys.* 445 (2006) 199–213.
- [31] M. Mimuro, T. Tschuchiya, K. Koyama, G.A. Peschek, in: G.A. Peschek (Ed.), *Bioenergetic Processes in Cyanobacteria*, 2011, pp. 211–238 (Chapter 9).
- [32] S. Santamaria-Hernando, T. Krell, M.-I. Ramos-Gonzalez, *PLoS One* 7 (2012) e40698.
- [33] M. Auer, A. Nicolussi, G. Schütz, P.G. Furtmüller, C. Obinger, *J. Biol. Chem.* 289 (2014) 31480–31491.
- [34] M. Kawamura, H. Inaoka, S. Obata, Y. Harada, *Prostaglandins Other Lipid Mediat.* 109–111 (2014) 14–22.
- [35] C.C. Goulah, G. Zhu, M. Koszelak-Rosenblum, M.G. Malkowski, *Biochemistry* 52 (2013) 1364–1372.
- [36] G. Zhu, M. Koszelak-Rosenblum, M.G. Malkowski, *Protein Sci.* 22 (2013) 1432–1438.
- [37] C. Su, E.H. Oliw, *J. Biol. Chem.* 271 (1996) 14112–14118.
- [38] F. Jerneřen, A. Sesma, M. Francheschetti, M. Hamberg, E.H. Oliw, *J. Biol. Chem.* 285 (2010) 5308–5316.
- [39] J.L. Meitzler, P.R. Ortiz de Montellano, *J. Biol. Chem.* 284 (2009) 18634–18643.
- [40] Y.S. Bae, M.K. Choi, W.-J. Lee, *Trends Immunol.* 31 (2010) 278–287.
- [41] A. Vizzini, D. Parrinello, M.A. Sanfratello, V. Mangano, N. Parrinello, M. Cammarata, *Dev. Comput. Immunol.* 41 (2013) 59–67.
- [42] N.B. Loughran, B. ÓConnor, C. ÓFágain, M.J. ÓConnell, *BMC Evol. Biol.* 8 (2008) 101.
- [43] J. Kessler, C. Obinger, G. Eales, *Thyroid* 18 (2008) 769–774.
- [44] A.L. Fidler, R.M. Vanacore, S.V. Chetyrkin, V.K. Pedchenko, G. Bhav, V.P. Yin, C.L. Stothers, K.L. Rose, W.H. McDonald, T.A. Clark, D.-B. Borza, R.E. Steele, M.T. Ivy, T. Aspirnauts, J.K. Hudson, B.G. Hudson, *Proc. Natl. Acad. Sci. U.S.A.* 111 (2014) 331–336.
- [45] G. Bhav, C.F. Cummings, R.M. Vanacore, C. Kumagai-Cresse, I.A. Ero-Tolliver, M. Rafi, J.-S. Kang, V. Pedchenko, L.I. Fessler, J.H. Fessler, B.G. Hudson, *Chem. Biol.* 8 (2012) 784–790.
- [46] B. Goblrirsch, R.C. Kurker, B.R. Streit, C.M. Wilmot, J.L. DuBois, *J. Mol. Biol.* 408 (2011) 379–398.
- [47] R. Singh, J.C. Grigg, Z. Armstrong, M.E.P. Murphy, L.D. Eltis, *J. Biol. Chem.* 287 (2012) 10623–10630.
- [48] E. van Bloois, D.E. Torres, *Appl. Microbiol. Biotechnol.* 86 (2010) 1419–1430.
- [49] S. Hofbauer, I. Schaffner, P.G. Furtmüller, C. Obinger, *Biotechnol. J.* 9 (2014) 461–473.
- [50] Y. Sugano, *Cell. Mol. Life Sci.* 66 (2009) 1387–1403.
- [51] T. Yoshida, Y. Sugano, *Arch. Biochem. Biophys.* 574 (2015) 49–55.
- [52] F.D. Ciccarelli, T. Doerks, C. von Mering, C.J. Creevey, B. Snel, P. Bork, *Science* 311 (2006) 1283–1287.
- [53] G. Mlynek, B. Sjöblom, J. Kostan, S. Fureder, F. Maixner, K. Gysel, P.G. Furtmüller, K. Djinović-Carugo, C. Obinger, M. Wagner, H. Daims, *J. Bacteriol.* 193 (2011) 2408–2417.
- [54] S. Hofbauer, M. Bellei, A. Sundermann, K.F. Pirker, A. Hagmüller, G. Mlynek, J. Kostan, H. Daims, P.G. Furtmüller, K. Djinović-Carugo, C. Oostenbrink, G. Battistuzzi, C. Obinger, *Biochemistry* 51 (2012) 9501–9512.
- [55] S. Hofbauer, C. Gruber, K.F. Pirker, A. Sundermann, I. Schaffner, C. Jakopitsch, C. Oostenbrink, P.G. Furtmüller, C. Obinger, *Biochemistry* 53 (2014) 3145–3157.
- [56] A. Sündermann, M.M. Reif, S. Hofbauer, C. Obinger, C. Oostenbrink, *Biochemistry* 53 (2014) 4869–4879.
- [57] I. Schaffner, S. Hofbauer, M. Krutzler, K.F. Pirker, G. Stadlmayr, M. Bellei, G. Mlynek, K. Djinović-Carugo, G. Battistuzzi, P.G. Furtmüller, H. Daims, C. Obinger, *Mol. Microbiol.*, submitted for publication.
- [58] T.A. Dailey, T.O. Boynton, A.N. Albetel, S. Gerdes, M.K. Johnson, H.A. Dailey, *J. Biol. Chem.* 285 (2010) 25978–25986.
- [59] J.A. Mayfield, N.D. Hammer, R.C. Kurker, T.K. Chen, S. Ojha, E.P. Skaar, J.L. DuBois, *J. Biol. Chem.* 288 (2013) 23488–23504.
- [60] S. Hofbauer, A. Hagmüller, I. Schaffner, M. Krutzler, G. Stadlmayr, H. Daims, C. Obinger, K. Djinović-Carugo, P.G. Furtmüller, *Arch. Biochem. Biophys.* 574 (2015) 36–48.
- [61] M. Sundaramoorthy, J. Turner, T.L. Poulos, *Structure* 3 (1995) 1367–1377.
- [62] M. Hofrichter, R. Ulrich, *Appl. Microbiol. Biotechnol.* 71 (2006) 276–288.
- [63] M. Hofrichter, R. Ullrich, M.J. Pecyna, C. Liers, T. Lundell, *Appl. Microbiol. Biotechnol.* 87 (2010) 871–897.
- [64] M. Hofrichter, R. Ullrich, *Curr. Opin. Chem. Biol.* 19 (2014) 116–125.
- [65] K. Piontek, E. Strittmatter, R. Ullrich, G. Gröbe, M.J. Pecyna, M. Kluge, K. Scheibner, M. Hofrichter, D.A. Plattner, *J. Biol. Chem.* 288 (2013) 34767–34776.
- [66] K. Tamura, D. Peterson, N. Peterson, G. Stecher, M. Nei, S. Kumar, *Mol. Biol. Evol.* 28 (2011) 2731–2739.



Dipl.-Ing. Andrea Nicolussi

* February 22nd, 1988 in Steyr, Upper Austria

Gablenzgasse 24/16

1160 Vienna

+43 650 6630820

andrea.nicolussi@gmx.net

Education

- 11/2013 – present **PhD program** *BioToP –Biomolecular Technology of Proteins*
University of Natural Resources and Life Sciences, Vienna
PhD thesis in Protein Biochemistry: “Enlightening the impact of covalent heme to protein bonds in ancestral peroxidases”
- 03/2011 – 10/2013 **Master’s program** *Biotechnology*
University of Natural Resources and Life Sciences, Vienna
Final exam with distinction
Master’s thesis in Protein Biochemistry: “Mechanism studies on a eukaryotic secreted catalase-peroxidase from *Magnaporthe grisea*”
- 10/2007 – 03/2011 **Bachelor’s program** *Food Science and Biotechnology*
University of Natural Resources and Life Sciences, Vienna
Bachelor’s thesis in Organic Chemistry: “Synthesis of 2-acetamido-2-deoxy-1,3,4,6-tetra-O-acetyl-β-D-glucopyranose and derivatives thereof”
- 10/2006 – 06/2007 **Diploma program** *Pharmacy* (change of program after 2 semesters)
University of Vienna
- 06/2006 **Higher School Certificate** *Öffentliches Stiftsgymnasium der Benediktiner*
Seitenstetten, Lower Austria

Professional experience

- 08/2016 – 12/2016 **Research stay**
Cell biological and *in vivo* experiments on the role of a heme peroxidase in the social amoeba *Dictyostelium discoideum*
University of Geneva, Switzerland
- 03/2015 & 01/2016 **Research stays**
Spectroelectrochemical determination of the reduction potentials of heme peroxidases
University of Modena and Reggio Emilia, Italy

- 10/2009 – present **Tutor**
 “Practical Course in Organic Chemistry” and
 “Practical Course in Biochemistry II”
 University of Natural Resources and Life Sciences, Vienna
- 08/2008 **Internship**
 Food laboratory (chemical, microbiological and enzymatic
 analysis of food and water samples)
 LebCo Lebensmittel Control GmbH
- 07/2008 **Internship**
 Quality Control (Analysis of raw materials and pharmaceutical
 products in a GMP and GLP environment including documentation)
 Dr. Peithner GmbH & Co

Awards

- 2017 Winner of the **PhD Student Young Investigator Travel Award**
 at the 10th International Human Peroxidase Meeting, Colorado
- 2016 Holder of the **University Fellowship “Boursier d’Excellence”**
 for the research stay at the University of Geneva, Switzerland

Conferences

- 2017 **10th International Human Peroxidase Meeting**
 Breckenridge, Colorado (Oral presentation)
LS² Annual Meeting
 Zürich, Switzerland (Poster presentation)
- 2016 **8th European Meeting on Oxizymes**
 Wageningen, Netherlands (Oral presentation)
- 2015 **9th International Human Peroxidase Meeting**
 Cologne, Germany (Oral presentation)
8th Conference on Recombinant Protein Production
 Palma de Mallorca, Spain (Poster presentation)
- 2014 **12th European Biological Inorganic Chemistry Conference**
 Zurich, Switzerland (Poster presentation)
7th European Meeting on Oxizymes
 Vienna, Austria (Poster presentation)

SCI publications

- 2017 **Nicolussi, A.**, Auer, M., Paumann-Page, M., Sevcnikar, B., Soudi, M., Zamocky, M., Hofbauer, S., Furtmüller, P. G., and Obinger, C. (2017) The impact of heme-protein crosslinking on structure and catalysis of prokaryotic and eukaryotic peroxidases. *Arch Biochem Biophys*, in preparation
- Nicolussi, A.**, Dunn, J. D., Mlynek, G., Bellei, M., Zamocky, M., Battistuzzi, G., Djinović-Carugo, K., Furtmüller, P. G., Soldati, T. and Obinger, C. (2017) Secreted Heme Peroxidase from *Dictyostelium discoideum*: Insights into Catalysis, Structure and Biological Role *J Biol Chem*, accepted on December 14th
- Nicolussi, A.**, Auer, M., Weissensteiner, J., Schütz, G., Katz, S., Maresch, D., Hobauer, S., Bellei, M., Battistuzzi, G., Furtmüller, P. G., and Obinger, C. (2017) Posttranslational modification of heme *b* in a bacterial peroxidase: the role of heme to protein ester bonds in ligand binding and catalysis. *Biochemistry* 56, 4525-38.
- 2016 Gasselhuber, B., Graf, M. M., Jakopitsch, C., Zamocky, M., **Nicolussi, A.**, Furtmüller, P. G., Oostenbrink, C., Carpena, X., and Obinger, C. (2016) Interaction with the redox cofactor MYW and functional role of a mobile arginine in eukaryotic catalase-peroxidase. *Biochemistry* 25, 3528-41.
- 2015 Gasselhuber, B., Carpena, X., Graf, M. M., Pirker, K. F., **Nicolussi, A.**, Sündermann, A., Hofbauer, S., Zamocky, M., Furtmüller, P. G., Jakopitsch, C., Oostenbrink, C., Fita, I., and Obinger, C. (2015) Eukaryotic catalase-peroxidase: the role of the trp-tyr-met adduct in protein stability, substrate accessibility and catalysis of hydrogen peroxide dismutation. *Biochemistry* 35, 5425-38.
- Zamocky, M., Hofbauer, H., Schaffner, I., Gasselhuber, B., **Nicolussi, A.**, Soudi, M., Pirker, K. F., Furtmüller, P. G., and Obinger, C. (2015) Independent evolution of four heme peroxidase superfamilies. *Arch Biochem Biophys* 574, 108-19.
- 2014 Auer, M., **Nicolussi, A.**, Schütz, G., Furtmüller, P. G., and Obinger, C. (2014) How covalent heme to protein bonds influence the formation and reactivity of redox intermediates of a bacterial peroxidase. *J Biol Chem* 289, 31480-91.

Additional skills

Languages	German (first language) ●●●●● English ●●●●○ Italian ●○○○○
IT skills	Microsoft Office (Word, Excel, Powerpoint) Specific software (e.g. SnapGene, ExPASy, PyMOL) CorelDRAW
Extracurricular activity	Member of Curriculum Committee of the PhD program BioToP (2016 – 2017)
Driving license	Austrian B